From the Adolf-Butenand-Institut, Chair of Physiological Chemistry at the
Biomedical Center, Faculty of Medicine,
Ludwig-Maximilians-University Munich and 4SC AG

Dissertation
zum Erwerb des Doctor of Philosophy (Ph.D.)
an der Medizinischen Fakultät der
Ludwig-Maximilians-Universität zu München

The potential of epigenetically-active small molecules in regulating metabolism - paving novel avenues for alternative treatment strategies

vorgelegt von:

Evangelia Tzika

aus:

Cholargos, Athen, Griechenland

Jahr:

2021

Mit Genehmigung der Medizinischen Fakultät der
Ludwig-Maximilians-Universität zu München

First evaluator: Prof Dr Axel Imhof

Second evaluator: Prof Dr Andreas Ladurner

Third evaluator: Prof Dr Aloys Schepers

Fourth evaluator: Prof Dr Ralph Rupp

Dean: ***Prof. Dr. med. dent. Reinhard Hickel***

date of the defense:

30 July 2021

Affidavit

Surname, first name

Street

Zip code, town

Country

I hereby declare, that the submitted thesis entitled

is my own work. I have only used the sources indicated and have not made unauthorised use of services of a third party. Where the work of others has been quoted or reproduced, the source is always given.

I further declare that the submitted thesis or parts thereof have not been presented as part of an examination degree to any other university.

Place, date

Evangelia Tzika

Signature doctoral candidate

LMU LUDWIG-MAXIMILIANS-UNIVERSITÄT MÜNCHEN

Dean's Office
Medical Faculty

MMRS MUNICH MEDICAL RESEARCH SCHOOL

Confirmation of congruency between printed and electronic version of the doctoral thesis

Tzika Evangelia

Surname, first name

Street

Zip code, town

Country

I hereby declare that the electronic version of the submitted thesis, entitled

The potential of epigenetically-active small molecules in regulating metabolism - paving novel avenues for alternative treatment strategies

is congruent with the printed version both in content and format.

Munich, 25 Aug 2021

Place, date

Evangelia Tzika

Signature doctoral candidate

Abstract

Metabolic disorders will be the number one non-communicable disease on a global scale by 2030. In the next 10 years, one billion people are estimated to suffer from disabling consequences of metabolic disorders and the global health expenditure specifically for diabetes is estimated to reach $845 billion by 2045. Lots of risk factors such as dietary intake, lack of exercise and other life style behaviors are considered to influence the development of metabolic disorders. However, despite the efforts that have been undertaken to unravel their potential causes, the underlying molecular mechanisms remain elusive. Some evidence suggested links between the pathogenesis of metabolic disorders and changes on chromatin and chromatin-modifying enzymes, which can contribute to a persistent dysregulated metabolic phenotype. Indeed, a rising number of studies links epigenetic alterations with the diagnosis and prognosis of metabolic disorders. Most studies have investigated the impact of altered metabolism on chromatin modifications via energy substrates. However, as of today, there is a lack of comprehensive studies examining how by modulating epigenetics metabolism is affected.

The current study has focused specifically on this route of interplay between epigenetics and metabolism. Importantly, a prerequisite for exploiting these findings for pharmacological intervention is a detailed understanding of how differential epigenetic modifications control cell metabolism. In the current study, I present, support and discuss novel data uncovering the interplay between epigenetics and metabolic pathways on a cellular level and highlight potential new avenues for alternative treatment strategies. Using live cell metabolic profiling of glycolysis and oxidative phosphorylation, mass spectrometry-based quantitation of over 40 distinct histone modifications, and quantitative proteomics, this work suggests a potential “histone code of metabolism”, which characterised specific metabolic states of cells and links those not only to histone PTMs but also potentially novel protein effectors.

Acknowledgements

I would like to thank the company sponsor where I performed experiments for providing me with the resources I needed to fulfil my PhD. I especially would like to thank Dr T Dreker for supervising me during my PhD. I also want to thank the biology team for supporting me when I was working in the company's lab spaces. I would also very much like to thank Prof Dr A Imhof for my project discussions and for giving me the opportunity to participate in the weekly meetings at the Biomedical Centre, departmental retreats and seminars and finally feedback and discussion on the thesis. I would also like to thank Mrs M Serefidou for introducing me into the Imhof lab spaces during my secondment. I would like to thank Mr A Venkatasubramani for helping me with the Skyline software for peptide peak assignments for histone samples. Moreover, I would like to thank my additional TAC members, Prof Dr A Ladurner and Prof Dr J Mellor, for their time and feedback during project meetings and discussions. Finally, I would like to thank the ChroMe network for organising helpful seminars spanning from programming to various other scientifically relevant topics and for valuable feedback and thoughts regarding my project.

Table of Contents

List of Figures

List of Tables

Abbreviations

Listed below are abbreviations used in this thesis. For proteins and genes, recommended symbols and names are used with common alternative names indicated when appropriate. Protein names are from UniProt (http://www.uniprot.org/) and gene names are from the Human Gene Nomenclature Committee (HUGO, http://www.genenames.org) and from the Ensembl genome browser (http://www.ensembl.org/index.html).

Abbreviation	Full name
2-OG	2-Oxoglutarate
ACN	Acetonitrile
ATP	Adenosine triphosphate
BCA	Bicinchoninic acid assay
BH	Benjamini-Hochberg
BWS	Beckwith-Wiedemann syndrome
DMEM	Dulbecco's modified Eagle's medium
DMRS	DNA methyl regions
DMSO	Dimethyl sulfoxide
DNMT	DNA methyltransferase
DTT	Dithiothreitol
ECAR	Extracellular acidification rate
ETC	Electron transport chain
FAD	Flavin adenine dinucleotide
FDA	Food and Drug Administration
FH	Fumarate hydrolase
HAT	Histone acetyltransferase
HD	Huntington's disease
HDAC	Histone deacetylase
HEPES	N-2-hydroxyethylpiperazine-N'-2-ethanesulfonic acid
HMTs	Histone methyltransferases
ICR	Imprinting control regions
IDF	International Diabetes Federation
IDH	Isocitrate dehydrogenase
KDM	Lysine demethylases
KMT	Lysine Methyltransferase
NAD	Nicotinamide adenine dinucleotide
NAFLD	Non-alcoholic fatty liver disease
NCD	Non-communicable diseases
PCA	Principal component analysis
PDE	Phosphodiesterase

PRMT	Arginine methyltransferase
PTMS	Post-translational modifications
PTPB	Protein tyrosine phosphatase of *Mycobacterium tuberculosis*
R-2-HG	R-2-hydroxyglutarate
RFU	Relative fluorescent units
ROR	Retinoid related orphan receptor
RT	Room temperature
RTT	Rett syndrome
SAM	S-adenosyl methionine
SDH	Succinate dehydrogenase
SRS	Silver Russel syndrome
TCA	Trichloroacetic acid
TCA	Tricarboxylic cycle
TFA	Trifluoroacetic acid

Chapter 1

Introduction

A similar discussion corresponding to some parts of the Introduction Chapter has been published by the author previously as a peer-reviewed Review – see list of Publications. Those parts have been adapted in accordance with the currently valid guidelines of the LMU.

1.1 Societal and clinical relevance of epigenetics and metabolism

According to World Health Organization (WHO) data, noncommunicable diseases (NCDs) are the leading cause of death globally (WHO, 2018). In particular, NCDs accounted for seven out of ten most frequent reasons of morbidity and mortality (WHO, 2019). It is alarming that the greatest part of NCDs consist of metabolic diseases. As reported in 2019 in the atlas of the International Diabetes Federation (IDF), diabetes will affect more than 700 million people by 2045 (IDF, 2019). The global health expenditure is estimated to rise to $845 billion by 2045 only for diabetes cases (Williams et al., 2020). Obesity and cardiovascular diseases are increasing (WHO, 2014) with obesity prevailing and estimated to affect 1 billion people globally by 2030 (Kelly et al., 2008). There are multiple projection studies forecasting that almost 50% of the population in the US and UK will be obese by 2030 (Finkelstein et al., 2012; Kopelman et al., 2007; Thomas et al., 2014; Y. Wang et al., 2008) and other studies analyse various EU countries as well, in regards to short and long term obesity rates (Janssen et al., 2020; OECD, 2017). It is essential to identify risk factors of predisposition for those diseases and work towards prevention management. In fact, prediction or increased risk of diabetes and heart diseases can be associated with a group of risk factors including high fasting blood sugar, high blood pressure and low HDL cholesterol levels. These and other abnormal physiological measures are described as the “metabolic syndrome" (NIH, 2016). The projection data mentioned above underline the pressing need to identify methods to prevent and treat the metabolic syndrome. Another important aspect to look into to improve prevention measures is to address yet unanswered questions about the fundamental pathology of metabolic diseases. There are many other determinants such as life style choices, like nutrition preferences and training routine that are thought to hold a role in the progression of metabolic diseases among different patients (Jumpertz von Schwartzenberg & Turnbaugh, 2015; Khera et al., 2016; Phillips, 2016; Zeevi et al., 2015). Furthermore, the molecular mechanisms framing the impact of metabolism on possible patterns of deregulated genes underpinning causality and progression of metabolic diseases, are far from being fully understood. Interacting factors are traded dynamically and reciprocally between epigenetics and metabolism, while constantly being regulated by multifactorial external stimuli, unravelling correlations among varying pathological states. The epigenome can be affected not only by immediate physiological effects like hormonal dysregulation

and adipose tissue generation but also from lifestyle factors and diet choices. For example, there is eminent evidence that eating preferences may impact gene transcription via epigenetic mechanisms (Etchegaray & Mostoslavsky, 2016; van Dijk et al., 2015). A few studies have been published pointing towards inheritance to the offspring (L. M. Nicholas et al., 2013; Rando & Simmons, 2015; Seki et al., 2012). A comprehensive analysis of genomic DNA methylation showed that children of parents impacted by the Dutch famine exhibited several DNA regions linked with growth and metabolism showing significantly differential methylation even 70 years later. These regions included genes implicated in control of birth weight and LDL cholesterol regulation (Tobi et al., 2015).

Dietary habits is not the only factor influencing epigenetic regulation of metabolism. There are more societal factors such as sleep patterns, meal timing and work shifts that trigger misalignment of the circadian rhythm. A study demonstrated that even one night of sleep deprivation leads to hypermethylation of different circadian clock genes, that are expressed in a tissue-specific manner. This results in increased insulin resistance and impaired glucose tolerance (Cedernaes et al., 2015; Donga et al., 2010; Fontana & Partridge, 2015; Morris et al., 2016). Additionally, metabolites are the substrates utilized in the formation of chromatin modifications and play a fundamental role in all biochemical pathways. It has been demonstrated that food-derived metabolites can be used as substrates for transcription factors and histone modifying enzymes. As a consequence, chromatin folding is affected, resulting in more compacted or more accessible areas of the genome and respectively to decreased or increased gene transcription (Fan et al., 2015b; Gut & Verdin, 2013; C. Lu & Thompson, 2012).

On the other hand, there is evidence indicating that epigenetics in turn could impact metabolic mechanisms and disease (Crunkhorn, 2011; Heerboth et al., 2014; Kwak & Park, 2016). However, the studies exploring metabolism via epigenetic alterations for example via histone PTMs are very limited and mainly focus on one target (see Chapter 1.3). Big network studies and multifaceted analyses focusing on altering metabolism via histone PTMs are currently missing. Also, there are no studies linking epigenetic inhibitors with metabolic regulation. Therefore, efforts exploring epigenetic targets as future candidates for drug development in metabolic diseases need to be further advanced. The aim

of my work was to add more clues in the interplay of epigenetics and metabolism and to help discover novel therapeutics to modify pathological states.

1.2 Epigenetics and metabolism in human disease

1.2.1 Rare diseases

Rare diseases by definition affect a very small number of people comparing to the general population. Our limited understanding of the underlying pathomechanisms and the lack of identified druggable targets are the main causes why there are so many rare diseases without treatment. Rare diseases comprise monogenetic as well as multifactorial disorders, albeit not all of them have a genetic background. The observed symptoms vary greatly and encompass birth dysplasia, gradual atrophy and in multiple cases extend to the onset of dysregulated metabolic phenotypes.

Rett syndrome (RTT; OMIM 312750) is a rare progressive neurodegenerative disease. It mainly affects young females and its symptoms include diminished brain volume, as well as speech and motor disabilities, breathing malfunctions, muscle atrophy and many metabolic complications. It is primarily caused by any of various mutations in the methyl-CpG-binding protein 2 gene (MECP2) (Kyle et al., 2016). The main role of MECP2 is to control chromatin structure and epigenetic imprinting. MECP2 selectively binds to methylated DNA and associates with chromatin-remodelling complexes (such as type I histone deacetylases, HDACs) to modulate gene transcription (Justice et al., 2013). Interestingly, MECP2 impacts various biological pathways on multiple levels and currently the molecular mechanisms from gene to phenotype are not entirely deciphered (Justice et al., 2013). However, a few published studies started to elucidate the underlying pathomechanisms behind RTT's metabolic symptoms. More specifically, one study showed that lipid metabolism was vastly influenced both in the brain and systemically in MECP2 null mice (Buchovecky et al., 2013). Another study described mitochondrial malfunction and abnormal morphology in patients with RTT, as well as murine models of MECP2 (Kriaucionis et al., 2006). In recent published work, MECP2 was identified as a regulator of lipid homeostasis. It was shown to recruit the repressor complex, NCoR1/SMRT - HDAC3, to its lipogenesis targets in hepatocytes. Furthermore, it was demonstrated that Mecp2 mutant

mice develop fatty liver disease and dyslipidaemia with similarities to HDAC3 liver-specific ablation (Kyle et al., 2016). These above data frame MECP2 as an important epigenetic modulator of metabolic homeostasis.

Albeit RTT being a better studied example, there are more rare diseases with a potential direct link among epigenetics and metabolism. Mutations of various epigenetic regulatory factors have in the past first been linked with cancer. It is now apparent that cell metabolism and cancer are tightly connected. For this reason, it does not come as a surprise that many genes which had previously been linked with cancer may also lead to metabolic disease phenotypes in the absence of cancer symptoms. More specifically, histone-lysine N-methyltransferase 2D (KMT2D,MLL4/MLL2, is a key H3 lysine 4 (H3K4) mono-methyltransferase (J.-E. Lee et al., 2013). It is mainly associated with acute myeloid leukaemia, lung and colon cancer (Rao & Dou, 2015). Furthermore, KMT2D mutations are linked with Kabuki syndrome, which is a multisystem congenital anomaly. Characteristics and symptoms of this syndrome include facial and skeletal dysmorphisms, mild to moderate intellectual disability and postnatal growth defects (Van Laarhoven et al., 2015). Mutations in the KMT2D gene are detected in 45–80% of patients. Whilst abnormalities of the musculoskeletal system are the primary characteristics of Kabuki syndrome, later in life patients also suffer from symptoms of metabolic deregulation.

Congenital heart disease progression is another pathology where KMT2D has been implicated to play a role although the exact mechanism is not clear (Zaidi et al., 2013). Even though the exact underlying molecular mechanism of KMT2D's influence on metabolism remains elusive and may be different from disease to disease, it has been previously demonstrated that mutations in Mll2 in mice cause impaired glucose tolerance and insulin resistance (Goldsworthy et al., 2013). Interestingly, KMT2D mutant mice were found exhibiting characteristics of mild non-alcoholic fatty liver disease (NAFLD) including increased levels of blood plasma cholesterol and triglycerides. Another study implicated KMT2D and KMT2C as modulating factors of the hepatic circadian clock which also play a role as co-activators of the circadian transcription factors retinoid-related orphan receptor (ROR)-α and -γ, that have been previously involved in regulating lipid metabolism (D.-H. Kim et al., 2015; Lau et al., 2008). It has also been shown before that KMT2D can also act as a coactivator of PPARγ within

the murine liver to control over-nutrition induced steatosis. Interestingly, the heterozygous Kmt2d+/- mice were resistant to hepatic steatosis triggered by over-nutrition (D.-H. Kim et al., 2016).

DNA methylation in mammals is linked with the epigenetic mechanism of parental imprinting, where the differential expression of one allele of a specific gene is directed by its parental origin. All imprinting control regions (ICRs) that have been identified so far are differentially DNA methylated regions (DMRs) on the two parental chromosomes and are heritably maintained in the developing embryo. The role of post-translational histone modifications (PTMs), however, is not straightforward. DMRs are featuring asymmetrical aggregation of various histone modifications on the two parental chromosomes and a demand for histone demethylation has been identified at some ICRs in order to establish germline DNA methylation (Ciccone et al., 2009). Imprinting disorders consist a group of 12 pathologies with similar clinical symptoms and common epigenetic patterns. They have been indicated to influence growth, development and metabolism (Livingstone & Borai, 2014). Silver–Russell syndrome (SRS) patients have in their vast majority a common underlying disease-linked epigenetic change; loss of methylation on chromosome 11p15 (Schönherr et al., 2006). In spite of this finding, the molecular aetiology underlying SRS remains elusive in a considerable fraction of patients. The most interesting genomic regions to examine differences in DNA methylation in SRS patients are CpG islands. This is due to the fact that methylation changes in these parts of the genome impact the direct epigenetic environment to modulate transcription of affected genes. Interestingly, genes coding for metabolic factors were particularly enriched at CpG islands that are differentially methylated in SRS patients (Prickett et al., 2015). This finding could possibly be a link among the observed metabolic symptoms of SRS patients, including type II diabetes, cardiovascular disorders and obesity (Wakeling et al., 2017).

A number of imprinted genes hold a key role in modulating energy homeostasis and glucose metabolism, such as DLK1, GRB10 and IGF2 (Livingstone & Borai, 2014). There are specific diseases like Beckwith–Wiedemann syndrome (BWS) that are linked with these genes and showcase their importance for normal metabolic regulation. BWS is a congenital disorder that is described by elevated expression ofIGF2, in most cases caused by a loss of DNA-mediated imprinting. 50% of BWS patients experience hypoglycaemia. This condition is caused by hyperinsulinism, instead of it being a direct

effect of Igf2. However, the underlying β-cell defect is yet to be elucidated (Adachi et al., 2013; Sparago et al., 2004). Studies investigating epigenetic implications have indicated that parental obesity can influence embryonic methylation of IGF2, linking these alterations with birth weight and the occurrence of metabolic syndrome later in life (Hoyo et al., 2012; Soubry et al., 2013). In animal models, parental caloric restriction impacts epigenetic modulation of Igf2 (S. Zhang et al., 2011). It has also been shown that transmission of a null Grb10 allele results in decreased adiposity, elevated lean mass and improved glucose tolerance possibly through the Igf1 signalling and controlled insulin secretion (Mokbel et al., 2014). Interestingly, hypomethylation of the GRB10 locus has been involved in the development of both SRS and Beckwith–Wiedemann syndromes (Koren & Palladino, 2016; Scott & Moore, 2012). One other possible factor controlling a transgenerational epigenetic disease predisposition is DLK1 (also referenced as preadipocyte factor 1) (Andersen et al., 2009). It had been shown that DLK1 was highly expressed in preadipocytes, and downregulation of Dlk1 correlated with adipocyte differentiation in vitro. Another study in an animal model indicated that a regulatory mutation causing partial loss of imprinting of the Dlk1-Dio3 cluster resulted in embryonic hypothyroidism in the offspring (Charalambous & Hernandez, 2013). More specifically, the animals exhibited postnatal hypothyroidism and impaired brown tissue generation because of increased expression of Dlk1, causing obesity, glucose intolerance and hypothyroidism.

Taken together, the increasing evidence suggests that chromatin modifications, DNA methylation and imprinting hold key roles in modulating metabolism, and their dysregulation in disease can lead to devastating outcomes. Furthermore, these epigenetic drivers of metabolism can be impacted by a range of non-genetic and extracellular cues, thereby mediating transgenerational effects on metabolism.

1.2.2 Cancer

Cancer is characterised by several defined hallmarks – and it has become clear that metabolism is one of them (DeBerardinis & Chandel, 2016; Vander Heiden & DeBerardinis, 2017). An increased uptake and metabolism of glucose by cancer cells in contrast to normal cells was first described by

Warbung (Warburg et al., 1927). Another phenotype observed in tumors is high glutamine demand, since this amino acid is a main nitrogen source for the biosynthesis of many cell components necessary for fast growth which is a typical characteristic of tumors (DeBerardinis & Cheng, 2010; Eagle, 1955; Nicklin et al., 2009). Metabolic pathways are strictly regulated because of their crucial function in cells. Importantly, this is not limited to just the direct energy requirements of the cell. It has previously been shown that the cellular uptake of glucose can also be modified by extracellular stimuli and not only by the immediate bioenergetic needs of a cell (Grassian et al., 2011). Similarly, tumor tissue might depend on cell interactions and nutrient in its microenvironment to achieve proliferation and the cancer-associated accelerated growth. In line with this, it has been demonstrated that several metabolic pathways are dysregulated in cancer and can be reprogrammed to facilitate the development of tumors despite the absence of essential nutrients (Boroughs & DeBerardinis, 2015).

Moreover, the origin and the cause of tumorigenesis, the microenvironment nutrient availability and potential of metastasis, could fuel stimulation of different metabolic pathways (Boroughs & DeBerardinis, 2015). As a consequence, profiling of tumor metabolic regulation came into focus in the past years (H. Wang et al., 2016; Yuneva et al., 2012). However, a caveat of tumor classification based on metabolic profiles is the observed heterogeneity. In particular, even parts of the same tumor exhibit high metabolic heterogeneity, as demonstrated by several studies that aimed to detect metabolic changes for tumor classification (Denkert et al., 2006; T. Li & Deng, 2017; Russell et al., 2017).

Even though there are genetic and histopathological differences, tumor development appears to frequently entail the activation of a defined cluster of pathways to sustain core functions such as redox balance, catabolism and anabolism (Cantor & Sabatini, 2012). The rewired metabolism of cancer cells could be a cause or a consequence of the multiple alterations in the epigenome which is interconnected with nutrient and metabolite availability. Indeed, it has been shown by several publications that metabolic alterations impact the epigenome to provoke more cancerogenic changes (L. Cai et al., 2011; Fan et al., 2015a; Feinberg et al., 2016; Pietrocola et al., 2015; Roe et al., 2017). Moreover, the epigenome may play a role in uncoupling normal metabolic functions to support tumorigenic growth.

A large number of metabolites hold centre roles as signalling molecules in epigenetic modulation in normal cells, including S-adenosyl methionine (SAM), which is essential for DNA methyltransferases (DNMTs) and histone methyltransferases (HMTs) (Rea et al., 2000), nicotinamide adenine dinucleotide (NAD) a cofactor for class III histone deacetylases (Galdieri & Vancura, 2012), flavin adenine dinucleotide (FAD) and 2-oxoglutarate (2-OG), that modulate lysine demethylases (KDM), acetyl-CoA, that is necessary for adding acetyl groups to histones by histone acetyl transferases (HATs). Hence, metabolites are participating in the regulation of all crucial stages in forming, controlling, and removing histone epigenetic modifications.

Onset of cancer is therefore highly impacted by the dysregulation of the cellular levels of those metabolites which establish direct routes of influencing the epigenome and subsequently affect cancer development (Kaelin et al., 2013; Mehrmohamadi et al., 2016). In line with this, mutations in isocitrate dehydrogenase 1 (IDH1) and IDH2, key metabolic enzymes, have been associated with glioblastoma and acute myeloid leukaemia (Losman et al., 2013). The altered enzymatic activity caused by these mutations results in the accumulation of the metabolite R-2-hydroxyglutarate (R-2HG). Increased levels of R-2HG influence the function of dioxygenases requiring 2-oxoglutarate (2-OG) as a co-substrate. Dioxygenases hold a key role in cells and include prolyl hydroxylases, cytosine hydroxylases, and histone demethylases. High levels of R-2HG inhibit the TET DNA- and JmjC histone-demethylase families and affect gene expression partially via a modified epigenetic state, defined by unsuccessful expression of cellular differentiation programs (Dang et al., 2009; Figueroa et al., 2010). Although in this case the production of R-2HG is associated with metabolic dysregulation, its impact on cancer development appears to be not linked with but instead to an absence of differentiation.

Another set of striking examples are fumarate hydratase (FH) and succinate dehydrogenase (SDH), mutations of which have been involved in many types of cancer. The result of these mutations are the increased amounts of their products, which are both intermediates of the tricarboxylic acid (TCA) cycle (M. Xiao et al., 2012). Although these mutations reprogram the TCA cycle metabolism (comparable to the mutations in IDH1/IDH2 mentioned above) the implication of fumarate and

succinate in tumor development may be associated with vast changes in the epigenome as they likewise influence dioxygenase activity (Kaelin et al., 2013; Laukka et al., 2016).

Although gene mutations linked to cancer growth signalling pathways are currently outnumbering known changes in metabolic enzymes, growing evidence supports the significance of metabolic pathways in causing and promoting tumorigenesis. Specifically, transcription regulators, which are key pathway modulators in glycolysis, hypoxia, androgen response, and lipid metabolism, act synergistically with KDM3A in cancer progression (S. Wilson et al., 2016, 2017). Additionally, DNA enhancer methylation was a powerful predictor of cancer associated gene expression in a study of 58 cancer cell types. Importantly, two thirds of the impacted genes (upregulated and hypomethylated) had known functions in metabolic processes (Van Damme et al., 2016).

1.3 Regulation of metabolism by histone modifications

1.3.1 Functional interplay between histone PTMs and metabolism

As previously discussed, there are studies that focus on how specific epigenetic changes affect metabolism. These studies are linking mainly DNA methylation changes or PTMs on metabolic enzymes with metabolic regulation. Moreover, research has been conducted mostly from the perspective how metabolic substrates influence histone PTMs. As mentioned above (Chapter 1.2.2), the natural fluctuations of cellular levels of various metabolites can directly influence chromatin modifications and epigenetic dynamics, as reviewed recently (Reid et al., 2017). Moreover, artificial perturbations in experimental models or through pathological alterations can use the same pathways of metabolic-epigenetic interplay. Examples include the work of Cluntun et al., who have described how increased glucose has led to increased glycolysis rates and through the production of Acetyl-CoA higher acetylation levels on histones H3 and H4 (Cluntun et al., 2015). Furthermore, Mehedint and colleagues described how maternal choline deficiency affects H3K9me and CpG methylation in the fetus (Mehedint et al., 2010). Importantly, the physiological relevance of those interactions cover both normal physiology, cancer, cell differentiation and others (Chisolm & Weinmann, 2018; Reid et al., 2017).

However much less is known how PTMs affect metabolism and specifically how histone PTMs regulate metabolism. To my knowledge, no comprehensive study has been published investigating a multitude of histone PTMs and their effects on metabolic regulation. Moreover, little is known about the effects of epigenetic small molecules on metabolism. A few select studies have investigated related aspects of metabolism, looking at single histone PTMs. Cai and colleagues reported increase of H3K9ac in the kidneys of diabetic mice (M. Cai et al., 2016) and other works have investigated various acetylation sites on the genes linked with diabetic nephropathy (X. Li et al., 2016). A functional role for chromatin modifications was suggested for diabetes, where loss of PRC2 mediated H3K27me3 led to glucose intolerance and diabetic phenotype of β cell islets in animal models (T. T. H. Lu et al., 2018). Furthermore, few studies are analysing how a specific small molecule impacts metabolism, although these studies are mainly focusing on pan HDAC inhibitors with little or no specificity for particular targets. For example, HDAC inhibitor sodium butyrate is found to increase acetylation on H3/H4 and increase oxygen consumption rate in treated flies (Peleg et al., 2016). In another study, FDA approved broad-spectrum (panobinostat, vorinostat) and selective (romidepsin) HDAC inhibitors were found to disrupt Warbung effect-related gene enhancers and was associated with decreased glycolytic levels, reversing the Warburg effect (Nguyen et al., 2020). However, there was no investigation of histone PTMs induced changes (apart from controlling the inhibitors' efficacy through H3K27ac levels). Abexinostat, another HDAC inhibitor was found to alter multiple genes regarding adipocytic and osteoblactic differentiation and H3K9ac levels were quantified (Ali et al., 2016). Entinostat, another HDAC inhibitor, was found to induce lipid synthesis in HepaRG cells, however the exact mechanism of action or potentially induced histone PTMs remain unknown (Nunn et al., 2016). It is important to point out that the disease that is predominantly investigated for potential effects of epigenetic small molecules, is cancer, even though there is a great range of various other metabolic syndromes and rare diseases that could be investigated after epigenetic inhibitor treatments since there is evidence of epigenetic deregulation linked with their underlying pathogenesis (as discussed in Chapter 1.2.1).

The lack of data in this important field has impeded fundamental and clinical research regarding the role of histone PTMs in metabolism and potential exploitable drug candidates and therapies. Bringing together in a systems-view three aspects – histone modifications, metabolic states,

and the proteome – will help to increase the understanding of their interplay, and to identify key modifiers of metabolism and future druggable targets.

1.3.2 Relevance for fundamental and clinical research

Despite the lack of wide-ranging studies on histone modifications and metabolism (See Chapter 1.3.1), a clear understanding of this is especially crucial to promote clinical research in the future, in tackling metabolic diseases and syndromes with metabolic phenotypes, such as cancer, immunological and neurodegenerative diseases.

To date, 10 therapeutics have been approved by the US Federal Drug Administration (FDA). The primary targets of those drugs are epigenetic mechanisms. Even though the majority of these approved medicines were initially for cancer treatment, now a growing number of compounds that target epigenetic proteins in other diseases is in preclinical and clinical development (Buocikova et al., 2020; Meighan-Mantha, 2017; Qi et al., 2016). In particular, the HDAC inhibitor valproic acid which had initially been developed for psychiatric disorders, is now under investigation in clinical trials for various types of cancer. Even though 30 years have passed from the initiation of clinical trials involving DNMT-inhibitors and HDAC-inhibitors, only the past 5 years have seen 2nd generation epigenetic drugs advancing from preclinical to clinical trials phases. These novel drugs are more potent, more specific and can target additional protein families, such as bromodomain and extra terminal protein (BET), mutant isocitrate dehydrogenase (IDH), lysine-specific demethylase 1A (LSD1/KDM1A), histone methyltransferase (HMT) and protein arginine methyltransferase (PRMT). Additionally, a recent but promising trend in the cancer therapy landscape is combination treatments of epigenetic drugs with other molecules (Ahuja et al., 2016; Dueñas-Gonzalez et al., 2014; Raynal et al., 2017).

In addition to cancer, epigenetic inhibitors could be one of the main agents to treat other types of disease. For instance, ESR1 and ESR2 are expressed in smooth vascular muscle cells. They are also usually hypomethylated in human atherosclerosis and folic acid deficiency is indicated to hold a role in endothelial dysfunction associated with aging and cardiovascular disease (J. Kim et al., 2007; Kok et al., 2015). In regards to several neurological disorders, epigenetic alterations are involved in the nervous system's memory, plasticity and aging (Jakovcevski & Akbarian, 2012). ORY-2001 was the

first epigenetic drug that entered clinical phase I for Alzheimer's (Maes et al., 2016; Meighan-Mantha, 2017). Another neurodegenerative disease for which epigenetic treatments are considered, is Huntington's (HD). The polyglutamine repeat sequence in the huntingtin protein, which causes the disease, has been shown to inhibit HATs, resulting in a reduction of acetylation on H3 and H4 histones. Several recent studies have demonstrated that HDAC-inhibitor treatment stops effects of HD in vivo – with other molecules still under investigation to elicit similar effects (Bürli et al., 2013; Duan, 2013; Gray, 2010). Other HDACi have also recently been employed to treat diabetes (Mau & Yung, 2014).

However, it still remains unknown how epigenetic inhibitors impact the underlying specific pathomechanisms. Novel ideas have evolved such as examining metabolic checkpoint inhibitors for cancer therapy and reversal of its progression (Scharping & Delgoffe, 2016). There is cause for optimism that in the coming years it will be possible to improve the control of the bidirectional relationship among epigenetic switches and metabolism and thereby address disease development. Moreover, metabolic alterations can be identified as early warning signs of many diseases such as neurodegeneration (Kennedy et al., 2016). Therefore, it is urgent to gain more knowledge in understanding the underlying mechanisms of how epigenetic drugs affect metabolic states to be able to discover disease biomarkers, therapeutic targets and design novel therapies. My study aims therefore to provide new insights into the interplay between epigenetics and metabolism and help to elucidate novel regulatory pathways and provide resources to aid in further drug discovery endeavours.

1.5 Publications relating to this study

Parts of the work described in this thesis have been published, are in preparation or submitted status to be published in peer reviewed journals:

- **Tzika, E.;** Dreker, T.; Imhof, A. *Epigenetics and metabolism in health and disease.* **Frontiers in Genetics, 2018.** https://doi.org/10.3389/fgene.2018.00361
- **Tzika, E**., et al.: The potential of epigenetically-active small molecules in regulating metabolism - paving novel avenues for alternative treatment strategies. Research paper. *(In preparation)*
- **Tzika, E**., et al.: Optimized seahorse XF assay for metabolic profiling. Technical Note. *(In preparation)*
- Sollner, F. (…), **Tzika, E.**, et al.: Protein ADP-ribosylation Regulates Human Mitochondrial DNA Replication. *(Submitted/under review)*

Chapter 2

Materials and Methods

2.1 Materials

2.1.1 Mammalian cell lines

HEK293T wild type and knockout cell lines were a kind gift from Dr. M. Volker Albert from Prof. Dr. A. Imhof lab at the Biomedical Centre. U2OS and HEK TREX cell lines were kindly provided by Ms. F. Soellner from Prof. Dr. A. Ladurner lab at the Biomedical Centre for a collaboration project.

2.1.2 Buffers and solutions

Non-commercial buffers and solutions were prepared in-house using standard sterile techniques. Buffers and solutions were prepared with ddH_2O (18.2MΩ) and autoclaved. Chemicals used to prepare the buffers were of molecular biology grade and obtained from Sigma Aldrich and other certified laboratory supply providers.

2.1.3 Enzymes and other materials

Commercial buffers, reagents, materials, kits and enzymes not prepared in the laboratory were used according to the manufacturers' instructions. The small molecules / compounds used in this study were acquired in ≥99% (HPLC) grade from the following providers: Selleck Chemicals Llc, Cayman Chemical and Tocris Bioscience. Some of the compounds used were part of the company sponsor proprietary chemical libraries. The list of those chemical compounds is given in Table 2.1.

2.2 Mammalian cell culture techniques

2.2.1 Propagation of mammalian cell lines

HEK293T (wildtype and knockout), HEK TREX (wildtype and knockout) and U2OS (wildtype and knockout) cell lines were grown in Dulbecco's modified Eagle's medium with 4.5 g/L glucose (DMEM,PAN Biotech), respectively supplemented with 10% fetal bovine serum (FBS, from Gibco), 100 U/ml penicillin and 100 µg/ml streptomycin (Gibco, Thermo Fisher Scientific) at 37ºC in 5% CO_2. All cell lines were split regularly every three days by trypsinisation at approximately 80% confluency. All experiments were performed with early passages of the cell lines and were discarded after eight passages of splitting.

2.2.2 Storage of mammalian cell lines

To prepare frozen stocks HEK293T (wildtype and knockout) cells, $6 \cdot 10^6$ cells were resuspended in 1 ml freezing medium (80% v/v FBS, 20% DMSO). All frozen cell stocks were stored at -80°C.

Frozen cells were thawed in RT. The defrosted cells were diluted in complete DMEM, pelleted and resuspended again in complete medium with antibiotics, followed by standard propagation at 37°C.

2.3 Seahorse XF methodology

2.3.1 72h treatment protocol for HEK293T wildtype and KO cell lines

300k/well cells were seeded in DMEM in 6 well plates and a selected inhibitor (full list of concentrations used can be found in Table 2.1) was added separately in each well. Two wells were used for each inhibitor and two wells for DMSO controls. Cells were incubated for 72h at 37 ^{o}C in a CO_2 incubator. One day prior to the experiment the sensor plate was hydrated as described by the manufacturer and placed in a non CO_2 incubator. Also, the seahorse XF was turned on to heat up at 37 ^{o}C. On the day of the experiment, cells were collected, washed in DPBS and resuspended in assay medium with pH at 7.4 at 37 ^{o}C (base medium was supplemented with 2mM L-glutamine, 1mM sodium pyruvate, 10mM glucose and 5mM HEPES buffer and passed through a sterile filter) with the freshly added inhibitor or DMSO. Each cell suspension was calculated to a number of 30k cells/seahorse XF well and 6 replicates were measured for each treatment. Optimisation steps performed in this study has previously shown that 30k HEK293T cells were optimal for seahorse XF measurements on the XFe96 (as described in the Results Chapter). Cells were then incubated for 1h at 37 ^{o}C in a non CO_2 incubator. In the meantime, Mito Stress Test reagents oligomycin (10uM), FCCP (10 uM), rotenone/antimycinA (5 uM) were loaded sequentially in ports A-C for each well in the sensor plate. After the end of the 1h incubation time, the cell plate was covered carefully with the sensor plate and placed into the seahorse XF (XFe96). Temperature equilibration, sensor and fiber optics optimisation lasted 20min in an automated procedure following the manufacturer's instructions. After that step, the run was initiated and lasted 90 min. The measuring module followed a 3 min mixing and 3 min measuring intervals of

OCR and ECAR at the beginning of the experiment and between each reagent injection. At the end of the run, the raw files were exported and analysed in the WAVE software (Agilent) and exported to Excel or other formats for further bioinformatic analysis (see the relevant Methods Chapter 2.6). First normalization of readouts was carried out using live cell staining after the completion of measurements. This procedure is described in the subchapter 2.3.5.

Chemical Compound ID	Concentration used in this study
SC 00107038	10uM
SC 00105914	0.75uM
SC 00106834	0.1uM
SC 00107029	1uM
SC 00106414	1uM
SC 00106835	1uM
SC 00107032	10uM
SC 00107048	2uM
SC 00106836	10uM
SC 00107036	160nM
SC 00107022	5uM
SC 00105711	50nM
SC 00107059	1uM
SC 00107063	0.5uM
SC 00107064	10nM
SC 00107067	363nM
SC 00107062	0.1uM
SC 00107050	120nM
SC 00107054	50nM
SC 00106842	15uM
SC 00107016	1uM
SC 00107059	1uM
SC00107019	30uM
SC 00107061	1uM
SC 00107049	2uM
SC 00107065	1.4uM
SC 00107066	250nM
SC 00107058	1uM
SC 00107052	100nM
SC00107051	220nM
SC 00107053	100nM
SC 00106838	7uM
SC 00106839	1uM
SC 00106951	1uM
SC 00107069	2uM
SC 00106960	20uM
Anacardic acid	8uM
SC 00106959	30uM
SC 00106841	12uM
SC 00106840	5uM

SC00106956	0.05uM
SC 00106845	0.4mM
SC 00106827	0.3uM
SC 00106829	4uM
SC 00106947	1uM
SC 00013575	0.5uM
SC 00106935	1uM
SC 00085956	1uM
SC 00106942	1uM
SC 00106949	5uM
SC 00101300	25uM
SC 00106934	500nM
SC 00106948	1.2uM
SC 00106945	1uM
SC 00106837	10uM
SC 00085937	1uM
SC 00106955	0.5nM
SC 00106946	0.3uM
SC 00106933	30nM
SC 00106843	1uM
SC 00106958	2uM
SC 00087771	8uM
SC 00095567	1uM
BI 00062343	0.25uM
SC 00106941	0.1uM
SC 0010LEV	10uM
SC 00107030	1uM
SC 00107014	225nM
SC 00106950	10uM
SC 00107025	0.3uM
SC 00107021	20uM
SC 00107015	5uM
SC 00107028	2uM
SC 00107024	1uM
SC 00107023	200nM
SC00107033	10uM
SC 00107017	0.5uM
BI 00062344	3uM
SC 00107026	2uM
SC 00107034	1.25uM
SC 00107018	60nM
SC 00107035	300nM
SC 00107037	100nM
SC 00107027	100nM
SC 00106826	10nM
SC 00106940	20uM
SC 00106943	5uM
SC 00106832	1uM
SC 00082039	5uM
Nicotinamide	21uM
SC 00106944	9uM
SC 00106939	20uM

SC 00106828	1uM
SC 00106961	20uM
SC 00106953	100uM
SC 00106954	8.4uM
SC 00106957	0.3uM
SC 00106831	25uM
SC 00106952	30uM
SC 00106833	5uM

Table 2.1.: List of small molecules / inhibitors employed in this study.

2.3.2 1h treatment direct injection protocol for HEK293T wildtype and KO cell lines

For the 1h protocol, cells were seeded in a concentration of 30k/SeahorseXF well in assay medium and incubated as described for the 72h treatment protocol. Each tested inhibitor was added in a concentration of 10x of the amounts described in Table 2.2 in port A of each well and other Mito Stress Test reagents were added sequentially in ports B-D at concentrations previously described. After the 1h incubation of the cells the sensor plate was placed on top of the cell plate. The combined plates were then placed in the XFe96 and after a 20 min equilibration the experiment measurements started by first injecting the inhibitors or control (DMSO) in the cells. OCR and ECAR were monitored for one hour and then the mito stress test was performed by injecting sequentially Oligomycin, FCCP and rotenone/antimycinA. The full run lasted 150 min. All other following steps were performed as previously described.

2.3.3 XF cell mito stress test analysis for HEK TREX and U2OS cell lines

HEK TREX and U2OS cell lines were firstly tested using the seahorse XF technology in different seeding numbers to determine the optimal cell numbers for the seahorse XF assay. After this optimisation step, cells were seeded at densities of 60,000 and 40,000 respectively into a XF96 cell culture microplate and on the day of the assay incubated for one hour in (180 ul/well) Mito Stress Test assay medium at 37°C in a CO_2 free incubator for 1h. The assay medium was buffered at pH 7.4 at 37°C. The medium contained 2 mM L-glutamine, 1mM sodium pyruvate, 10 mM glucose and 5mM HEPES buffer.

The oxygen consumption rate (OCR) and extracellular acidification rate (ECAR) were measured in a XF96 extracellular flux analyzer (Agilent Technologies). Three basal measurements were performed and then H_2O_2 was injected in port A of separate wells in final well concentrations of 0.1 mM, 0.5 mM and 1 mM (where indicated) and measured for 1h. Then continued with sequential injections of 10 uM oligomycin A (port B), 10 uM FCCP (port C), and 5 uM rotenone/antimycin A (port D) in each well of the plate. The concentrations of the above known electron transport chain (ETC) inhibitors are the ones used for port injections in the seahorse XF96 sensor plate. Three measurements were performed after the addition of each ETC inhibitor to determine the ATP turnover, the spare respiratory capacity and the non mitochondrial respiration effects. Live cell count was performed at the end of the assay to normalise the seahorse XF assay readouts (see next paragraph).

2.3.4 Protein concentration normalization

After the end of the seahorse XF assay 150 ul of seahorse XF assay medium were removed from each well and 50 ul of lysis buffer (RIPA buffer and 100x protein inhibitors; in 5ml RIPA buffer add 50 ul 100x protein inhibitors) was added to the remaining 50 ul of assay medium and cells in each well plate. Then an incubation step followed at 4 ˚C for 5 min while shaking. The plate was stored at -20 ˚C if it was to be processed later. Protein concentration of mammalian whole cell extracts was determined according to the BCA method using Sigma Aldrich's QuantiPro BCA assay kit, following the manufacturer's instructions. The appropriate sample buffer was used as blank control. A standard curve based on at least six BSA standards of known concentrations was used to calculate the protein concentration of the samples based on their absorbance at 562nM. For each sample, 6 measurements were performed.

2.3.5 Live cell normalization

After the end of the seahorse XF assay well volumes were brought to 200 ul (from 247ul). Calcein AM reagent was prepared by adding 12 ul of DMSO (vortex and spin down) and diluted with 1800 ul cold PBS (vortex and spin down).The tube was always covered with aluminium foil. The whole procedure of preparing the calcein AM reagent and addition to plate wells was done under minimum light. 25 ul of calcein AM mix with PBS was added at 4 uM final concentration in each well, covered

with plate lid, aluminium foil and briefly and gently shaken on the bench. Incubation for 30 min in 37 ˚C followed. A specific file was set up and optimised for a Tecan Ultra plate reader for the seahorse XF plates including all parameters for the specifications of this plate. The plate reader was always turned on at least 10 min before the plate readout and set to 30 ˚C. Fluorescence mode was selected and wavelengths at 485 nm excitation and 535 nm emission. Z position (~11551 uM) and manual gain (28-32) were determined separately in every experiment and 10 flashes option was mostly used. Mirror selection was set at dichroic 2. After the plate readout staining evaluation and qualitative cell viability (cell equal distribution on well) under UV light was performed. The staining and analysis of the normalisation results was performed in replicated for each sample. Two blank measurement values were deducted from the other sample values and then these results were applied as normalisation step on the WAVE (Agilent) software that was used for the seahorse XF assay analysis.

2.4 Histones extraction and sample preparation

2.4.1 Histones extraction

After HEK293T cells were treated in triplicates with selected inhibitors (3 technical replicates x 30 selected inhibitors and DMSO controls) for 72h in 6 well plates at concentrations as noted on Table 2.1, cells were trypsinised and suspensions were placed in 15 ml falcon tubes. Cells were collected by centrifugation at 300 g for 5 min at 4˚C, washed and resuspended in 5ml DPBS. Another centrifugation step followed at 300 g for 5 min at 4˚C, supernatant was removed and pellets were resuspended in 1.8 ml DPBS and placed into labelled Eppendorf tubes. Cells were collected by centrifugation, supernatant was removed and cells were frozen at -80˚C. After collection of all samples at the company labs, the protein extraction steps and histones preparation for mass spectrometry analysis was done following the protocol provided by Dr Ignasi Forne at the ZFP facility in the Biomedical Centre. Essentially, cell pellets were left on the bench for 3 min and 200 ul of H_2SO_4 (~100-200 ul/10^6 cells) was added in all samples and brief vortexing for 30 sec followed to break the pellets. The Bioruptor was used until all pellets were completely dissolved (10x30 sec ON, 10x30 sec OFF). Samples were then placed in the cold room, 4˚C, rotating on a bench wheel overnight. After overnight

cell suspensions were centrifuged (30 min, 4°C, 20800 g) to separate the extracted histones (supernatant) from cell debris and other proteins (pellet). Simultaneously, another centrifuge was set up at 4°C. Under the fume hood, supernatants were transferred (~200 ul) to new labelled tubes. Next, if sample concentration was not previously measured to be 300 uM = 10^6 HEK293T cells, all concentrations were measured and adjusted to same concentrations using BCA assay as previously described. 300 uM of protein is the required protein concentration starting material amount for the histone sample analysis protocol procedure that was provided by the facility. Proteins were precipitated adding H_2SO_4 and TCA: TCA was added in the supernatants of all samples (TCA volume= supernatant volume x 26/74). Samples were inverted once and placed in 4°C for 2h. Cell precipitates were placed at -80°C further analysis. Also, the amounts of samples that were not used in the current experiment were stored in separate tubes as back up samples for future experiments at -80°C. After the 2h incubation time, samples were centrifuged at 4°C in the cold room for 30 min at 20800 g. Samples were then placed on ice and the supernatant was discarded. The histone pellets (haze) lied on the side walls of the tubes or sometimes was not obvious and it was scattered around the tube walls. This step was followed by 4 wash steps of the histone hazes with 500ul ice cold acetone (kept at -20°C) followed by centrifugation at 4°C for 15min at 20800 g. Special care was taken to keep the labelling on the tubes and to not be removed from the acetone washes. Also, when acetone was removed around 20 ul was left in the tube in order to not disturb the histone pellets. The pipet tip had to not touch the tube walls or the bottom of the tube as the histone haze turned transparent and it was prone to sample loss if the handling was not delicate. The histone pellets-hazes were then air dried for 15 min under the fume hood. Dried histone pellets were resuspended with 14 ul HPLC water (histone pellets were often on the side of the tubes and around the walls up to the tube height of 500 ul). Then, 4 ul of Laemmli and 2 ul DTT were added in final sample volumes as in the table below:

Ingredient	**Concentration**	**Volume**
DTT (1M in 100uM TRIS)	10% (100mM) of final volume	2ul
Laemli 5x	1x	4ul
HPLC H_2O	n/a	14ul
Final volume		20ul

After brief resuspension to bring histone pellets into solution, a quick spin down followed (nano centrifuge up to 2000 rpm). If colour changed to orange yellow, pH was adjusted by adding 1 ul of 2M TRIS. Samples were frozen at -20^{o}C until loading into polyacrylamide gels.

2.4.2 SDS polyacrylamide gel electrophoresis and trypsinisation

Histone proteins were separated according to their molecular weight using SDS-PAGE. Pre-cast 8%-16% 10-12 sample Tris-Glycine gels were used. Proteins were denatured by heating at 95^{o}C for 5 min. After 1 min incubation on bench a brief centrifugation step followed to collect the sample at the bottom of the tube. 10 ul of each histone sample was loaded in each well and 4 ul of a protein marker was used in every run. The gels were run at 80 V for 20 min and then at 160 V for 1 h in running buffer (900 ml H_2O + 100 ml 10x running buffer) prepared in house. After the end of the run, gels were cracked open from the cassette following the manufacturer's method and place in 10 cm plastic dishes with lids and washed 2x with H_2O. Next, 20-30 min staining step with Coomassie (prepared in house) followed and then a destaining step (buffer prepared in house) of the gels for 30-40 min. Gels were then placed under the hood to carefully extract the histone gel bands from each sample. A razor was used to cut between 11.5 kDa and 17 kDa of the marker bands respectively for each sample which corresponds to the range of size of the histones H1H2, H3, H4. For this, gels were placed on a glass lighted surface with small amount of HPLC water and gel bands were carefully cut in small pieces and placed in tubes with HPLC water respectively for each sample. Razor and glass surface was cleaned with ethanol after extraction of each sample histone bands. The same procedure was followed until the collection of all 98 samples. After removal of the containing HPLC H_2O another 200 ul of HPLC H_2O was added to the samples and gel pieces were incubated for 1min in RT (gel pieces were covered with H_2O). Then H_2O was removed and 2x destaining steps followed. 200 ul of destaining solution (50% ACN/50 mM NH_4HCO_3) was added and samples were placed for 30 min at 37^{o}C (shaking). This procedure of destaining was repeated until gel bands were fully destained. After the last destaining step and removal of the destaining solution, (2x) 200 ul of H_2O was added at the samples for 5 min in RT (no shaking) and then removed. (2x) addition of 200 ul 100% ACN followed for 5 min in RT (no shaking) and then removed. The gel pieces turned white and all remaining ACN was removed by

spinning down the samples. 20 ul of 100% propionic anhydrite/acetic anhydrite was added to the gel pieces (1:10 of final volume, in the current protocol final volume was 200 ul) and another 40 ul of 100 mM NH_4HCO_3. Lids had to be pressed closed for 30 sec because of the CO_2 production of the reaction. Then another 140 ul of 1 M NH_4HCO_3 and lids had to be pressed closed for 2 min. Then lids were opened to release the CO_2. pH was confirmed to be acidic or up to 7. If pH was not within the acidic range, 1M of ambic was added (~10 ul each time after checking the pH). The solution from previous steps was placed in shaking conditions for 45 min at 37ºC. After the incubation time ended, wash steps followed; 5x: 200 ul, 100 mM NH_4HCO_3, 5 min, (no shaking) RT, and solution was removed every time before starting the new step. Then another 5x wash steps with H_2O (200ul H_2O, no shaking, 5 min RT, solution was removed in between). Finally, 3x steps with 200 ul 100% ACN followed (no shaking, 5 min, RT, solution was removed every time before starting the new step). The whole amount of ACN was removed by a brief spin down to collect it and pipet it of the tube.

A mix of acylated SpikeTides (JPT Innovative Peptide Solutions, provided by BMC Mass Spec facility) were used in concentrations of 3 ul, 5 ul and 10 ul for 25 ng/ul histones concentration sample to determine which is a suitable concentration for detection using an Orbitrap LTQ and a Q Exactive.

An amount of 3 ul spike tides mix was selected to be used in each sample as below while working on ice for the trypsinisation step:

Reagent	**Sample**
Spike tides (master mix)	3 ul
Trypsin (100 ng/ul in 100 mM NH_4HCO_3)	(25 ng/ul in 100 mM NH_4HCO_3) 27.5 ul
100Mm NH_4HCO_3	79.5 ul
Final volume	110 ul

An incubation step of 20 min on ice followed. 120 ul of 50 mM Ambic was added to fully cover the gel pieces and then they were incubated overnight at 37 ºC (shaking).

2.3.3 Histone peptide extraction

At this step, peptides were extracted from the gel pieces. 100 ul of 50 mM ambic was added to cover them and gel pieces were incubated for 10 min in RT. Then, a sonication step followed for 3 min. The supernatant was transferred to low binding tubes (SN1) and another 100 ul of solution (50% ACN/0.1% TFA) was added to the gel pieces. Then, a sonication step followed for 3 min, incubation for 10min in RT, spin down and supernatant (SN2) was transferred in the low binding tube. The last step was repeated once more and the supernatant was transferred. 2X steps of adding 70 ul – 100 ul, 100% ACN to the gel pieces followed and then gel pieces were sonicated for 3 min, incubated for 10 min in RT, spined down) and the supernatant was transferred to the low binding tube (SN3 to SN2+ SN1). Samples were then placed balanced to evaporate in the Speedvac at 30ºC. Evaporation of around 350 ul of sample volume was usually observed to last about 5h.

2.4.4 Mass spec histone sample preparation

C18 Purification

Desalting of samples was performed using C18 tips. Samples were prepared for loading on the C18 by being resuspended in 30 ul 0.1% TFA and an addition of 5 ul 1% TFA. pH was checked to be between pH 2 and pH3. C18 tips were prepared for binding of the peptides following manufacturer's procedures by using 20 ul MetOH (conditioning and cleaning of the cartridge) and centrifuged at 1000 g for 1 min. Then, addition of 20 ul 0.1% TFA/80% ACN (wetting of cartridge) followed and tips were centrifuged at 1000 g for 1 min. 20 ul of 0.1% TFA (equilibration) was added with care to not fully dry the cartridge after the short centrifugation step (1000 g for 1 min). The cartridges were placed in new tubes to collect the samples. Samples were loaded on the cartridges (2 x 20 ul) and spun down at 1000 g for 1 min. Then samples were (2x) reloaded and spun down at 1000 g for 1 min. The samples were loaded 3 times in total and were bound on the C18 cartridges. The flow through was stored (FT) for later analysis steps with carbon tips. 2x wash steps (20 ul 0.1% TFA) followed and then cartridges were placed in new low binding tubes. 3X elution steps and brief centrifugation (10UL 0.25% TFA/ 80%ACN, 1000g for 1min) followed (EL1) and samples were stored at -20ºC.

Carbon tips

The more hydrophilic and smaller peptides are not efficiently bound on the C18 cartridges and to increase the turnover carbon tips were used on the initial flow through from the C18 tips. Carbon tip beds were prepared by three (10 ul 100%ACN) wetting steps (30 sec, 1000 rpm) and 3x (10 ul 0.1%TFA) equilibration (30 sec, 1000 rpm) steps. Then, carbon tips were placed in new low binding tubes and the sample was loaded 3x-5x (FT from C18). Then, 5x (10 ul 0.1%TFA) wash steps followed and carbon tips were placed in new tubes. The samples were then bound on the carbon tips. Finally, 3x 15 ul (70% ACN/0.1% TFA) elution (EL2) steps followed. The 45 ul volume of samples was reloaded once more on the tips. EL1 and EL2 were combined and briefly centrifuged for 10 sec. The samples were then placed in Speedvac for evaporation and stored at -20^{o}C. Prior to mass spectrometry runs samples were resuspended in 12 ul 0.1%TFA and were then given to the BMC mass spec facility. The samples were injected into a nano LC-MS/MS Q Exactive for analysis following the facility standard procedures. Raw files were imported into Skyline. A peptide library for Skyline was provided by the Mass Spec facility. This library was used to identify peptide peaks based on mapped mass and retention times in the individual control and drug-treated samples, followed by manual review to ensure peaks were properly called by the Software. Peptide abundance was quantified following the procedure as described before (Feller et al., 2015). The effect of drug treatments was then calculated and depicted as log2-ratio of intensities in drug-treated samples versus control (DMSO)-treated samples.

2.5 Whole proteome analysis

2.5.1 Mass spectrometry whole proteome sample preparation

72h drug-treated cell samples and vehicle controls were separately washed 1x in PBS, briefly treated with trypsin to achieve singe cell status and after half a minute DMEM used to culture HEK293T was added to inactivate the trypsin. Cells were then pelleted (4 min, 1000 rpm) and washed sequentially 3x in ice cold PBS with centrifugation in between and removal of PBS. The cell pellets

were snap frozen in liquid nitrogen were shipped to DC Biosciences in dry ice for protein extraction and further analysis steps.

2.5.2 Sample processing

Upon reception, proteins were extracted and cell lysates were subjected to protein quantitation. Each sample was brought to ~100 µg of protein, which was estimated that corresponds to $0.33*10^6$ cells. After adjustment of protein concentration, samples were trypsin digested, reduced and alkylated and then labelled with TMT-11plex following the instructions of the manufacturer (ThermoFisher Scientific). Each set of TMT constituted of 10 drug-treated samples and one control from one replicate), which were combined and cleaned-up (total: 3 TMT-11plex-labelled samples per replicate). Each sample was fractionated by high pH reversed phase chromatography into 4 fractions. Final peptide samples were analysed by LC-MS/MS/MS on a Fusion Tribrid Orbitrap instrument using a data dependent, MultiNotch MS3 acquisition method at the proteomic facility of the School of Life Sciences, University of Dundee (DC Biosciences). The raw spectra file output was analysed in MaxQuant against a human proteome database as described (Tyanova et al., 2015) with quantification carried out on MS3 level. Protein IDs with quantification were exported for further analyses in Excel or using R Bioconductor environment. All data from the proteomic dataset are represented as log2 fold-change of intensities in drug-treated vs DMSO (control)-treated samples.

2.6 Statistical analyses

2.6.1 Statistics

Unless otherwise stated, the figures present the average values of at least three independent biological experiments +/- SEM or Standard Deviation, as described in the figure legends and Results. Asterisks (*) indicate statistical significance (* $p<0.05$; ** $p<0.01$; *** $p<0.001$), based on unpaired,

two-tailed distribution Student's t test. Correlations were calculated using Pearson's correlation coefficient (r).

2.6.2 Seahorse XF analysis

All Seahorse XF experiments were normalized to the number of living cells using the Live Cell counting method (as described above). For each well, the OCR (oxygen consumption rate, in pmol/min) and ECAR (extracellular acidification rate, in pmol/min) data from the Seahorse XF were divided by the RFU (relative fluorescence units) as determined by the Live Cell staining after the assay. These normalized metabolic readout data (in pmol/min/RFU) were then used as the basis for further analyses. First, the measurement intervals for defined metabolic states were defined (the time points indicate representative timepoints from a specific experiment):

72h experiment				
Phase	**First measurement**	*(min)*	**Last measurement**	*(min)*
Start of exp		*0*		
Drug or DMSO incubated*	1	*1.35*	3	*14.83*
Oligomycin injected	4	*21.75*	6	*35.18*
FCCP injected	7	*42.17*	9	*55.60*
ROT/ANT injected	10	*62.53*	12	*75.98*

*As cells were pre-incubated in Drug or DMSO prior to the experiment, the first measurement cycle already includes the effect of the drug.

1h experiment				
Phase	**First measurement**	*(min)*	**Last measurement**	*(min)*
Start of exp		*0*		
Baseline prior to injection	1	*1.35*	3	*14.82*
Drug or DMSO injected	4	*21.75*	13	*82.27*
Oligomycin injected	14	*89.22*	16	*102.68*
FCCP injected	17	*109.67*	19	*123.15*
ROT/ANT injected	20	*130.13*	22	*143.63*

Based on these measurement cycles, the following metabolic states were defined:

- **Basal metabolic rate**: average of the normalized metabolic rates of the first three measurements. For the 72h experiments, the effect of drug treatments on the basal rate was calculated by comparing the fold-change of this basal metabolic rate in drug-treated samples versus control (DMSO)-treated samples. For the 1h experiments, the drug effect was calculated

by subtracting the baseline rate (average of first three measurements) from the average of three measurements 11,12 and 13 (i.e. 1h after drug injection).

- **Maximal respiration**: maximal respiration in the Mito Stress Test is defined as the metabolic rate after treatment of cells with Oligomycin and FCCP, corrected for the non-mitochondrial respiration (measurable as remaining metabolic rate after treatment with ROT/ANT). In these experiments, maximal respiration was therefore calculated by taking the average of the three measurements after FCCP injection (measurements 7,8, 20, 9 for 72h experiments, measurements 17, 18, 19 for 1h experiments) and subtracting the average of three measurements after ROT/ANT injection (measurements 10, 11, 12 for 72h experiments, measurements 20, 21, 22 for 1h experiments).

For each compound, six technical replicates were prepared and measured on each Seahorse XF multi-well plate. These six technical replicates were averaged and the averages used for further calculation. To allow comparison of experiments carried out on different dates and across different treatments, each plate contained (at least) two DMSO controls constituted of six technical replicates. All metabolic values were normalized to the average basal rate of this (or the average of several) DMSO control(s). Effects of drug treatments in comparison to DMSO control were calculated and represented as fold-change (for initial metabolic analyses) or log2 fold change (for all analyses where seahorse XF, proteomic and histone PTM data are compiled).

2.6.3 Bioinformatic analyses of metabolic, proteomic and histone PTM data

In addition to the fundamental analyses and graphs outlined above, advanced analyses and representations were prepared in R (Version 4.0.0 “Arbor Day” using the R Studio (Version 1.3.959) with various packages as described below, including the Bioconductor environment (Version 3.12.0), in part with bioinformatics support and collaboration. As first step to perform unbiased data clustering and generate heatmaps, the ideal number of clusters was determined. For this, the fviz_nbclust() function from package factoextra (Version 1.0.7) was applied to the log2-transformed data of all three datasets, using the gap statistics method. For the following clustering and heatmap generation the ComplexHeatmap package for Bioconductor was employed (Version 2.6.2), using the Euclidian

distance method as clustering algorithm. To elucidate enrichment of biological pathways in different drug-treated samples, the STRINGdb package was used (Version 2.2.0). Enrichment p values were calculated using hypergeometric testing. The number of significantly differentially expressed proteins was compared to the number of proteins within a term of the ontology (biological process terms) and the total number of proteins in the background. In this analysis, only the proteins detected in the experiment were used as background (instead of the whole proteome as an alternative) as this gives more accurate results. Benjamini-Hochberg (BH) multiple testing correction was also applied to the p-values.

In order to identify common themes and correlations across the three different datasets, multivariate linear modelling was employed using the linear modelling function lm() from package stats (Version 3.6.2) in R. In particular, four separate regression models were made: 1) Basal OXPHOS 72h versus all acetylated histone PTMs; 2) Maximum OXPHOS 72h vs all acetylated histone PTMs; 3) Basal Glycolysis 72h versus all methylated histone PTMs; 4) Maximum Glycolysis 72h vs all methylated histone PTMs. In each model, linear regression was carried out with the metabolic values as x-values and histone PTM levels for each analyzed histone peptide as y-values across the 30 treatments.

Principal Component Analysis (PCA) was employed to identify clusters and underlying correlations in the datasets. PCA was carried out in R Studio using the prcomp() function of the PCA tools package in Bioconductor (Version 2.2.0) with the settings center = TRUE and scale = TRUE. Based on the output of the PCA, six different types of graphs were generated. The correlation matrix was generated using the corrplot() package (Version 0.8.4) based on the PCA output of cos2 values – depicting how much of the variability of a given observation (e.g. histone mark) was represented by a given principal component of the PCA (Dim1, Dim2, ...). The quality of representation based on cos2 was depicted using the fviz_cos2() function from the package factoextra (Version 1.0.7) with choice = var for the 4 most important principal components (Dim1, Dim2, Dim3, Dim4). The "Scree" plot, which explains how much of the observed variance in a data set is explained by a given principal component, was made using fviz_eig() from the package factoextra (Version 1.0.7). To depict the distribution of "PCA Individuals" (i.e. drug treatment samples) and identify possible similar groupings

across Principal Components, and to depict distribution of "PCA Variables" (i.e. histone modifications, or metabolic readouts) and their groupings, fviz_pca_ind() and fviz_pca_var() were used, respectively, with the coloring representing the quality of representation per dimension for Individuals (cos2), or contribution (contrib), for Variables, again from the package factoextra (Version 1.0.7). "Biplots" were generated using fviz_pca_biplot() from the package factoextra (Version 1.0.7)

The employed Pearson multivariate correlation was carried out to identify and visualize correlations and anticorrelations across all three different data sets. For this, the data sets were consolidated so that the 30 different drug treatments constituted the rows, while the metabolic readouts (72h base, 72 max, 1h base, 1h max), histone PTMs (e.g. H3K927me3), and individual protein levels (e.g. RPS9) constituted 5096 columns (in excel). Pearson correlations were computed using the correlate() package (Version 0.8.4) in R across different subsets of the consolidated data set - for example comparing the four metabolic states against protein levels. The resulting correlation matrices were plotted using the corrplot() package, with coloring indicating the degree of correlation (Pearson's r), with r close to 1 indicating a high positive correlation and r close to -1 indicating a high negative (anti-) correlation. Thresholds of correlations that were depicted or not depicted are described in the figure legends and the text.

Chapter 3

Results

3.1 Aim of this study

The aim of this project was to investigate and characterize the interplay between epigenetics and metabolism. For this, the effects of small molecule-induced changes of histone post-translational modifications (PTM) on levels of cellular proteins and cellular metabolism were measured. Clarifying the link between the induced and characterized PTM patterns, protein expression levels and metabolic pathway regulation will help finding strategies to interfere with pathologic or dysregulated metabolic states (e.g. in tumor cells or adipocytes) by epigenetic modulation. The first step to achieve this goal was to identify and optimize an appropriate metabolic assay. Literature review and existing usage within the research network led to the selection of the seahorse XF assay. However, significant optimisations were required to make the assay fit for the project purposes and to be able to screen 100 epigenetic compounds for induced cellular metabolic changes. Subsequently, histone PTM changes induced by the treatment with selected small molecules were investigated by a quantitative histone-targeted mass spectrometric approach. This was followed by a whole proteome analysis to investigate protein changes induced by those epigenetically active compounds. Finally, novel findings between histone PTMs and induced protein changes and metabolic effects were evaluated using unbiased statistical methods and interpreted in light of the relevant literature. The final aim of this work was that its results could be used as the groundwork for exploration of potential new treatments for metabolic disorders and other diseases with aberrant metabolism, including cancer.

3.2 Establishment of the seahorse XF assay

3.2.1 Challenges of existent seahorse XF assay

The seahorse XF metabolic assay as used historically before and as described in literature (Muller et al., 2019; Swain et al., n.d.) proved to be challenging to use. Most problems were stemming from very low reproducibility of experimental results, which made statistical analysis impossible to perform. The factors that caused low reproducibility were the unequal cell distribution across the assay wells' surfaces, unequal and generally very low cell adherence and finally the normalisation method

used as the final assay step to calculate an accurate cell number per well. For each of these issues, solutions were identified and the assay was optimised accordingly to upgrade the seahorse XF assay.

3.2.2 Optimised vs commonly used seahorse XF protocol

In initial measurements, technical replicates usually presented with a large variation of oxygen consumption rate (OCR) in time course measuring basal respiration over a period of one hour (variation of ca. 16% in an example experiment as depicted in Fig 3.1A). After applying the commonly used normalization method based on measuring protein concentration (BCA assay after end of the experiment), the technical variation increased dramatically (to 36% in the representative example experiment depicted in Fig 3.1B). The protein concentration normalisation method itself usually presented large and consistently over 30% variation amongst the three technical replicates (43% in the presented example), likely caused by the small number of cells per well that had to be used in the protein measurement assay. After the optimisation of the protocol as described under the methods chapter 2.3, technical replicates presented on average not more than 15% OCR variation for basal respiration (12% in the example experiment shown in Fig 3.1C). Importantly, after application of the new and optimized normalisation method of fluorescence-based live cell number counting, the variation between technical replicates dropped to 5% (Fig 3.1D). After the optimisation of the seahorse XF protocol, problems regarding cell distribution and attachment (Fig 3.2A, B) were resolved (Fig 3.2C, D).

3.3 Metabolic screening

3.3.1 Seahorse XF assay experimental approach types: 72h assay and 1h assay

To realise the metabolic profiling of small molecules, two different assays were established and implemented. As fully capturing significant downstream effects of drug treatments on protein level and metabolic phenotype would rely on allowing histone PTM changes to take effect, followed by altered gene expression and further downstream changes in protein levels, a 72h incubation with drugs was used. Equally important, a shorter, 1h, real-time measurement of the drugs' impact on metabolism was employed to gather insights on potential effects that are not mediated by histone PTM changes but

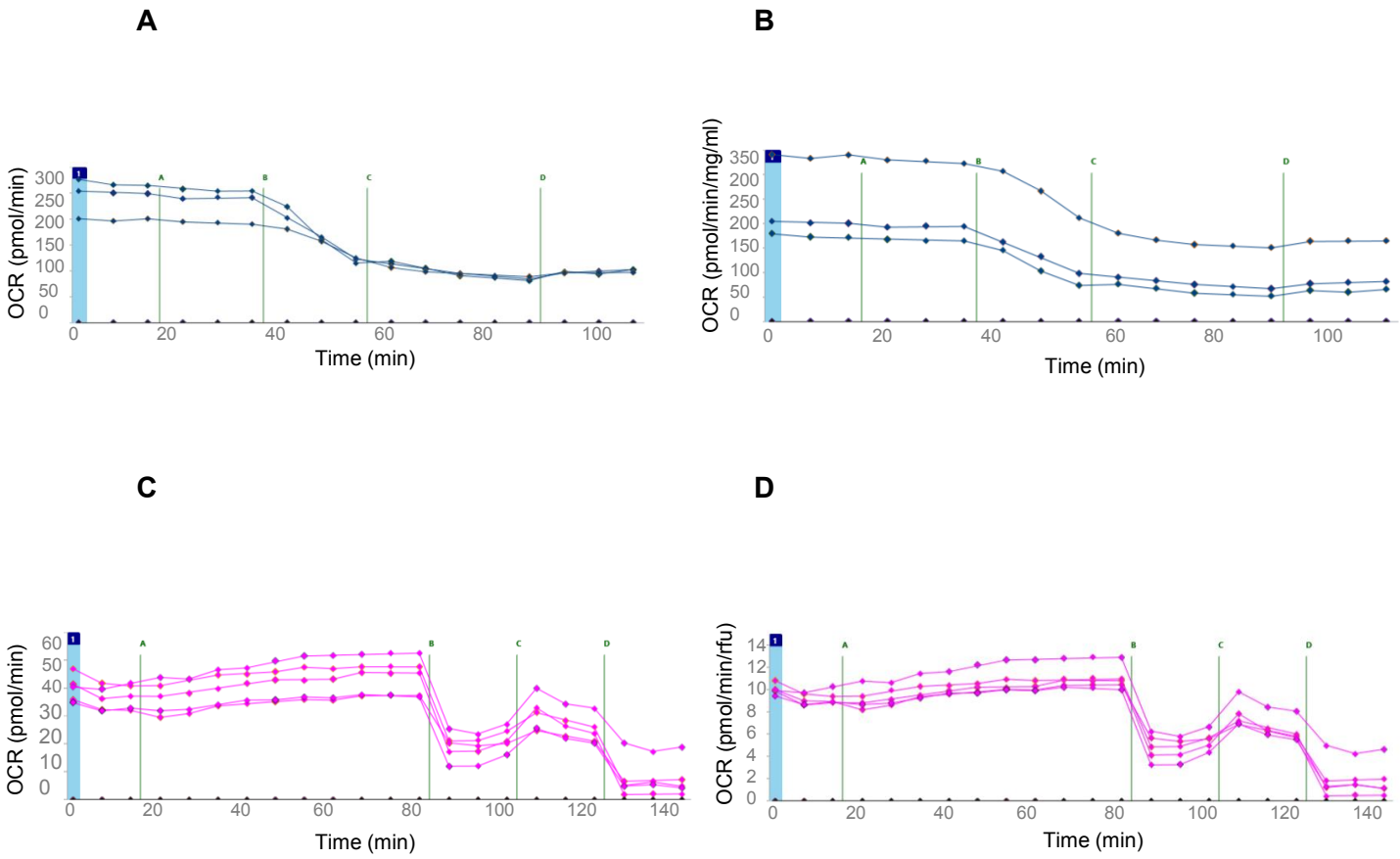

Figure 3.1. Optimization of seahorse XF assay led to more reliable experimentation and significantly reduced variation between technical replicates (more than 30% on average).

For the comparison, basal respiration rates of HEK293T cells are measured. The y-axis represents OCR (pmol/min) and x-axis represents time (min). Depending on the normalisation method applied the y-axis represents OCR ([pmol/min]/[mg/ml]) for the protein concentration and OCR ([pmol/min]/RFU) for the live cell number counting normalisation.

A. Results obtained with the commonly-used seahorse XF protocol before normalization. Three technical replicates are shown with relative standard deviation of 16%.

B. Results obtained with the commonly-used seahorse XF protocol after applying BCA-based normalization method. Three technical replicates are shown with 36% relative standard deviation. The BCA values between the three technical replicates had 43% relative standard deviation despite similar cell numbers as determined by counting.

C. Results obtained with the optimized seahorse XF protocol. Five technical replicates are shown with relative standard deviation of 12%.

D. Results obtained with the optimized seahorse XF protocol after applying the normalization method of live cell counting. The relative standard deviation of live cell numbers between technical replicates was 6%. The values of the five technical replicates after applying the normalization method showed a relative standard deviation of 5%.

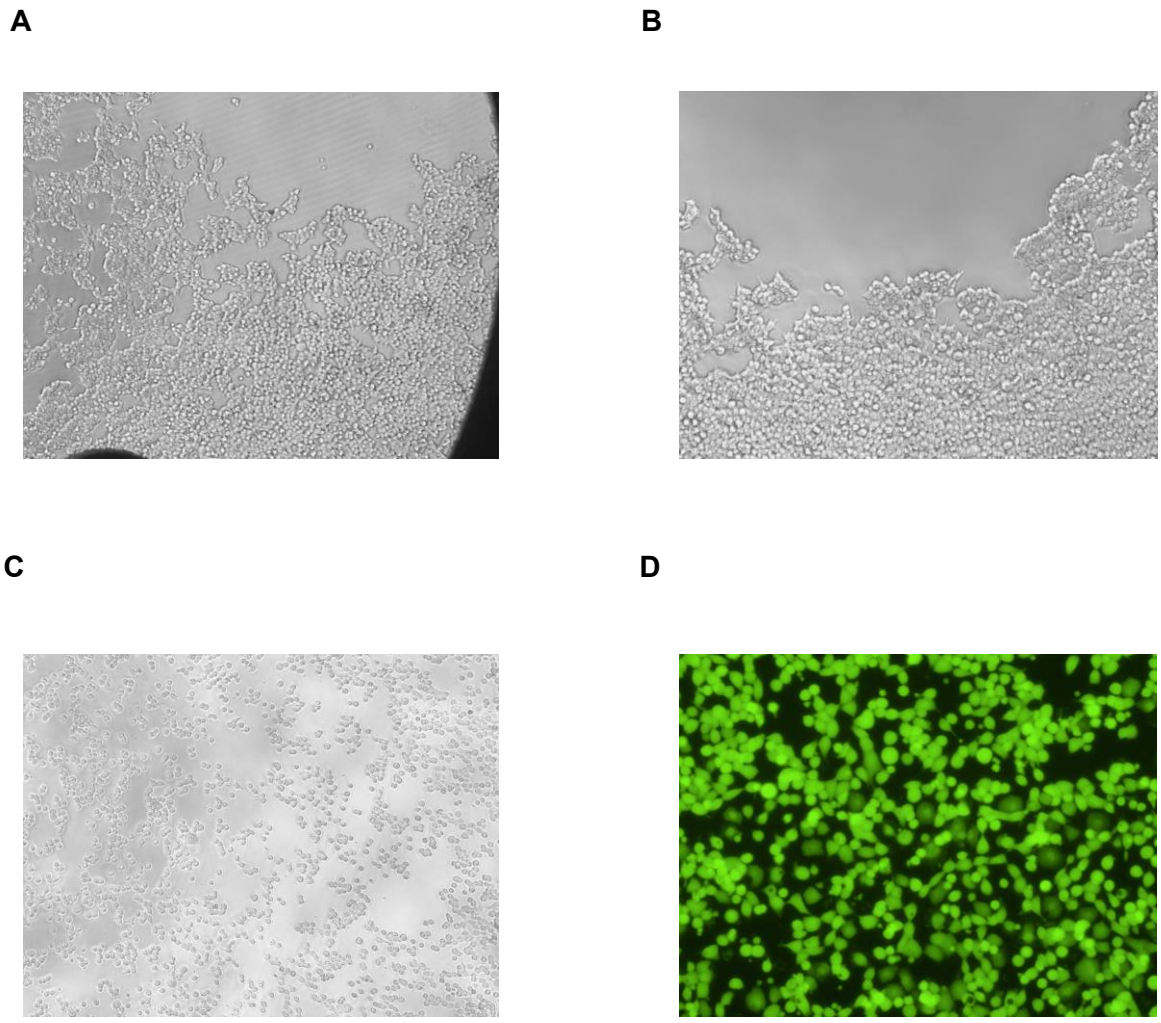

Figure 3.2. The optimised seahorse XF protocol resolved multiple assay issues and reduced experimental variation.

A. Light microscopic image of HEK293T cells obtained before the assay using the commonly-used seahorse XF protocol. Cells showed "edge effect", non-equal distribution, and clusters within the population.

B. Light microscopic image of HEK293T cells obtained after the assay using the commonly-used seahorse XF protocol. Cells commonly detached, making normalization challenging.

C. Light microscopic image of HEK293T cells obtained before the assay using the optimized seahorse XF protocol. The optimized protocol achieved equal single cell distribution, resolution of the edge effect, and equal cell attachment.

D. Fluorescence microscopy image of HEK293T cells after performing the optimized protocol. Cells were equally distributed across the well bed.

direct interactions of the small molecules with metabolic processes. This was intended to identify fast-acting drugs but also serve as a control to allow selection of drugs that predominantly exert their metabolic effects via epigenetic mechanisms including alterations of protein expression patterns rather than direct modification of the activity of metabolic enzymes.

For the first type of experiments (Fig 3.3A), HEK293T cells were treated with inhibitors for 72h and then counted and placed in the seahorse XF plate with seahorse XF medium with the respective drug. Afterwards, they were placed in the seahorse XF instrument for the mitochondrial stress test. After the performance of the assay, results were normalized using cell density as measured with the live cell number fluorescence counting approach. The other type of experimental set up involved seeding of HEK293T in the seahorse XF plate in assay medium and injection of epigenetic inhibitors directly during the assay in the instrument where measurements were performed for 1h (Fig 3.3B). This essentially allowed a real-time tracking of the metabolic response of live cells to the small molecules. After 1h of measurements, the mitochondrial stress test was performed. After the completion of the assay cells were normalised to live cell number as described in Materials and Methods (Chapter 2.3.5 and 2.6.2).

3.3.2 Typical readouts of the seahorse XF assay

During the performance of the seahorse XF assay, measurements of both oxygen consumption and extracellular acidification rates can be monitored simultaneously. For the current project, mitochondrial stress tests were performed for the metabolic screening. During the mitochondrial stress test, multiple parameters can be obtained in one assay to assess mitochondrial function and oxygen consumption rate (OCR) including basal respiration, ATP production linked respiration, maximal respiration, proton leak and nonmitochondrial respiration (Fig 3.4). At the same time, the rate of glycolysis can be measured in the form of extracellular acidification rate (ECAR). Each of the 100 screening experiments followed this aforementioned approach and provided deep underlying data traces. The following comparative and integrating statistical analyses relied on four key metabolic parameters: basal (resting) OCR, basal ECAR, maximum (“stressed”) OCR and maximum ECAR. The calculation of those parameters is described in Materials and Methods Chapter 2.6.2.

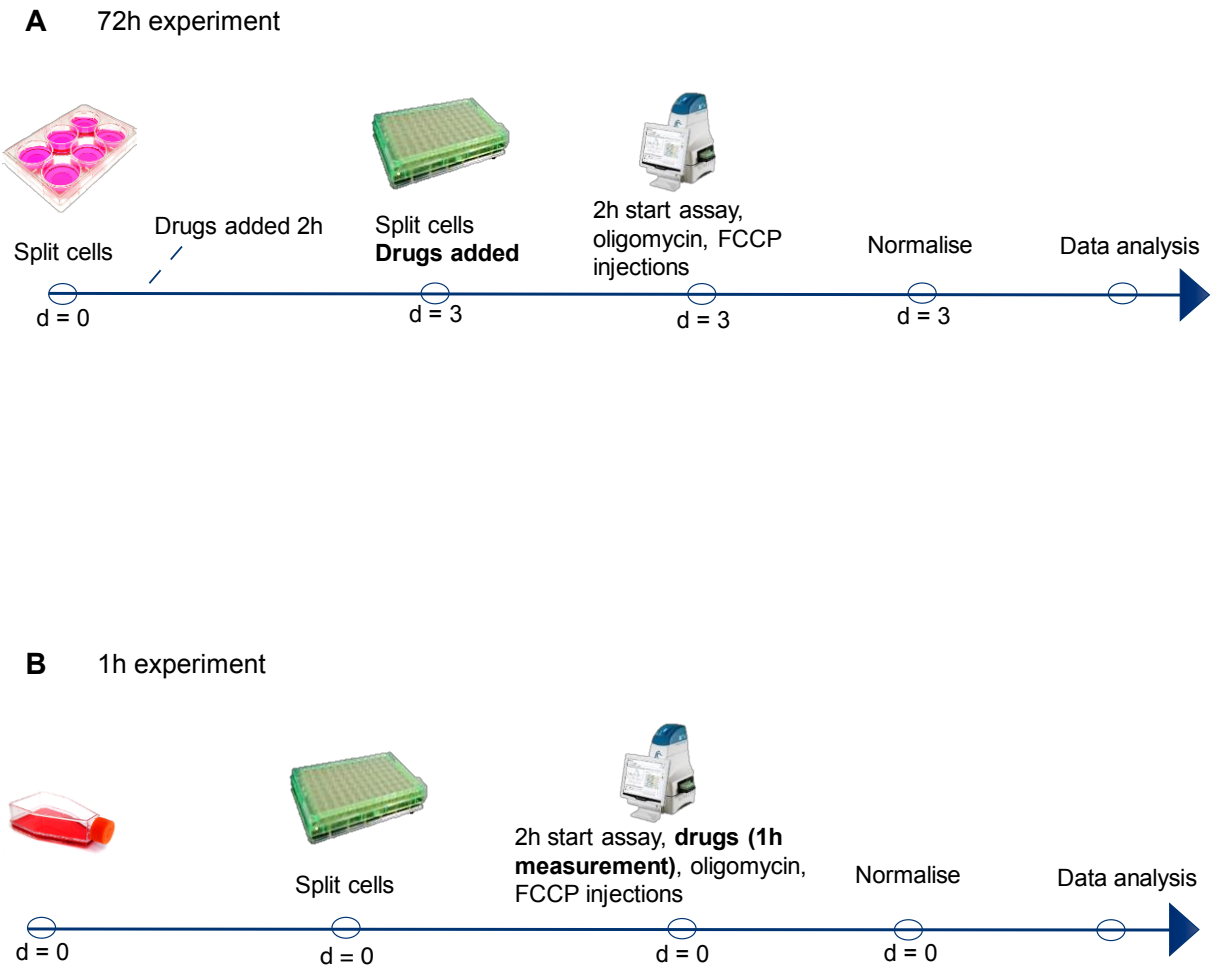

Figure 3.3. Seahorse XF assay experimental approach.

A. Experiment type 1: 72h assay. HEK293T cells were grown in standard growth medium supplemented with appropriate concentrations of tested inhibitors for 72h. Before the seahorse XF assay, cells were harvested, counted and reseeded in seahorse XF assay plates with assay medium supplemented with drug. Following the seahorse XF assay and mitochondrial stress test performance, live cell number and viability was assessed and used for normalization.

B. Experiment type 2: 1h assay. Before the seahorse XF assay, HEK293T cells were harvested, counted and reseeded in seahorse XF assay plates with assay medium. Direct injection of drugs during the seahorse XF assay was performed in the seahorse XF device using the respective ports of the assay plate. Measurements were monitored for 1h, followed by the mitochondrial stress test. Live cell number and viability was assessed and used for normalization.

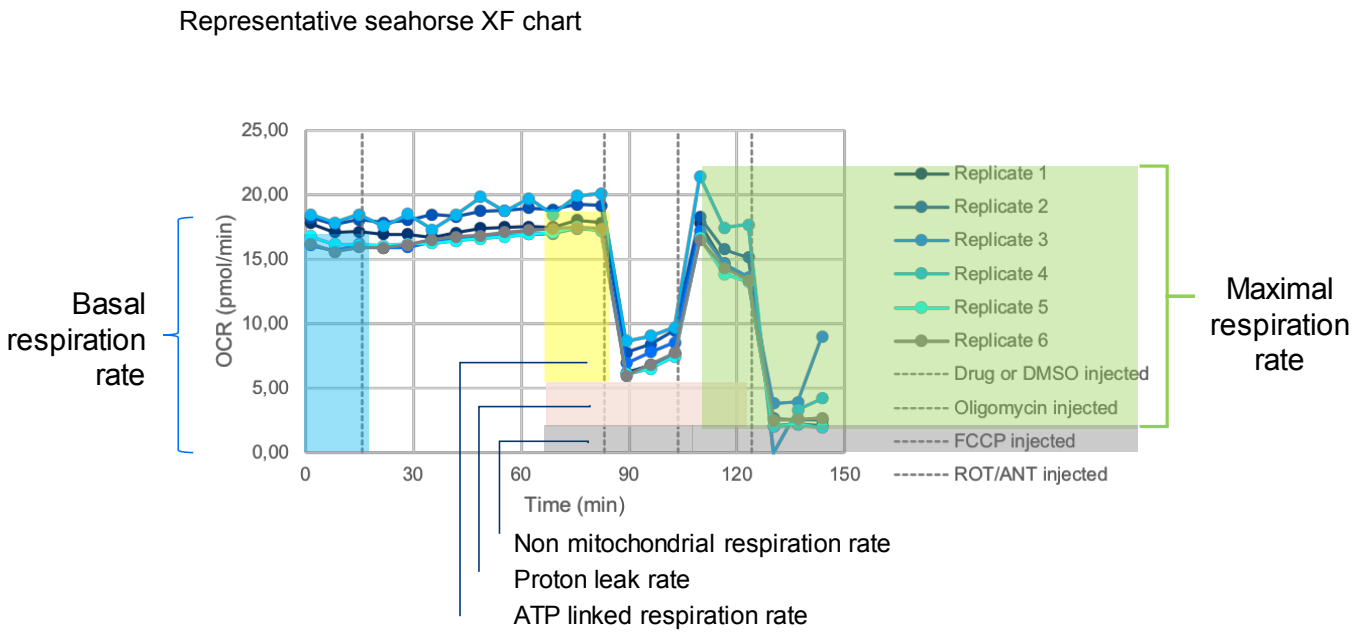

Figure 3.4. Typical readouts of the optimized seahorse XF assay mitochondrial stress test. Experiment type 2, direct injection of drug: 6 technical replicates of HEK293T cells are shown. Y-axis shows OCR (pmol/min) and x-axis shows time (min). The parameters measured during the mitochondrial stress test are basal respiration, maximal respiration, ATP-linked respiration, proton leak and non-mitochondrial respiration. Dotted vertical lines indicate the time points of sequential injections during the mitochondrial stress test: drug or DMSO, oligomycin, FCCP, rotenone/antimycin.

3.3.3 Compounds targeting epigenetic reader and writer proteins can significantly alter metabolism

100 epigenetically active compounds were screened for metabolic effects using the seahorse XF assay and the mitochondrial stress test. An overview of the selected compounds and employed concentrations can be found in (Table 2.1) in the Materials and Methods Chapter 2.3.1. The 100 initial compounds were selected to represent a wide variety of known and suspected epigenetically active small molecule compounds. Major classes of chromatin-modifying enzymes were covered (e.g. histone deacetylases, histone methyltransferases) and compounds both with broad or very specific activity were included.

The consolidation of the 100 individual experiments revealed that many epigenetically active compounds alter basal respiration and glycolysis after the 72h drug treatment (Fig 3.5A). HAT inhibitors (SC00106951, SC00107069, SC00106960) targeting NAT10 (GNAT family), Tip60 (MYST family), p300/CBP respectively, decreased respiration with SC00106960 increasing both respiration and glycolysis. HDAC inhibitors, and molecules targeting epigenetic reader domains resulted in various metabolic effects. In the cases of inhibitors SC00105711 and SC00107059, the observed 1h metabolic effects could hint at potential off target effects. Methyltransferase inhibitors containing classic SET domains generally decreased metabolism or showed no effects. One exception was inhibitor SC00107035 targeting KMT3C (alternative name SMYD2) which contains an interposed SET domain by MYND domain and therefore KMT3C is classified as a different group of SET domain containing methyltransferases (Abu-Farha et al., 2007; Brown et al., 2006; Tsuda & Komatsu, 2010). Several tested methyltransferase inhibitors which target the non-SET domain methyltransferase DOT1L, showed no effect compared to control. PRMT methyltransferase inhibitors showed heterogeneous effects. In contrast to the significant alterations observed at 72h, the 1h of treatment with epigenetic compounds showed much less pronounced metabolic effects on the basal respiration and glycolysis (Fig 3.5B). Five notable exceptions to these observations were one HAT inhibitor (SC00106959), two epigenetic reader domain compounds (SC00107049, SC00106842) and a demethylase inhibitor (SC00106834).

A 72h basal cellular metabolism

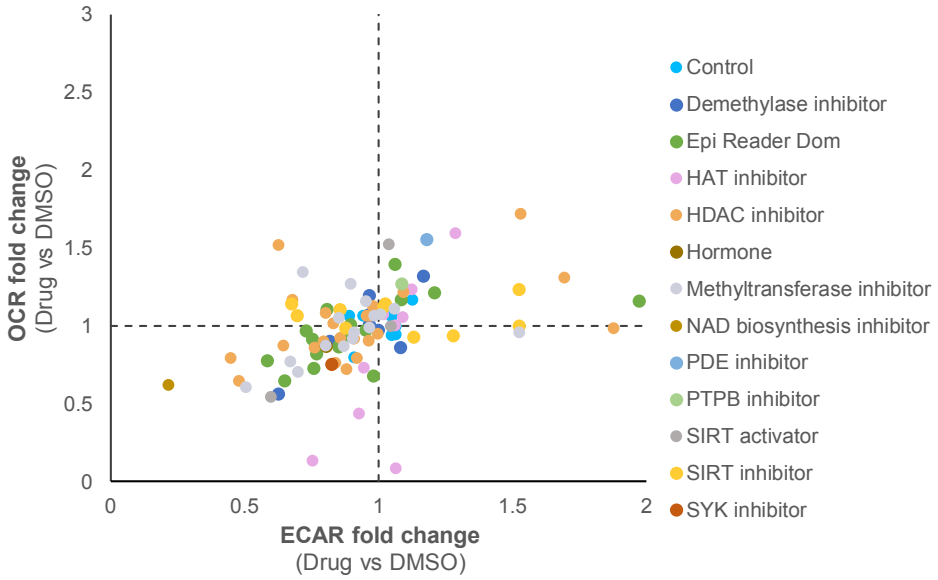

B 1h basal cellular metabolism

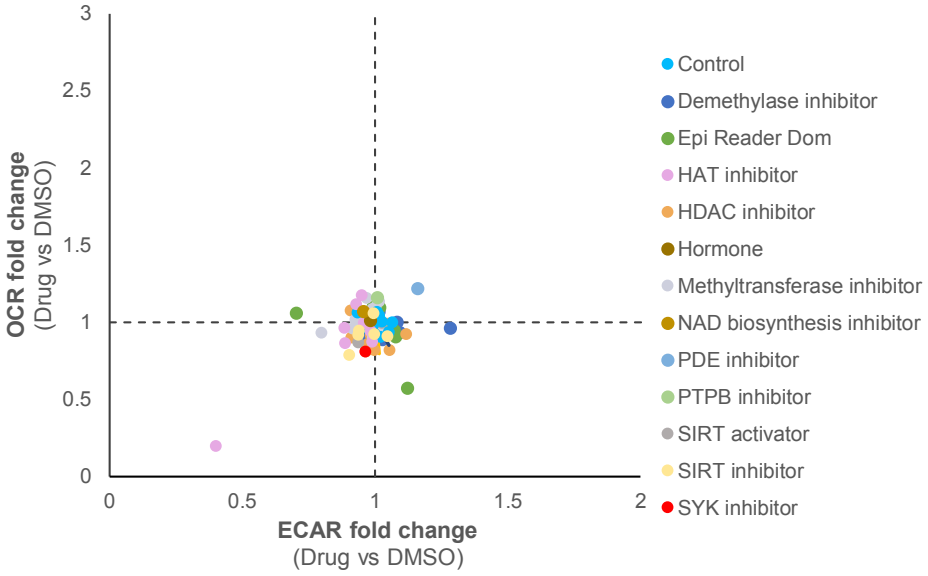

Figure 3.5. Compounds targeting epigenetically-active proteins significantly altered metabolism – basal respiration and glycolysis.

A. Basal respiration and basal glycolysis rates after 72h drug treatments. Each dot represents cells treated with a distinct drug. Values indicate fold-change of readouts in drug-treated cells vs DMSO (control). OCR fold change (y-axis) is plotted against ECAR fold-change (x-axis).

B. Basal respiration and basal glycolysis rates after 1h drug treatments. Each dot represents cells treated with a distinct drug. Values indicate fold-change of readouts in drug-treated cells vs DMSO (control). OCR fold change (y-axis) is plotted against ECAR fold-change (x-axis).

72h treatments with those molecules resulted in more pronounced maximal respiration and corresponding glycolysis rates in the mito stress test (Fig 3.6A). 1h treatments with epigenetic compounds presented fewer metabolic effects comparing to 72h treatments. However, the 1h readouts of maximal respiration/glycolysis were more pronounced than the basal rates, corresponding to the fact that the cells are "stressed" from the addition of oligomycin and FCCP and therefore potentially more sensitive to disturbance by the added compounds. Epigenetic reader domain inhibitors, HAT and methyltransferase inhibitors were the two drug classes that showed most metabolic effects after 1h (Fig 3.6B). This could be hinting possibly at non-specific effects and activity in the cytoplasm in addition to the epigenetic mechanisms those compounds are generally known for.

3.4 Epigenetic proteins regulate metabolism

Very few comprehensive metabolic characterizations of mammalian cells under different conditions have been published to date. A limited set of studies focused on individual epigenetic regulatory proteins and their potential involvement in metabolism (Nguyen et al., 2020; J. Yang et al., 2017; T. Zhang et al., 2020). In particular, no screening study linking epigenetic proteins and metabolism has been published to the author's knowledge. Therefore, the seahorse XF assay was used to measure the metabolic phenotype of cell lines deficient in specific epigenetic proteins, including DOT1L, KMT9, PARP1 and MacroD1. Furthermore, the results helped to test the screening approach and validity of results so far, potentially demonstrating that there can be causative relationship between the activity/presence of an epigenetic regulator and metabolism. The selected knockout cell lines therefore were used as specific examples to support that the observed correlations between histone PTM changes and metabolic changes caused by epigenetically active compounds could be underlined by causative relationships (for instance signaling cascades), as discussed in Chapter 4

3.4.1 Effects of genetic alterations of HEK293T DOT1L and KMT9

To look into more detail in the metabolic effects of KMT methyltransferase inhibitors for the DOT1L domain and SET domain methyltransferases, the metabolic characteristics of two types of knockout cell lines were analysed using the seahorse XF assay: HEK293T DOT1L KO and HEK293T

A 72h maximal cellular metabolism

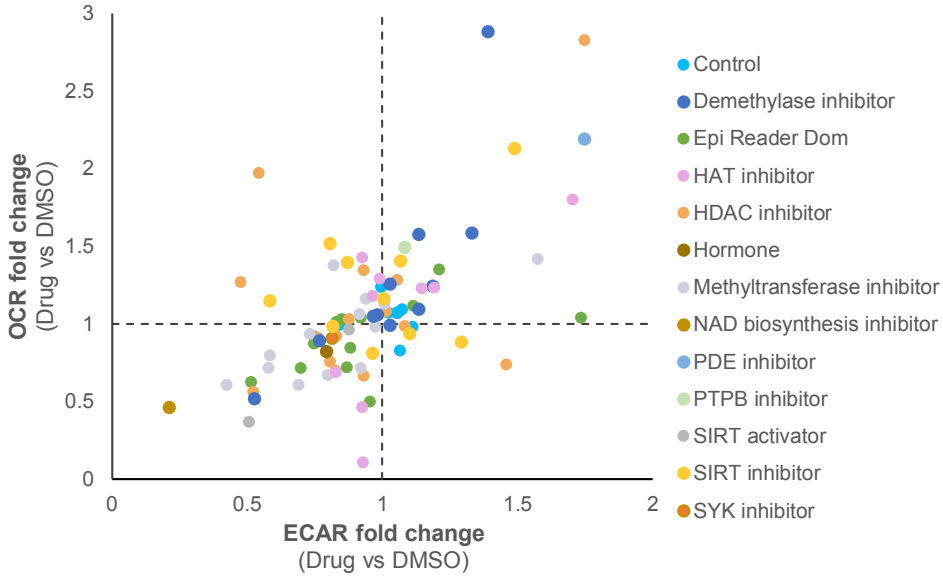

B 1h maximal cellular metabolism

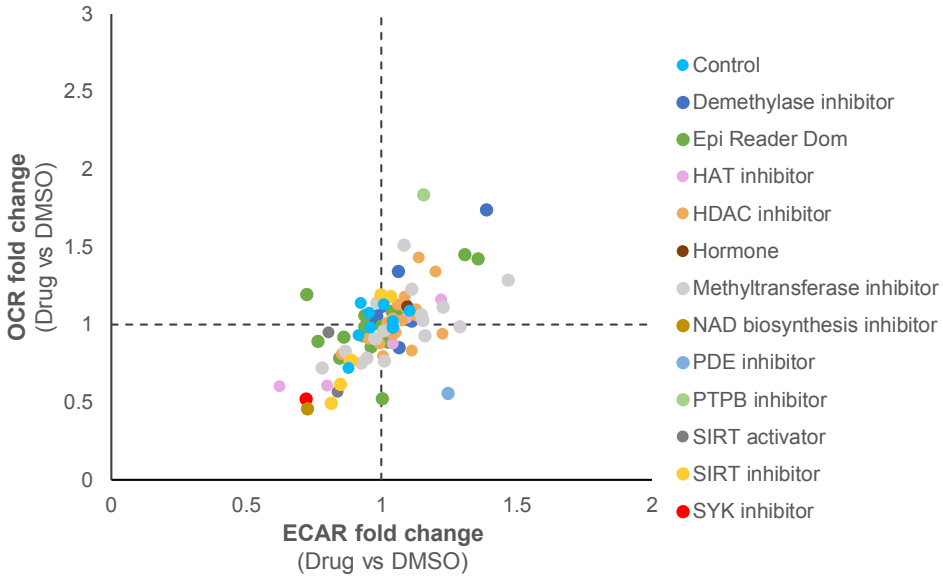

Figure 3.6. Compounds targeting epigenetically-active proteins significantly altered metabolism – maximal respiration & glycolysis.

A. Maximal respiration and maximal glycolysis rates after 72h drug treatments. Each dot represents cells treated with a distinct drug. Values indicate fold-change of readouts in drug-treated cells vs DMSO (control). OCR fold change (y-axis) is plotted against ECAR fold-change (x-axis).

B. Maximal respiration and maximal glycolysis rates after 1h drug treatments. Each dot represents cells treated with a distinct drug. Values indicate fold-change of readouts in drug-treated cells vs DMSO (control). OCR fold change (y-axis) is plotted against ECAR fold-change (x-axis).

KMT9 KO. Basal respiration was significantly increased in the case of DOT1L KO comparing to WT and KMT9 KO (Fig 3.7A). In the HEK293T KMT9 KO, basal glycolysis was significantly reduced comparing to WT and HEK293T DOT1L KO (Fig 3.7B) while DOT1L KO seem to have increased basal glycolysis. Maximal respiration was slightly increased in DOT1L KO comparing to WT and KMT9 KO (Fig 3.7C). Maximal glycolysis was significantly reduced in KMT9 KO comparing to WT and DOT1L KO (Fig 3.7D).

In line with the above consolidated results, respiration measurements over time showed that KMT9 KO was similar to WT (Fig 3.8A, C) but presented significantly reduced glycolysis (Fig 3.8B). In contrast to these results, cells treated with DOT1L or KMT inhibitors for 72h showed no metabolic effect compared to control when measured on the seahorse XF. This could potentially be explained if the employed inhibitors do not fully inhibit the cellular activity of DOT1L, thereby allowing enough remaining activity so that no downstream effect on metabolism was observed despite the inhibitor treatments. The KMT9 KO metabolic effects were in line with the effects caused by inhibitors targeting SET domain methyltransferases, as all SET domain KMT inhibitors led to reduced metabolism (Fig 3.5A, Fig 3.6A).

3.4.2 Upon cellular stress, HEK293T DOTL1 KO increase both glycolysis and mitochondrial respiration, while WT and KMT9 KO cells show minimal responses

Interestingly, absence of DOT1L increased the respiration and glycolysis potential of HEK293T when exposed to stress after sequential injections of oligomycin and FCCP during the mitochondrial stress test (Fig 3.9). In contrast, WT and KMT9 KO showed minimal responses during the mitochondrial stress test. The DOT1L KO showed preference to oxidative phosphorylation at basal state but used both oxidative phosphorylation and glycolysis under stress conditions.

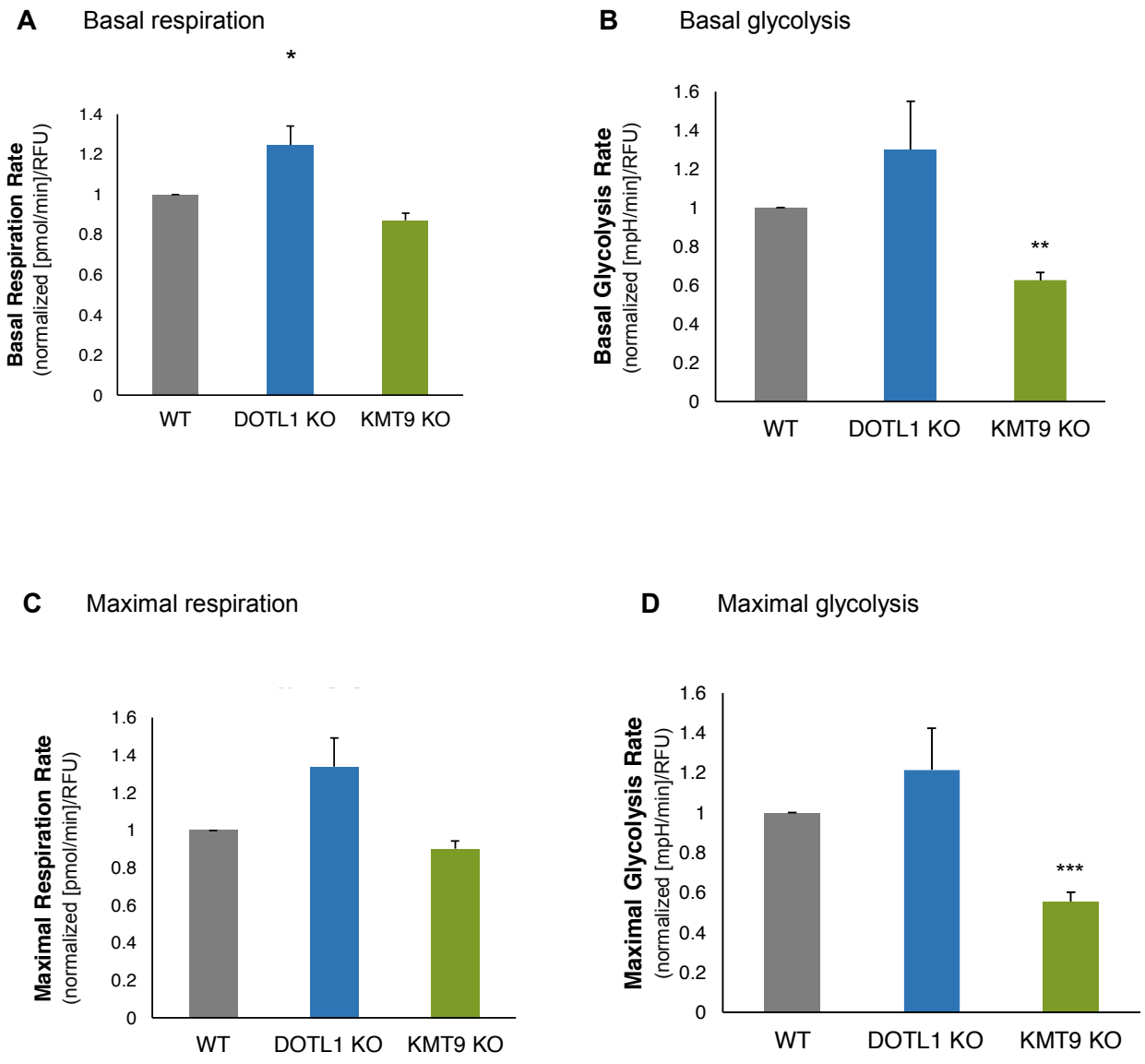

Figure 3.7. Epigenetic proteins regulated metabolism: confirmation using HEK293T DOT1L and KMT9 KO cell lines.

The results shown are compiled of n=3 biological replicates for the KMT9 KO and n=5 biological replicates for the WT and DOT1L KO.

A. Y-axis indicates normalized basal respiration rates ([pmol/min]/RFU). Results from KO cell lines are depicted relative to WT.

B. Y-axis indicates normalized basal glycolysis rates ([mpH/min]/RFU). Results from KO cell lines are depicted relative to WT.

C. Y-axis indicates normalized maximal respiration rates ([pmol/min]/RFU). Results from KO cell lines are depicted relative to WT.

D. Y-axis indicates normalized maximal glycolysis rates ([mpH/min]/RFU). Results from KO cell lines are depicted relative to WT.

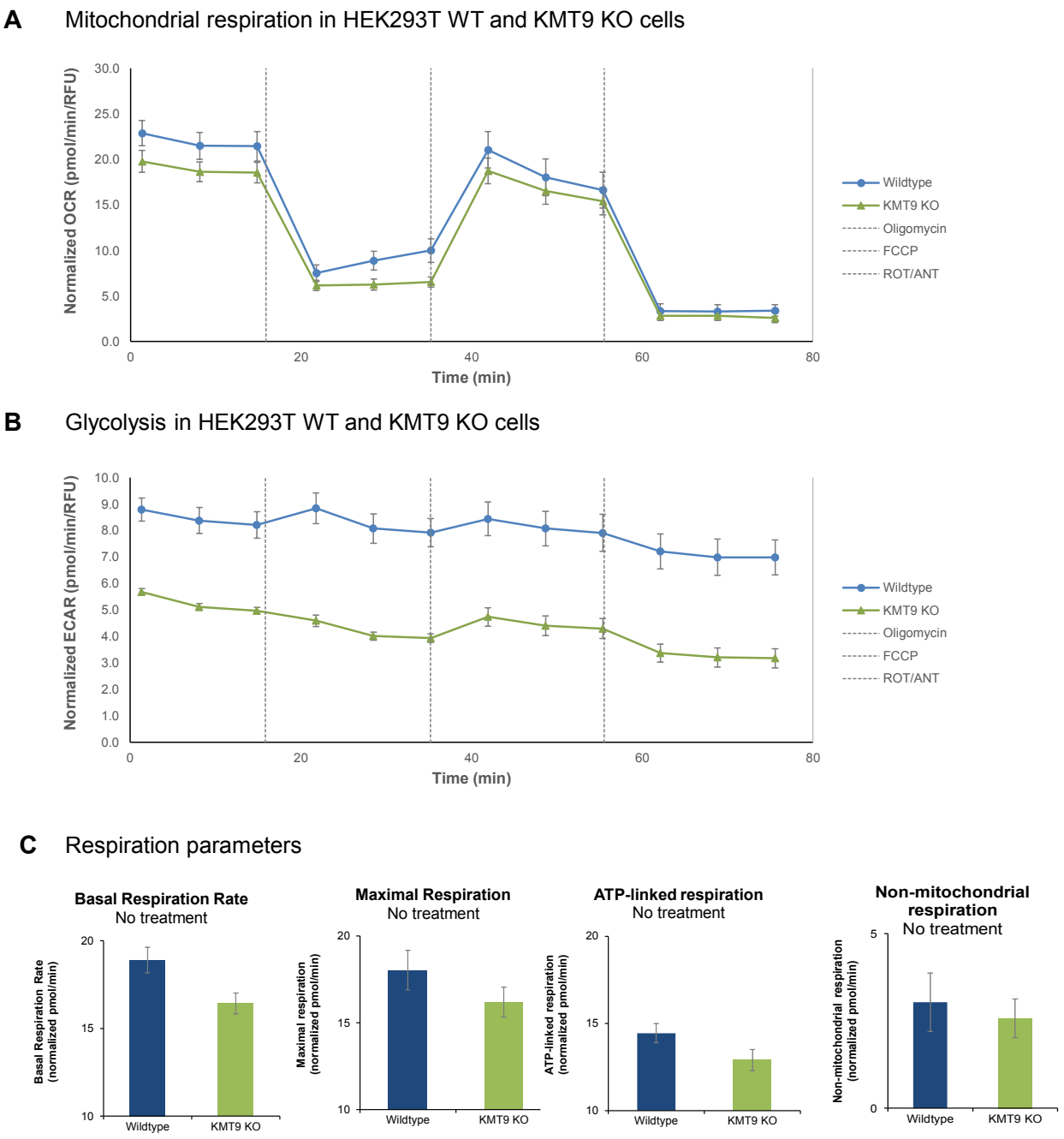

Figure 3.8. Detailed analysis of HEK293T KMT9 KO cell line revealed significantly reduced glycolysis with mitochondrial respiration similar to WT.

A. Seahorse XF analysis of mitochondrial respiration of HEK293T WT vs KMT9 KO. N=3 biological replicates; error bars: SEM, 6 technical replicates per condition per biological repeat. X-axis represents time (min) and y-axis normalized OCR ([pmol/min]/RFU).

B. Seahorse XF analysis of glycolysis rate of HEK293T WT vs KMT9 KO. N=3 biological replicates; error bars: SEM, 6 technical replicates per condition per biological repeat. X-axis represents time (min) and y-axis represents normalized ECAR ([mpH/min]/RFU).

C. Normalized respiration rate parameters measured with seahorse XF (see A).

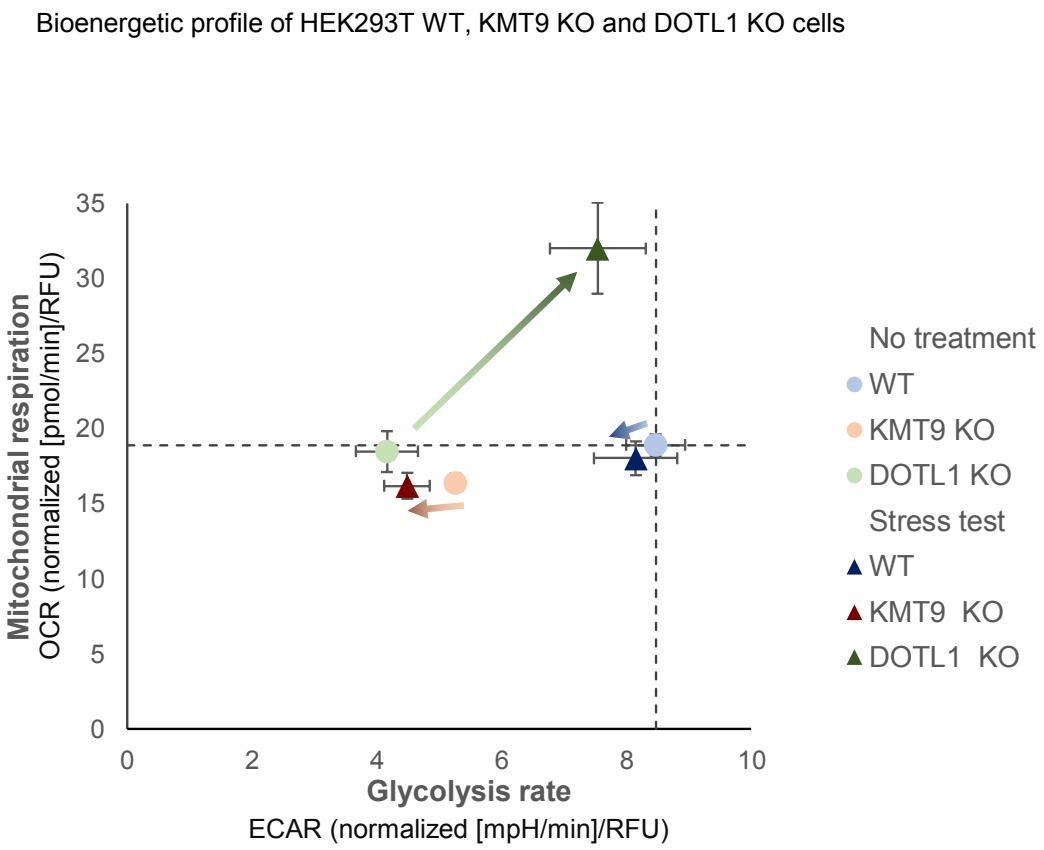

Figure 3.9. Upon cellular stress, HEK293T DOTL1 KO increased both glycolysis and mitochondrial respiration, while WT and KMT9 KO cells showed minimal responses.
Cellular respiration and glycolysis rates before (light-colored round symbols) and after the mitochondrial stress test (dark-colored pyramid symbols). N=3 biological replicates for KMT9 KO and n=5 biological replicates for WT and DOT1L KO. There were 6 technical replicates for each biological repeat. X-axis represents normalized ECAR ([mpH/min]/RFU) and y-axis represents OCR ([pmol/min]/RFU). No treatment indicates the basal rates for OCR and ECAR and stress test indicates rates after injections of oligomycin and FCCP.

3.4.3 MacroD1 regulates metabolism in HEK TREX cells by promoting oxidative respiration and inhibiting glycolysis

To expand the investigations to a protein that is known to have a physiological function in mitochondria but outside of the oxidative phosphorylation pathway, MacroD1 knockout cell lines were employed. MacroD1, a macrodomain-containing ADP-ribosyl hydrolase, is mainly localized in mitochondria and targets ester bonds of ADP-ribosylated phosphorylated double-stranded DNA ends, promoting a reversal of DNA damage response (Agnew et al., 2018). MacroD1 has been implicated in the pathogenesis of various cancer types but its role in metabolism has not been investigated so far. The HEK TREX KO of the mitochondrial protein MacroD1 appeared to have decreased respiration and increased glycolysis comparing to WT (Fig 3.10A, B). Basal respiration rate, ATP linked respiration, nonmitochondrial respiration and proton leak rates appeared similar to WT. Maximal respiration rate though was significantly increased in the MacroD1 KO comparing to WT (Fig 3.10C).

3.4.4 MacroD1 regulates metabolism in U2OS cells by promoting oxidative respiration and inhibiting glycolysis

The effects seen on HEK TREX cell line were confirmed on the U2OS cell line for the MacroD1 protein (Fig 3.11A, B); MacroD1 KO showed decreased respiration and increased glycolysis comparing to WT. It was interesting to investigate whether poly(ADP-ribose) polymerase (PARP), an enzyme that senses DNA damage by adding poly ADP substrates, would have an opposite metabolic effect than MacroD1. PARP1 has the opposite function from MacroD1 as it adds ADP substrates and MacroD1 is a mono hydrolase removing these marks (Alemasova & Lavrik, 2019; Jankevicius et al., 2013; Tallis et al., 2014). PARP1 KO presented slightly higher respiration to WT and similar glycolysis. MacroD1 KO appeared to have both basal and maximal respiration rates decreased comparing to WT (Fig 3.11C). Under stress conditions and after the performance of the mitochondrial stress test the results showed that lack of MacroD1 influenced negatively the basal respiration rate and maximal respiration rate comparing to WT. PARP1 KO showed slight increase of maximal respiration rate comparing to WT after the performance of the mitochondrial stress test (Fig 3.12). To study the role of MacroD1 in metabolism under conditions of DNA damage stress, cells were pre-treated with

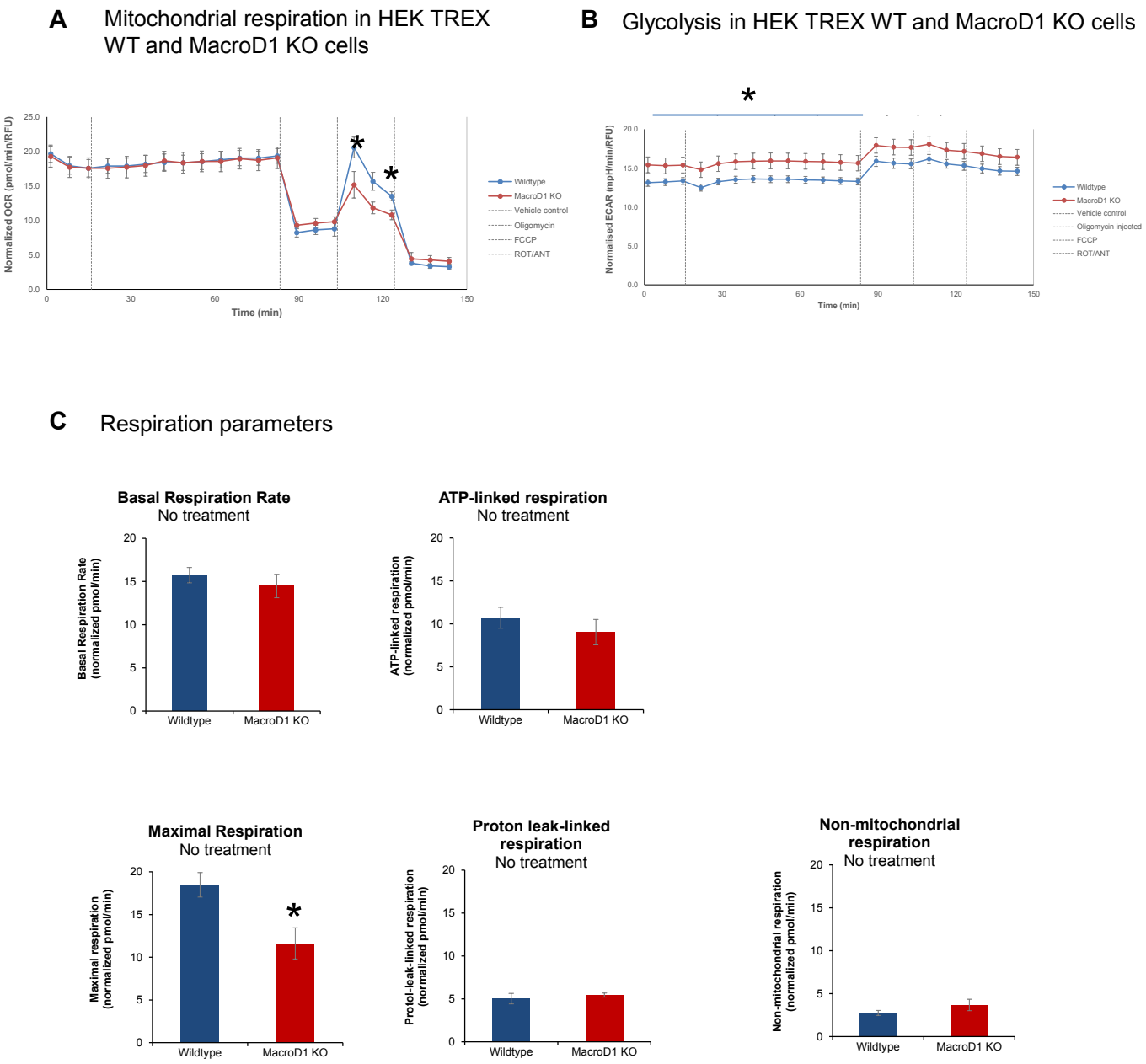

Figure 3.10. MacroD1 regulated metabolism in HEK TREX cells by promoting oxidative respiration and inhibiting glycolysis.

A. Seahorse XF analysis of mitochondrial respiration of HEK TREX WT vs MacroD1 KO. N=4 biological replicates; error bars: SEM, 6 technical replicates per condition per biological repeat. X axis represents time (min) and y axis represents normalized OCR ([pmol/min]/RFU)

B. Seahorse XF analysis of glycolysis rate of HEK TREX WT vs MacroD1 KO. N=4 biological replicates; error bars: SEM, 6 technical replicates per condition per biological repeat. X axis represents time (min) and y axis represents normalized ECAR ([mpH/min]/RFU)

C. Normalized respiration rate parameters measured with seahorse XF (see A).

A Mitochondrial respiration in U2OS WT, MacroD1 KO and Parp1 KO cells

B Glycolysis in U2OS WT, MacroD1 KO and Parp1 KO cells

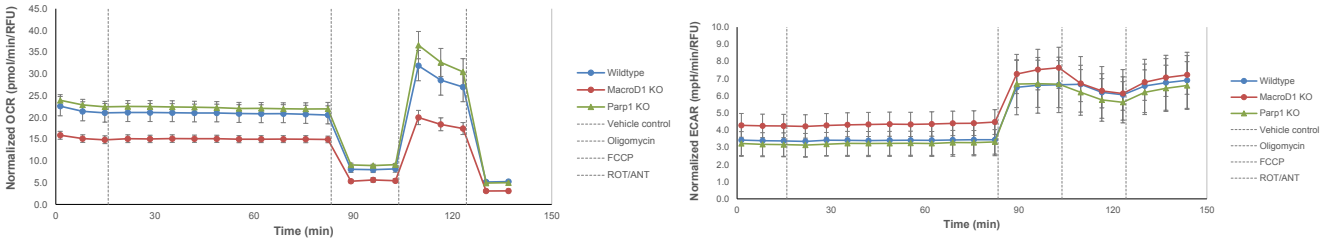

C Respiration parameters

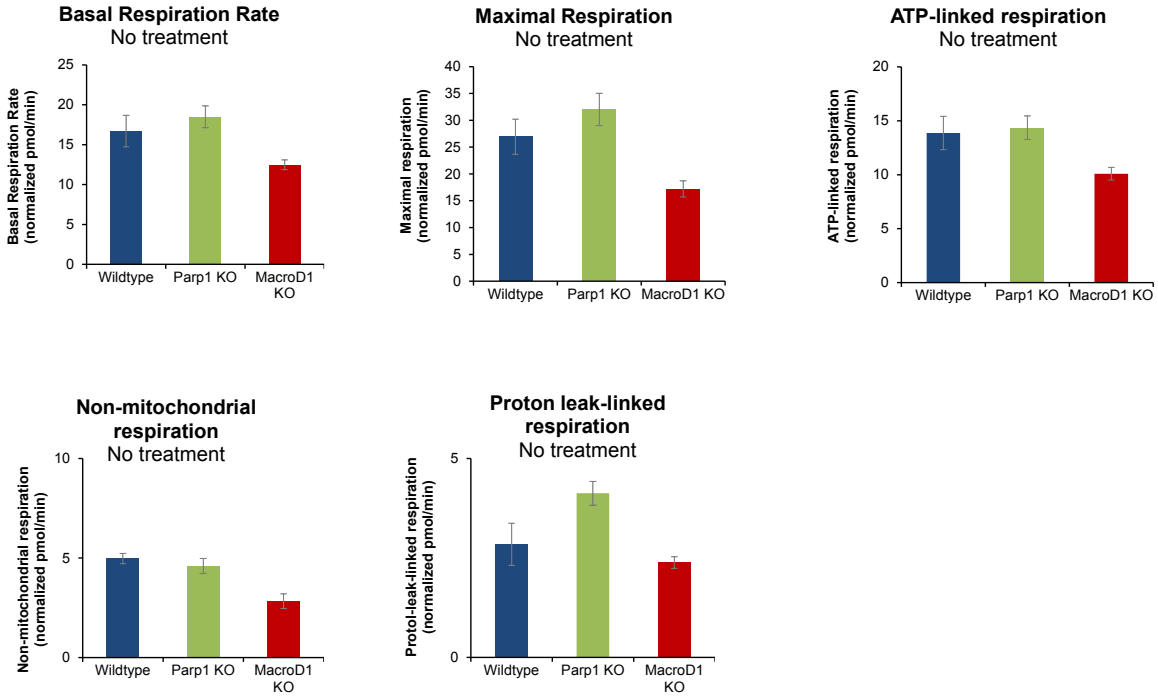

Figure 3.11. MacroD1 regulated metabolism in U2OS cells by promoting oxidative respiration and inhibiting glycolysis.

A. Seahorse XF analysis of mitochondrial respiration of U2OS WT vs MacroD1 KO and Parp1 KO. N=6 biological replicates; error bars: SEM, 6 technical replicates per condition per biological repeat. X-axis represents time (min) and y-axis represents normalized OCR ([pmol/min]/RFU)

B. Seahorse XF analysis of glycolysis rate of U2OS WT vs MacroD1 KO and Parp1 KO N=6 biological replicates; error bars: SEM, 6 technical replicates per condition per biological repeat. X-axis represents time (min) and y-axis represents normalized ECAR ([mpH/min]/RFU)

C. Normalized respiration rate parameters measured with seahorse XF (see A).

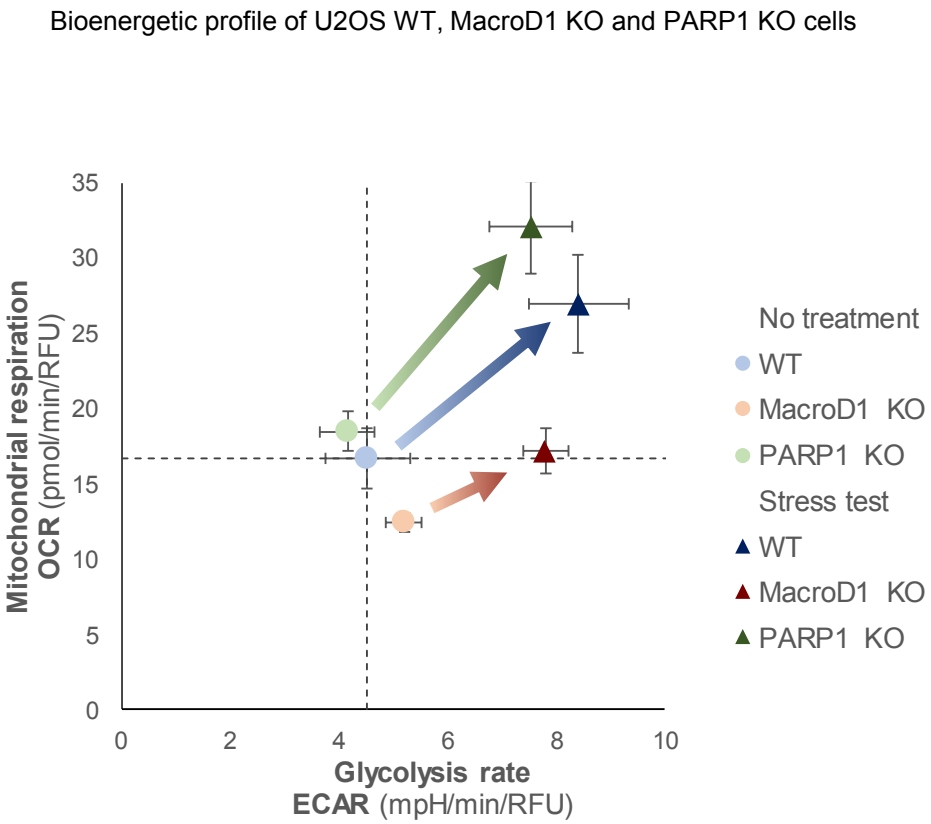

Figure 3.12. U2OS MacroD1 KO reduced the response to cellular stress compared to WT and PARP1 KO.

Cellular respiration and glycolysis rates before (light-colored round symbols) and after the mitochondrial stress test (dark-colored pyramid symbols). N≥3 biological replicates for MacroD1 KO and n ≥ 3 biological replicates for WT and PARP1 KO. There were 6 technical replicates for each biological repeat. X-axis represents normalized ECAR ([mpH/min]/RFU) and y-axis represents OCR ([pmol/min]/RFU). No treatment indicates the basal rates for OCR and ECAR and stress test indicates rates after injections of oligomycin and FCCP.

various concentrations of H_2O_2. Indeed, even under these conditions, the seahorse XF time course experiments showed a similarly reduced maximum oxidative phosphorylation in the MacroD1 KO cells, while glycolysis rates were also higher, similar to the non-H_2O_2-stressed cells (Compare Appendix Fig A.5 to A.8 and Fig. 3.11, 3.12). Together these results suggested that MacroD1 in U2OS cells has a positive regulatory role to promote oxidative phosphorylation, while it has an inhibitory role on glycolysis. In line with their oppositive functions in ADP-mediated protein modifications, PARP1 knockouts led to opposite effects on metabolism.

3.5 Pharmacophore fragment analysis did not show a correlation between underlying drug structure and metabolic readouts of 100 inhibitors

The results of the initial screening of 100 epigenetically active inhibitors showed a diverse picture of drug-induced responses on cellular metabolism. Importantly, small molecules targeting the same group of cellular proteins showed apparently different results (Fig 3.5 and Fig 3.6). This prompted the question whether the metabolic effects could be explained by factors other than their effects on epigenetic inhibitors described on the literature. One way to investigate this is the pharmacophore fragment based analysis, which is an unbiased way to assess the contribution of pharmacologically active sub fragments of drugs irrespective of their known or suspected activity (Khanna, 2012; Nicolaou, 2014; Wasko et al., 2015). Pharmacophore analysis was performed in silico in collaboration with BioNTech Small Molecules, using the MOE software**,** providing an annotation of the 100 screened chemicals with distinct pharmacophore clusters. After acquiring the results from BioNTech Small Molecules, two types of compounds clustering (1: fragment cluster based; 2: MOE gpiDAPH3 based) were used to group the drug inhibitors. As shown in Fig. 3.13A, the screened compounds were distributing in 4 large “macro” groups, combining criteria from both clustering methods as defined by statistical proximity within a fragment cluster or MOE gpiDAPH3. To correlate the cellular metabolic effect of the compounds with pharmacophores, 72h inhibitor treated HEK293T basal respiration rates from all compounds (Fig 3.5 and Fig. 3.6) were divided in 9 groups depending on the effects on respiration and glycolysis (Fig 3.13B top row of the table). For example, cluster 1 “up up”, described all inhibitors causing increased oxidative phosphorylation and glycolysis upon

A

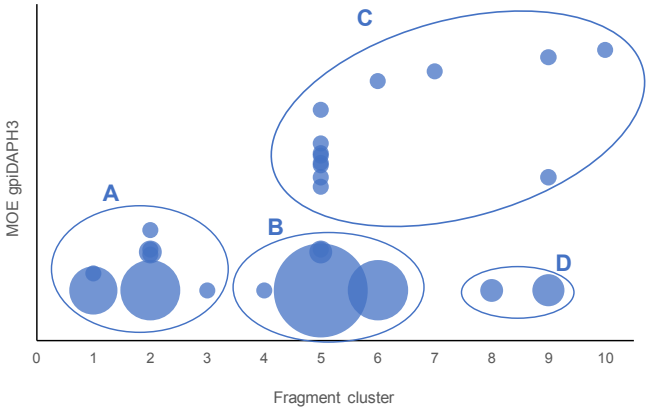

B

Seahorse 72h basal

Type of compound		cluster 1	cluster 2	cluster 3	cluster 4	cluster 5	cluster 6	cluster 7	cluster 8	cluster 9
OCR / ECAR response		Up Up	Up NC	Up Down	NC Up	Down Up	Down NC	NC Down	Down Dow	NC NC
Fragment cluster	1	0	0	0	1	0	2	2	0	5
	2	0	2	0	1	0	0	1	2	11
	3	0	0	0	0	0	0	0	0	1
	4	0	0	0	0	0	0	0	0	0
	5	0	3	1	3	0	3	4	0	27
	6	1	1	0	1	0	0	2	3	6
	7	0	0	0	0	0	0	0	0	0
	8	0	1	0	0	0	0	0	0	1
	9	1	0	0	0	0	1	0	1	2
	10	0	0	0	0	0	0	0	0	1
Macro classes	A	0	2	0	2	0	2	3	2	17
	B	1	4	1	4	0	0	5	3	30
	C	0	0	0	0	0	3	1	0	5
	D	1	1	0	0	0	1	0	1	2

C

Seahorse 72h max

Type of compound		cluster 1	cluster 2	cluster 3	cluster 4	cluster 5	cluster 6	cluster 7	cluster 8	cluster 9
OCR / ECAR response		Up Up	Up NC	Up Down	NC Up	Down Up	Down NC	NC Down	Down Down	NC NC
Fragment cluster	1	1	2	0	0	0	3	3	0	1
	2	3	1	0	0	0	1	0	3	9
	3	0	0	0	0	0	0	0	0	1
	4	0	0	0	0	0	0	0	0	0
	5	2	5	1	1	0	4	2	2	24
	6	1	1	1	0	1	0	1	4	5
	7	0	0	0	0	0	0	0	0	0
	8	1	0	0	0	0	0	0	0	1
	9	1	0	0	0	0	1	0	2	1
	10	0	0	0	0	0	1	0	0	0
Macro classes	A	4	3	0	0	0	4	3	3	11
	B	3	6	2	1	1	1	3	5	26
	C	0	0	0	0	0	4	0	2	3
	D	2	0	0	0	0	1	0	1	2

Figure 3.13. Pharmacophore fragment-based analysis did not show underlying drug structure similarities to explain metabolic readouts of 100 inhibitors.

A. Pharmacophore analysis using MOE software**.** The screened compounds cluster in 4 large groups defined by statistical proximity within a fragment cluster or MOE gpiDAPH3.

B. 72h basal respiration rates were used to cluster the inhibitors in the macro classes corresponding to the fragment cluster method (Up: at least 30% increase comparing to control for OCR or ECAR, Down: at least 30% decrease comparing to control for OCR or ECAR, NC/NC: no change comparing to control for OCR or ECAR)

C. 72h maximal respiration rates were used to cluster the inhibitors in the macro classes corresponding to the fragment cluster method.

treatment comparing to control.

Then the distribution of the compounds along the10 pharmacophore fragment-based clusters were compared to the 9 metabolic groups (Fig 3.13B). In addition, the 4 macro classes of compounds identified were used to compare the compounds within each class with the compounds grouped in each metabolic group (Fig 3.13B). A possible correlation between fragment clusters and metabolic clusters would be identified if all or most inhibitors of one metabolic cluster would associate within one fragment cluster. However, no such exclusive grouping was observed, meaning that no possible chemical structure similarities were identified that could explain the obtained metabolic effects from the metabolic screening. Similar analysis was performed for the 72h maximal respiration rates (Fig 3.13C) and 1h basal respiration rates and 1h maximal respiration rates (Appendix Fig A.1-4). Eventually, this study revealed that a specific metabolic effect could be triggered from drugs with varying structures and varying targets. This result led to the investigation of commonly regulated epigenetic modifications as an intermediate step and basis to design next steps of identifying commonly regulated epigenetic targets that introduce similar metabolic effects described in the next Chapters.

3.6 Epigenetically active compounds alter metabolism, histone PTMs and protein expression; identification of commonly affected targets

3.6.1 Epigenetically-active compounds cluster in distinct groups based on their metabolic impact on HEK293T cells

To take an alternative approach to analyze the data hierarchical clustering was performed. In contrast to the method described in 3.5 (which was a supervised method based on predefined binary groups) this approach allowed clustering of compounds and respective induced metabolic effects in an unbiased manner. For this, seahorse XF results were normalised to control and transformed into log2 ratios and clustered based on similarity of their metabolic readouts, as described in Chapter 2.6. Basal and maximal respiration rates for both 1h and 72h treatments were analysed as well as basal glycolysis and maximal glycolysis for both experiment types (Fig 3.14A). Three distinct metabolic effect groups were identified. The metabolic effects were synergistic where both oxidative phosphorylation and

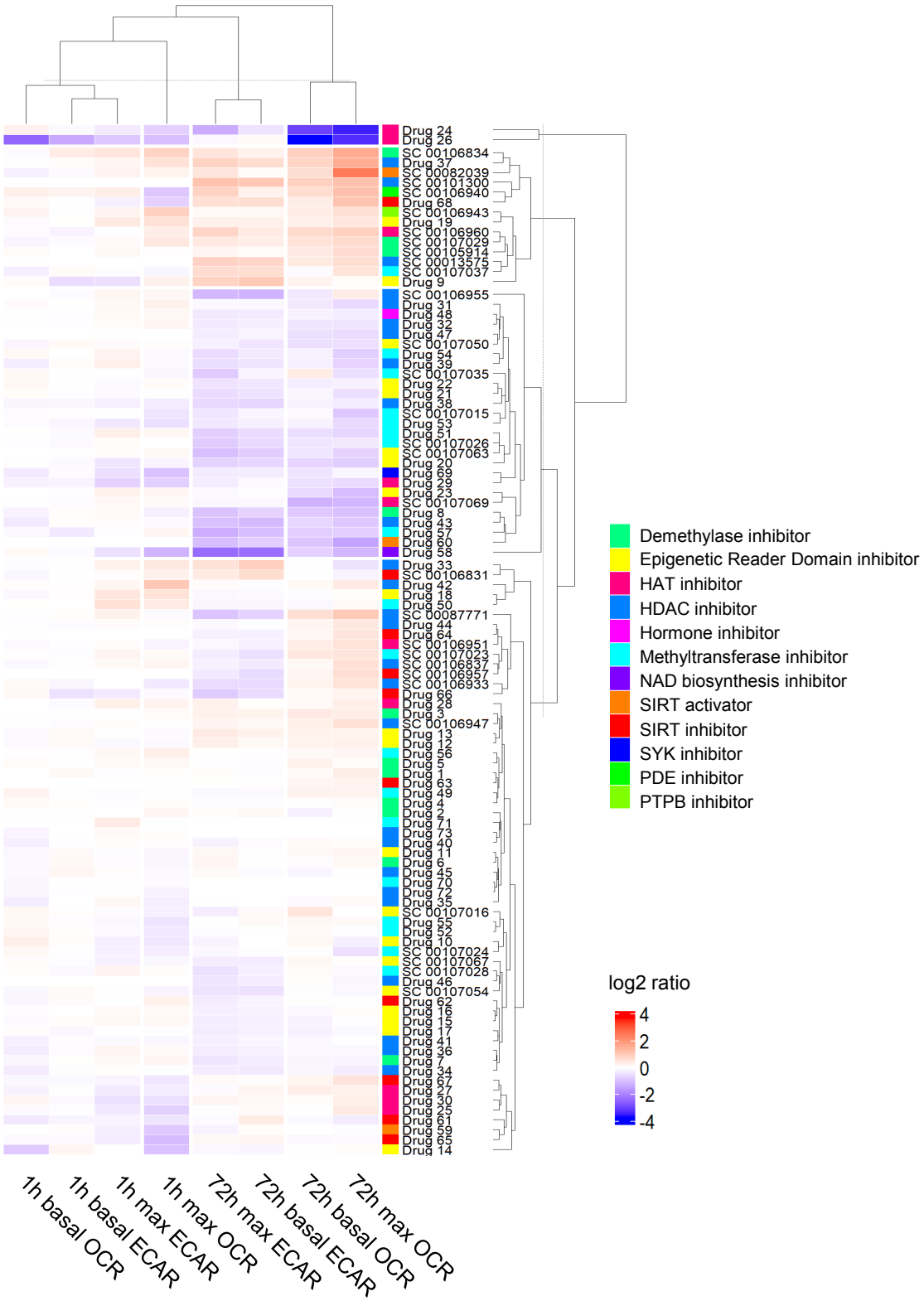

Figure 3.14. Epigenetically-active compounds clustered in distinct groups based on their metabolic impact on HEK293T cells.

Hierarchical clustering and heatmap of 100 epigenetically-active compounds based on their metabolic profiles measured with seahorse XF. The results are normalised to DMSO (control). Upregulation in drug- vs DMSO-treated cells is indicated in red and downregulation is indicated in blue. All four measured mitochondrial stress test parameters from both 72h and 1h experiments are represented: basal OCR, basal ECAR, maximal OCR and maximal ECAR.

glycolysis were decreased or both increased, and antagonistic were oxidative phosphorylation was increased and glycolysis was decreased. There were almost no cases were oxidative phosphorylation was decreased and glycolysis increased. The relative lack of this type of observation (which would be similar to Warbung effect) was in line with expectations since the cell lines used were not cancer derived and the drugs used were mainly described as anticancer treatment candidates. Interestingly, different classes of inhibitors caused similar metabolic effects. Furthermore, distinct drug groups such as HDAC inhibitors were identified causing increase in oxidative phosphorylation and decrease in glycolysis (Fig 3.14).

3.6.2 Criteria for selection of 30 inhibitors out of 100 initially studied compounds

To look into more detail for molecular mechanisms involved in affecting metabolism via epigenetics, 30 compounds were selected for follow-up experiments (Fig 3.15A). The criteria for compound selection were: to cause a 30% change in metabolism compare to control; to present no 1h effects to reduce likelihood of unspecific and non-histone effects; absence of cell toxicity; and to be known to target specific proteins.

Compounds included in the selection had to cause a 30% change in metabolism comparing to control, present no 1h effects to reduce likelihood of unspecific and non-histone effects, show no cell toxicity and have a specific target. The selected epigenetically active compounds covered various inhibitor classes such as HAT, HDAC, methyltransferase inhibitors and others (Fig 3.15B).

An overview of the 30 selected compounds is presented in Table 3.1 (below). Three classes of HAT inhibitors targeting nuclear HATs were selected. SC00106951 HAT inhibitor main target is NAT10 (GCN5 HAT family), SC00107069 targeting Tip60 (MYST HAT family) and SC00106960 targeting P300/CBP. The selected HDAC inhibitors were covering various targets from the HDAC subfamilies. For instance, HDAC inhibitor SC00106933 was selected that is targeting class I (HDAC1) (refer to Table 3.1 for more details on the other inhibitors).

A Selection of compounds for in-depth analyses

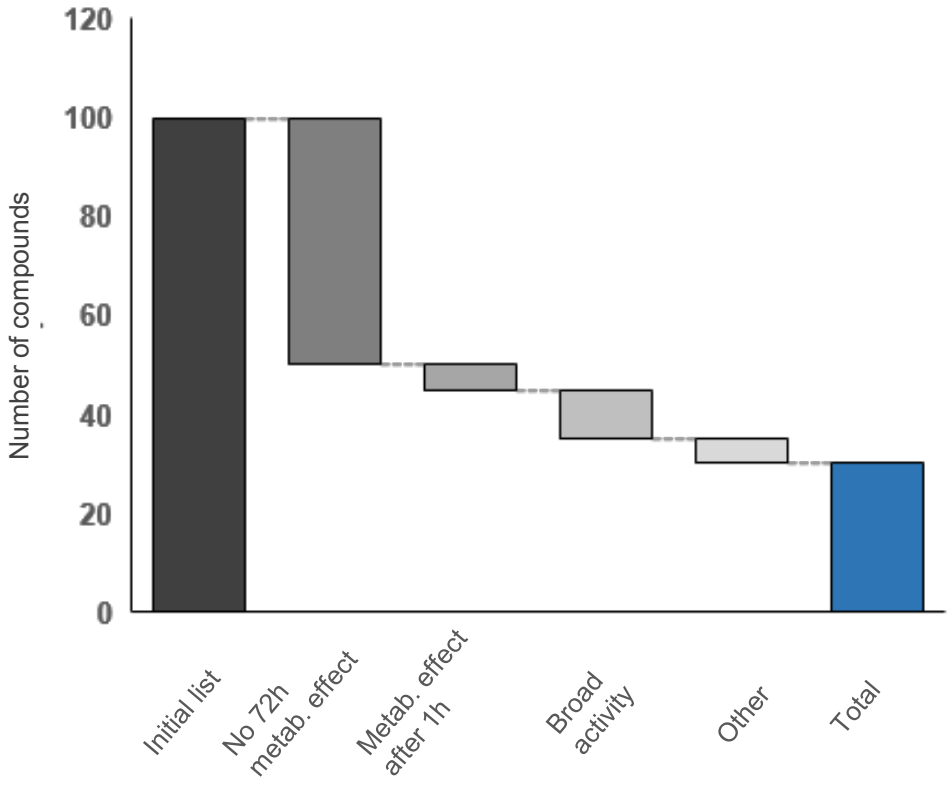

B Distribution of selected compounds across chemical classes

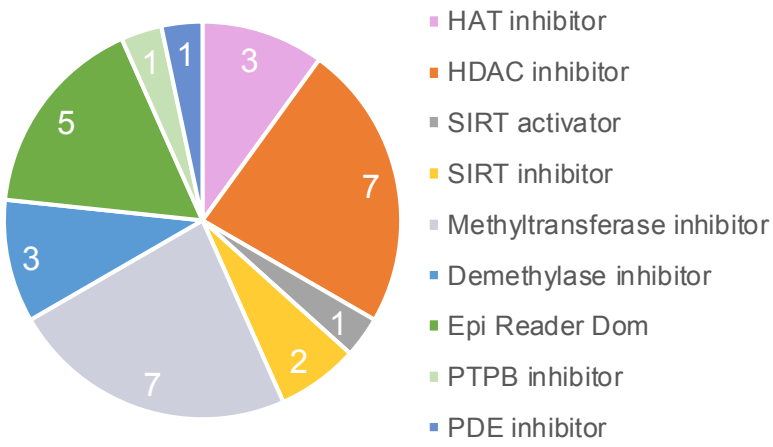

Figure 3.15. Criteria for selection of 30 inhibitors out of 100 initially studied compounds.

A. The figure represents the criteria used for selecting 30 compounds out of the initial pool of 100 drugs.

B. 30 compounds covering all functional classes were selected for follow up analyses.

Chemical Compound ID	Chemical group	Concentration used in this study
SC 00087771	HDAC inhibitor	8uM
SC 00106933	HDAC inhibitor	30nM
SC 00106837	HDAC inhibitor	10uM
SC 00106955	HDAC inhibitor	0.5nM
SC 00106947	HDAC inhibitor	1uM
SC 00013575	HDAC inhibitor	0.5uM
SC 00101300	HDAC inhibitor	25uM
SC 00107069	HAT inhibitor	2uM
SC 00106951	HAT inhibitor	1uM
SC 00106960	HAT inhibitor	20uM
SC 00107026	KMT inhibitor	2uM
SC 00107028	KMT inhibitor	2uM
SC 00107024	KMT inhibitor	1uM
SC 00107037	PRMT inhibitor	100nM
SC 00107015	PRMT inhibitor	5uM
SC 00107035	KMT inhibitor	1uM
SC 00107023	KMT inhibitor	1.25uM
SC 00107029	KDM inhibitor	1uM
SC 00106834	KDM inhibitor	0.1uM
SC 00105914	KDM inhibitor	0.75uM
SC 00107050	Epigenetic reader domain targeting	120nM
SC 00107067	Epigenetic reader domain targeting	363nM
SC 00107063	Epigenetic reader domain targeting	0.5uM
SC 00107016	Epigenetic reader domain targeting	1uM
SC 00107054	Epigenetic reader domain targeting	50nM
SC 00106831	Sirtuin inhibitor	25uM
SC 00106957	Sirtuin inhibitor	0.3uM
SC 00082039	Sirtuin activator	5uM
SC 00106943	Other molecule	5uM
SC 00106940	Other molecule	20uM

Table 3.1.: Overview of 30 small molecules selected for further detailed study in proteomics and histone PTM analyses

3.6.3 Selected 30 compounds cluster in three distinct groups based on their effect on respiration and glycolysis

As previously discussed (Fig 3.15A, B), 30 inhibitors were selected out of 100 that were following certain criteria. Hierarchical clustering was performed to study the metabolic effects and potential correlations of drug type / cellular target group with downstream metabolic effects of the 30 selected inhibitors (Fig 3.16). The results of the seahorse XF experiments were normalised to control and transformed into log2 ratios and underwent hierarchical clustering followed by heatmap generation. Three distinct metabolic effect groups were identified using this approach. Interestingly, while in the original clustering of 100 drugs many chemical groups contributed to similar metabolic

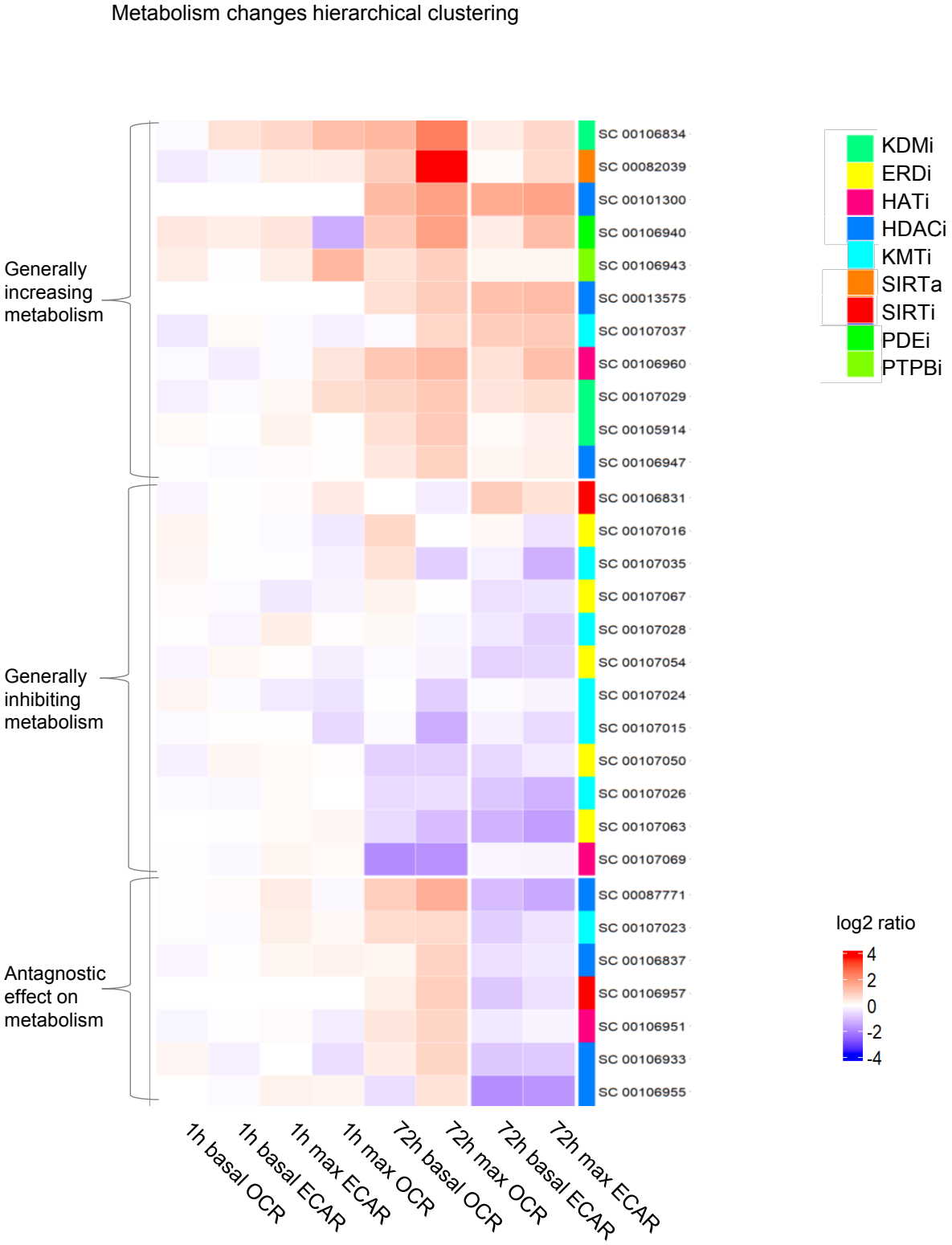

Figure 3.16. Selected 30 compounds clustered in three distinct groups based on their effect on respiration and glycolysis.

Hierarchical clustering and heatmap of 30 epigenetically-active compounds based on their metabolic profiles measured with seahorse XF. The results are normalised to DMSO (control). Upregulation in drug- vs DMSO-treated cells is indicated in red and downregulation is indicated in blue. All four measured mitochondrial stress test parameters from both 72h and 1h experiments are represented: basal OCR, basal ECAR, maximal OCR and maximal ECAR.

effects (Fig 3.14), heterogeneity of types of inhibitors grouped per metabolic effect group, was reduced to a minimum of 2 to 3 inhibitor classes for the selected 30 drugs (Fig 3.16). This may point to the notion that certain inhibitor classes could cause specific metabolic effects like the selected methyltransferase inhibitors which mainly caused a decrease to both glycolysis and oxidative phosphorylation comparing to the untreated cells (Fig 3.16). A potential reason for this more stringent outcome is that inhibitors with off-target effects and immediate (1h) effects that had a high likelihood of not mediating their cellular impact via chromatin mechanisms were not selected for this analysis of 30 drugs, therefore allowing for a more focussed and specific correlation analysis between cause and effect within the limited group of 30 inhibitors These promising results prompted a further investigation of the potential regulation of cellular metabolism by common epigenetic mechanisms.

3.6.4 72h treatments with epigenetic drugs cause a wide range of histone PTM changes

To investigate possible epigenetic mechanisms involved in inducing the observed metabolic changes I looked first into specific histone PTMs. Specifically, histone PTM changes induced by the 72h inhibitor treatments were analysed using mass spectrometry, focusing on H3 and H4 methylation and acetylation marks in HEK293T cells. Three biological replicates for each 72h treatment for all 30 inhibitors were performed and histones were extracted, separated and analysed using an online nano LC MS/MS QExactive system, as detailed in Materials and Methods (Chapters 2.4 and 2.6) Identification of the histone mass spec peaks was done using the skyline software and quantification was performed following a standard method developed by the Imhof group (Feller et al., 2015). Data quality analysis is depicted in Fig A.9 (Appendix), showing that while control samples showed very low inter-sample variability (Fig A.9A), the different compound treatments had much higher deviation from the PTM mean levels (Fig A.9A). Furthermore, some compounds elicited very large changes versus the control, both increasing or decreasing PTM levels vs control, while others were more similar to the control (Fig A.9B). To define PTMs that were significantly altered in the treated samples comparing to control, hierarchical clustering analysis of PTM changes was performed, and showed that the compounds were grouped into distinct subsets depending on their target and inhibitor classification. For instance (and as expected) HDAC inhibitors mainly increased acetylation marks and

were grouped next to each other, classic SET domain methyltransferase inhibitors SC00107024, SC00107026, SC00107028, induced anticipated PTM changes such as H3K27me3 and H3K27me2 decrease and unmodified H3K27 increase and were grouped in the same subset (Fig 3.17).

In contrast to HDACi and methyltransferase inhibitors, inhibitors of epigenetic reader domains, HAT and demethylase inhibitors showed a bigger variability of induced epigenetic marks within each chemical group. These results urged a further investigation of underlying epigenetic mechanisms involved in metabolic regulation, since various epigenetic marks were found associated with similar metabolic activity. It was also not clear if the epigenetic marks induced affected transcription and protein levels of specific proteins, which then could be the mediators of induced metabolic changes. To examine this, whole proteome analysis was performed to monitor changes induced by the selected inhibitors.

3.6.5 Based on their effect on the whole cell proteome, epigenetically-active drugs can be clustered in four distinct groups

To investigate the role of specific proteins and epigenetic enzymes in the regulation of metabolic activity, proteome changes due to inhibitor treatments were investigated (see chapters 2.5 & 2.6). Whole proteome analysis before and after a 72h treatment with the selected 30 inhibitors resulted in the identification of more than 5000 proteins. Protein changes were clustered in 4 major groups (Fig 3.18 and 3.19). Cluster 1 and 2 contained proteins that were altered due to HDAC inhibitor treatment. Interestingly, protein IDs included ZNF292 and CPT1A which are downstream of HIF1A and found to regulate glycolysis in different studies (O. Xia et al., 2009a; C.-H. Yao et al., 2018). Additionally, clusters 1 and 2 contained proteins that were affected by HAT inhibitor treatment. Proteins changed after methyltransferase inhibitor treatments were clustered in groups 1,2 and 4 whereas proteins affected from demethylase inhibitor treatment were clustered in groups 3 and 4. Interestingly, proteins differentially expressed due to epigenetic reader domain inhibitor treatments were mainly clustered in group 4. Proteins enriched in group 4 included AFF4 which is interacting with HIF1A related targets (Galbraith et al., 2013). In comparison to the initial metabolic screening analysis, hierarchical clustering of both histone PTMs and whole proteome changes presented that

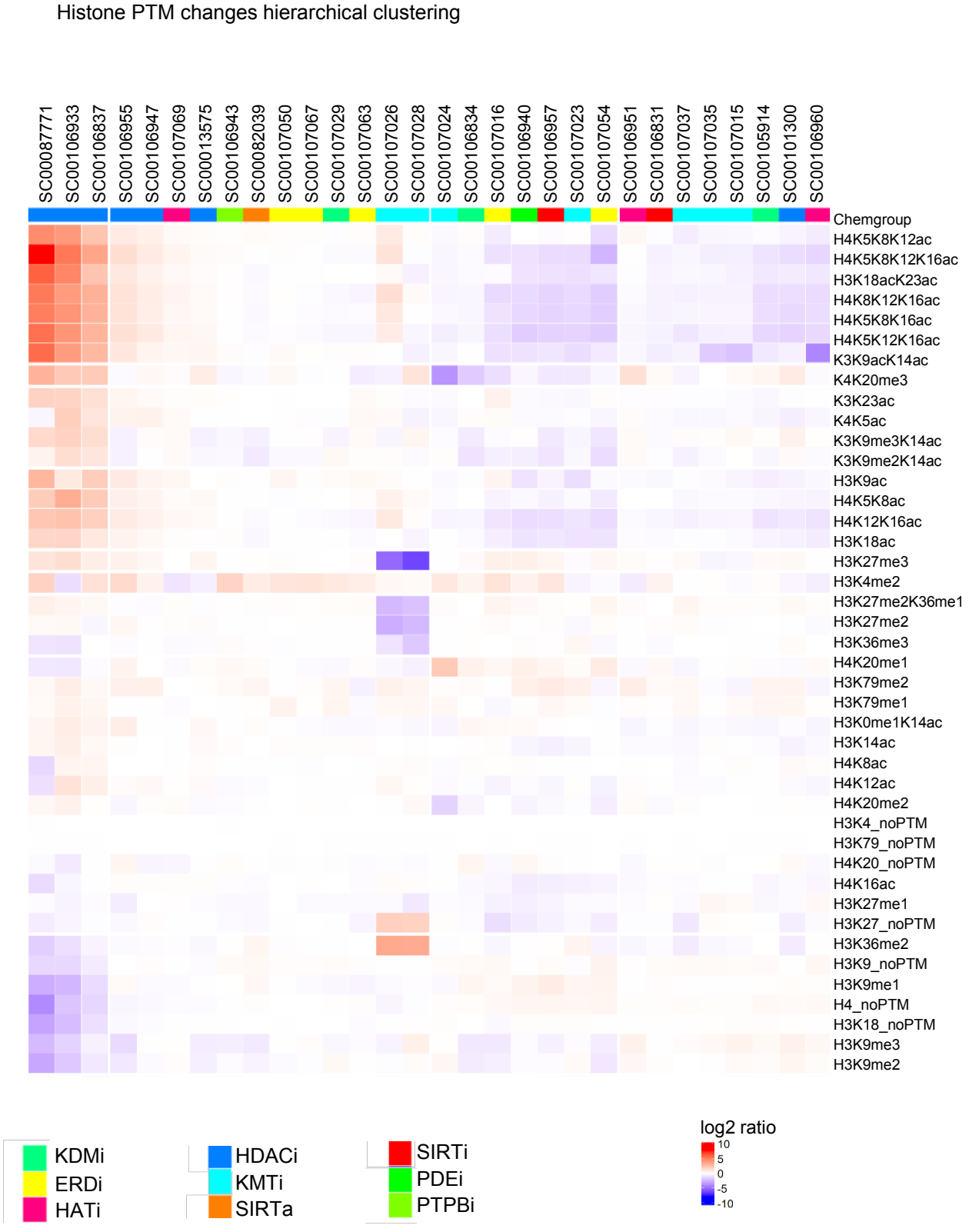

Figure 3.17. 72h treatments with epigenetic drugs caused a wide range of histone PTM changes. Hierarchical clustering and heatmap of histone H3 and H4 methylation and acetylation changes induced by 30 epigenetically-active drugs. The results are normalised to DMSO (control). Upregulation in drug- vs DMSO-treated cells is indicated in red and downregulation is indicated in blue. N =3 biological replicates.

Figure 3.18. Based on their effect on the whole cell proteome, epigenetically-active drugs could be clustered in four distinct groups.

Hierarchical clustering and heatmap of proteomic changes induced by 30 selected epigenetically-active drugs. Upregulation of proteins is indicated in red and downregulation of proteins is indicated in blue. Minimal log2 fold-change threshold for analysis was 1.11.

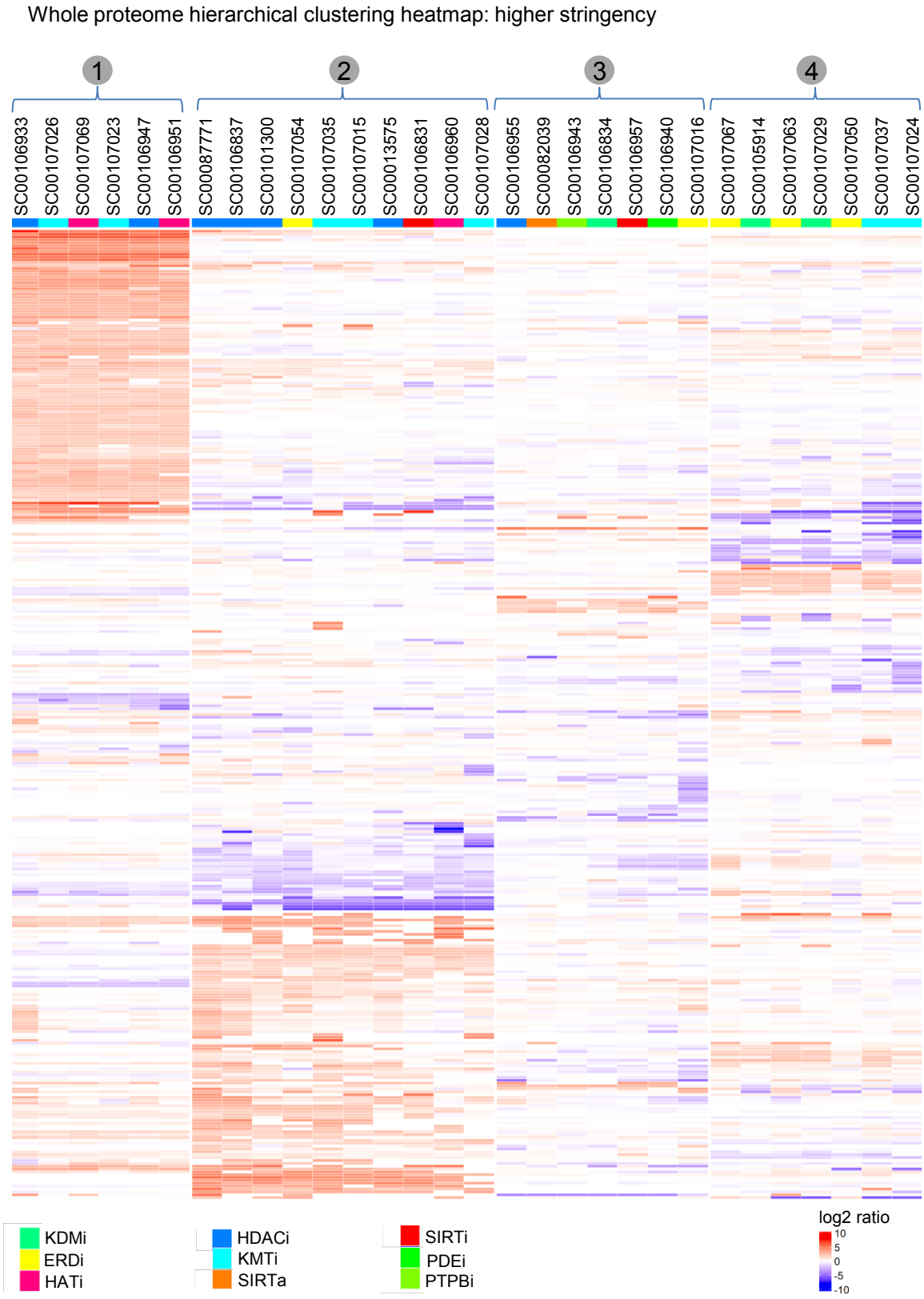

Figure 3.19. Based on their effect on the whole cell proteome, epigenetically-active drugs could be clustered in four distinct groups – also at higher analysis stringency.

Hierarchical clustering and heatmap of proteomic changes induced by 30 selected epigenetically-active drugs. Upregulation of proteins is indicated in red and downregulation of proteins is indicated in blue. Minimal log2 fold-change threshold for analysis was 1.55.

there might be overarching themes across the drug induced changes and possible antagonistic effects within the same chemical drug groups. These initial promising results prompted a further analysis for each of the chemical groups with greater emphasis on identifying histone PTM patterns as well as protein candidates that could have a relevant effect on epigenetics or metabolism (Chapter 3.7 and 3.8, as well as Discussion Chapter 4.1).

3.7 Analysis of interplay between histone modifications, proteomic changes and metabolic phenotype in different chemical drug classes

3.7.1 HDAC inhibitors

In order to better understand the specific effect HDAC inhibitors may have on epigenetic marks and metabolism, the hierarchical clustering was performed selectively for all 7 HDAC inhibitors. Both the metabolic and histone PTM analysis showed emergence of two different large clusters of response to HDAC inhibitor treatments (Fig. 3.20, A and B). In particular, a group of 4 HDAC inhibitors (SC00106933 targeting class I HDAC1; SC00106955 targeting class I HDAC1/2; SC00087771 targeting class I HDAC1/3 and class IV HDAC11; SC00106837 targeting class IIA HDAC4) decreased glycolysis while increasing oxidative phosphorylation (Fig 3.20A, four HDAC inhibitors from the left). Interestingly, three out of these four (SC00106933, SC00106837, SC00087771) also behaved the same way in the histone PTM analysis (Fig. 3.20, B, three inhibitors from the right): all three of them significantly increased cellular levels of transcription-promoting histone PTMs such as histone acetylation, while decreasing major repressive marks such as H3K9me3. This observation could potentially point to a correlation between generally higher levels of transcription (high histone acetylation, low repressive histone methylation) and suppression of glycolysis. Behaving differently, three HDAC inhibitors caused less pronounced effects on histone PTMs (Fig. 3.20B, left side). Of those three, two (SC0013575, SC106947) which both target class I (HDAC1, HDAC3) showed the same pattern in the histone PTM analysis, but with generally very mild effects.

One of the seven HDAC inhibitors, SC00101300, behaved differently from all the others, showing different results in the histone PTM analysis, causing a global reduction of H3/4 acetylation

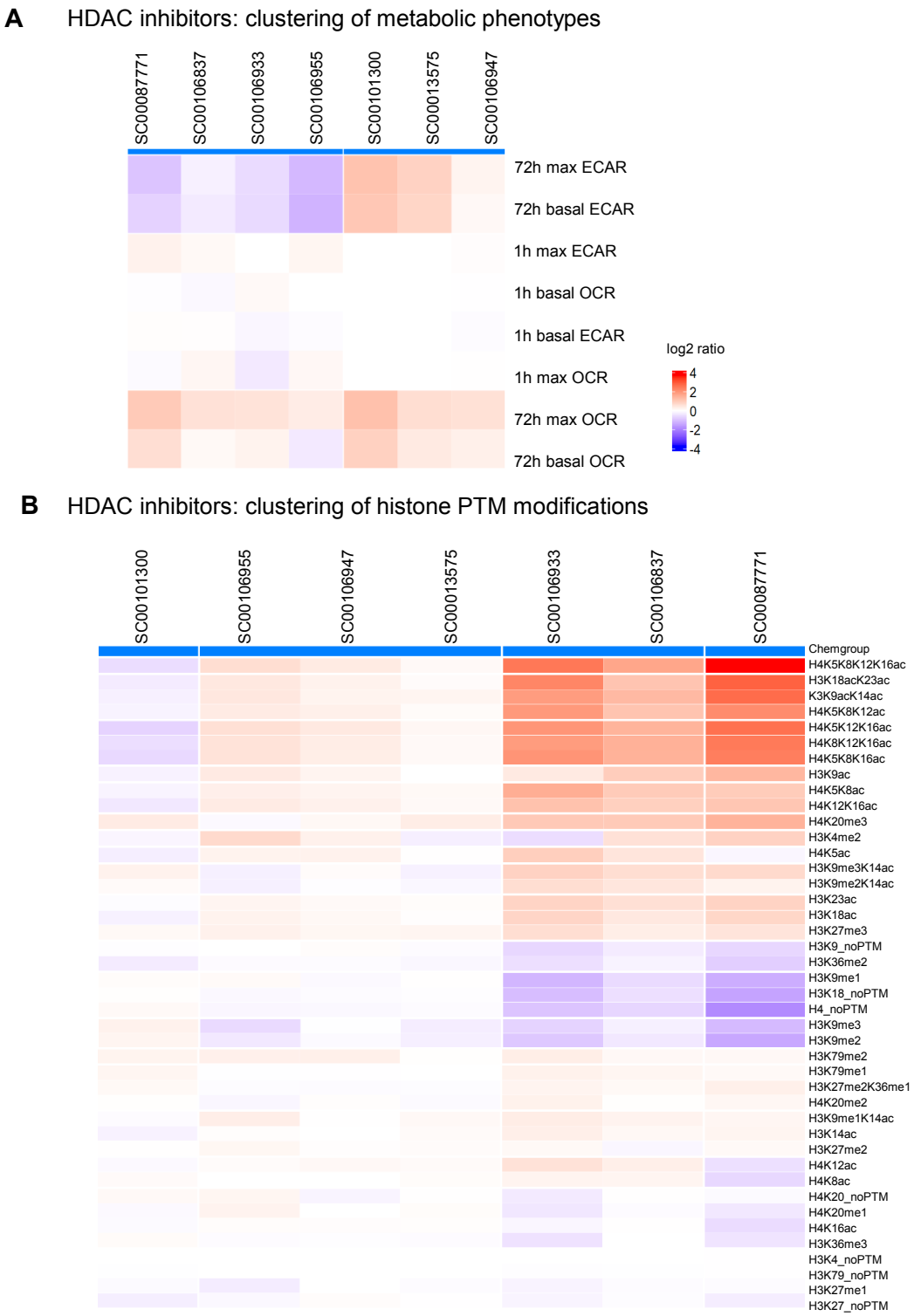

Figure 3.20. HDAC inhibitor treatments of HEK293T cells caused correlating formation of distinct metabolic and PTM phenotype clusters.

A. Hierarchical clustering an heatmaps of the selected HDAC inhibitors. 72h treatments with selected HDAC inhibitors induced metabolic changes, while 1h treatments did not lead to significant effects comparing to control.

B. 72h treatments with selected HDAC inhibitors induced histone PTM changes comparing to control. Three apparent clusters could be identified.

(Fig. 3.20B, left). Indeed, it is the only tested selective HDAC class IIA inhibitor, targeting HDACs 4/5/7/9 (Lobera et al., 2013). Importantly, it has previously been shown that SC00101300 does not increase acetylation of histone H3 and H4, but rather increases acetylation of H1 and H2A/H2B (Choi et al., 2018; Su et al., 2020). Although it is known that H1 and H2A/H2B can be heavily modified, I am not aware of research that has been published on linking acetylation of H1 and H2A/H2B with metabolic regulation. Moreover, it has been shown that class IIA HDACs are present in the cytoplasm, shuttling between cytoplasm and nucleus, in contrast to the class I HDACs which are nuclear and class IIB which are cytoplasmic (Verdin et al., 2003). Interestingly, HDAC4 acetylates lysine residues on HIF1A and regulates hypoxia and cancer (Geng et al., 2011) and inhibition of class IIA inhibitors decreased HIF1A acetylation (Qian et al., 2006). Therefore, the observation of this unusual behaviour could be explained by the different targeting activity of this specific inhibitor on HDAC class IIA in contrast to the other HDACs. Furthermore, this "outlier" result uncovered a potentially new role of H1/H2 acetylation in metabolism (which due to the experimental design was not measured in the histone PTM work) which could be the basis for further analysis in the future.

In conclusion, the experiments with HDAC inhibitors showed that all HDAC inhibitors increased oxidative phosphorylation. However, only the subset of HDAC inhibitors that caused strong hyperacetylation of H3/4 caused reduction of repressive methylation marks and a downregulation of glycolytic activity. This observation is important as employing HDACs to reverse the Warburg effect would therefore only be efficient for the 4 HDAC inhibitors with this specific profile. On the contrary, HDAC inhibitors that do not result in expected acetylation changes could even be detrimental by further increasing glycolysis, therefore supporting the Warburg effect and tumour growth.

To link the direct epigenetic effect of inhibitors with the downstream physiological effect, the proteomic changes were analysed. Overall, in line of the HDAC inhibitors' strong effect on metabolism, metabolism-related proteins were generally highly enriched. The STRING database (version10.0) was used for the enrichment analysis for biological processes, cellular components and molecular functions for the proteins identified from the proteomics analysis (only biological processes enrichment is shown, Fig. 3.21). The significantly enriched annotation terms that are summarised in

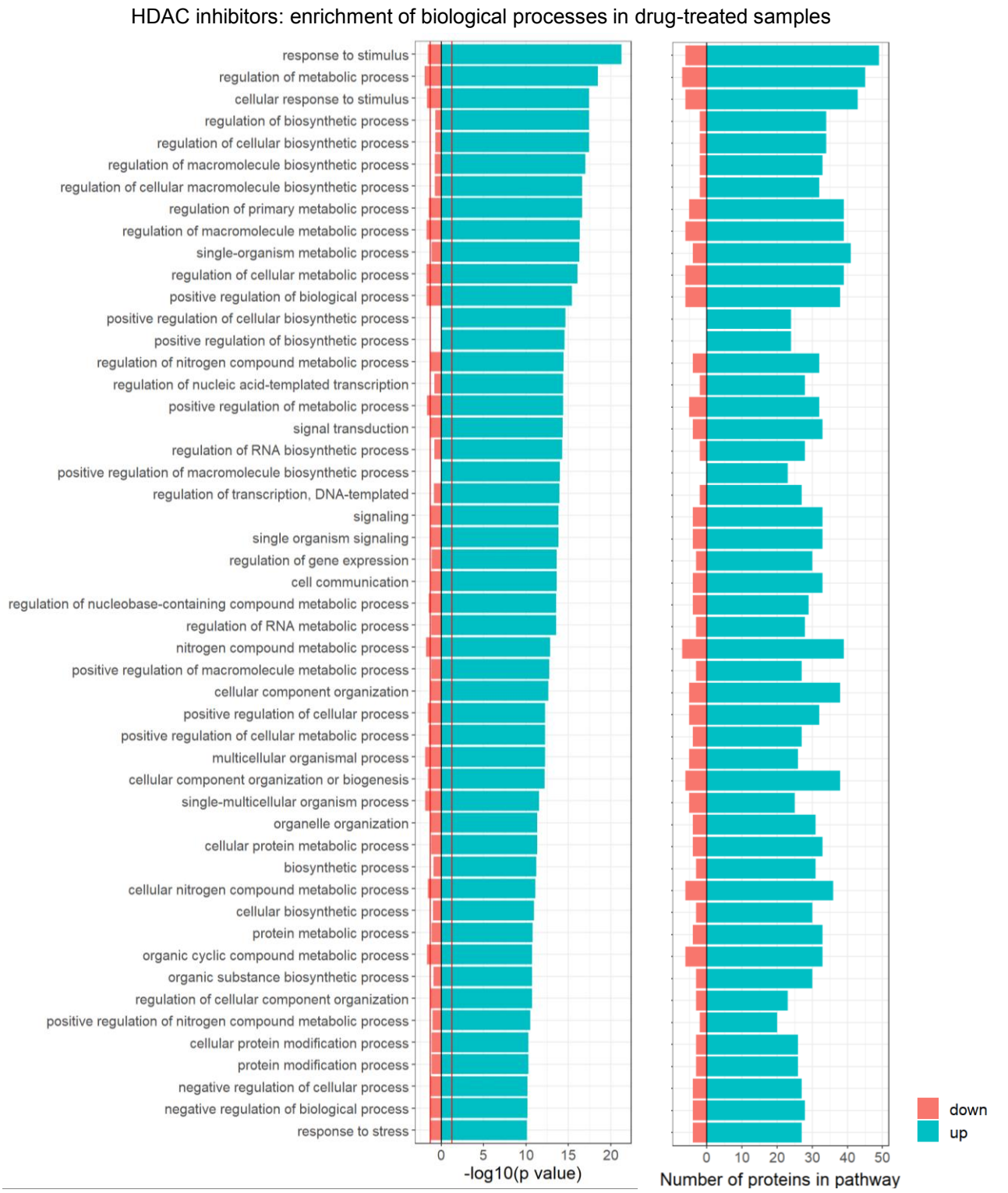

Figure 3.21. HDAC inhibitor treatment caused significant upregulation of metabolic pathways. Enrichment analysis of HEK293T cells treated with HDAC inhibitors. Enrichment analysis is based on the set of proteins differentially expressed across the seven HDAC treatments (minimal log2 fold-change threshold for analysis 1.11) using biological process terms. Enriched terms were ranked based on their statistical significance (-log10 p-value, left). The corresponding number of differentially expressed proteins per biological process is depicted on the right part of the figure.

Fig 3.21 showed $p<0.05$. Interestingly, many regulators of metabolism were affected, such as chromatin remodelling enzymes, transcription factors and signal transduction proteins.

The hierarchical proteome clustering on protein level resulted in four separate groups (Fig. 3.22). Here, it became apparent that the distinctions between groups are finer than on the histone PTM level: the right-most HDAC inhibitor "cluster 4" (SC00106837, SC00087771) caused the same PTM and metabolic effects, linked by a similar proteomic profile. Furthermore, the HDAC inhibitor "cluster 3", comprising SC00101300 and SC0001375 caused same PTM and metabolic effects. Whereas the proteomic profiles looked similar, they were associated with very different effects on metabolism (down vs upregulation of glycolysis). One potential explanation for this observation may be that in contrast to global PTM analyses, changes of the levels of a few critical proteins can have a significant impact on physiological functions. In line with this hypothesis, several proteins linked to the regulation of metabolism were enriched in either cluster 3, or cluster 4 – suggesting that those transcription factors and chromatin regulators could be involved in switching between high or low glycolysis (Fig. 3.23). For example, proteins ZNF292 and CPT1A are known to be involved in metabolic processes although their role is not fully uncovered yet (see Chapter 3.6.5). It has previously been shown that they are downstream of HIF1A and under hypoxic conditions CPT1A is downregulated (Fillmore & Lopaschuk, 2013; D. A. Nicholas et al., 2019; C.-H. Yao et al., 2018) and ZNF292 is upregulated (Del Rey et al., 2017; Nauta et al., 2017; O. Xia et al., 2009b), leading to increased glycolysis. In this current work, CPT1A was increased and ZNF292 was decreased after HDAC inhibitor treatments (cluster 4) which was associated with decreased glycolysis (Fig 3.20-23). Interestingly, hypoxia-induced key factors HIF1A and HIF2A were not enriched in the proteomic samples of this study. This observation suggests that these two factors (ZNF292, CPT1A) may independently act of HIF1A/HIF2A under normoxia and may play a role in regulating metabolism by upregulating glycolysis. Moreover, there were another 9 HIF-associated proteins enriched in cluster 4. In cluster 3, five different HIF-associated proteins were enriched. GUF1 and ADIPOR1 were downregulated versus control, both of which are HIF induced and shown to increase glycolysis which is in line with the current findings (Mora-García et al., 2017; Zhu et al., 2018) (Fig 3.23). The activation of a glycolysis-promoting partial HIF network by cluster 4 HDAC inhibitors may therefore contribute to the specific observed metabolic results and

Figure 3.22. HDAC inhibitor treatments of HEK293T cells caused significant changes in whole proteome with three types of patterns observed across the seven compounds.
Hierarchical clustering and heatmap of protein level changes after treatment with selected HDAC inhibitors. Minimal log2 fold-change threshold for analysis was 1.11.

HDAC inhibitors: identified proteins with at least 3-fold change comparing to control cluster 3 and 4

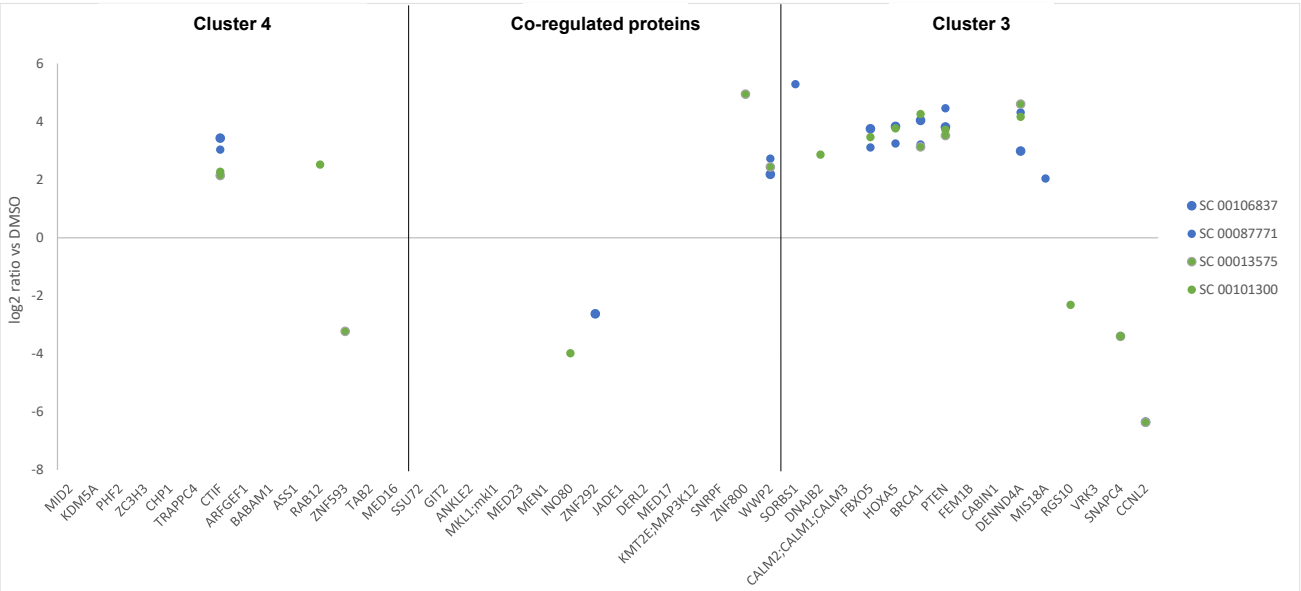

Figure 3.23. Detailed depiction of proteins most affected by HDACi treatments revealed highly changed proteins between "cluster 3" and "cluster 4" which appeared superficially similar based on whole-proteome hierarchical clustering heatmaps (Fig. 3.22)

Enrichment analysis of HEK293T cells treated with HDAC inhibitors. Enrichment analysis is based on the set of proteins differentially expressed across the seven HDAC. Depicted are proteins that showed the largest fold-change vs the control samples upon inhibitor treatment

would warrant further investigation, as naturally the focus of research on HIF network/metabolism-regulation has been on its effect under hypoxic conditions.

Although all the discussed HDAC inhibitors affected some parts of the HIF regulatory network, the particular components activated differ between clusters 3 and 4. Indeed, HDACs are important for HIF activity and are positive regulators of HIF stability (S. Kim et al., 2007; Sang & Chen, 2011; Schoepflin, 2016). The HIF pathway plays an important role in tumor metabolism by modulating Warbung effect and HIF-induced glycolysis under hypoxia leads to tumor cell survival (Courtnay et al., 2015; Dabral et al., 2019; Semenza, 2007; L. Xia et al., 2020). Cancer treatments inducing the Warburg effect through increased glycolysis such as HDAC inhibitors SC00101300 and SC0001375 may therefore elicit undesired side-effects that promote tumor survival. On the other hand HDAC inhibitors repressing HIF activity may be better candidates to address drug resistance and metastasis potential.

3.7.2 HAT inhibitors

Three HAT inhibitors were selected from the initial metabolic screening. The metabolic profiling showed three different responses, with each HAT inhibitor causing a different metabolic effect.

SC00106960, an inhibitor of p300/CBP and SC00107069, a selective Tip60 inhibitor (MYST family of HATs), caused opposite metabolic effects (Fig 3.24A). While SC00106960 increased both oxidative phosphorylation and glycolysis after 72h, SC00107069 decreased both metabolic readouts after 72h. Interestingly, these two inhibitors also induced a range of different PTM marks (Fig 3.24B). This in turn could result in different protein expression profiles between these two drugs. In line with this, the proteomics analysis of SC00107069 and SC00106960 showed very diverse profiles of enriched proteins (Fig 3.25). In contrast to other drug classes, the HAT inhibitors showed some 1h metabolic effects (Fig 3.24A). These 1h effects caused by SC00106960 and SC00107069 could potentially be explained by the fact that p300/CBP and Tip60 have been found to regulate a number of

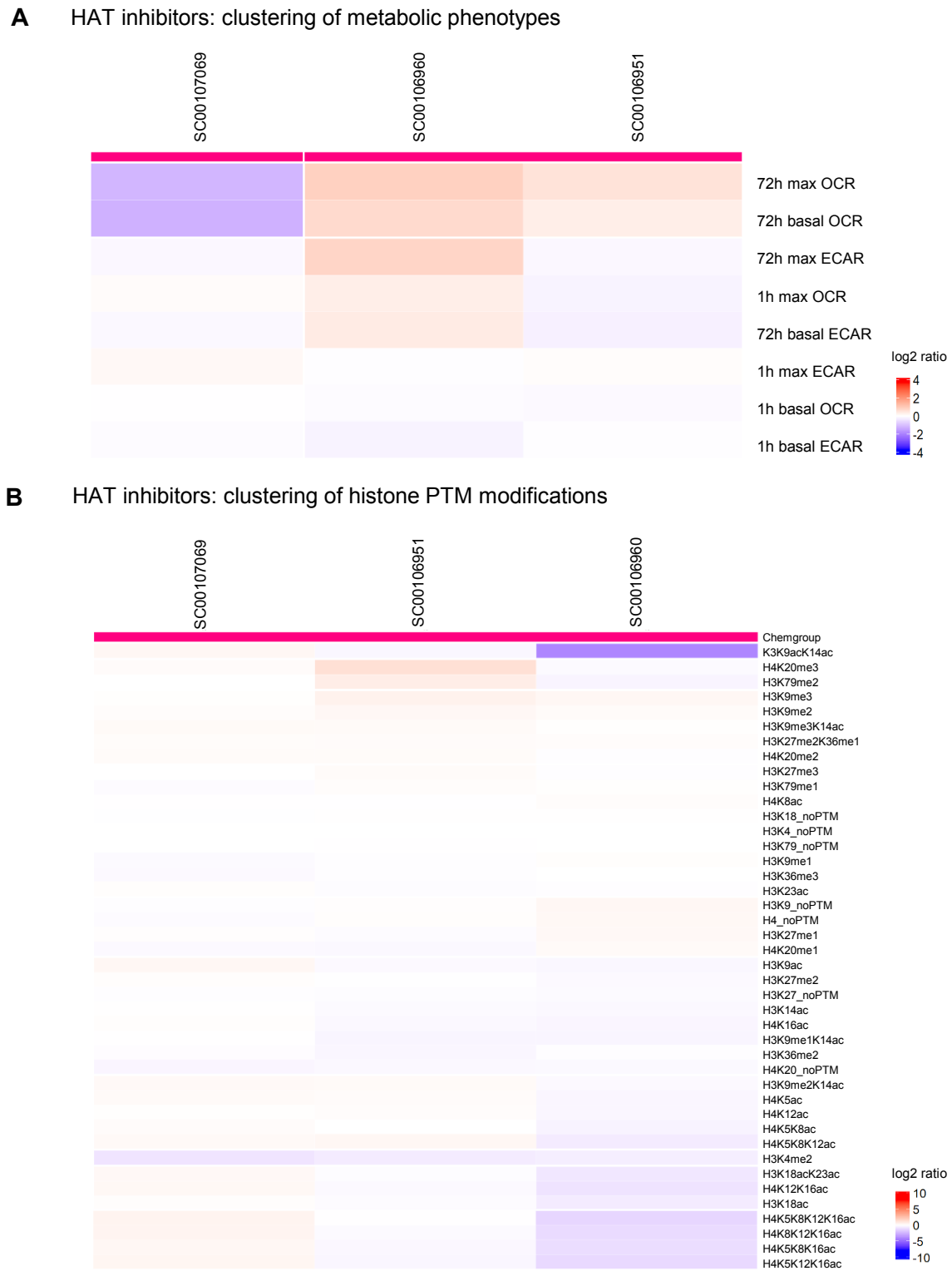

Figure 3.24. HAT inhibitor treatments of HEK293T cells caused correlating formation of distinct metabolic and PTM phenotype clusters.

A. Hierarchical clustering an heatmaps of the selected HAT inhibitors. 72h treatments with selected HAT inhibitors induced metabolic changes. In the case of 6960 and 6951, 1h treatments lead to altered metabolic effects comparing to control.

B. 72h treatments with selected HAT inhibitors induced histone PTM changes comparing to control.

Figure 3.25. HAT inhibitor treatments of HEK293T cells caused significant changes in whole proteome with two types of patterns observed across the three compounds.
Hierarchical clustering and heatmap of protein level changes after treatment with selected HAT inhibitors. Minimal log2 fold-change threshold for analysis was 1.11.

non-histone proteins, including metabolic enzymes in nucleus and cytoplasm without the intermediate step of transcription regulation (Guan & Xiong, 2011; Xiong & Guan, 2012).

Active transcription-associated H3K4me2 was decreased by all three inhibitors which is in line with repressive function of HAT inhibitors. Interestingly, H3K4-specific demethylase KDM5A was increased more than 40-fold in SC00106951 and SC00107069 (not identified in SC00106960 which had the weakest decrease of H3K4me2 vs control). This is similar to the observation in HDAC inhibitor-treated samples where higher levels of KDM5A were associated with lower levels of H3K4me2 and inhibition of glycolysis.

SC00106960 treatment significantly reduced acetylation of transcription-associated H3K9 and H3K14, while causing a slight increase of repressive H3K9me2/3 (Fig. 3.24B). A similar effect on the relative levels of H3K9ac versus H3K9me2/3 was observed in SC00106951, albeit to a slightly lower degree comparing to SC00106960.

A main writer of H4 acetylation, JADE1, was found more than 20-fold upregulated in SC00107069. JADE1 was not changed in SC00106951 vs control and it was not identified in the SC00106960 samples. In line with this, increased acetylation of H4 sites was detected only in the case of SC00107069. This unexpected increase of some histone acetylation in a HAT-inhibitor treated sample could therefore potentially be traced to induced overexpression of a non-targeted HAT, potentially as a compensatory mechanism. A similar effect has been described upon ablation of specific HAT enzymes in *Drosophila* cells (Feller et al., 2015).

SC00106951, an inhibitor of NAT10 (GNAT family of HATs), showed a different metabolic response compared to the other two HAT inhibitors, exhibiting an antagonistic metabolic profile, similar to some HDAC inhibitors discussed before (Chapter 3.7.1). Interestingly, two histone modifications were highly increased only in the case of SC00106951 – namely H3K79me2 and H4K20me3. Interestingly, these two modifications – especially H4K20me3 – were also significantly increased in the group of three HDAC inhibitors that induced the same antagonistic metabolic effect as SC00106951, leading similarly to increased oxidative phosphorylation and decreased glycolysis (SC0087771, SC00106837, SC00106933 – see Fig. 3.20A, B).

Surprisingly, the treatment-induced proteomic changes for SC00106951 were similar to SC00107069 (Fig 3.25, Fig 3.26) and showed a significant enrichment for proteins involved in transcription, lipid and fatty acid homeostasis. Importantly, several of the proteins with the highest change of protein levels upon HATi-treatment were affected in the same direction and extent by SC00106951 and SC00107069 (Fig 3.27). In particular, mediator complex proteins MED23, MED16 and MED17 were significantly increased after treatment with these two inhibitors (at least 4 fold increase comparing to control) but unchanged to control in SC00106951. The mediator complex subunit MED16 transduced NRF2-activating signals into antioxidant gene expression (Sekine et al., 2016). Moreover, other mediator complex components including MED1, MED14, and MED23 are required for the development of adipocytes, lipid homeostasis, glucose and lipid metabolism (Chu et al., 2014; Ge et al., 2002; Iida et al., 2015; Jia et al., 2004, 2009; Toth et al., 2004; W. Wang et al., 2009). MED23 is required for MAPK/ELK signalling which regulates Krox20,a transcription factor induced in an insulin- triggered adipogenesis cascade (G. Wang et al., 2005; W. Wang et al., 2009). MED15, CDK8 and CycC are involved in SREBP-mediated gene transcription and subsequent de novo lipogenesis (F. Yang et al., 2006). SREBPs transcriptional activity is controlled through recruiting specific transcriptional cofactors, including the mediator complex (Näär et al., 1999; F. Yang et al., 2006) and CBP/p300 (Giandomenico et al., 2003), which is inhibited by SC00106960. Additionally, mediator has been involved in other aspects of metabolism, including fatty acid oxidation, phospholipid biosynthesis, and bile acid metabolism. TAB2, adapter protein which is needed to activate TAK1 (Omori et al., 2012) which is also involved in the lipid regulation via SREBP (Sho Morioka1 et al., 2016) was also enriched after treatment with these two drugs. Interestingly by inhibiting CBP/p300 with SC00106960 mediator complex subunits and TAB2 where either not identified or significantly downregulated. Although fatty acid metabolism was not measured in the seahorse XF experiments, the proteome analysis suggested that while proteins of fatty acid degradation were almost not altered in both SC00107069 and SC00106951, they were significantly decreased in SC00106960 comparing to control (Fig 3.28). Interestingly, cells treated with SC00106960 had very high levels of glycolysis and oxidative phosphorylation, which could suggest that this treatment induces increased reliance on glycolysis instead of fatty acid metabolism for energy generation. Similarly, proteomic changes for

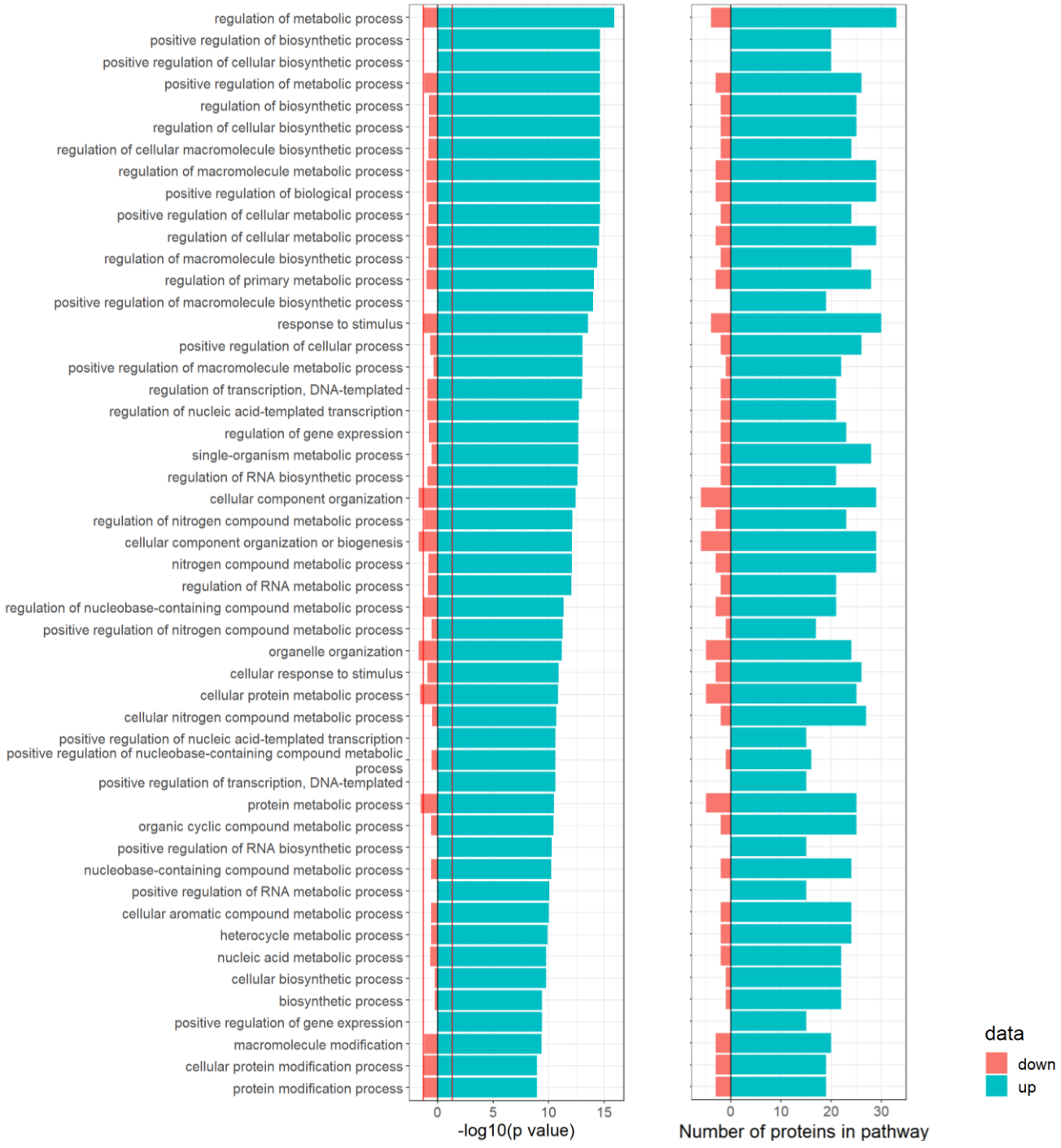

Figure 3.26. HAT inhibitor treatments causes significant upregulation of metabolic pathways
Enrichment analysis of HEK293T cells treated with HAT inhibitors. Enrichment analysis is based on the set of proteins differentially expressed across the three HAT treatments (minimal log2 fold-change threshold for analysis 1.11) using biological process terms. Enriched terms were ranked based on their statistical significance (-log10 p-value, left). The corresponding number of differentially expressed proteins per biological process is depicted on the right part of the figure.

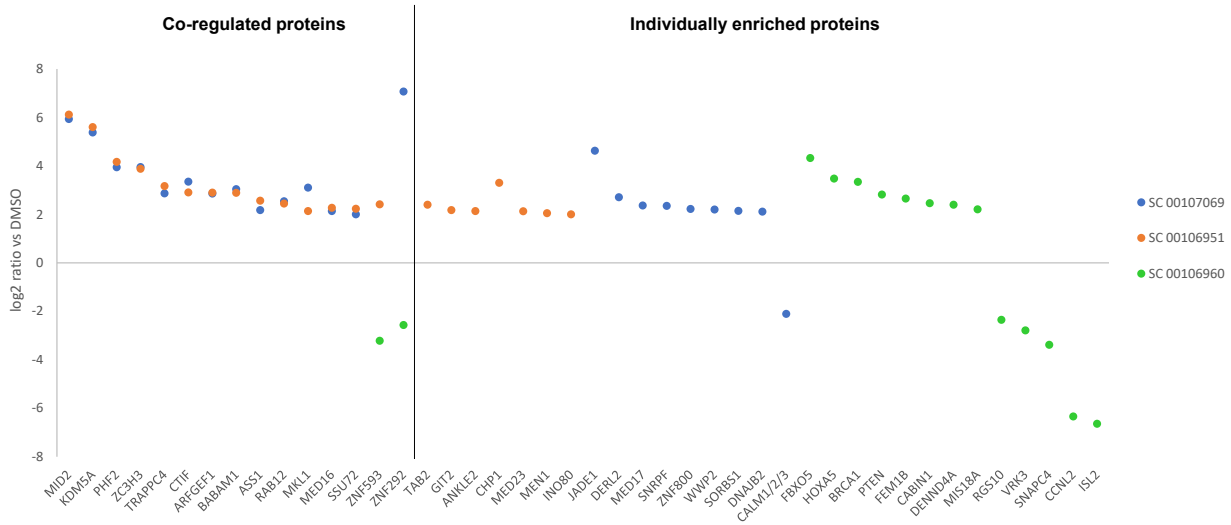

Figure 3.27. Several of the most-differentially expressed proteins overlapped between HATi treatments SC00106951 and SC00107069.

Enrichment analysis of HEK293T cells treated with HAT inhibitors. Enrichment analysis is based on the set of proteins differentially expressed across the HAT treatments. Depicted are proteins that showed the largest fold-change vs the control samples upon inhibitor treatment

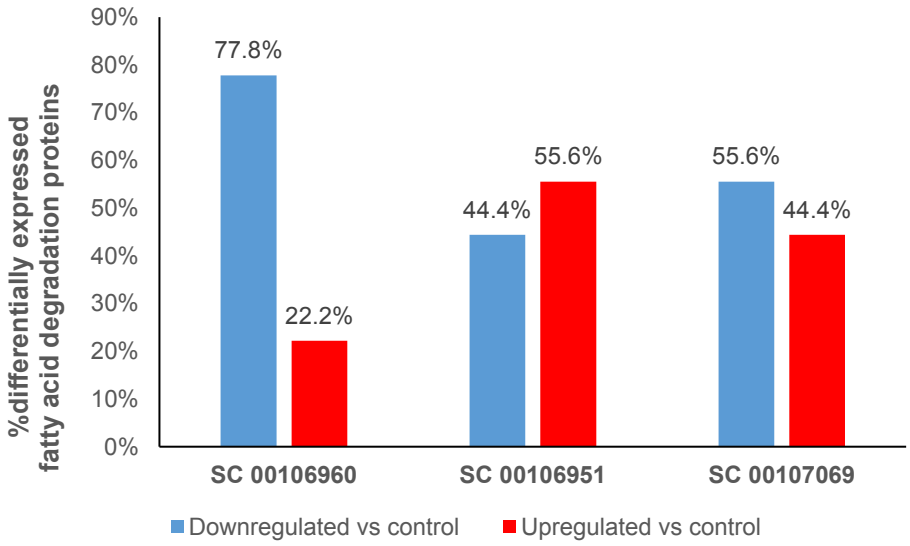

Figure 3.28. HAT inhibitor SC00106960 mostly downregulated fatty acid metabolism proteins
Enrichment analysis of HEK293T cells treated with HAT inhibitors. Enrichment analysis is based on the set of proteins differentially expressed across the three HAT treatments (minimal log2 fold-change threshold for analysis 1.11) using biological process terms. The number of up- or downregulated proteins belonging to fatty acid degradation pathways was counted as fraction of all proteins in the pathway.

fatty acid biosynthesis and elongation were also opposite: the two similarly behaving drugs SC00107060 and SC00106951 induced a strong upregulation of fatty acid biosynthesis proteins compared to SC00106960 which presented almost no change in fatty acid biosynthesis enzyme levels (not shown). In conclusion, these results demonstrated that HAT inhibitors may be implicated not only in glycolysis and oxidative phosphorylation, but that those metabolic phenotypes also extend to fatty acid metabolism, although this hypothesis remains to be demonstrated in future experiments. In the set of treatments, high induced levels of glycolysis correlated with higher levels of fatty acid degrading enzymes (SC00106960), while on the other hand, inhibition of glycolysis was associated with higher levels of fatty acid biosynthesis enzymes (SC0010760, SC00106951).

3.7.3 Methyltransferase inhibitors

Seven methyltransferase inhibitors were selected after the initial metabolic screening for further analysis of induced histone PTMs and protein changes. Interestingly, three metabolic groups were identified. The majority of the drugs caused a decrease of maximal oxidative phosphorylation and glycolysis with almost no effect on the basal oxidative phosphorylation rates (Fig. 3.29A). Only one drug, SC00107037, a PRMT5 inhibitor, increased the maximal oxidative phosphorylation and glycolysis after 72h treatment. One more drug, SC00107023 which is a KMT5A inhibitor, increased oxidative phosphorylation and decreased glycolysis. Interestingly, all SET domain- containing methyltransferase inhibitors decreased maximal respiration capacity and glycolysis (Fig. 3.29A).

When looked on the histone PTM marks induced by the inhibitor treatments three groups were identified (Fig. 3.29B). One group containing SC00107024 and SC00107037, a second group containing SC00107035, SC00107015, SC00107023, and a third group containing SC00107026 and SC00107028. The inhibitors SC00107026 and SC00107028 induced almost the same marks, in line with them both targeting the same enzymes - KMT6A and KMT6A/B respectively. More specifically, KMT6 (EZH2) targets H3K27me1/2/3 and after treatment with the respective inhibitors there was a significant decrease of these methylation marks. The major difference between both inhibitors was that SC00107026 presented a significant increase of all H4 related acetylation marks. In the case of SC00107028, H3K9me2/3 was increased compared to control, while in the case of SC00107026 was

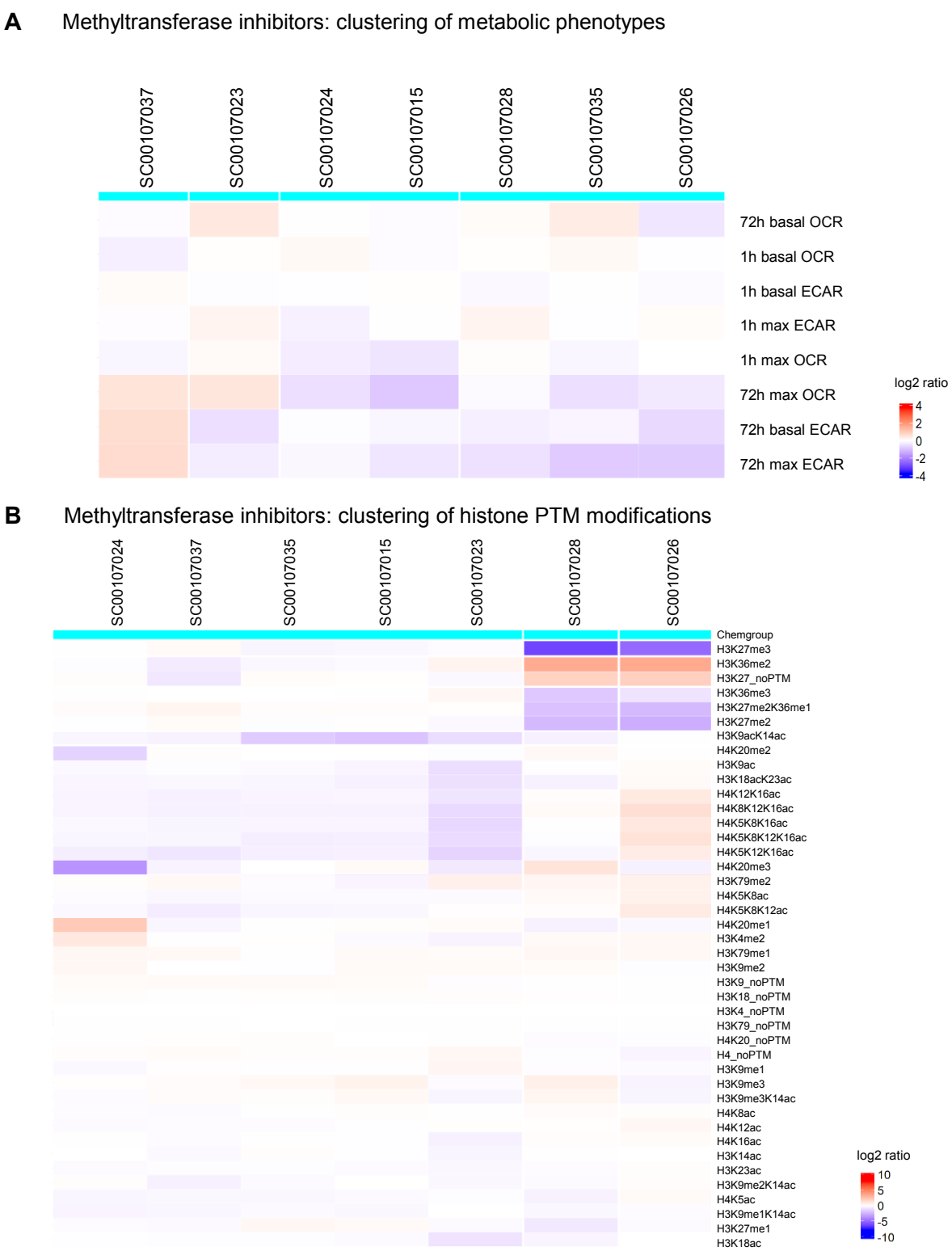

Figure 3.29. Methyltransferase inhibitor treatments of HEK293T cells cause correlating formation of distinct metabolic and PTM phenotype clusters.

A. Hierarchical clustering an heatmaps of the selected methyltransferase inhibitors. 72h treatments with selected methyltransferase inhibitors induced metabolic changes, while 1h treatments did not lead to significant effects comparing to control.

B. 72h treatments with selected methyltransferase inhibitors induced histone PTM changes comparing to control. Three apparent clusters could be identified.

slightly decreased. In the case of SC00107028, H4K20me1 was decreased, H4K20me2/3 were increased but not in the SC00107026. One potential reason could be that SC00107028 also targets EZH1. EZH1 displays weaker effects on H3K27me1/2/3 than the EZH2 and can only partially compensate to H3K27me3 after loss of EZH2 (Holoch & Margueron, 2017; N. Liu & Zhu, 2017). EZH1 binds directly on nucleosomes in contrast to EZH2 that requires JARID2 to do so. Thus, EZH1 holds a compaction ability of chromatin as it binds tighter to it in contrast to EZH2 that lacks this characteristic (Holoch & Margueron, 2017; N. Liu & Zhu, 2017). In addition, EZH1 can also form a non-canonical PRC2 complex that is associated with active transcription (Bowen Xua, Kyle D. Konzeb, Jian Jinb, 2015; Henriquez et al., 2013; Riising & Helin, 2012; Stojic et al., 2011). Another intriguing but controversial issue would be the tissue-specific compensation of EZH2 activity by EZH1 and restoration of the H3K27me3 mark in a selection of EZH2 target genes (Weipeng Mu, Joshua Starmer, Yoichiro Shibata, Della Yee, 2017). As the relative Kd of SC00107028 for EZH1 and EZH2 in HEK293T cells is not known, it is possible that the observed fewer protein changes in SC00107028 comparing to SC00107026 are explained by this inhibitor targeting primarily or at least to a stronger degree EZH1. Interestingly, It has been indicated that the oncogenic protein EZH2 positively regulates HIF1A which in turn stimulates glycolysis, contributing to the Warburg effect and progression of tumorigenesis(Pang et al., 2016). In this study, there was decreased glycolysis after inhibitor treatments with SC00107028 and SC00107026 which might be linked to inhibition of EZH2.

Interestingly, SC00107024, a KMT5B/C (writer of H4K20me2/3) inhibitor, reduced H4K20me2/3 (Fig. 3.29B). KMT5B (Suv4-20h1) targets H4K20me1 and H4K20me2 to form H4K20me3. In line with this, inhibition of KMT5B/C led to an increase of H4K20me1 comparing to control, as the cellular steady state balance shifted from the (often described as transcriptionally repressing, see Discussion Chapter 4.1) di- and trimethylated form of H4K20 to the (often described as transcriptionally activating, see Discussion Chapter 4.1) mono-methylated H4K20 (H4K20me1 is substrate but cannot be generated by KMT5B). KMT5B mainly acts as a transcriptional repressor in context to H4K20me1/2/3-regulated genes (Faundes et al., 2018). Moreover, H3K4me2, representing a specific tag for epigenetic transcriptional activation, was increased by SC0010724. In a clinical study, H3K4me2 and H4K20me1/2/3 were looked at as possible prognostic coregulated marks for various

cancer types (Schneider et al., 2011). Taken together, while the connection between H3K4me2 and H4K20me1 is not yet fully explained, treatment with SC00107024 showed that these activating transcription marks may be connected which warrants further investigation in the future.

On the other hand, SC00107023 an inhibitor of H4K20 monomethyltransferase KMT5A (SETD8), showed H4K20me1 and H4K20me2 equal to control and only H4K20me3 was reduced. Although this was unexpected, it has been shown by others that SC00107023 may not fully inhibit KMT5A, while another methyltransferase MMSET/NSD2 may be taking the role of monomethylating H4K20 when SETD8 is inhibited (Gursoy-Yuzugullu et al., 2017).

The last of the lysine methyltransferases targeted with inhibitors in this study, KMT3C (SMYD2), catalyses H3K4me3 and H3K36me2 (Hyun et al., 2017; Kaniskan et al., 2018). In line with this, inhibiting KMT3C with SC00107035 resulted in decrease in H3K36me2 (Fig 3.29B; H3K4me3 was not part of the tested peptides).

Histone arginine methyltransferase inhibitors SC00107037 and SC00107015 target specifically PRMT5 and PRMT4, respectively. Treatments with these inhibitors did not induce significant alterations on tested histone lysine residues comparing to control. A direct measurement of arginine methylation was not conducted due the design of the study focussing on histone lysine acetylation and methylation. However, SC00107037 was the only inhibitor that decreased H3K36me2, while - as expected - EZH2 inhibitors significantly increased it and other inhibitors had no effect. H3K27me3 was slightly increased comparing to control after PRMT5 inhibition with SC00107037. It has been hypothesized that there is a crosstalk between inhibition of PRMT5 and other methylation marks like H3K27me3 (F. Liu et al., 2020). PRMT5-mediated histone arginine methylation antagonizes transcriptional repression by Polycomb complex PRC2 (F. Liu et al., 2020). H3K36me2 could therefore be another mark where the crosstalk between inhibition of arginine methyltransferases and other lysine marks is active. Furthermore, it has been demonstrated that H3K36 methylation antagonizes PRC2-mediated H3K27 methylation (Yuan et al., 2011). In line with this, the antagonistic effect was seen in the inhibitors directly targeting H3K27me3 and increasing H3K36me2 as a result and the opposite.

As SC00107037 was the only inhibitor in this group that increased levels of glycolysis, its results were analysed in more detail in the following steps for PTMs and proteome changes. PRMT5 inhibition has been shown to improve fatty liver disease through increasing PPARα and PGC-1α levels, mitochondrial biogenesis and β-oxidation (Huang et al., 2018). The results of the current study suggest that inhibiting PRMT5 favours β-oxidation. β-oxidation is directly linked with oxidative phosphorylation. Electrons are passed from β-oxidation to oxidative phosphorylation via NAD and FADH2 oxidation. This may be linked with the observed increase in oxidative phosphorylation after treatment with SC00107037 (Fig. 3. 29A). Having higher β-oxidation may therefore provide a source of electrons for elevated oxidative phosphorylation. Moreover, these pathways share substrates that interact biochemically and there is ample evidence for physical interactions between proteins of β-oxidation and oxidative phosphorylation. Furthermore, defects in either of these two intimately linked pathways have been shown to disturb or inhibit the other and cause metabolic diseases (Arpa et al., 2009; Gargus et al., 2003; Nouws et al., 2014; Sumegi & Srere, 1984; Taylor et al., 2012; Tyni et al., 1997). Proteome analysis showed that also specific glycolytic proteins are increased after SC00107037 treatment, such as PXN (Fig 3.31). PXN mutations have been linked with cell migration and metastasis, cancer metabolism and alterations in mitochondrial dynamics and respiratory activity, having been associated with promoting mobilization of different sources of fuel for glycolysis (Curtis et al., 2019; Kawada et al., 2013).

As with other epigenetic compounds, proteins differentially expressed due to treatments with KMT inhibitors were highly enriched for proteins involved in metabolic regulation (Fig. 3.31). Interestingly, IKBKB a regulator of NFkb pathway and mainly known for its role in inflammation regulation, was significantly decreased after SC00107037 treatment (Fig. 3.32). It has been shown that IKBKB deficient cells exhibit elevated aerobic glycolysis (Reid et al., 2016) which is in line with the current project findings (Fig 3.29A and 3.30). Treatment with SC00107037 significantly altered PXN, IKBKB linked with elevated glycolysis. In addition to PXN and IKBKB, other proteins like PABPN1 that play an important role in the regulation of glycolytic muscle fibres (Trollet et al., 2010) linked with altered glycolysis and muscle wasting in aging (Olie et al., 2019) were altered (Fig 3.30 and 3.32). PRMT5 which induces symmetric di-methylation on histone H4R3 and H3R8, generally acts as

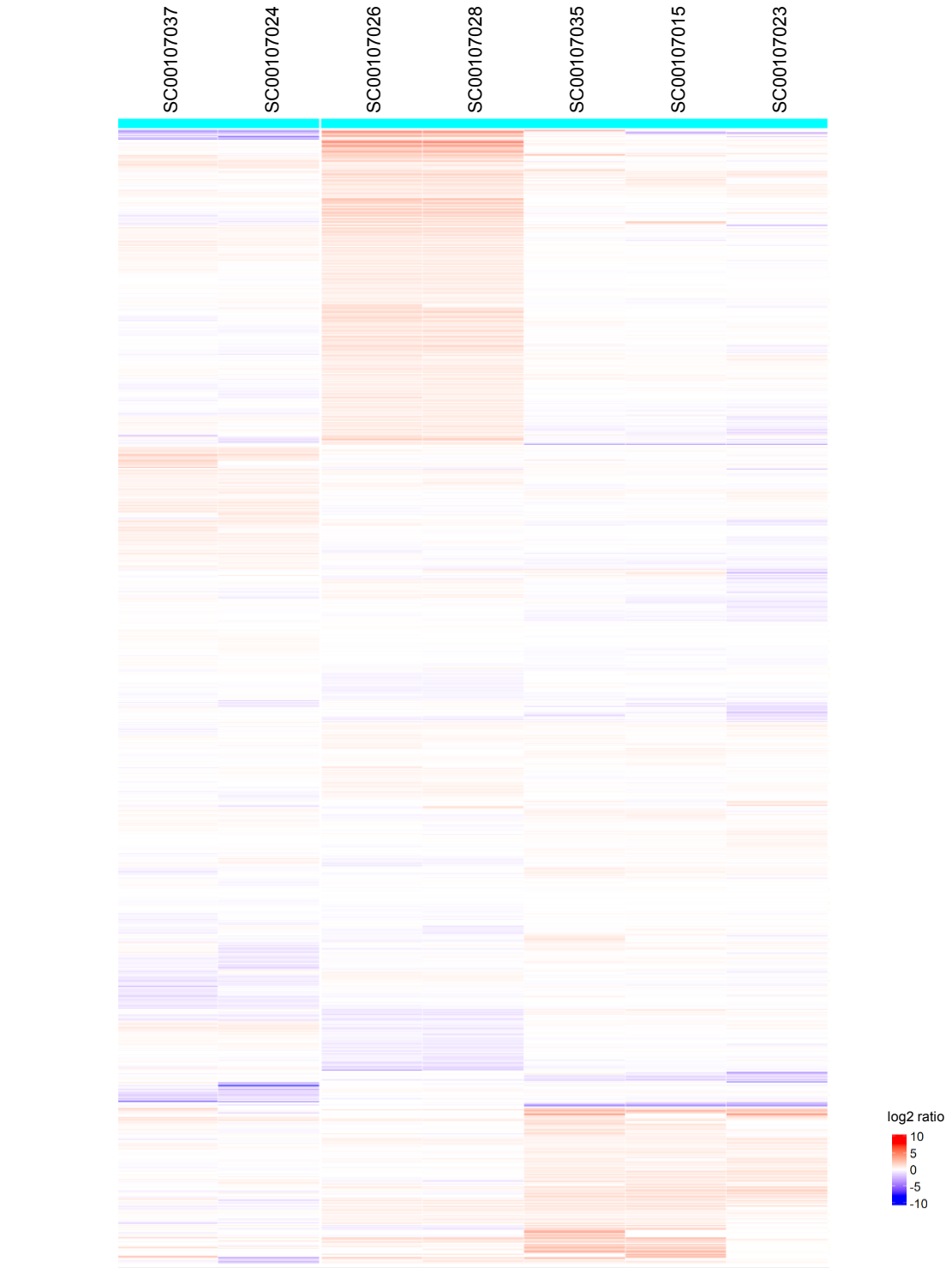

Figure 3.30. Methyltransferase inhibitor treatments of HEK293T cells caused significant changes in whole proteome with two types of patterns observed across the compounds.
Hierarchical clustering and heatmap of protein level changes after treatment with selected methyltransferase inhibitors. Minimal log2 fold-change threshold for analysis was 1.11.

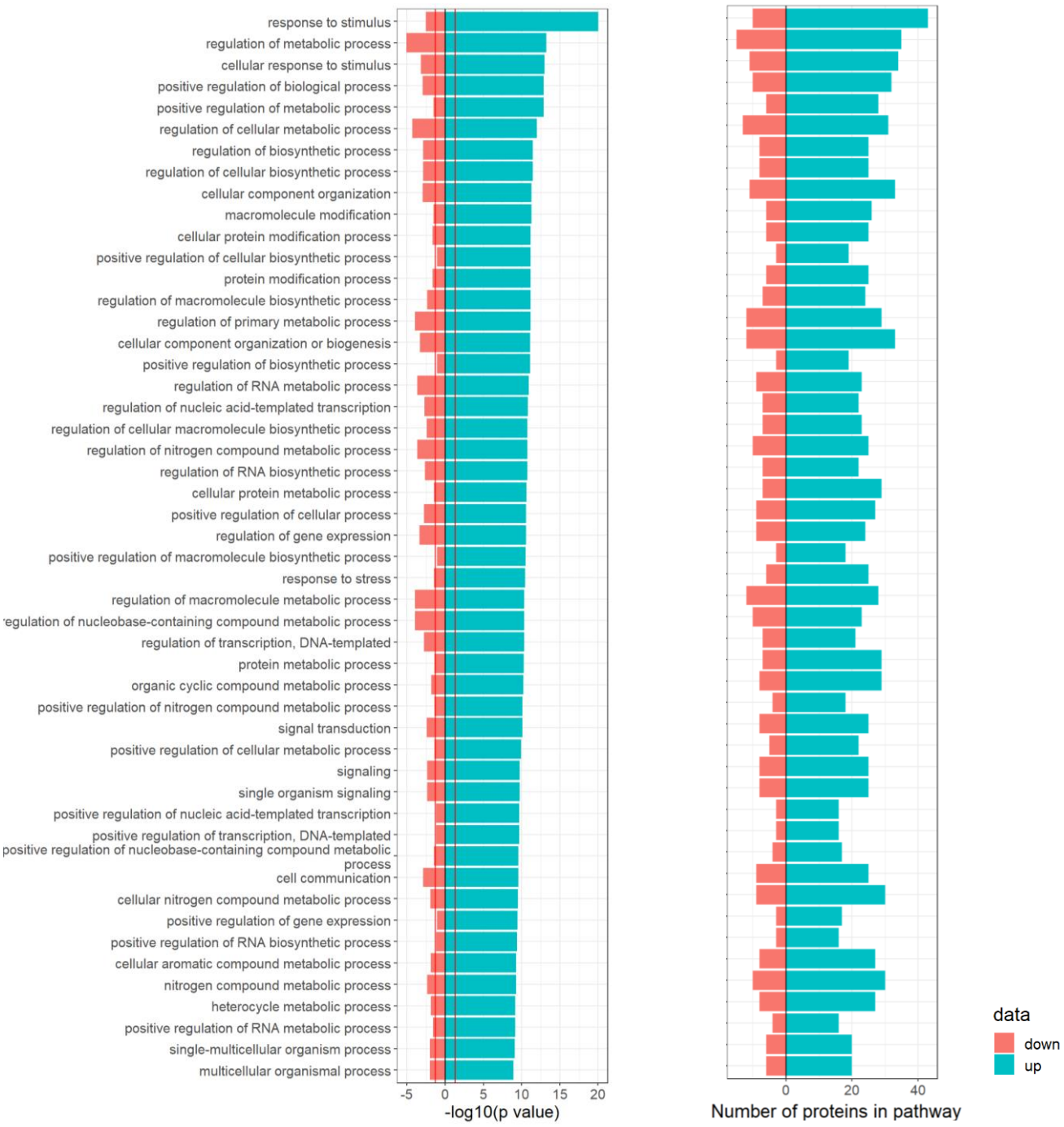

Figure 3.31. Methyltransferase inhibitor treatments causes significant upregulation of metabolic pathways

Enrichment analysis of HEK293T cells treated with methyltransferase inhibitors. Enrichment analysis is based on the set of proteins differentially expressed across the three methyltransferase treatments (minimal log2 fold-change threshold for analysis 1.11) using biological process terms. Enriched terms were ranked based on their statistical significance (-log10 p-value, left). The corresponding number of differentially expressed proteins per biological process is depicted on the right part of the figure.

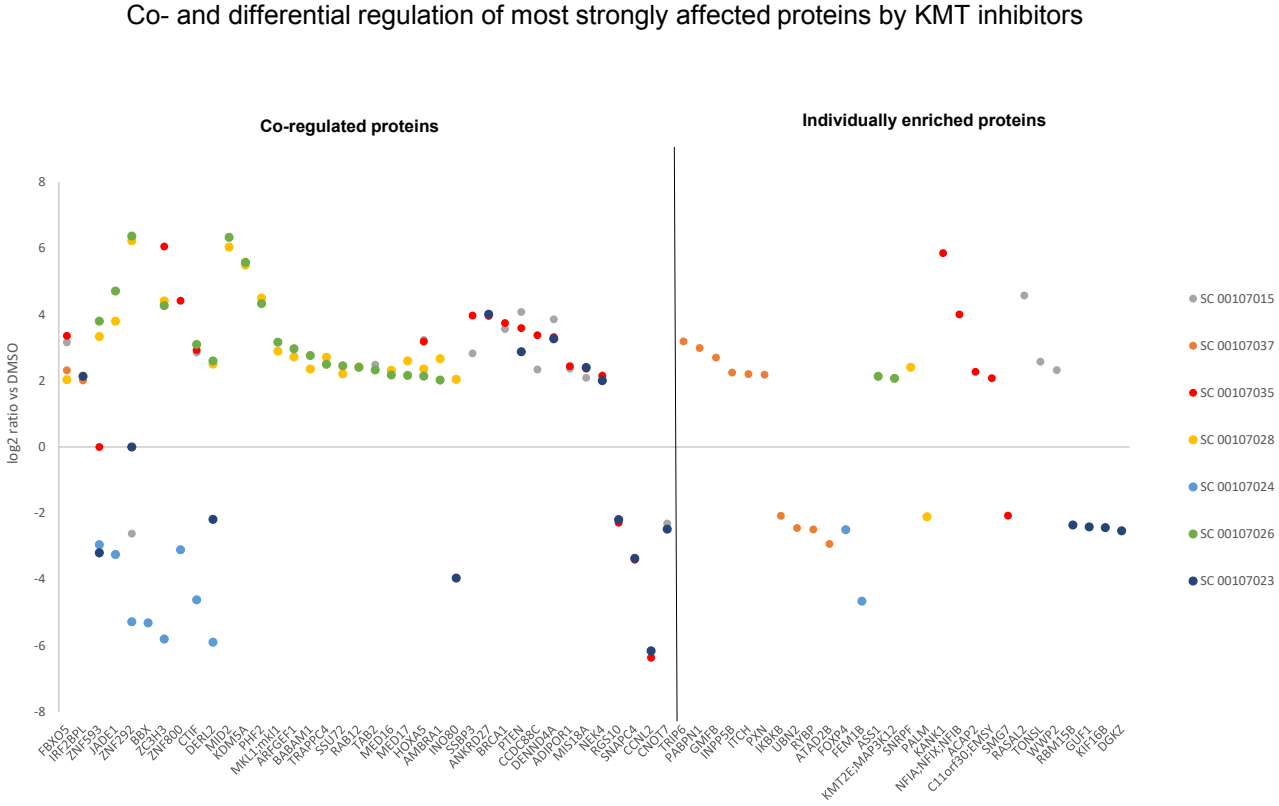

Figure 3.32. Depiction of the most highly differentially-expressed proteins after KMT-inhibitor treatments

Enrichment analysis of HEK293T cells treated with KMT inhibitors. Enrichment analysis is based on the set of proteins differentially expressed across the KMT inhibitors. Depicted are proteins that showed the largest fold-change vs the control samples upon inhibitor treatment

repressive marks for gene expression (Greenblatt et al., 2016). On the contrary, asymmetric di-methylation on H4R3 and H3R17, deposited by the type I enzymes PRMT1 and CARM1 (PRMT4), respectively, is often found on regulatory regions of active genes (Greenblatt et al., 2016). In line with these observations, the PRMT4 inhibitor SC00107015 induced very different protein changes comparing to PRMT5 inhibitor SC00107037 and opposite metabolic profiles (Fig 3.29A and Fig 3.30/3.32).

In the case of SC00107023, the protein changes appeared to be very similar to SC00107035 and SC00107015. However, treatment with SC00107023 increased oxidative phosphorylation and no other treatment apart from SC00107037 and SC00107035 did so. IRF2BPL was the only protein that was commonly increased only in SC00107037 and SC00107023 (Fig 3.32). IRF2BPL variants have been linked with different neurodevelopmental disorders like Rett Syndrome which is also linked with various metabolic anomalies (Neul et al., 2020; Tran Mau-Them et al., 2019). IRF2BPL role is fairly new and it is not extensively studied yet. Mitochondrial defects have been found in this study of patients with DEE and variants of IRF2BPL (Tran Mau-Them et al., 2019). Also IRF2BPL has been linked with female neuroendocrine system regulation (Heger et al., 2007). INO80 was also found decreased (Fig 3.32) which is linked with lower glycolysis and increase of genes in the oxidative phosphorylation pathway (W. Yao et al., 2016). ANKRD27 was increased in the case of SC00107035 and SC00107023 (Fig 3.32), where there was an increase in oxidative phosphorylation and decrease in glycolysis (Fig 3.29A). In SC00107037, where both oxidative phosphorylation and glycolysis were increased, ANKRD27 was not affected comparing to control. Interestingly, ANKRD27 has been linked as a HIF1A target gene under hypoxia. Interestingly, AFF4, which is also upregulated by inhibitors SC00107035 and SC00107023 has been linked with ANKRD27 (Galbraith et al., 2013). Supporting a potential role of both ANKRD27 and AFF4 in the link between epigenetic and metabolism, they are also upregulated by epigenetic reader domain targeting-molecules (SC00107016, SC00107067, see Chapter 3.7.5) and HDAC inhibitor SC0010008771.

Treatments with SC00107026 and SC00107028 caused the same metabolic changes and induced similar histone PTMs (Fig 3.29A and B). Moreover, the protein changes induced by these two drugs were almost identical (Fig 3.30 and 3.32).

Taken together, the analysis of methyltransferase inhibitors revealed a picture very different to the one captured by HDAC and HAT inhibitors. In line with their much more specific targeting profiles, methyltransferase inhibitors elicited more differential histone PTM profiles, as well as proteomic changes. Interestingly despite this diversity, all except a PRMT5 inhibitor decreased glycolysis rate irrespective of the role of their targeted histone modification (i.e. repressive or activating). However, certain themes emerged in combination with other inhibitor classes that are discussed in chapter 3.8 and Chapter 4.1.

3.7.4 Demethylase inhibitors

From the initial eleven demethylase inhibitors investigated in the metabolic profiling, three passed the filtering criteria and were further analysed. All three (SC00107029, SC00105914, SC00106834) caused highly similar metabolic effects, leading to a significant upregulation of oxidative phosphorylation and a slightly less pronounced upregulation of glycolysis (Fig 3.33A). The majority of the other eight demethylase inhibitors showed similar phenotype of increased overall metabolic activity, with only two showing a decrease of 10% or more versus control (Fig 3.14 and Fig 3.15). The filtered histone demethylase inhibitors therefore seemed to comprise a comparably consistent small molecule inhibitor group in relation to their metabolic effects.

Both SC00106834 and SC00107029 primarily target histone demethylase KDM5B, which is a key H3K4me demethylase. In line with the inhibition of KDM5B, an increase in H3K4me2 was observed in samples treated with either of the two inhibitors (Fig. 3.33B). SC00106834 is a highly specific inhibitor for KDM5B – and resulted in a histone PTM picture in line with the expected increased transcription from higher levels of H3K4me2, as well as decreased repressive methylation marks H3K9me2/3 and H4K20me2/3 and increased transcription-associated mark H4K20me1 (Beck et al., 2012b; Zhibin Wang et al., 2008). However, acetylation was generally not increased and the repressive mark H3K27me3 was not decreased, suggesting that the effect of this drug may be limited to a certain subset of target genes, or that KDM5B's target genes in turn repress other genes. In contrast to SC00106834, SC00107029 is known to have some more broad-spectrum activity, including KDM6A and KDM6B. In line with this, the histone PTM profile results differed from the more specific

Figure 3.33. Demethylase inhibitor treatments of HEK293T cells cause correlating formation of distinct metabolic and PTM phenotype clusters.

A. Hierarchical clustering an heatmaps of the selected demethylase inhibitors. 72h treatments with selected demethylase inhibitors induced metabolic changes. 1h treatments caused pronounced effects comparing to control.

B. 72h treatments with selected demethylase inhibitors induced histone PTM changes comparing to control.

KDM5B-targeting SC00106834, despite the strong expected upregulation of H3K4me2. Interestingly, H3K79me1/2 was also increased by this drug treatment. Only recently, a demethylase specific for H3K79 was identified – KDM2B (J. Kang et al., 2018) and it is possible that the employed small molecule may also target KDM2B, leading to the increased levels of H3K79me1/2. On the other hand, SC0010519, which targets LSD1, showed a modest increase in H3K4me2 and H3K9me2, which are histone modifications LSD1 is known to demethylate (Hyun et al., 2017).

The hierarchical clustering of the metabolic phenotype, as well as of the histone PTMs unexpectedly showed a higher similarity between SC00107029 and SC00105914, despite the fact that they target different demethylases (KDM5A/6A/B, and LSD1, respectively (Fig. 3.33A, B).

Common to all three demethylase inhibitor-treated samples were unexpectedly decreased levels of histone acetylation, especially on histone H4 (Fig. 3.33B). The main writer of bulk histone H4 acetylation in vivo is thought to be JADE1, as part of the HBO1 complex (Foy et al., 2008). Indeed, JADE1 protein levels were reduced in all samples, with highest reduction of more than 10.5-fold versus control samples observed for SC00105914, which also showed the largest decrease in H4 acetylation. This observation potentially could link the global loss of H4 acetylation in conjunction with high levels of H3K4me2 through downregulated expression of a key acetylation writer – possibly JADE1.

Furthermore, a crucial reader of acetylated histones with known transcriptional-regulation functions, bromodomain-containing ATAD2B, was downregulated more than 7-fold vs control in both the SC00107029 and SC00105914 samples. Although its cellular function is not yet fully understood, several studies indicate that the combination of its bromodomain with its intrinsic ATPase activity is an important positive regulator of receptor-induced genes but also can act as generalist enhancer of transcription (Cochran et al., 2019; Lloyd & Glass, 2018), the loss of this epigenetic effector may mediate transcriptional repression downstream of treatment with demethylase inhibitors.

In respect to enrichment for proteins differentially regulated by the treatments, demethylase inhibitors showed the most divergent picture across all chemical groups – presenting an almost equal distribution of significantly up- as well as downregulated proteins in most of the enriched gene ontology terms (Fig. 3.34 and 3.35). The most significantly enriched protein groups were regulation of metabolic processes and gene expression, in line with the strong observed metabolic phenotypes. In

Figure 3.34. Demethylase inhibitor treatments of HEK293T cells cause significant changes in whole proteome changes with two types of patterns observed across the three compounds. Hierarchical clustering and heatmap of protein level changes after treatment with selected methyltransferase inhibitors. Minimal log2 fold-change threshold for analysis was 1.11.

Figure 3.35. Demethylase inhibitor treatments causes significant upregulation of metabolic pathways

Enrichment analysis of HEK293T cells treated with demethylase inhibitors. Enrichment analysis is based on the set of proteins differentially expressed across the three demethylase treatments (minimal log2 fold-change threshold for analysis 1.11) using biological process terms. Enriched terms were ranked based on their statistical significance (-log10 p-value, left). The corresponding number of differentially expressed proteins per biological process is depicted on the right part of the figure.

order to understand better the connection between the induced histone PTMs, proteomic changes and observed metabolic phenotype, differentially expressed proteins were mapped against the consensus KEGG glycolysis pathway. Out of 67 proteins associated with glycolysis, 50 were quantified in the relevant proteomics samples. Interestingly, SC00106834 showed a high fraction of downregulated proteins across glycolysis, while both SC00107029 and SC00105914 had more balanced up/downregulated ratios (Fig. 3.36A). This was confirmed by a more detailed review of the differentially expressed proteins, where SC00107029 and SC00105914 formed a subcluster and had several important glycolytic enzymes upregulated vs control, while SC00106834's proteins were mostly downregulated (Fig. 3.36B). This observation was further confirmed by similar patterns of protein expression in the TCA cycle and oxidative phosphorylation (data not shown). Therefore, the unbiased subclustering predicted by the seahorse experiments could be explained by patterns of PTMs as well as protein levels of relevant metabolic pathways.

In summary, the analysis of these three histone demethylase inhibitors suggested that the intended primary cellular target of a demethylase inhibitor is not necessarily a good predictor of its effects on overall histone PTMs, proteome changes or the metabolic effects. On the contrary, unbiased hierarchical clustering of histone PTMs suggested an unexpected grouping of unrelated demethylase inhibitors (SC00107029 and SC00105914) that also correlated with similar proteomic profiles (and similar levels of highly differentially-regulated transcriptional regulators) and metabolic phenotypes.

3.7.5 Epigenetic reader domain inhibitors

Epigenetic reader domains as part of different protein classes play a key role in transcription regulation (Borck et al., 2020). However, regulation of metabolism via specific domain motifs is not well understood. Five inhibitors were therefore selected after the metabolic screening for further analysis of the induced histone PTMs and protein changes. Four targeting bromodomains (BET and non BET) and one targeting MBT (malignant brain tumor) family chromatin interacting transcriptional repressors were included. The inhibitors were of known broad spectrum activity like the SC00107063 which inhibits BRD2/4/9 and CECR2 and some were selective for specific targets like the MBT member L3MBTL3 antagonist SC00107050. Three metabolic groups were identified, drug treatments

A Demethylase inhibitors: subclustering based on regulation of glycolytic enzymes

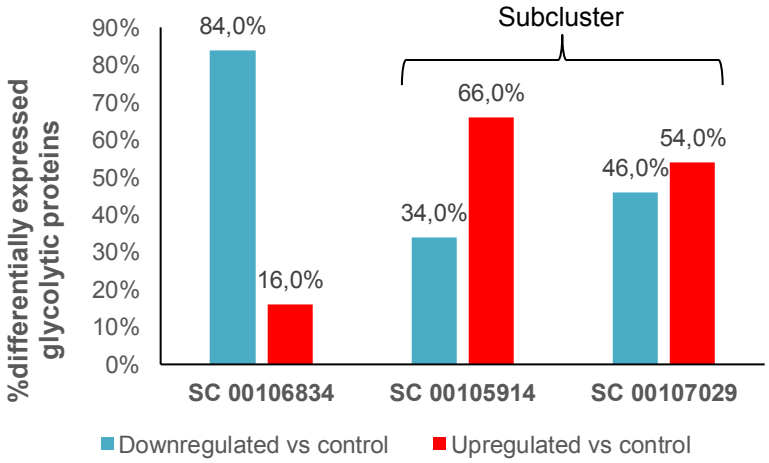

B Demethylase inhibitors: detailed analysis of differentially expressed glycolysis genes

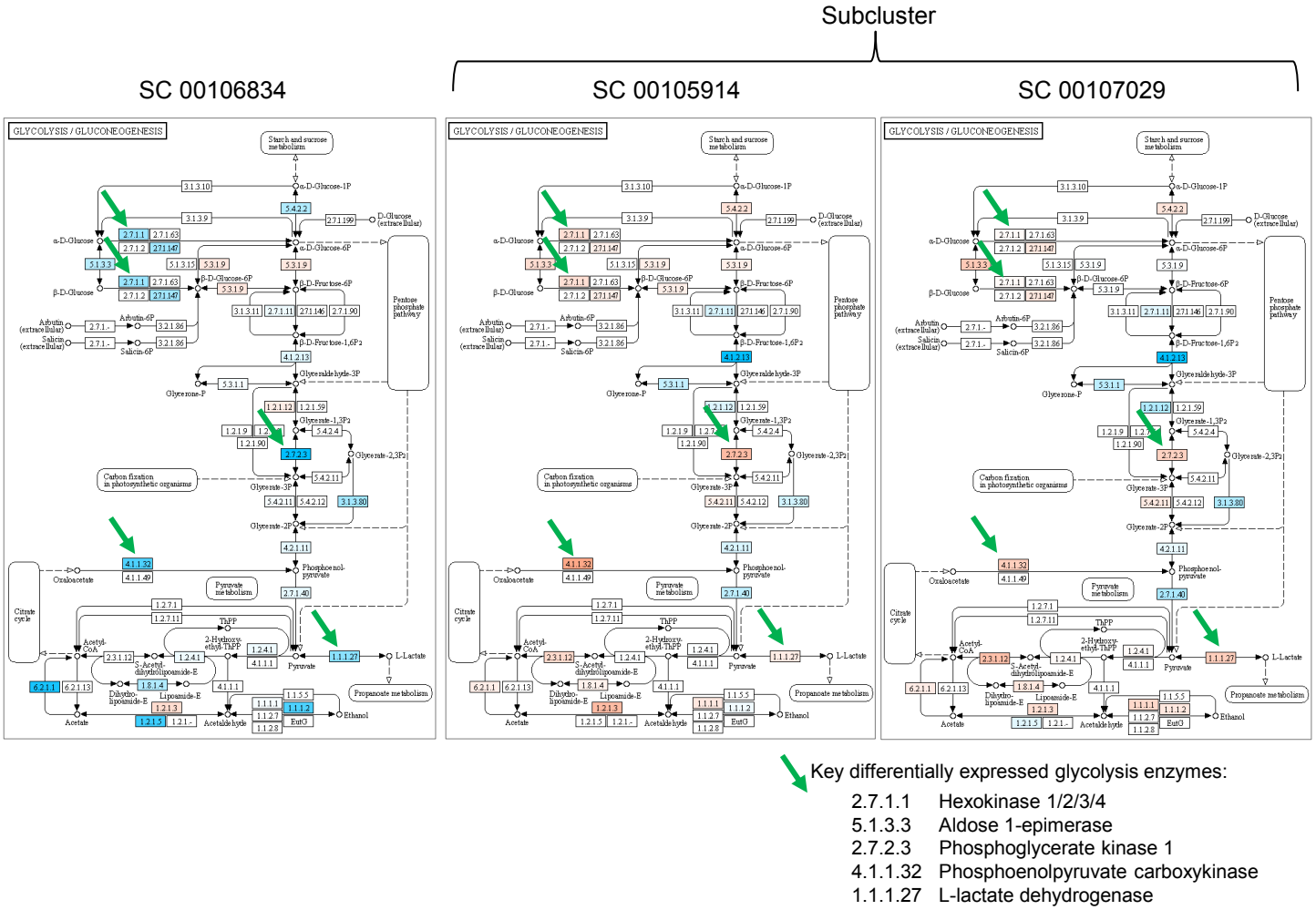

Figure 3.36. In-depth analysis of glycolytic proteins and pathways in samples treated with demethylase inhibitors.

A. Glycolytic proteins regulation in demethylase inhibitors

B. KEGG ontology glycolysis pathway for demethylase inhibitors

that decreased both oxidative phosphorylation and glycolysis, drugs that caused antagonistic effects by increasing oxidative phosphorylation and decreased glycolysis and one drug caused no effect in oxidative phosphorylation but decreased glycolysis (Fig 3.37A). Interestingly all inhibitors decreased glycolysis. SC00106063 and SC00107050 decreased both oxidative phosphorylation and glycolysis after 72h treatment. SC00107016, a selective BRD2/3/4 inhibitor caused antagonistic effects and SC00107067, a CREBBP and p300 bromodomain inhibitor, also caused antagonistic effects. SC00107054, selective for BRD2/4/T, did not alter oxidative phosphorylation but decreased glycolysis.

Bromodomains are readers of acetylated lysine and even though SC00107016 and SC00107054 have similar targets with BRD2/3/4 and BRD2/4/T, respectively, they did not induce the same effects on oxidative phosphorylation. However, as expected they did show an almost identical histone PTMs map with few different marks. For instance, in the case of SC00107016 H3K4me2 was increased but not in the case of SC00107054 and H3K9ac was also increased after treatment with SC00107016. The other three inhibitors induced only mild effects on histone PTMs although H3K4me2 was significantly upregulated after treatment with all inhibitors apart from the case of SC00107054 where there was no change comparing to control. It has been shown before that inhibition of demethylation of H3K4 causes autophagy in cancer and inhibitors of LSD1 as well as SC00107050 and others have the same effect (Zhen Wang et al., 2017a). Also, only in the case of the MBT domain inhibitor SC00107050 another mark H3K79me1 was elevated comparing to control. Regarding L3MBTL3, it binds to multiple methylated sites on histone H3 (Zhen Wang et al., 2017b). SC00107050 competitively binds to the lysine methyl binding pocket of the L3MBTL3 MBT domain and displaces mono or dimethylated lysine peptides versus unmethylated or trimethylated lysine.

SC00107063 and SC00107067 clustered next to each other in the unbiased hierarchical clustering for protein changes (Fig 3. 38). However, their targets are different; BRD(2,3,4,T), non BET and CREBBP, p300 respectively. Distinct proteins that are differently affected from each other could explain the opposite effects on oxidative phosphorylation (Fig 3.37A and Fig 3.38). Protein Fem1b was significantly decreased in SC00107063 but not in the case of SC00107067. Deprivation of Fem1b has been linked with abnormal glucose homeostasis and functional defect in insulin secretion

Figure 3.37. Demethylase inhibitor treatments of HEK293T cells caused correlating formation of distinct metabolic and PTM phenotype clusters.

A. Hierarchical clustering an heatmaps of the selected demethylase inhibitors. 72h treatments with selected epigenetic reader domain inhibitors induced metabolic changes.

B. 72h treatments with selected epigenetic reader domain inhibitors induced histone PTM changes comparing to control.

Figure 3.38. Epigenetic reader domain inhibitor treatments of HEK293T cells caused significant changes in whole proteome with two types of patterns observed across the compounds.

Hierarchical clustering and heatmap of protein level changes after treatment with selected epigenetic reader domain inhibitors. Minimal log2 fold-change threshold for analysis was 1.11.

(D. Lu et al., 2005). Also, RYBP was decreased in SC00107067 but not in SC00107063. RYBP is involved in the ubiquitination of H2AK119ub and network with PRC1 and PRC2 but the role of this protein in metabolism is not fully known (Morey et al., 2013).

Interestingly, in the present study there were other findings that suggested a possible metabolic role of RYBP – RYBP was decreased in the case of SC00107037 a PRMT5 inhibitor, and SC00107029 a methylation inhibitor. FOXP4 was also significantly decreased comparing to control in the case of SC00107063. The FOX family of proteins have been found to participate in multiple cellular processes. However, only recently FOXO proteins have been investigated in relation to cancer metabolism and metabolic regulation in more general terms (Yadav et al., 2018). In that regard, FOXP4-AS1 was found to play a role in oxidative phosphorylation and TCA cycle in cancer (X. G. Liu et al., 2020). It has also been indicated that FOXO3a-SIRT6 axis is negatively correlating with a number of aerobic glycolytic genes in melanoma patients (Dong et al., 2020). FOXP1 was found to play a central role in the response of hair follicle cycle to oxidative stress as FOXP1 deficient hair follicles showed increased ROS and shorter anagen phase (Zhao et al., 2015). AFF4 was increased only in the case of SC00107067 but not SC00107063. AFF4 together with BRD4, which is a target of SC00107063, has been linked with HIF1A related targets which are induced under hypoxia (Galbraith et al., 2013). In other drug classes AFF4 was also found increased when oxidative phosphorylation was increased and glycolysis decreased (methyltransferase inhibitors SC00107023 and SC00107035 and HDAC inhibitor SC00107771). Furthermore, ACTR8 which holds a central role in the INO80 complex and is related to HIF1A response, was downregulated only in SC00107067 (increased oxidative phosphorylation) but not in any other inhibitor. (INO80 was not changed in SC00107067). On the other hand, methyltransferase inhibitors SC00107026 and SC00107028, increased INO80 but there was no change in ACTR8 and oxidative phosphorylation was unaltered comparing to control. Therefore, ACTR8 may be an important regulator of oxidative phosphorylation.

SC00107067 and SC00107016 increased oxidative phosphorylation but they showed a different PTM profile. They targeted different proteins and as a result they caused different protein changes. SC00107054 and SC0010705016 induced similar histone PTMs marks and even though they appeared to cluster together after hierarchical clustering of protein changes there are couple of proteins

that were differentially regulated that could explain the effect of SC00107016 on increasing oxidative phosphorylation and that SC00107054 induced no effect on respiration. For example, ZNF292 as previously discussed, ADIPOR1, PTEN and Cabin1 were only a few proteins that were differentially expressed between the two different treatment samples.

As expected SC00107050, due to its selectivity on the L3MBTL3 target, induced only few protein changes and showed a different proteomic profile comparing to the other four bromodomain inhibitors. For instance, NR2F2 which represses genes crucial for electron transport chain activity and mitochondrial dynamics leading to decreased oxygen consumption rates (Wu et al., 2015) and CLN6 were found altered only after treatment with SC00107050. Mutations in CLN6 cause the neuronal disease ceroid lipofuscinosis type 6 (Arsov et al., 2011; Kollmann et al., 2013). Maybe the target protein L3MNTL3 is a crucial therapeutic candidate for ceroid lipofuscinosis type 6 and it would be very interesting to further investigate. Also, other proteins linked with glucose homeostasis and cellular metabolism were altered. For example, Fem1b (B. Kang & Sun, 2014) and CTIF were altered comparing to control which are found to be involved in overfeeding and adipose tissue metabolism (Perfilyev et al., 2017). Furthermore, the FOX family of proteins have previously linked with cancer metabolism and FOXP4 was decreased significantly comparing to control after treatment with SC00107050. Taken together, epigenetic reader domain inhibitors did show similar effects with other drug classes like methyltransferase and HDAC inhibitors, with significant impact on the levels of metabolically-relevant proteins (Fig. 3.39) but they also presented other PTM and protein changes indicating that these drugs affect metabolism via different routes.

3.7.6 SIRT inhibitors and SIRT activator

Sirtuins are a very special class of HDACs dependent on NAD+ and have previously been linked with metabolism regulation (Chang & Guarente, 2014; German & Haigis, 2015; Guarente et al., 2018; Houtkooper et al., 2012; Nogueiras et al., 2012; J. Yu & Auwerx, 2009). SC00106831 is a specific SIRT2 inhibitor and SC00106957 is a SIRT1 inhibitor. SC0082039 has been described as a SIRT1 activator. Performance of metabolic profiling of SC00106831 and SC00106957 showed opposite responses: SC00106831 mainly increased glycolysis and slightly decreased oxidative

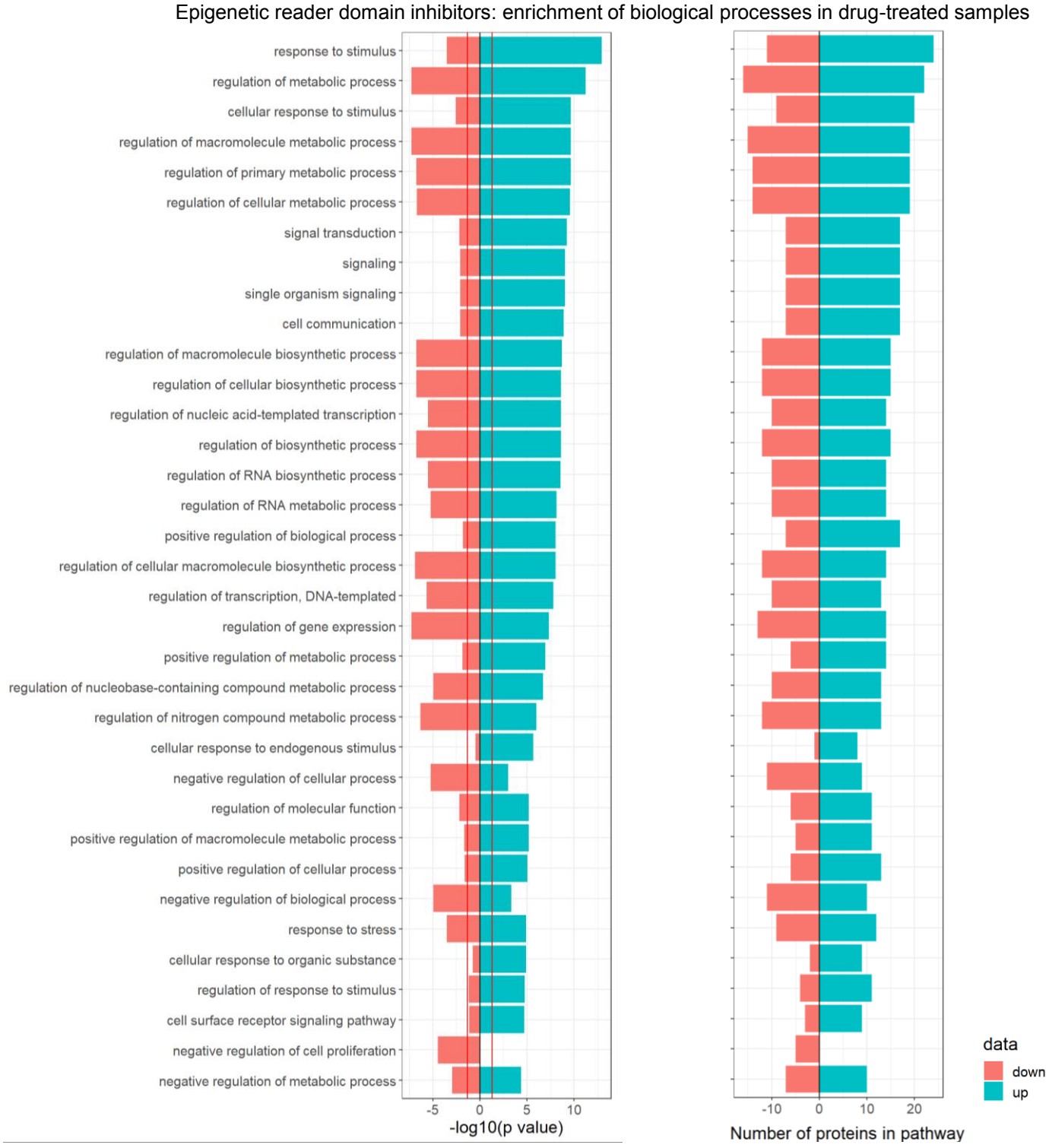

Figure 3.39. Epigenetic reader domain inhibitor treatments causes significant upregulation of metabolic pathways

Enrichment analysis of HEK293T cells treated with epigenetic reader domain inhibitors. Enrichment analysis is based on the set of proteins differentially expressed across the five epigenetic reader domain inhibitor treatments (minimal log2 fold-change threshold for analysis 1.11) using biological process terms. Enriched terms were ranked based on their statistical significance (-log10 p-value, left). The corresponding number of differentially expressed proteins per biological process is depicted on the right part of the figure.

phosphorylation. On the other hand, SC00106957 increased oxidative phosphorylation and decreased glycolysis (Fig 3.40A). Oxidative phosphorylation and glycolysis were increased after the treatment with the SIRT activator SC0082039 (Fig 3.40A).

Looking at the immediate effects (after 1h treatments), the two SIRT inhibitors behaved differently: the SIRT2 inhibitor SC00106831 induced 1h effects, while the SIRT1 inhibitor SC00106957 did not show 1h effects. One possible explanation is that SIRT2 is localized primarily in the cytoplasm, and therefore may have direct effects on metabolic cytoplasmatic enzymes, while SIRT1 is primarily nuclear and is known to target nuclear transcription regulators such as p300, MOF, Ezh2 (Martínez-Redondo & Vaquero, 2013).

Overall, histone PTM changes induced by the treatments were very weak, especially comparing to the Type I/II HDAC inhibitors (compare Fig. 3.40B with Fig. 3.20B). Especially the SIRT2-treated samples showed almost control-level histone PTMs for all different marks. These observations were in line with the localization of SIRT1 and SIRT2. Unexpectedly, in contrast to other HDAC inhibitors, treatments with SC00106831 and SC00106957 significantly reduced acetylation marks. Also, treatments with the inhibitor SC00106957 and the activator SC0082039 increased specific methylation marks (Fig 3.40B). The observed acetylation pattern may be caused by SIRT1 regulating other chromatin modifiers, rather than direct action on lysine histone residues.

In line with the only moderate histone PTM changes, SIRT inhibitors and activator caused few protein level changes comparing to other HDAC inhibitors (Fig 3.41). Consistent with this, pathway enrichment analysis showed significantly fewer enriched proteins per pathway comparing to other inhibitor groups (Fig. 3.42 and 3.43). SIRT1 and SIRT2 inhibitors induced different protein changes. Only one protein, WWP2, was found to be increased in both cases in the same way by almost 2 fold. In addition, proteins that were identified in both samples were not affected in the same way between the two inhibitors. That could explain the opposite metabolic changes after the treatment with those inhibitors. In the case of SC00106831 a few proteins that are downstream of HIF1A were downregulated, including ZNF292 and ZNF593 which are upregulated in hypoxia which leads to increased anaerobic glycolysis (Loftus et al., 2017; Nauta et al., 2017; O. Xia et al., 2009a).

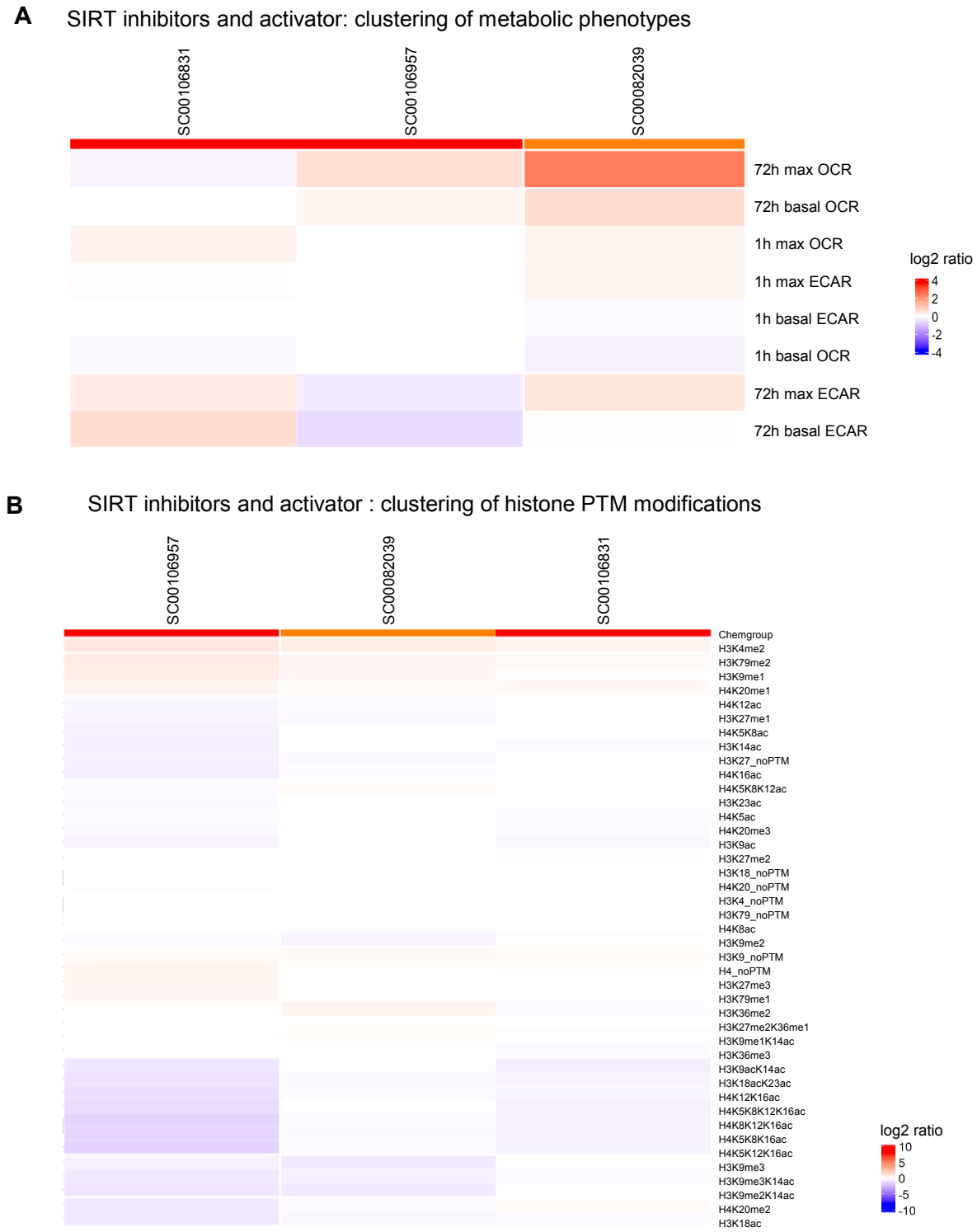

Figure 3.40. SIRT inhibitor and activator treatments of HEK293T cells cause correlating formation of distinct metabolic and PTM phenotype clusters.

A. Hierarchical clustering an heatmaps of the selected SIRT inhibitors and activator. 72h treatments with selected SIRT inhibitors and SIRT activator induced metabolic changes. 1h effects were induced comparing to control

B. 72h treatments with selected SIRT inhibitors and SIRT activator induced histone PTM changes comparing to control.

Figure 3.41. SIRT inhibitors and SIRT activator treatments of HEK293T cells cause significant changes in whole proteome changes.

Hierarchical clustering and heatmap of protein level changes after treatment with selected SIRT inhibitors and activator inhibitors. Minimal log2 fold-change threshold for analysis was 1.11.

SIRT activator: enrichment of biological processes in drug-treated samples

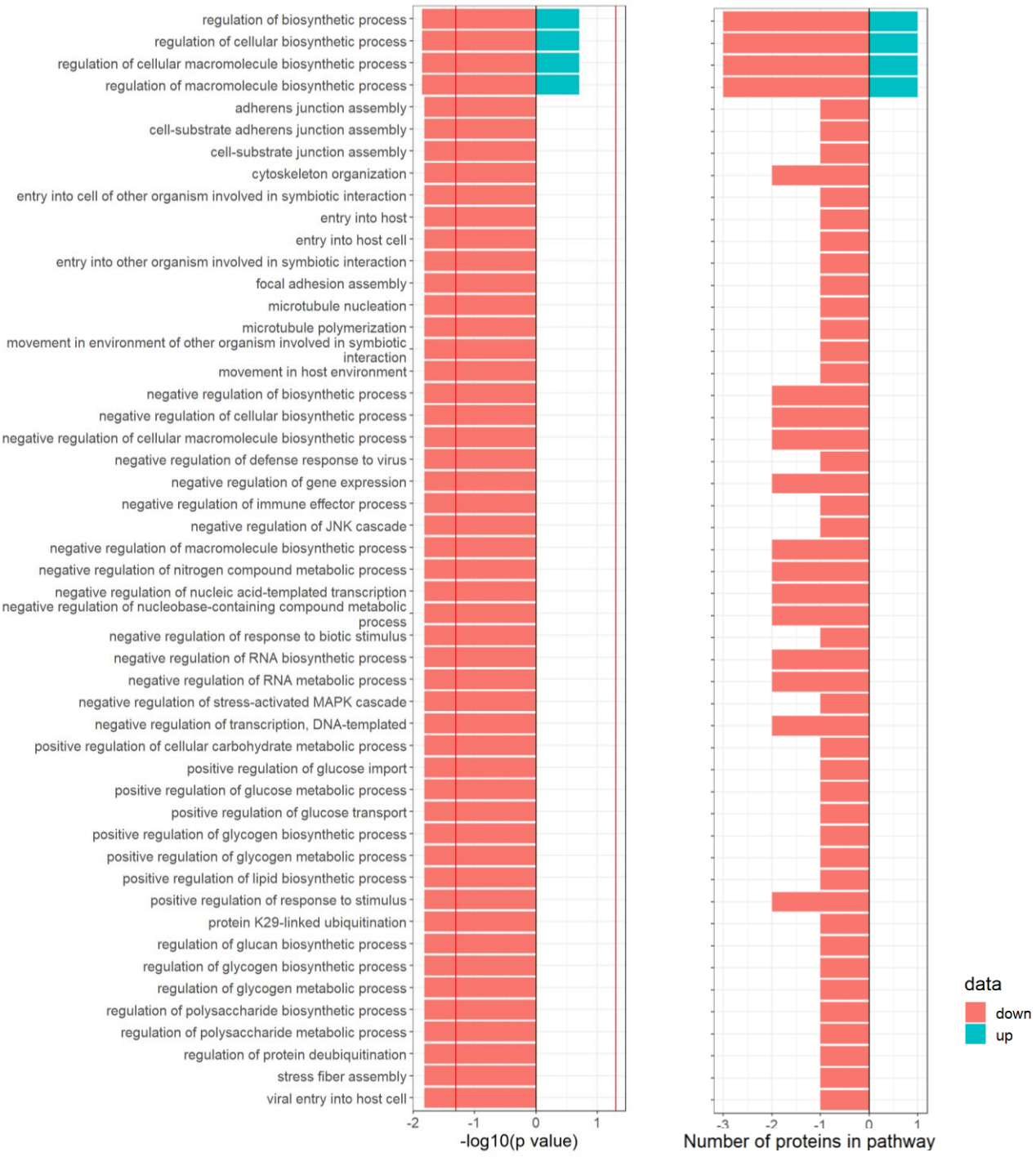

Figure 3.42. SIRT activator treatment biological process enrichment

Enrichment analysis of HEK293T cells treated with SIRT activator. Enrichment analysis is based on the set of proteins differentially expressed with SIRT activator treatment (minimal log2 fold-change threshold for analysis 1.11) using biological process terms. Enriched terms were ranked based on their statistical significance (-log10 p-value, left). The corresponding number of differentially expressed proteins per biological process is depicted on the right part of the figure.

Figure 3.43. SIRT inhibitors treatment causes significant upregulation of metabolic pathways
Enrichment analysis of HEK293T cells treated with SIRT activator. Enrichment analysis is based on the set of proteins differentially expressed with SIRT activator treatment (minimal log2 fold-change threshold for analysis 1.11) using biological process terms. Enriched terms were ranked based on their statistical significance (-log10 p-value, left). The corresponding number of differentially expressed proteins per biological process is depicted on the right part of the figure.

Other proteins that have been linked with metabolism were differentially regulated by the treatments. In particular, IREB2 which is linked with alterations in mitochondrial function and homeostasis was upregulated in both SIRT activator and SIRT1 inhibitor SC00106957 where oxidative phosphorylation was increased comparing to control. Furthermore, ITCH, which is linked with increased oxidative capacity (Jiang et al., 2020) was significantly downregulated in the case of the SIRT activator, in line with the increased oxidative phosphorylation induced after the treatment with this drug (Fig 3.40A an 3.41). ITCH deficiency has been previously shown to halt fatty liver disease caused by obesity (Marino et al., 2014) and from plaque formation in atherosclerosis via SIRT6 breakdown and SREBP2 which led to decreased cholesterol levels, reduced hepatic steatosis, increased mitochondrial oxidative capacity and shift to fatty acids as energy source (Stöhr et al., 2015).

Overall, the SIRT inhibitors and activator affected metabolism but they did not induce expected PTMs changes as the other HDAC inhibitors. However, many proteins that were differentially enriched comparing to control could explain the metabolic differences presented after the treatment with those drugs. Therefore, the observed effect of sirtuins on metabolism could be mediated partially by PTMs and a few key metabolic proteins whose expression is affected, and partially directly by regulating targets in the cytoplasm.

3.7.7 Epigenetic effects of two inhibitors with cytoplasmic targets

In addition to focusing the analytical work on small molecules that directly target epigenetic proteins, two compounds were selected where a clear connection with chromatin regulation has not been identified so far. SC00106943 is a specific inhibitor of the cytoplasmic ubiquitous PTP1B (protein-tyrosine phosphatase 1B), an important negative regulator of insulin-induced glycolysis (Tiganis, 2013).

In line with the small observed difference in the metabolic readout between treatment and control, cellular levels of glycolytic proteins were not affected or slightly downregulated by treatment with SC00106943 (Fig. 3.44A, Fig. 3.46). While PTP1B's primary function relates to the deactivation of activated insulin receptor, more functions have been uncovered – including the regulation of several

important signaling cascades that regulate transcription, such as inflammation-associated JAK-STAT and growth-regulating PI3K-AKT pathways (Feldhammer et al., 2013; Valverde & González-Rodríguez, 2011). The seahorse XF results suggested that in addition to the known immediate effects on glycolysis, PTP1B could influence oxidative phosphorylation via altered gene expression, as levels of oxidative phosphorylation were elevated after 72h treatment but not after 1h treatment (Fig. 3.44A). In line with a potential undescribed chromatin-mediated function of PTP1B, levels of histone H3K4me2 were elevated (Fig. 3.44B). Furthermore, changes across the proteome were observed (Fig. 3.45), including proteins involved in insulin signaling (e.g. more than 15-fold downregulation of SORBS1, which is required for insulin-mediated glucose import), as well as levels of transcription regulators (e.g. RNA polymerase II CTD phosphatase RPAP2, transcription factors).

SC00106940 is a naturally occurring flavonoid that has direct antioxidative functions as a scavenger of reactive oxygen species, but it can also modulate the activity of cytoplasmatic proteins (Dajas et al., 2013; Tuorkey, 2016). In line with these known cytoplasmatic effects, comparably strong effects on metabolism were observed already after 1 hour of treatment with this drug (Fig. 3.44A). The observed significant reduction of histone H3 and H4 acetylation by this treatment was unexpected, but could in fact be explained by the recent discovery that SC00106940 decreases histone acetyltransferase activity and can directly bind HATs (S. A. Ganai et al., 2018; A. Kim & Yun, 2017). The proteomic expression profile of SC00106940-treated cells could therefore be a consequence of the putative in vivo inactivation of HATs, which in turn could be responsible for the observed metabolic effects after longer treatment durations (Fig. 3.45, Fig. 3.44A).

Taken together these two small molecules, both of which are investigated as potential drug candidates in metabolic, neurological or oncological indications, demonstrated that despite a generally-accepted cytoplasmic mechanism-of-action, epigenetic modulators may be affected by treatments which in turn can have relevant consequences on the cells's energy and signaling homeostasis. It is therefore important to consider epigenetic effects and their consequences also in cases where the primary drug targets seem to be limited to the cytoplasm.

Figure 3.44. PDE and PTPB inhibitors

A. 72h and 1h treatments with selected PTPB and PDE inhibitors induced metabolic changes comparing to ctrl.

B. 72h treatments with selected PTPB and PDE inhibitors and activator induced histone PTMs comparing to ctrl.

Figure 3.45. PTPB and PDE inhibitors. Proteome (1x) induced changes after 72h treatment with selected compounds

Hierarchical clustering of protein changes after treatment with selected PTPB and PDE inhibitor and activator compound

Other inhibitors: pathway mapping for SC00106943

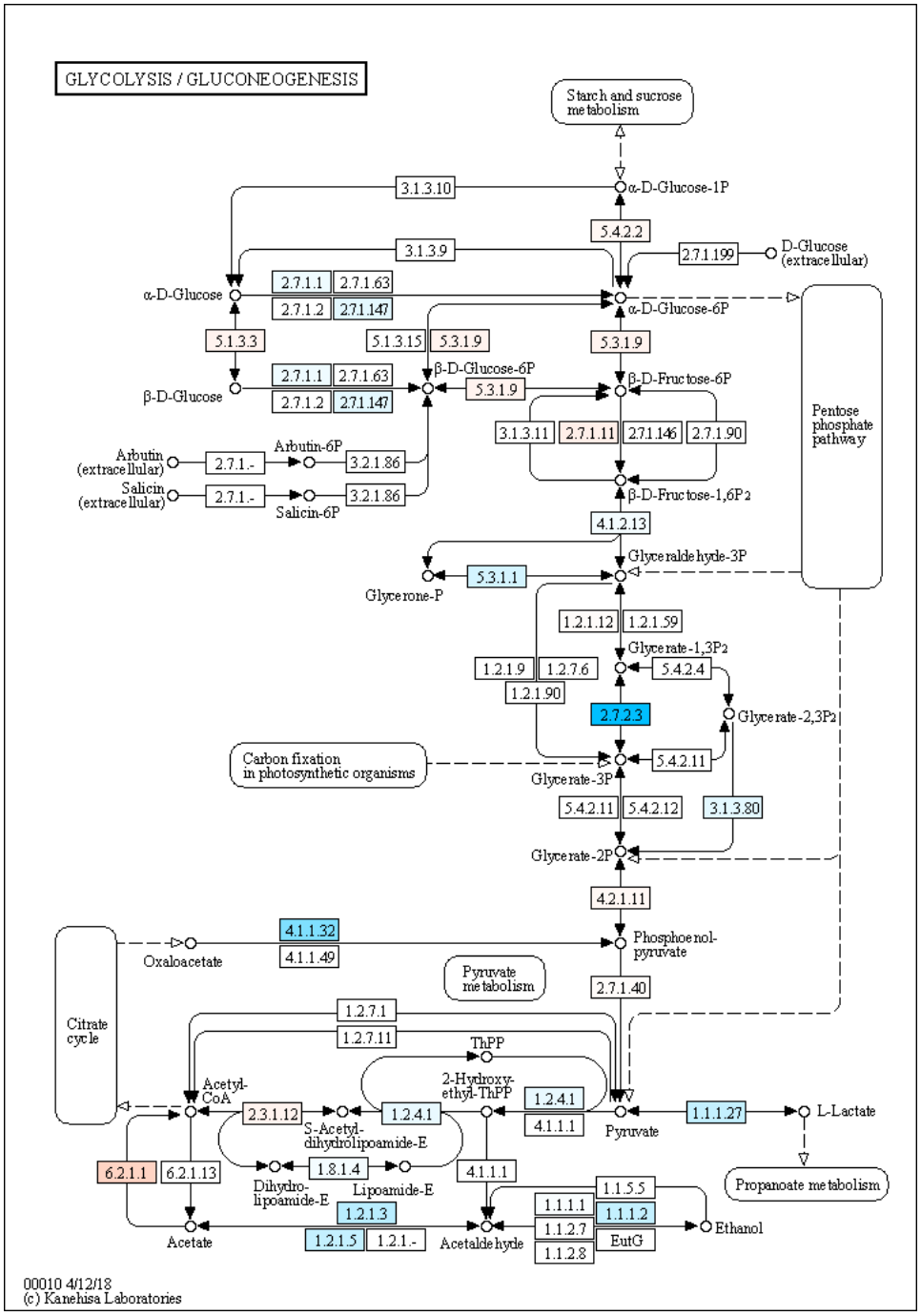

Figure 3.46. Glycolysis pathway mapping of PTP1B inhibitor SC00106943

Glycolysis pathway mapping of proteins identified using quantitative mass spectrometry of whole-cell extracts in samples from control-treated or SC00106943-treated HEK293T cells. The map depicts the canonical human glycolytic pathway obtained from KEGG. Colors indicate upregulation (red) or downregulation (blue) in drug-treated samples relative to the control sample.

3.8 Overarching links between epigenetics and metabolism

The Chapter 3.7 focussed on the effects of individual inhibitor treatments on the three experimental assays, metabolism, histone PTMs and the cellular proteome. Common themes among those readouts were identified for each chemical group. To look into prevalent epigenetic marks influencing metabolism irrespective of the drug treatment that caused them, various types of correlation analyses were performed. More specifically, the purpose of this second type of analysis presented in this Chapter 3.8 and Chapter 4.1 was to use the set of 30 inhibitors as a tool to experimentally induce various changes in metabolism and PTMs to create many different combinations of cellular states. Each cellular state was defined by all analysed histone PTMs (e.g. high H3/H4 acetylation), the state of metabolism (e.g. high oxidative phosphorylation, low glycolysis) and the relative level of proteins in the proteome. By comparing all variations and common features from all the cellular states, statistical analyses were then used to identify common rules that link those states.

3.8.1 Acetylation changes correlate with decreased glycolysis

As a first step, multivariate linear modelling between all measured histone PTM levels and metabolic states was performed for all drug treatments. This analysis determines if direct linear correlations exist between any of the histone PTM marks and a given metabolic state.

This analysis demonstrated that acetylation levels on histone H4 were significantly correlated with basal and maximal glycolysis rates, as well as maximal oxidative phosphorylation but not with basal oxidative phosphorylation (Fig. 3.47A-D). In contrast, using this type of analysis, histone methylation did not appear to be significantly correlated with oxidative phosphorylation or glycolysis (Appendix Fig A.10). When this analysis was restricted to HDAC and HAT inhibitors, in order to more directly assess the impact of acetylation changes on metabolism, higher acetylation of H4 peptides correlated with a decrease in glycolysis. However, no correlation with oxidative phosphorylation changes was identified. Oxidative phosphorylation was in most cases increased irrespective of the acetylation changes in H4 peptides. These results indicate that acetylation marks on peptides H4K5K8ac, H4K12K16ac, H4K5K12K16ac, H4K5K8K16ac, H4K5K8K12K16ac, H4K5K8K12ac, H4K8K12K16ac maybe involved in modulating glycolysis.

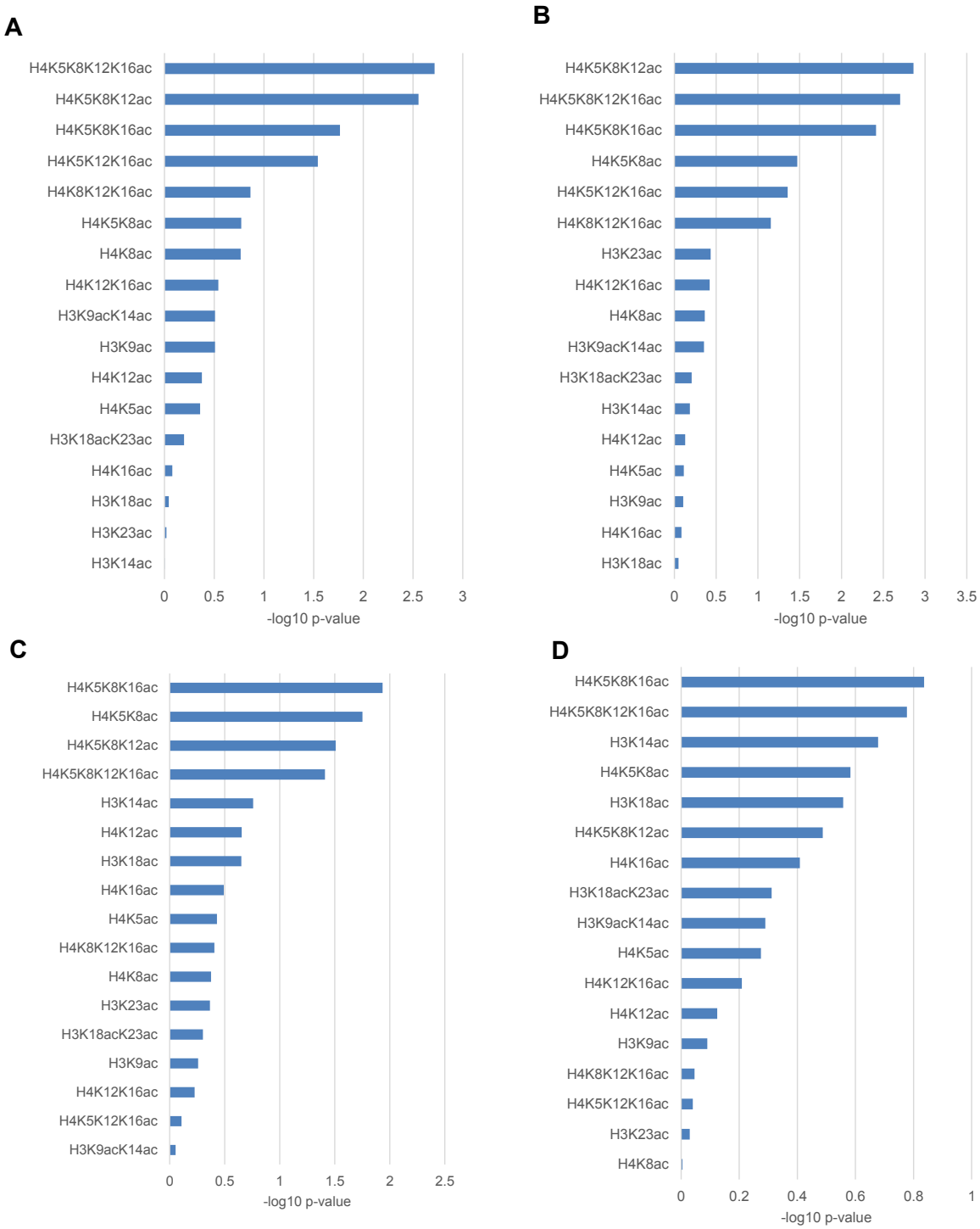

Figure 3.47. Correlation of acetylation marks on H3 and H4 and metabolic states

Multivariate linear modelling was performed between all histone PTMs levels and metabolic states induced by treatments with 30 different drug candidates. Values depict -log 10 p value where p>1.3 indicates a significant correlation (corresponding to p<0.05) between the respective PTM and metabolic state.

A. Correlation between histone lysine acetylation and basal glycolysis

B. Correlation between histone lysine acetylation and maximum glycolysis

C. Correlation between histone lysine acetylation and maximum oxidative phosphorylation

D. Correlation between histone lysine acetylation and base oxidative phosphorylation

A similar correlation was detected when all drug inhibitor classes were selected for comparison, however as their impact on cellular acetylation levels was generally less pronounced, also the impact on glycolysis was more limited. In conclusion, the main drivers of this effect were HDACs and HATs which led to strong changes of histone acetylation levels and at the same time lower rates of glycolysis. As the multivariate linear modelling is less sensitive to potential correlations between different variables, for instance if variables correlate but in a non-linear way, more advanced and powerful ways to analyse were employed next, including Principal Component Analysis (PCA) and correlation matrices, as discussed in Chapters 3.8.2, 2.8.3 and 4.1. Importantly, the key observation from this linear modelling – anticorrelation between histone acetylation and glycolysis – was confirmed with both alternative statistical methods.

3.8.2 Identification of opposing chromatin modification networks

As an alternative and more powerful unbiased analysis approach, Principal Component Analysis (PCA) was carried out as described in Materials and Methods Chapter 2.6.3. This allowed to get insights about the connections between histone acetylation and methylation patterns (this Chapter) and moreover, possible clustering with cellular metabolic states (Chapter 3.8.3). 75% of data variance of histone PTM levels was explained by combined principal components one to three (PC1-3, Fig 3.48 A). Different modifications were explained to different degrees by the first two (PC1/2) or third and fourth dimensions (Fig 3.48B, C). For example, the variances of histone PTM acetylation (e.g. H3K18acK23ac) were almost completely explained by PC1 (Fig 3.48B), while H3K27me1 was mostly represented in dimensions 3 and 4 (Fig 3.48C). This means that while some modifications usually are either correlated (e.g. different H3 acetylation on various residues) or anticorrelated (e.g. H3 acetylation and H3K9me3), other modifications are not directly linked to those mechanisms, and their levels changes largely independently of other PTMs.

To make this point clearer, the variation of all histone PTM levels across all PCA dimensions was calculated and plotted (Fig 3.49). Importantly, this type of analysis does not indicate whether a given observation is correlated or anti-correlated but it can point to histone modifications that are regulated by the same or overlapping pathways if they are represented in the same dimension / principal

A PCA fraction of variance by PC dimension

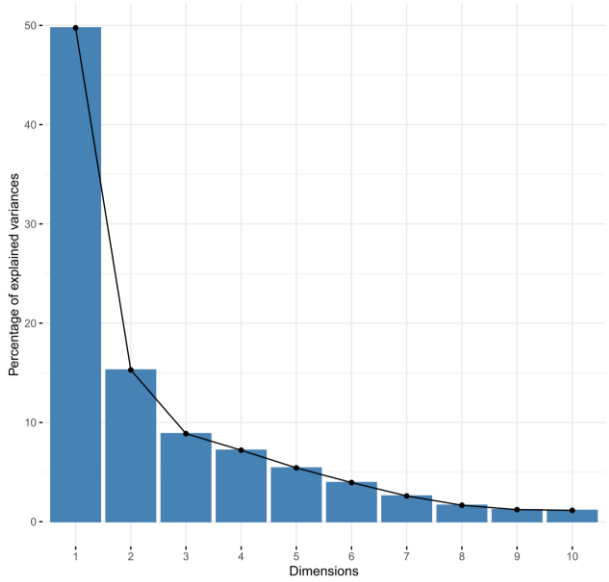

B PCA variance per variable (histone PTM), cumulative PC1+2

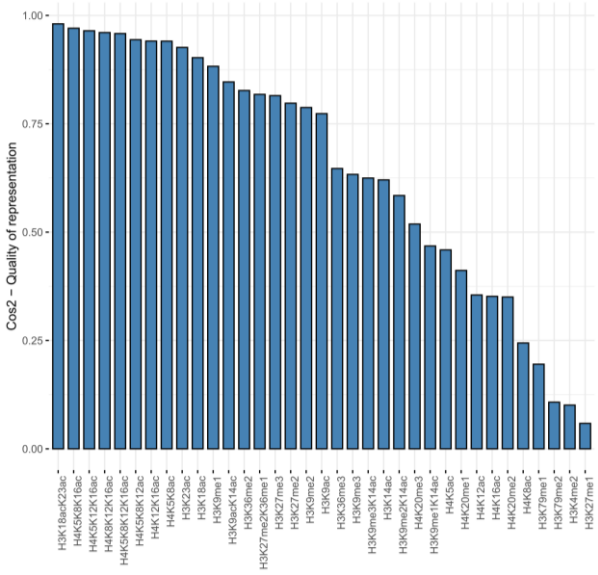

C PCA variance per variable (histone PTM), cumulative PC3+4

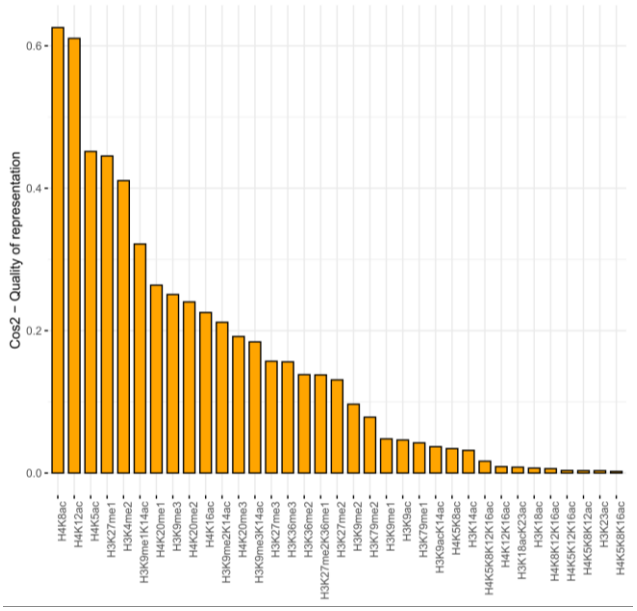

Figure 3.48. PCA analysis of acetylation and methylation marks on H3 and H4 induced by treatments with 30 different small molecules.

A. 75% of data variance was explained by PC1-3

B. Acetylation and methylation percentage variance explained by PC1 and PC2

C. Acetylation and methylation percentage variance explained by PC3 and PC4

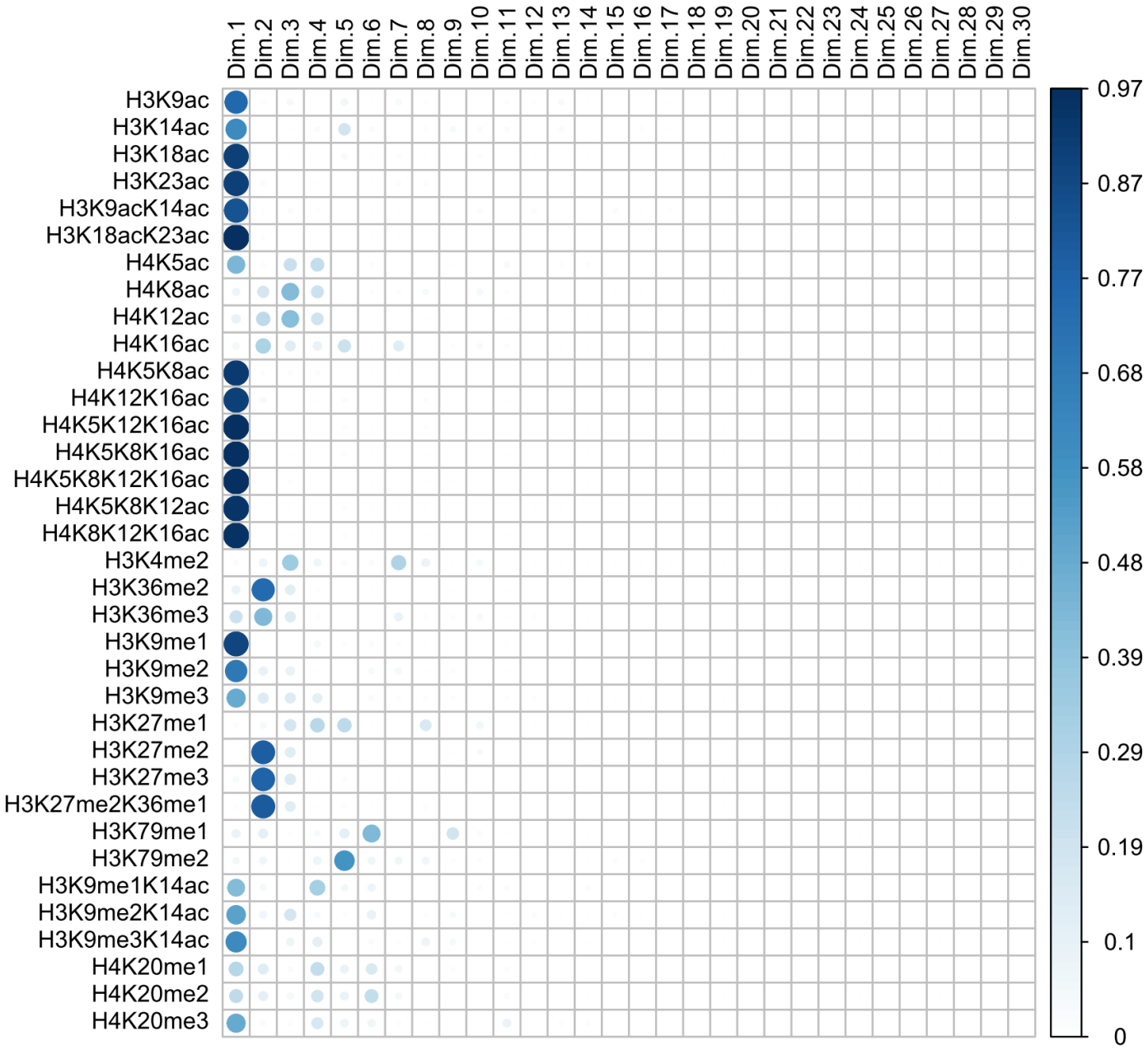

Figure 3.49. PCA analysis of acetylation and methylation histone modifications on H3 and H4 induced by treatments with 30 small molecules across all principal components

Degree of data representation across PCA dimensions PC1-30. The size and colour of bubble indicates a higher degree of representation in a specific dimension for the respective PTM mark, ranging from 0 (0%) to 1 (100%), as depicted in the legend on the side of the diagram.

component. As shown in Fig 3.49, a large fraction of the observed variation of histone PTMs was explained by PC1, including for instance H3K9ac and H3K9me2, two marks that are antagonistically regulated in cells. However, there were some notable exceptions: Acetylation changes on H4 were observed in the same PC dimension (PC1) as H3K9me1/2/3 and H4K20me3. In contrast, activating marks H3K36me2/3 were linked with repressive H3K27me2/3 through PC dimension 2. Interestingly, H3K79 was more variable than other modifications, varying in 2-3 dimensions on its own (Fig 3.49). As exemplified by H3K79 methylation but identified also by other histone PTMs, this analysis showed that different modification states of the same residue were linked through different PC dimensions: e.g. H3K79me1 in PC6, while H3K79me2 in PC5. This therefore potentially pointed to different regulatory networks with other histone modifications and cellular factors, in order to mediate different cellular functions

Furthermore, this analysis suggested that some modifications were not explained by common transcription regulation mechanisms. In particular, modifications that play clearly defined roles in general transcription such as H3K9ac, H4K5K8ac, H3K9me1/2/3 were explained by the same dimension (PC1). On the other hand, histone PTM marks that have been linked with more diverse epigenetic functions like transcription initiation (H3K4me2), transcription elongation (H3K36me2/3), and transcriptional silencing (H3K27me3) were explained by different dimensions but not PC1 (Fig 3.49). Interestingly, there were modifications like H3K27me1, H4K20me1/2/3, H3K79me1/2 that were present in more than four dimensions pinpointing a great variability in the biological activities of these marks. A more detailed picture of the possible activities of these histone modifications and possible links with metabolism are described in the discussion in chapter 4.1.

As seen in the PCA Biplot (Fig 3.50), histone acetylation was mostly explained by PC1, in line with the location of several HDAC inhibitors including SC00106933, SC00106837, S00107771. On the other hand, the variation of methylation levels of PTMs H3K27me2/3 and H3K36me2/3 in the PCA Biplot is mainly explained in PC2, in line with the location of several methylation inhibitors including SC00107026 and SC00107028. The effects of other inhibitors were to a larger degree explained by other dimensions, e.g. PC3 and PC4.

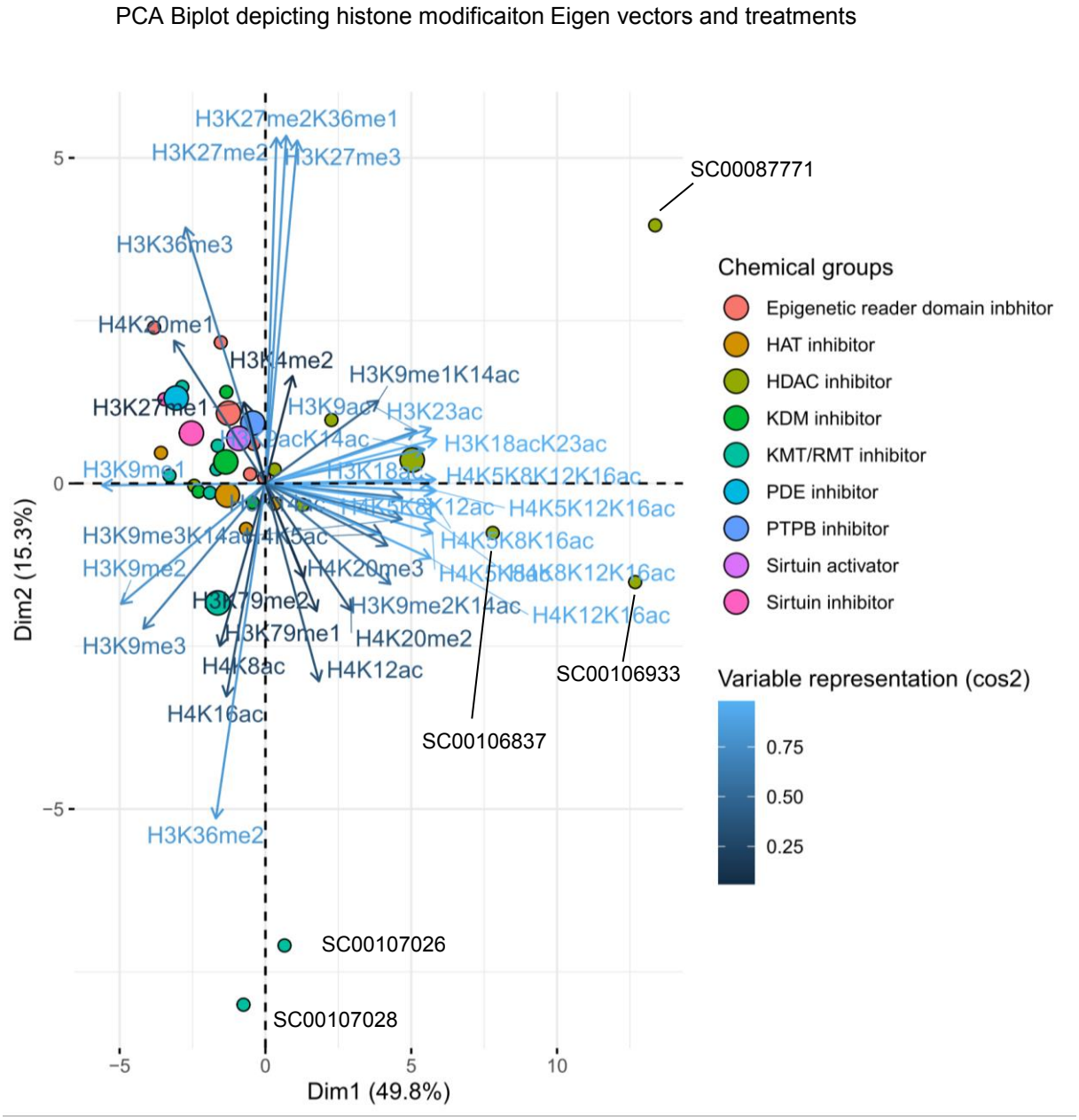

Figure 3.50. PCA Biplot of histone acetylation and methylation modifications on H3 and H4 induced by treatments with 30 different small molecules.

Biplot of PC1 (Dim1) and PC2 (Dim2). Each drug group is differentially coloured and each dot represents one drug. The length and the colour of Eigen vectors represents a higher or smaller degree of correlation of the specific histone PTM (named at the end of each arrow) with the respective PC. The orientation of the Eigen vectors indicates correlation or anticorrelation with a specific PC. The bigger sized bubbles represent the statistical center of each drug group.

To specifically look at the type of the correlation between these histone marks (correlated or anticorrelated), the eigenvectors were plotted along PC1 and PC2 (Fig 3.51). The length of the eigenvectors shows how much the specific variable is correlated with the dimension it is close to and the arrows depict the direction of the correlation. For example, H4K12K16ac (and others) and H3k9me1/2/3 were previously described to be explained by PC1 (Fig 3.49). From Fig 3.51, it becomes clear that these marks did appear to be commonly explained by PC1 and anticorrelated, as their eigenvectors lie close to the PC1 (Dim1) axis but face in different directions. This is in line with the data that supports that histone acetylation is linked mainly with transcription activation whereas H3K9me1/2/3 with transcriptional repression. Interestingly, H3K27me2/3 (repression) faced to a degree in a similar direction as H3K36me3 (elongation) and opposite to H3K36me2 (initiation). Also, H3K4me2 (initiation) was in the same direction with the repressive H3K27me2/3 but most of this data was explained in the dimensions (PCs) 3 and 4 where there was no correlation between them but rather H3K4me2 was anticorrelated with H3K27me1. The eigenvector of the variable mark H4K20me1 (variability seen before (Fig 3.49) was spanning across different dimensions. Indeed, in PC1 and 2 it was in the same direction of H3K36me2, H3K27me1 and opposite of H4K20me2/3 (Fig 3.51). In PC3 and PC4, H4K20me1 appeared to have opposite activities of H3K27me1 but remained anti-correlated with H4K20me2/3.

3.8.3 Metabolic regulation via specific histone methylation and acetylation marks

To specifically investigate the correlation of either histone acetylation or methylation patterns with metabolism, a PCA was carried out – this time including the metabolic assay readouts induced by the 30 small molecule treatments in addition to histone acetylation/methylation as additional variable (while the analysis in Chapter 3.8.2 did not include the metabolic readouts).

In the resulting PCA, acetylation/metabolism data were explained by PC1 to almost 70%, which is in contrast to methylation/metabolism data, where only 26% of variance was explained by PC1 (Fig 3.52 A, B). Therefore, methylation appeared to be more variable than acetylation or that the cooccurring observations between methylation and metabolism could be explained in more diverse

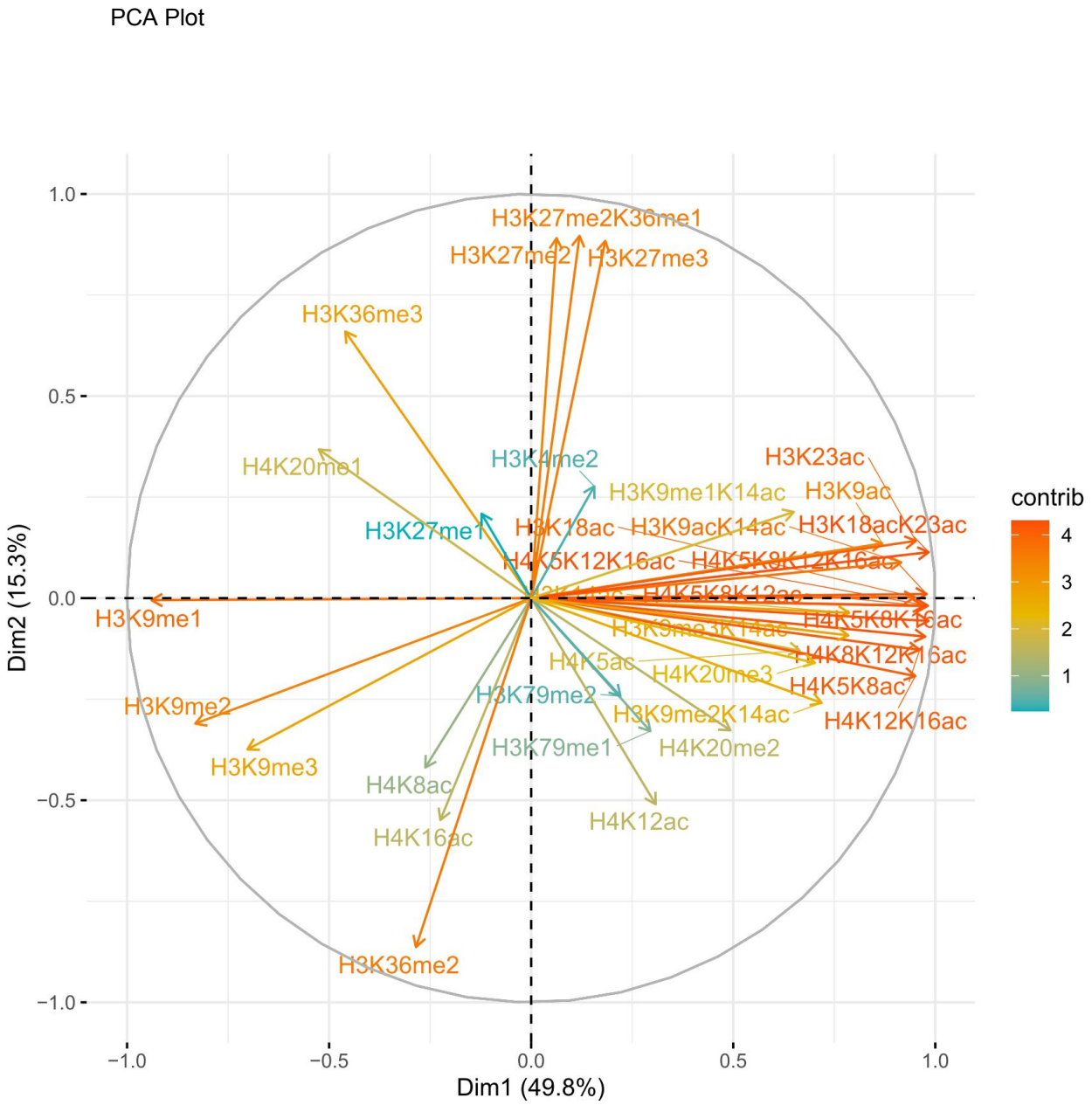

Figure 3.51. Depiction of variables of the PCA plot of acetylation and methylation marks on H3 and H4 of 30 drug candidates

Representation of PC1 and PC2. The length and the colour of Eigen vectors represents a higher or smaller degree of correlation of the specific PTM mark with the respective PC. The orientation of the Eigen vectors indicates correlation or anticorrelation with a specific PC.

A PCA fraction of variance by PC dimension: histone methylation & metabolism

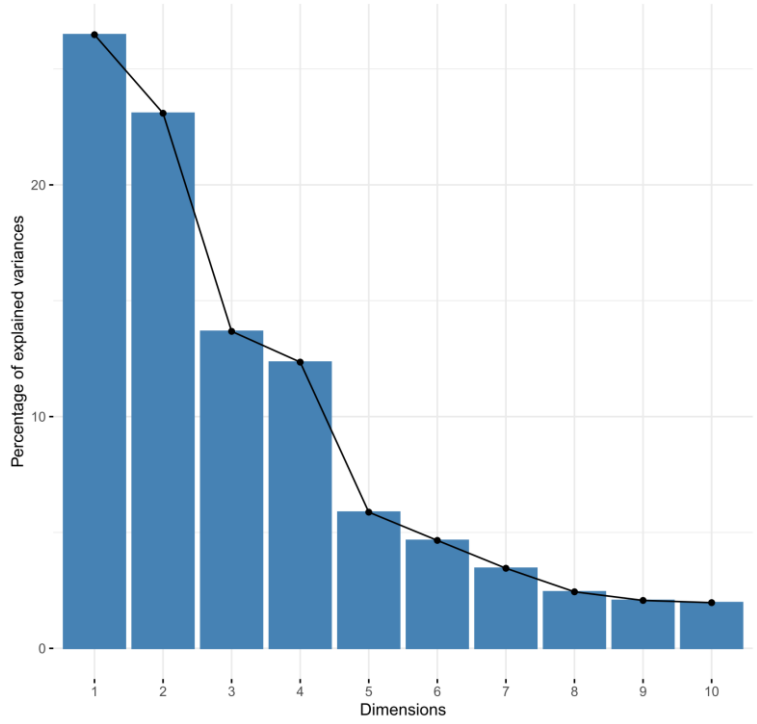

B PCA fraction of variance by PC dimension: histone acetylation & metabolism

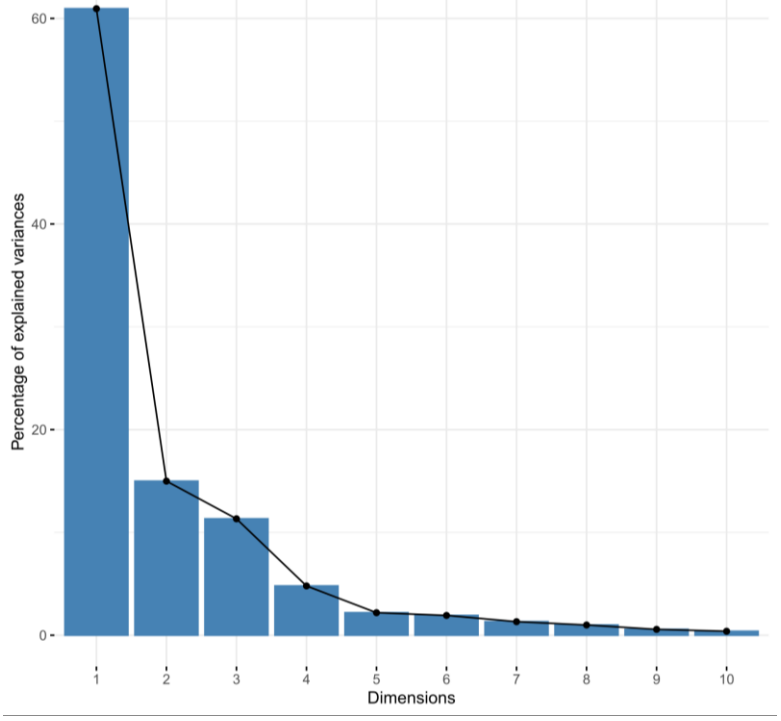

Figure 3.52. PCA analysis of acetylation and methylation histone PTMs on H3 and H4, as well as metabolic readouts (glycolysis and oxidative phosphorylation) induced by treatments with 30 different small molecules

A. Percentage of methylation and metabolism variance explained by each principal component.

B. Percentage of acetylation and metabolism variance explained by each principal component.

ways. This is in line with the more general effect, partially physically, that acetylation has on chromatin, while methylation is written and read by more specific enzymes and reader proteins. Regarding specific methylation modifications and the metabolic readouts oxidative phosphorylation and glycolysis, 76% of the data was explained by PC1-4, with 50% of the data explained by PC1-2 (Fig 3.52 A). Specifically, oxidative phosphorylation was explained by PC4 and to a lesser degree by PC2, in contrast to glycolysis readouts that were explained by more than 4 dimensions, but to a significant part in PC3 (Fig 3.53). This analysis suggested that oxidative phosphorylation was explained by different epigenetic regulatory pathways than glycolysis and that the overlap between those epigenetic pathways that regulate them is minimal. The fact that oxidative phosphorylation and glycolysis can be controlled independently is well described. In fact, normal tissues strongly rely on their ability to enter into "glycolytic states" or "oxidative state", and also tumor cells can switch between both states more dynamically (or hybridically) than previously thought when the Warburg effect was first formulated (Jose et al., 2011; D. F. Wilson, 2017; L. Yu et al., 2017). However, the differential regulation by epigenetic networks had not been demonstrated comprehensively so far, as was the case in this study through induction of the changes using epigenetically-active small molecules.

Next, specific histone modifications that grouped with glycolysis were identified. For histone acetylation, almost all modifications grouped in the same dimension (PC1) together with a fraction of the variance of glycolysis (Fig 3.54). Interestingly, a large part of the glycolysis variation relating to histone acetylation grouped with mono-modified H4K5ac, H4K12ac, suggesting a potential role of those residues in regulating glycolysis (to a small degree, as dimension 3 only related to 11% of observed variation). The analysis of the eigenvectors along PC1 and PC2 showed that H4K5ac and H4K12ac were strongly anti-correlated to both base and maximal glycolysis (Fig 3.55), in line with the previous observations from the linear regression analysis in Chapter 3.8.1. On the other hand, methylation marks H3K9me1/2/3 and H4K20me1/2/3 grouped with glycolysis in PC1, while H3K4me2, H3K9me3, H3K27me1 (but not H3K27me2/3) grouped in PC3, suggesting that these two groups of modifications (defined by PC1 and PC3) regulate different aspects of glycolysis (Fig 3.53). In fact, the analysis of the distribution of the eigenvectors showed that as an example for the case of H4K20, only the mono-methylated form H4K20me1 correlated with higher levels of glycolysis, while

PCA variation matrix across all PC dimensions and variables (histone methylation)

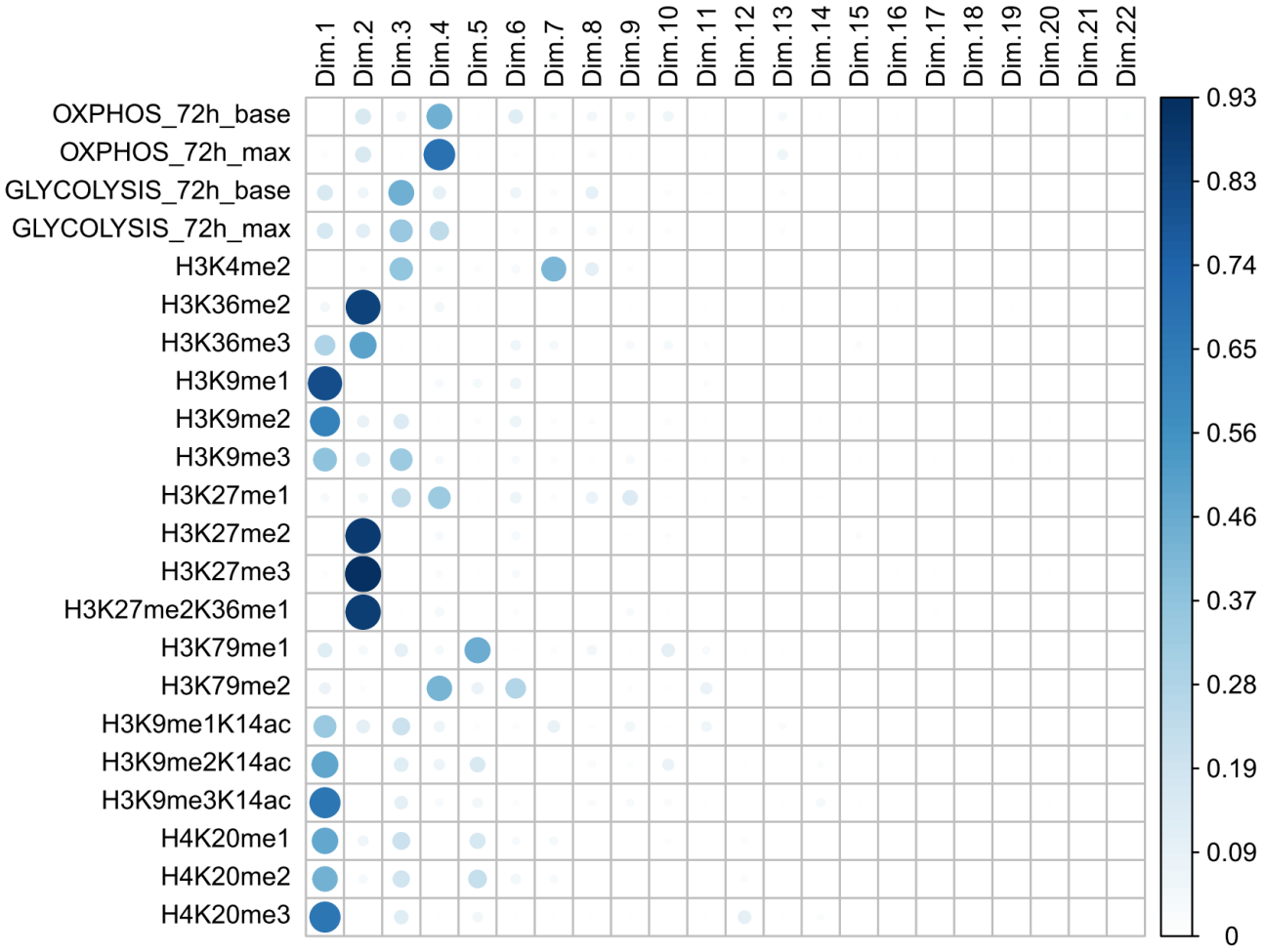

Figure 3.53. PCA analysis of methylation histone modifications on H3 and H4, as well as metabolic readouts, induced by treatments with 30 small molecules across all principal components

Degree of data representation across PC1-30. The size and colour of bubble indicates a higher degree of representation in a specific dimension for the respective PTM mark, ranging from 0 (0%) to 1 (100%), as depicted in the legend on the side of the diagram.

PCA variation matrix across all PC dimensions and variables (histone acetylation)

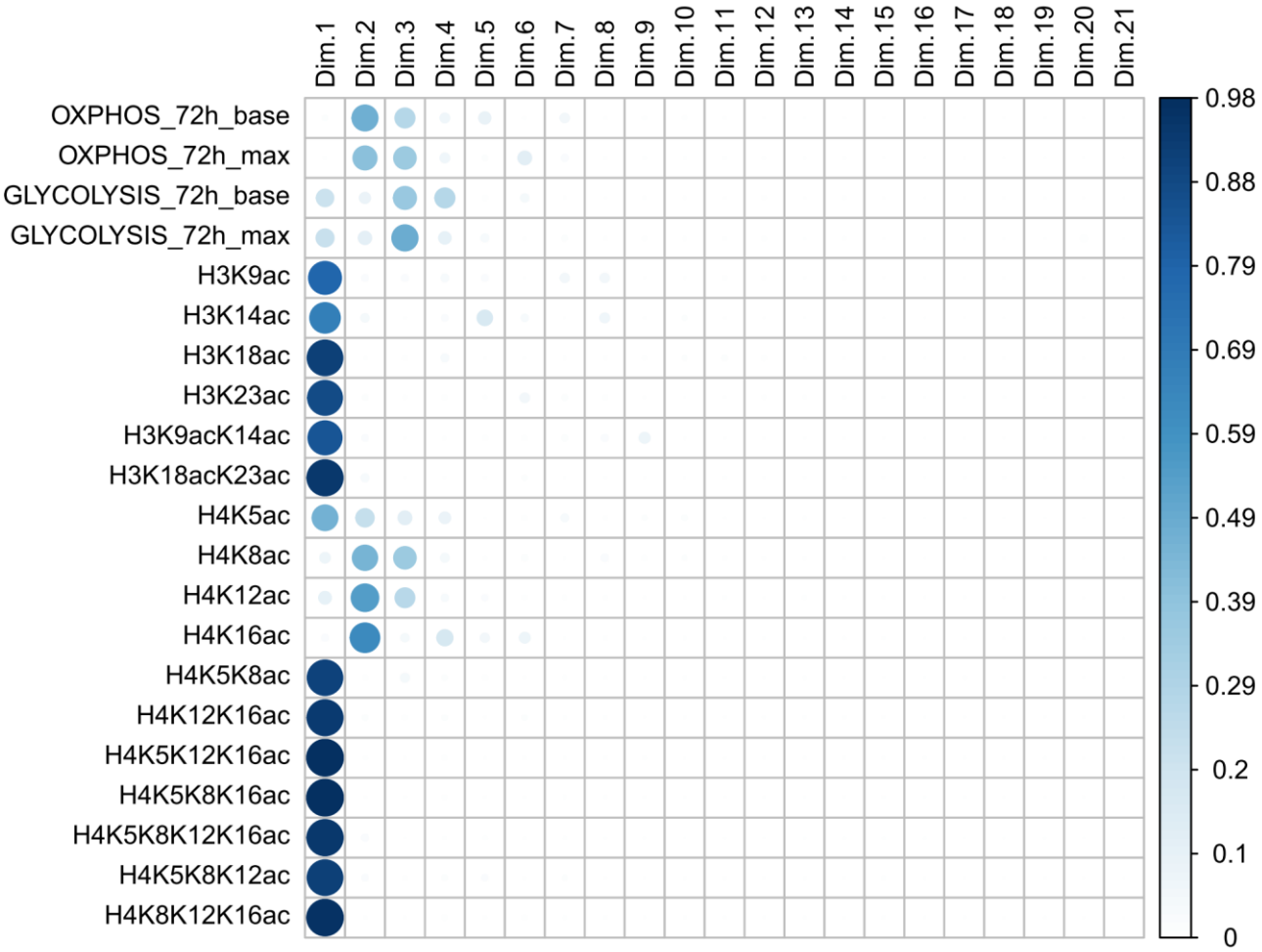

Figure 3.54. PCA analysis of acetylation histone modifications on H3 and H4 induced by treatments with 30 small molecules across all principal components

Degree of data representation across PC1-30. The size and colour of bubble indicates a higher degree of representation in a specific dimension for the respective PTM mark, ranging from 0 (0%) to 1 (100%), as depicted in the legend on the side of the diagram.

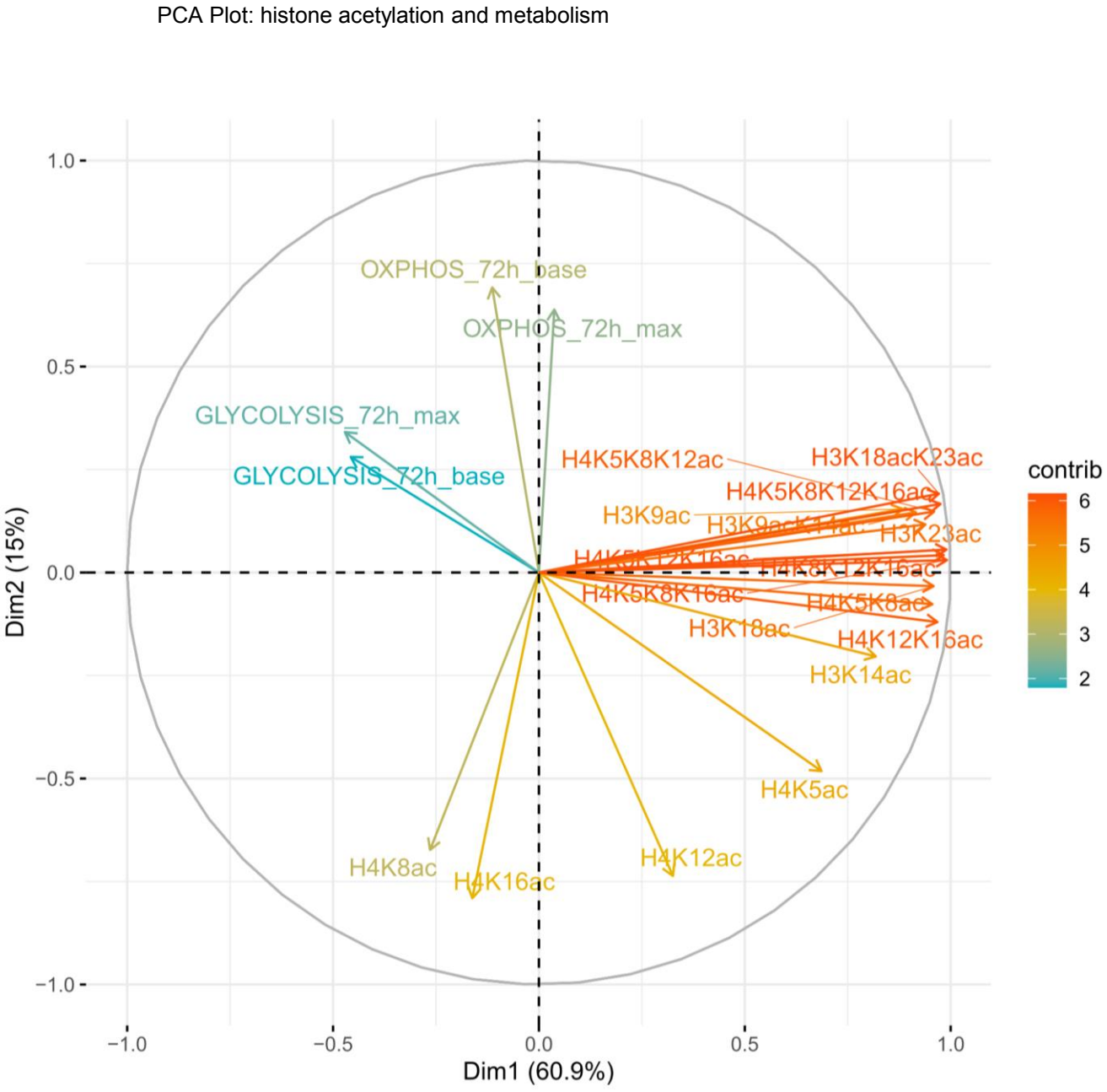

Figure 3.55. Depiction of variables of the PCA plot of acetylation histone modifications on H3 and H4 induced by treatments with 30 small molecules and metabolic states

Representation of PC1 and PC2. The length and the colour of Eigen vectors represents a higher or smaller degree of correlation of the specific PTM mark or metabolic state with the respective PC. The orientation of the Eigen vectors indicates correlation or anticorrelation with a specific PC.

H4K20me2 and me3 indicated an anti-correlation (Fig 3.56). This repeated observation of H4K20's involvement in glycolytic regulation, differentiated by mono vs di/trimethylation, could be related to the different roles of H4K20me1 vs H4K20me2/3 in transcription although not fully characterised and (see for instance Chapter 3.7.2, 3.7.3, 3.7.4).

As introduced above, a different set of PTMs grouped with oxidative phosphorylation: regarding acetylation, specifically H4K8ac and H4K16ac showed strong correlation (Fig 3.54), which was confirmed by the representation of eigenvector analysis, where those two histone acetylation marks anticorrelated with high levels of oxidative phosphorylation (Fig 3.55). The difference to the histone PTM pattern of glycolysis was even more prominent for methylation marks. Histone PTMs specifically grouping with oxidative phosphorylation (but not glycolysis) were transcription-elongation-associated H3K36me2/3, repressive H3K27me2/3 (in PC2) as well as H3K79me2 (in PC4) (Fig 3.54). Interestingly, the seemingly unintuitive observation of grouping with both a transcription-associated mark such as H3K36me2/3 and the repressive H3K27me2/3 was clearly explained by the eigenvector analysis of oxidative phosphorylation vs methyl PTMs, that clearly showed that H3K27me2/3 strongly correlated (pointed in same direction) as oxidative phosphorylation vectors, while H3K36me2 was anti-correlating (Fig 3.56). These observations suggested that oxidative phosphorylation co-occurred in cells with higher levels of repressive chromatin and lower levels of active ongoing transcription elongation.

In addition to modifications that occurred mostly with either oxidative phosphorylation or glycolysis (but not both), high levels of some histone modifications were observed together both with high levels of glycolysis and high levels of oxidative phosphorylation, namely H3K27me2/3, while high levels of H3K36me2 anti-correlated with both metabolic activities. Therefore, most (especially methylation) histone PTMs seemed to have a specific correlation with either glycolysis or oxidative phosphorylation, with the exception of the above-mentioned marks.

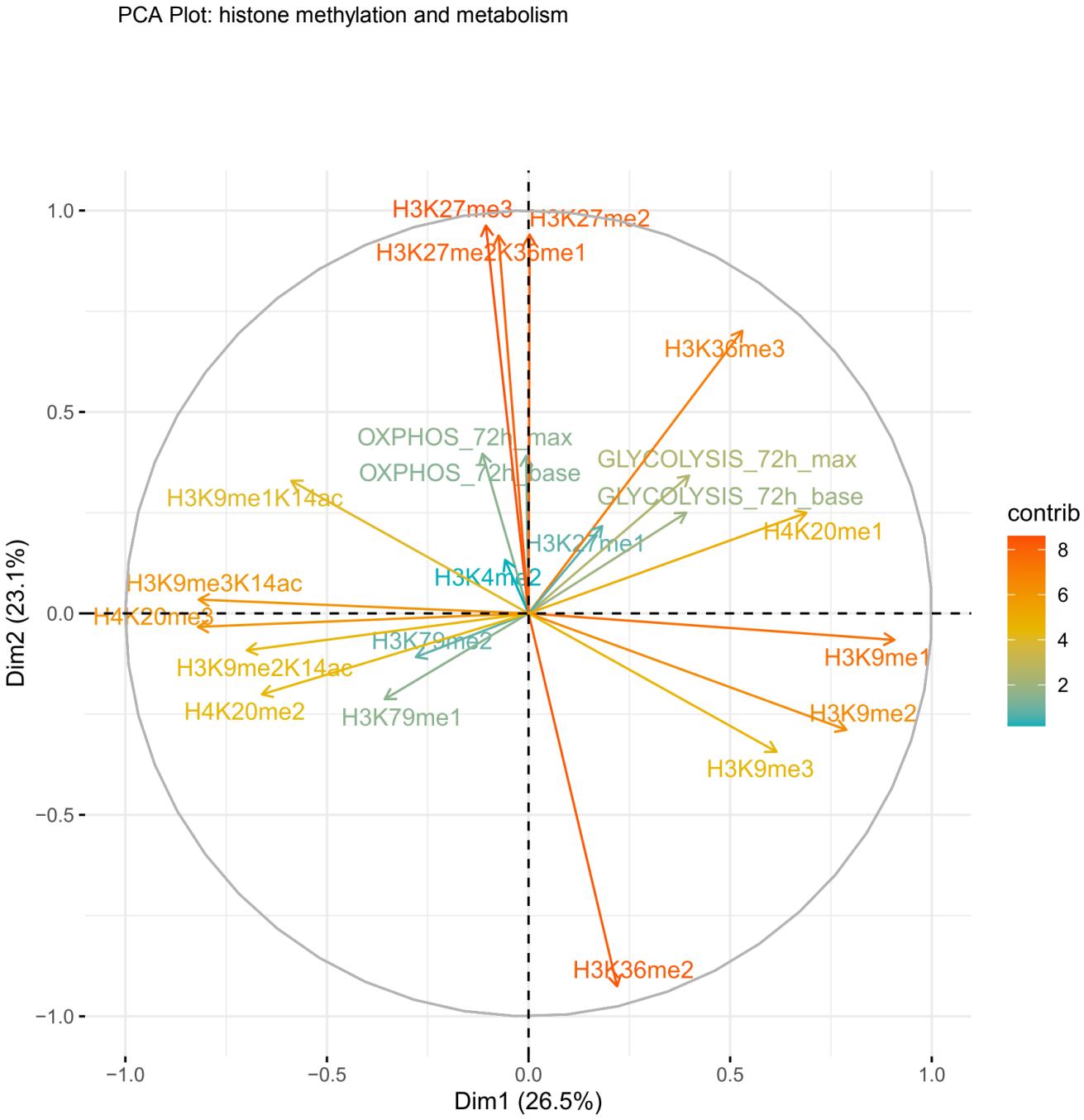

Figure 3.56. Depiction of variables of the PCA plot of methylation histone modifications on H3 and H4 induced by treatments with 30 small molecules and metabolic states

Representation of PC1 and PC2. The length and the colour of Eigen vectors represents a higher or smaller degree of correlation of the specific PTM mark or metabolic state with the respective PC. The orientation of the Eigen vectors indicates correlation or anticorrelation with a specific PC.

Chapter 4

Discussion

4.1 Identification of new metabolic regulatory networks and potential drug targets

Using a different analysis approach (correlation matrix based on multivariate Pearson's correlation), the results of the overarching analysis (Chapter 3.8) were summarized for histone PTM networks (Fig. 4.1), histone PTMs correlating with metabolism (Fig. 4.2) and identification of protein targets correlating with different metabolic states (Fig. 4.3). These analyses confirmed the two previous statistical approaches (linear modelling, PCA). It is important to note that interactions derived from this study were based on comparing cellular states (metabolism, histone PTMs, proteome) induced by small molecule treatments, while in many cases in other literature, the experimental approaches described native cellular states. The key observations from this correlation analysis were:

1. Additional histone PTM networks were identified. Apart from expected network interactions, this study uncovered several relationships – especially so far uncharacterised in response to drug treatments (see results Chapter 3.8 and below in Chapter 4.1.1)
2. The overarching analysis clearly showed that histone PTMs can be classified in three different groups in relation to their potential impact/interplay with metabolism: a) PTMs that define a high glycolytic signature, in a sense a histone code of glycolysis; b) PTMs that define a high oxidative phosphorylation signature; and c) PTMs that are increased in cells with high glycolysis and oxidative phosphorylation. No such comprehensive review of chromatin-metabolism has been carried out as of today (see below in Chapter 4.1.2). Generally, the "high glycolysis code" was marked by histone modifications associated with transcriptional repression (low acetylation, high H3K9me2/3, high H3K27me2/3). In turn, the "high oxidative phosphorylation" code was marked by a much more diverse set of histone PTMs, characterised by high H3K79me2 and H3K27me2/3 and low H4K16ac and H3K9me2/3.
3. Several proteins that correlated with either glycolysis or oxidative phosphorylation induction/repression induced by the 30 different small molecules were identified. While some of these proteins appeared to be implicated with metabolic functions through previous studies, this analysis uncovered a range of proteins that could play new roles in regulating and modulating metabolic pathways (see below in Chapter 4.1.3).

4.1.1. Histone PTM networks

Although it was not the focus of this study to shed light into novel histone PTMs networks, the data allowed to look into novel interactions caused by epigenetic treatments and possibly link them to altered metabolism. Different histone PTM interactions were identified and described in the chapter 3.8. Those networks were largely operating as expected. For example, H3K36me2, a transcription elongation mark, anti-correlated with H3K27me3, a transcriptional repression mark (Laugesen et al., 2019; U.Selker, 2017) (Fig 3.57, 4.1). Another example was that H3K27me1 correlated with H3K36me3. H3K27me1 is a less abundant H3K27 methylation state (estimated at 5-10% of all histones in contrast to >50% for H3K27me2) that accumulates within the gene bodies of transcribed genes, promotes transcription, and is regulated by Setd2-dependent H3K36me3 deposition (Ferrari et al., 2014a; Laugesen et al., 2019). Furthermore, H3K9ac anticorrelated with H3K9me2/3 (transcriptional repression); moreover, acetylation marks correlated with each other and H3K4me2, a key transcription activation mark, which in turn anticorrelated with H3K9me2/3 which is a repressive mark (Fig 4.1). Apart from expected network interactions as outlined above, this study uncovered several new relationships especially so far uncharacterised in response to drug treatments.

In particular, H3K79me2 a transcription activating mark (Wood et al., 2018) that has been linked with DNA damage response and cell differentiation, anticorrelated with H3K27me1/2/3, H3K36me3 and others (Fig 4.1). H3K27me1, like H3K79me2 is also linked with active transcription and H3K27me2/3 with transcriptional repression. However, in the current study, H3K79me2 appeared to anticorrelate with H3K27me1 and to a lower degree with H3K27me2/3. These histone modifications (H3K79me2 and H3K27me1) have not usually been examined together in the same studies and under the same experimental conditions. Therefore, the different behaviour of the modifications in this study could point towards a yet undescribed regulatory network of both modifications. To support this possibility and emphasizing a specific role in metabolism, it is interesting to point out that H3K27me1/2/3 is participating in PRC2 dependent cell dedifferentiation in diabetes, as loss of PRC2 led to hyperglycaemia independent cell dedifferentiation mimicking diabetes (T. T. H. Lu et al., 2018). On the other hand, increase of the transcription activation modification H3K79me2 under hyperglycaemic conditions was suspected to contribute to diabetic renal fibrosis (Goru et al., 2016).

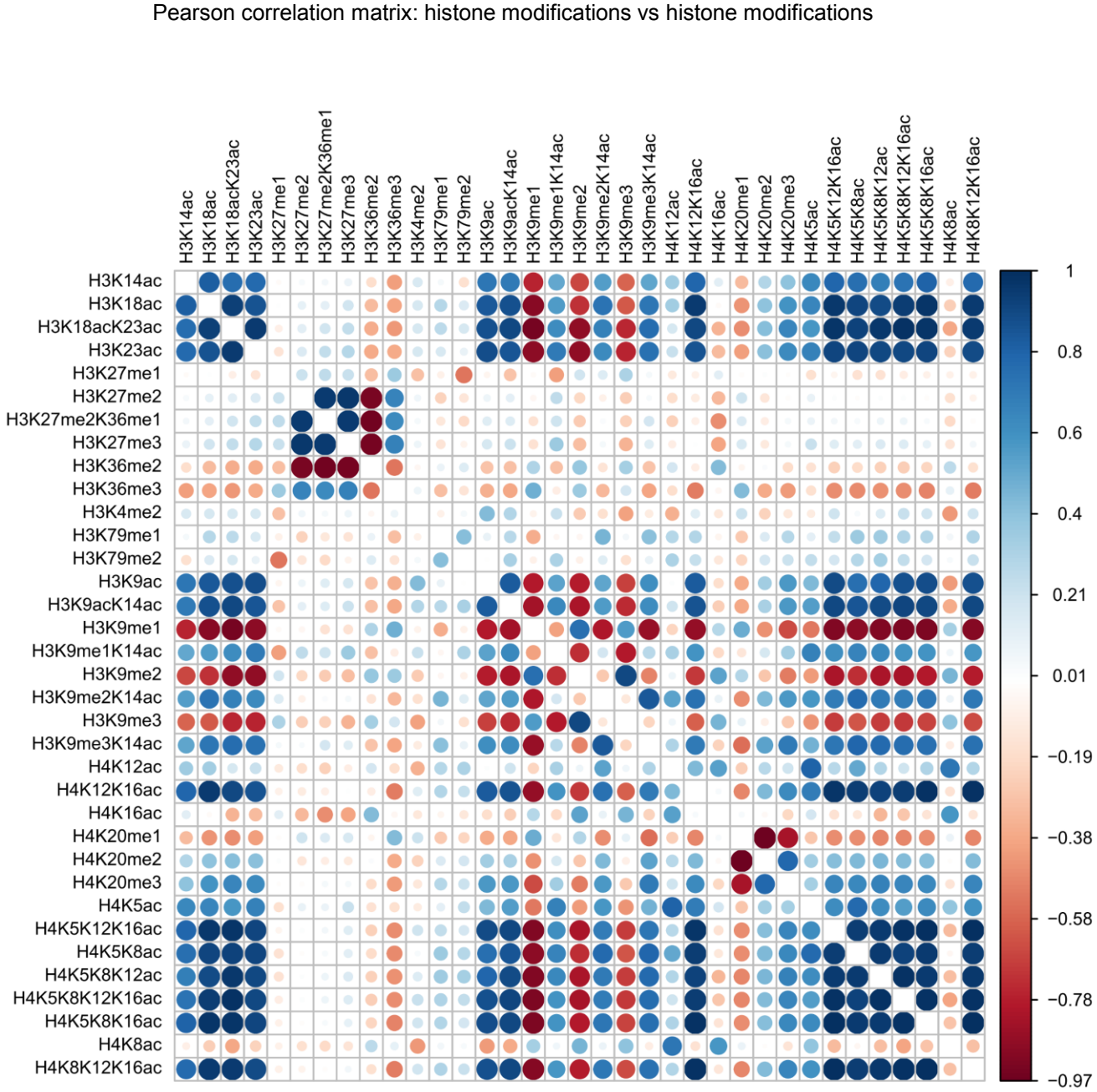

Figure 4.1. Pearson correlation analysis of acetylation and methylation modifications on histones H3 and H4 induced by treatments with 30 different small molecules

Correlation matrix based on Pearson's correlation coefficient. The size and colour of the bubble indicates a higher degree of correlation between respective PTM marks, as shown on the right-hand side legend, ranging from strong anticorrelation (red, -1) to strong correlation (blue, +1). The threshold for correlations selected in this graph was +/- 0.95.

Therefore, these two marks and their anticorrelating relationship may constitute a novel switch of metabolic regulation, being linked to opposite metabolic phenotypes: they both correlated with glycolysis but had opposite relationship with oxidative phosphorylation. H3K27me1 anticorrelated with oxidative phosphorylation and H3K79me2 correlated with oxidative phosphorylation (Fig 4.2).

Another example of a novel interaction are the three methylation states of H4K20, H4K20me1/2/3 (Fig 4.1). Specifically, H4K20me1 anticorrelated with H4K20me2/3, in line with the fact that those modifications are catalysed by different enzymes and are thought to associate with different cellular functions (Hyun et al., 2017). H4K20me1, even though it has usually been associated with active transcription (Beck et al., 2012b; Lv et al., 2016; L. Xiao et al., 2019), showed a more diverse picture in this study: while it correlated with transcription elongation-associated H3K36me3 and transcription-activation-associated H3K4me2, it anticorrelated with most acetylated H3 and H4 residues. Similarly, H4K20me1 also correlated with H3K9me1/2/3. On the contrary, H4K20me3, traditionally thought to be linked with inactive transcription (Beck et al., 2012a; Lv et al., 2016; Okamoto et al., 2017), correlated with all acetylation marks, and anticorrelated with H3K9me1/2/3. Interestingly, more recent studies have started to link H4K20me3 with a role in active transcription and associations with active histone modifications (Xu & Kidder, 2018). H4K20me2 has no well characterised function to date and no link with transcription has been identified. However, in the current study, H4K20me2 presented an identical correlating profile with H4K20me3. These correlation analyses showed that H4K20me1 and H4K20me2/3 have very distinctive profiles regarding their interaction within the histone code and that their response pattern caused by epigenetic small molecules may be different than their native distribution across genes as described in previous studies. This is also a novel interaction in regards to metabolic regulation effects. As presented in the interrelations of the histone code and metabolic states of the current study, H4K20me1 correlated with glycolysis as H3K9m1/2/3 did but H4K20me2/3 anticorrelated with glycolysis.

Another example is the H3K9me1/2/3. H3K9me1/2/3 is usually linked with inactive/repressed genes and heterochromatin (Jih et al., 2017; Ninova et al., 2019; Salzberg et al., 2017). Indeed, H3K9me1-3 strongly anticorrelated as expected with histone acetylation (Fig 4.1). However, unexpectedly, all three modifications also showed correlation with H3K36me3, which is usually

distributed along actively-transcribed gene bodies (Fig 4.1). Interestingly, in a recent study a subset of genomic regions including Zinc-finger protein (ZFP) genes and repetitive DNA were characterised by this uncommon combination of H3K36me3 and H3K9 methylation (Supplemental materials in (T. T. H. Lu et al., 2018)). However, these regions were not investigated and the function of this remains unclear but the response to epigenetically-active molecules described here suggests a potentially relevant role and warrants further investigation.

Although the focus of this study has not been to identify new histone PTM networks in native cellular states, the above few examples have indicated that previously undescribed or less characterised interactions could be physiologically relevant for metabolic regulation. Specifically, the current study is different from what has been published, in that it allowed analysis of the impact of epigenetically-active small molecule inhibitors on chromatin PTM networks. Furthermore, those changes could be brought into perspective of the co-occurring metabolic and proteomic changes, as discussed in the following Chapters 4.1.2 and 4.1.3.

4.1.2 Interplay between histone PTMs and metabolism

In the results Chapter 3.8, the overarching analysis showed that histone PTMs could be classified in three different groups in relation to their potential impact/interplay with metabolism: a) PTMs that are linked with a high glycolytic signature, the histone code of glycolysis b) PTMs that are linked with a high oxidative phosphorylation signature c) PTMs that are linked with both oxidative phosphorylation and glycolysis (Fig 4.2).

A strong and consistent result from this study was that most acetylation marks are anticorrelating with glycolysis. At first glance this may appear counterintuitive to the normal function of glycolytic physiology, as high rates of glycolysis would lead to production of high levels of cellular acetyl-CoA, the substrate of histone acetyltransferases. Indeed, other studies have shown that when there is increase of available intracellular glucose there is an increase in glycolysis and also histone acetylation (Cluntun et al., 2015). It is important to note that this is a fundamentally different perspective and mechanism, as that study tracked the increase of glucose through glycolysis and then measured effects on chromatin. To understand the relationship between metabolism and epigenetics, it

Pearson correlation matrix: histone modifications vs metabolism

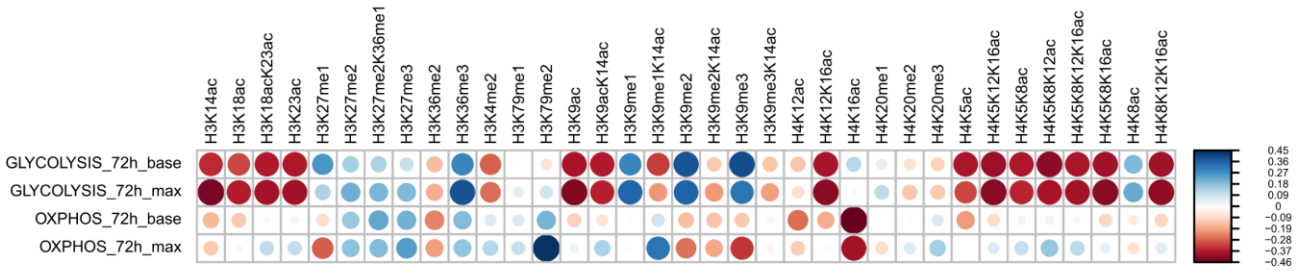

Figure 4.2. Pearson correlation analysis of acetylation and methylation modifications on histones H3 and H4 with metabolic readouts, induced by treatments with 30 different small molecules

Correlation matrix based on Pearson's correlation coefficient. The size and colour of the bubble indicates a higher degree of correlation between respective PTM marks, as shown on the right-hand side legend, ranging from strong anticorrelation (red, -1) to strong correlation (blue, +1). The threshold for correlations selected in this graph was +/- 0.50.

becomes clear that it strongly depends if, either a metabolic substrate (such as glucose), or on the other hand, histone PTMs are changed.

In my current study, the perspective was from an opposite route of that described in Cluntun et al. - by first altering epigenetic states (histone acetylation) to measure potential outcomes on metabolic flow. My study has shown that in general higher levels of acetylation were associated with a decrease in glycolytic activity, and vice versa (see detailed discussions in Chapter 3.7). So far, only an indicative relationship between treatment of cells with HDAC inhibitors, followed by increased acetylation and decreased glycolysis had been demonstrated, and was often limited to cancer cells (Fang et al., 2019; Q. Li et al., 2018; Nguyen et al., 2020). However, my study now shows that anticorrelation between histone acetylation and glycolysis is a general concept not limited to HDAC inhibitor treatments that links the status of chromatin with metabolic states (see Fig 4.2, Chapters 3.7.1-3.7.7 and Chapter 3.8).

In addition to the specific observations regarding histone acetylation and glycolysis, metabolism and epigenetics interplay has been mostly studied from the route of altering metabolism, e.g. with nutrients and analysing resulting epigenetic changes. Individual studies and reviews have described changes in specific histone modifications as responses to metabolic changes (Cluntun et al., 2015; Dutta et al., 2016). There are also studies and reviews discussing the relationships of metabolic intermediates regulating histone PTMs (Campit et al., 2020; Fan et al., 2015c; Suganuma & Workman, 2018).

However, the metabolic and epigenetic interplay from the route of altering epigenetics to investigate metabolism has not been studied to the same extent. In fact, the scopes of the few available studies altering epigenetics to study metabolism were rather limited. They are mostly focusing on one or very few epigenetic marks. using usually one or very few inhibitors, which in most cases belonged to the same drug class, e.g. HDAC inhibitors, without showing effects on metabolism (Feldman et al., 2013; Lavarone et al., 2019; Stein et al., 2018; Wapenaar & Dekker, 2016). Furthermore, they have also mainly focused on epigenetic changes of metabolic enzymes or other proteins that at a later stage affect metabolism and not how histone PTMs marks affect metabolism directly (Gerhäuser, 2012). On the other hand, some studies have investigated how treatments with epigenetic inhibitors alter

metabolism without analysing histone PTMs or protein changes (Amoêdo et al., 2011; S. Y. Kim et al., 2020; Nunn et al., 2016; Wardell et al., 2009). From these studies, only few have discussed how specific histone PTM marks, for example acetylation, can impact metabolism – with all of them focusing on the pathophysiology of diabetes (Hadden & Advani, 2018; X. Li et al., 2016; T. T. H. Lu et al., 2018; Zhong & Kowluru, 2010).

Indeed, this is the first time that a study characterises and correlates metabolic signatures of PTMs, the glycolytic histone PTM code or the oxidative phosphorylation PTM code addressing more than 40 histone PTMs states using epigenetic inhibitors covering all different epigenetic drug classes. This current study has comprehensively aimed to characterise a multitude of PTMs and metabolic states to come to a more systematic understanding bringing together all three aspects; histone PTMs, proteomic changes and metabolic profile alterations as responses to histone epigenetic alterations.

As mentioned above, acetylation marks anticorrelated with glycolysis with the exception of H4K16ac and H4K8ac. Interestingly, these two acetylation marks were anticorrelated with oxidative phosphorylation. H4K8ac is mainly found in active promoters of genes (Zhibin Wang et al., 2008) while H4K16ac is linked with both active and repressed transcription (Shogren-Knaak et al., 2006). A reduction of H4K16ac is also linked with cancer (Fraga et al., 2005). Therefore, these two histone modifications may play a more specialized role in regulating metabolism and pathological states.

Another key chromatin modification, H3K9me1/2/3, was found to correlate with glycolysis, while H3K9me2/3 anticorrelated with oxidative phosphorylation. Interestingly, H3K9me2 demethylation via Phf2 was found to regulate glucose and prevent NAFLD progression – a major and highly prevalent metabolic syndrome (Bricambert et al., 2018). H3K9me1 was found to be the one modification preserved under SAM depletion in the expense of loss of me2/3 (Haws et al., 2020). Furthermore, the complete absence of an interplay between H3K9me1 and oxidative phosphorylation but a very strong correlation with glycolysis points to a potentially very interesting role for the monomethylated H3K9: which could potentially be exploited to fight cancer cells, that often have higher levels of glycolysis. Targeting monomethylated H3K9 may therefore be an avenue to reduce the Warburg effect essential for cancer cell survival.

A key histone modification involved in active transcription, H3K4me2, was anticorrelated with glycolysis and H3K9me1. In fact, this observation is in line with the fact that higher levels of histone acetylation were anticorrelated with glycolysis, suggesting that on a global level, higher levels of active transcription (demonstrated by high H3K4me2 and high histone acetylation) corresponded with lower glycolysis activity (Fig 4.2). Interestingly, this is similar to other studies showing that H3 acetylation and H3K4me1 were anticorrelating with H3K9me1 under hyperglycaemin/hyperinsulinemic conditions (Gupta et al., 2012). My study adds another aspect to those results, as it shows firstly, that all H3K9 methylation marks (not just H3K9me1) correlate with glycolysis, and secondly, that H3K9me2 and H3K9me3 but not H3K9me1 anticorrelate with oxidative phosphorylation (Fig 4.2).

Further substantiating a potential overarching theme between lower levels of transcriptional activity and glycolysis was the observation that also H3K27me2/3, associated with transcriptionally inactive/repressed genes, correlated with glycolysis (Ferrari et al., 2014b). A further interesting observation was that two different usually repressive marks – H3K9me2/3 and H3K27me2/3 – behaved differently regarding oxidative phosphorylation (Fig 4.2). Moreover, and as seen for several other histone modifications, the monomethylated form of H3K27 behaved opposite to H3K27me2/3 relating to oxidative phosphorylation (H3K27me1 was correlating with glycolysis and anticorrelating with oxidative phosphorylation while H3K27me2/me3 correlated with both).

Also, H4K20me1 was correlating with glycolysis and anticorrelating with oxidative phosphorylation while H4K20me2/3 were anticorrelating with glycolysis and correlating with oxidative phosphorylation. In most studies H4K20me1 is linked with active transcription and H4K20me3with inactive transcription and nothing is known for the role of H4K20me2. There are no studies linking H4K20me1/2/3 with metabolism and specifically with the metabolic pathways oxidative phosphorylation and glycolysis. There is one study in mice fed with high fat diet were the offspring presented higher H4K20me1 on the gene promoter of leptin, suggesting that H4K20me1 could be involved in transgenerational transmission of epigenetic memory states of metabolism(Masuyama & Hiramatsu, 2012). Only one additional study has so far indicated at an involvement of H4K20me1 specifically in regulating some metabolic genes without phenotypic readouts of the metabolic states (Nikolaou et al., 2017). No more data is available, especially for the

higher methylation states of H4K20 and metabolic regulation. The current study presents that H4K20me1/2/3 has a different role across glycolysis and oxidative phosphorylation regulation, the network of other histone PTMs induced together with H4K20me1/2/3, potential protein candidates affected and a set of inhibitors with which H4K20me1/2/3 levels can be altered to further study this specific modification. It is the first time that a more complete set of data is presented regarding H4K20me1/2/3 and its role in metabolic regulation.

Work has been published analysing the relation between various histone marks, although not in regard to metabolism, as discussed above (Maitituoheti et al., 2020; C. Zhang et al., 2014). In summary, there has not been a study to date describing a potential histone PTM code of glycolysis or oxidative phosphorylation. A "histone code" for metabolism could prove useful for further research and drug development, as proven by work on the epigenetic code / clock of aging, characterised by specific patterns of DNA methylation (Hannum et al., 2013; Horvath, 2013) and epigenetic clocks of aging combined with progression of metabolic diseases, again using DNA methylation analyses (Corso-Díaz et al., 2020; H. S. Lee & Park, 2020). My study suggests that generally, the "high glycolysis code" was characterised by histone modifications associated with transcriptional repression (low acetylation, high H3K9me2/3, high H3K27me2/3). In turn, the "high oxidative phosphorylation" code was marked by a much more diverse set of histone PTMs, characterised by high H3K79me2 and H3K27me2/3 and low H4K16ac and H3K9me2/3. Similarly to the epigenetic codes of aging, this could allow further fundamental research and act as prognostic markers for metabolic diseases or diseases with metabolic phenotypes, such as cancer. This in turn could be the base to target new drug candidates to shift metabolic states – as demonstrated by the first time metabolic/chromatin/proteomic characterisation of the epigenetically-active small molecules studied and presented here.

4.1.3 Putative new protein regulators of metabolism

In the findings discussed up to now regarding histone PTM interactions (4.1.1) and histone PTMs in relation to metabolism (4.1.2) links with other published studies and generation of hypotheses were more direct than the proteome results discussed in this subchapter. In the proteome results presented in Chapter 3, when differentially expressed proteins were analyzed for enriched GO terms

for biological processes (for example Fig 3.22), regulation of metabolic process was amongst the most prominent results. This implied that there could be a direct effect of epigenetic inhibitors on key metabolic enzymes. However, the results were less straightforward. In particular, GO terms covering metabolic processes (e.g. "Regulation of metabolic process") includes not only key metabolic enzymes but also transcription factors and other regulators of metabolism. As analyses of many individual proteins in the results chapter and overarching topics revealed, most of the enriched proteins in this category where in fact transcription factors and pathway regulators - not metabolic enzymes.

Although metabolic enzymes are strongly regulated by immediately-acting mechanisms, such as substrate-, product-, and allosteric regulation, they are subject to long-term changes in abundance through transcriptional, posttranscriptional and posttranslational regulation (Bulik et al., 2016; Madhukar et al., 2015; Metallo & Vander Heiden, 2013; Wolfinbarger, 2017; Xiong & Guan, 2012). The observed lack of changes in key metabolic enzymes could mean that the epigenetic compounds did not directly affect the enzyme genes but instead targeted other proteins which then acted on the enzymes. In line with this, several known regulators of posttranscriptional and posttranslational regulations were identified throughout this study (e.g., PIKFYVE, COQ7, MAGEB2, RASA1, SYK).

Indeed, most of the identified and enriched proteins were not previously discussed in other studies regarding metabolism or were transcription factors or other regulatory enzymes. However, I wanted to investigate deeper those protein interactions and their effects on metabolism. On this subchapter, I therefore discuss the overview of protein interactions and then via correlation analyses I am focusing on a subset of proteins that correlate with specific PTMs marks and metabolism. There is not much known about these protein candidates and their relationship with metabolism. However, based on several selected protein examples I will discuss a few potential links and possible directions for future research.

In order to identify proteins at the centre of regulatory networks affected by the epigenetic drugs, a protein-protein correlation analysis was performed. This analysis would show if the protein levels of different proteins are correlated after treatment with the epigenetic drugs. When depicting only the most stringent protein-protein correlations ($r > 0.99$), two proteins were revealed at the centre of large regulatory networks: DHRS2 and KDM5A. DHRS2, lipid metabolism (Gabrielli & Tofanelli,

2012) dehydrogenase/reductase member 2 (DHRS2) belongs to the short-chain alcohol dehydrogenase/reductase (SDR) superfamily, which includes NAD/NADP dependent proteins, which are functionally involved in a number of intermediary metabolic processes and in the metabolism of lipid signalling molecules. KDM5A is a H3K4me2/3 demethylase and therefore plays an important role in transcriptional regulation (Kirtana et al., 2020). As discussed in Chapter 3.7.2, KDM5A was more than 40-fold enriched in two HAT-inhibitor-treated samples and associated with reduced H3K4me2 and lower glycolysis. Moreover, KDM5A has been implicated in regulating mitochondrial metabolism through regulating expression of mitochondrial pyruvate carrier 1 (MPC-1) (Jiujie Cui., 2019). Both DHRS2 and KDM5A strongly correlated with a large number of other proteins, as shown in the Table below:

Network node	Correlation direction	Protein IDs
DHRS2	Correlating with DHRS2	ARIH1, CORO1A, ELOVL4, GMPPB, HADHB, KANK1, LMNA, MLEC, MIF2, NEFM, PGM3, TERF2
	Anti-correlating with DHRS2	ATX10, BID, EIF1AX, H2AFY2, IGE/F2BP1, IRAK1, KRR1, MAZ, NCL/I, PRUNE, RPP25, RPRD1A, SET, SETD7, XPO1
KDM5A	Correlating with KDM5A	ANKLE2, AREGEE1, ATRX, BLOC1S3, CEIF1, CEP131, CLASRP, FAM98A, FOXJ3, NDUFA9, NKAP, PHF2, PNISR, PRPE38B, PRPF4B, RSRC1, SHOC2, SNAP23, SNRP70, SON, SREK1, SRSF4, SIK38, TMEM263, USP24, XPC
	Anti-correlating with KDM5A	CAMSAP2, LAGE3

Surprisingly, between DHRS2 and KDM5A there were no similar proteins identified participating in the correlations, suggesting that they were involved in two separate regulatory networks. The expectation was that because these two proteins were affecting so many other proteins (or were affected by many other proteins) that they would play a central role in regulating the observed metabolic phenotypes, as it has been implied by other studies indirectly. However, neither DHRS2 nor KDM5A correlated directly with metabolic states, as shown in Figure 4.3 ($r>0.6$). Furthermore, none of the protein candidates which (anti)-correlated with DHRS2/KDM5A (Table above) were found in metabolism-protein correlations (Fig 4.3).

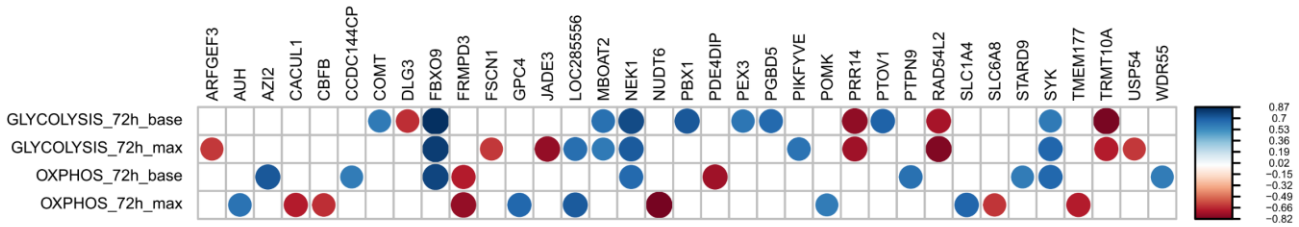

Figure 4.3. Pearson correlation analysis of acetylation and methylation modifications on histones H3 and H4, as well as proteins, induced by treatments with 30 different small molecules

Correlation matrix based on Pearson's correlation coefficient. The size and colour of the bubble indicates a higher degree of correlation between respective PTM marks, as shown on the right-hand side legend, ranging from strong anticorrelation (red, -1) to strong correlation (blue, +1). The threshold for correlations selected in this graph was +/- 0.80.

In summary, the employed epigenetic drugs affected these two central proteins and their associated (statistical) interaction partners but the changes did not seem to be relevant for metabolism. This unexpected observation demonstrated that experimental assays that focus only on most affected proteins or protein clusters from a treatment may not be the most biologically (in this case metabolically) relevant candidates – and may lead to wrong clues on identifying protein candidates for drug treatments that regulate metabolism.

A very different set of 35 proteins was found to correlate (or anti-correlate) with metabolic states (at r>0.8, see Fig 4.3) and 139 proteins at r>0.5 (see Appendix Fig A.11), including for example PIKFYVE, ARFGEF3, FBXO9, SYK, JADE3, TRMT10A, PDE4DIP. Clearly, the proteins showed a broad spectrum of correlations with metabolism: there were two proteins that correlated with both oxidative phosphorylation and glycolysis, SYK and FBXO9. Three proteins anticorrelated with both oxidative phosphorylation and glycolysis, JADE3, PDE4DIP, DLG3. There was only one protein identified in the current analysis that simultaneously correlated with glycolysis and anticorrelated with oxidative phosphorylation, PECR which is participating in fatty acid biosynthesis (elongation). Interestingly, no proteins were identified for the opposite effect (correlation with oxidative phosphorylation and anticorrelation with glycolysis). Moreover, some proteins were focused on either glycolysis or oxidative phosphorylation, without affecting the other metabolic readout (e.g. ARFGEF3, PIKFYVE, for glycolysis, AZI2, SUV39H1 for oxidative phosphorylation). These results could indicate that the identified proteins either up- or downregulated metabolism at the same time, or individually, with the notable exception of PECR. A common regulation of both metabolic cascades indeed would make sense, as in normal cells glycolysis is the central feed-in of electrons for the oxidative phosphorylation, which may get uncoupled in cancer cells (Warburg effect).

To investigate if some of the above-mentioned proteins that are correlating with metabolic states were also linked with specific epigenetic codes, a segmentation analysis was performed, as depicted in the Venn diagram in Fig 4.4. Of the 139 proteins correlating with metabolic states (at r>0.5), only 25 were found to significantly correlate with specific histone PTMs (at r>0.8 for protein-PTM correlations, resulting in 98 protein IDs). Amongst those were, for instance, PIKFYVE, ARFGEF3, FBXO9, SYK. While these outputs may provide the source for future in-depth analysis, the following

two examples are provided to demonstrate some of the uncovered observations: ARFGEF3 was identified as anticorrelating with glycolysis, while PIKFYVE correlated with glycolysis (Fig 4.3).

	ARFGEF3	***PIKFYVE***
Metabolic impact	Increased ARFGEF3 with decreased glycolysis	Increased PIKFYVE with Increased glycolysis
Histone acetylation *(H3K14ac, H3K18ac, H3K18ac, H3K23ac, H3K9ac, H4K12ac, H4K5ac,…)*	Increased ARFGEF3 with increased acetylation	Decreased PIKFYVE with increased acetylation
Histone methylation *H3K27me1/2/3; H3K36me3; H3K9me1/2/3; H4K20me1*	Increased ARFGEF3 with decreased methylated histone PTMs	Decreased PIKFYVE with decreased methylated histone PTMs
Histone methylation *H4K20me2/3*	Increased ARFGEF3 with increased methylated histone PTMs	Decreased PIKFYVE with increased methylated histone PTMs

In summary, ARFGEF3 and PIKFYVE follow the previously described PTM patterns of glycolysis (see Chapter 4.1.2). Therefore, these two proteins – together with the other 23 that overlapped between PTMs and metabolism – could be initial targets to modulate glycolysis via epigenetic pathways in cells. Indeed, ARFGEF3 (alternatively known as BIG3) has indirectly been implicated as negative regulator of glucose metabolism on a physiological/systemic way, BIG3 knockout mice showed hyperglycaemia, evidence of its role as a regulator on a single-cell level has not been published so far (H. Li et al., 2014). This current study now suggests that indeed ARFGEF3 may be a negative regulator for glycolysis on a single cell level. Conversely, some evidence suggests that PIKFYVE may be important for glucose homeostasis, including through the regulation of glucose uptake into cells (Ikonomov et al., 2007, 2016; Y. Liu et al., 2013).

As mentioned above, PECR was the only protein that presented an opposite correlation between oxidative phosphorylation and glycolysis (correlated with oxidative phosphorylation and anticorrelaed with glycolysis), as shown in Fig A.11. Interestingly, PECR highly correlated with H3K27me1 (which correlated with glycolysis and anticorrelated with oxidative phosphorylation) and anticorrelated with H3K27me2/3 (correlated with both oxidative phosphorylation and glycolysis). Another interesting finding is that PECR was highly correlated with H4K20me1 (correlated with glycolysis and anticorrelated with oxidative phosphorylation) and anticorrelated with H4K20me2/3 (anticorrelated with glycolysis and correlates with oxidative phosphorylation). It is interesting to look at this relationship between PECR and H4K20me1/2/3 and H3K27me1/2/3. These histone PTMs

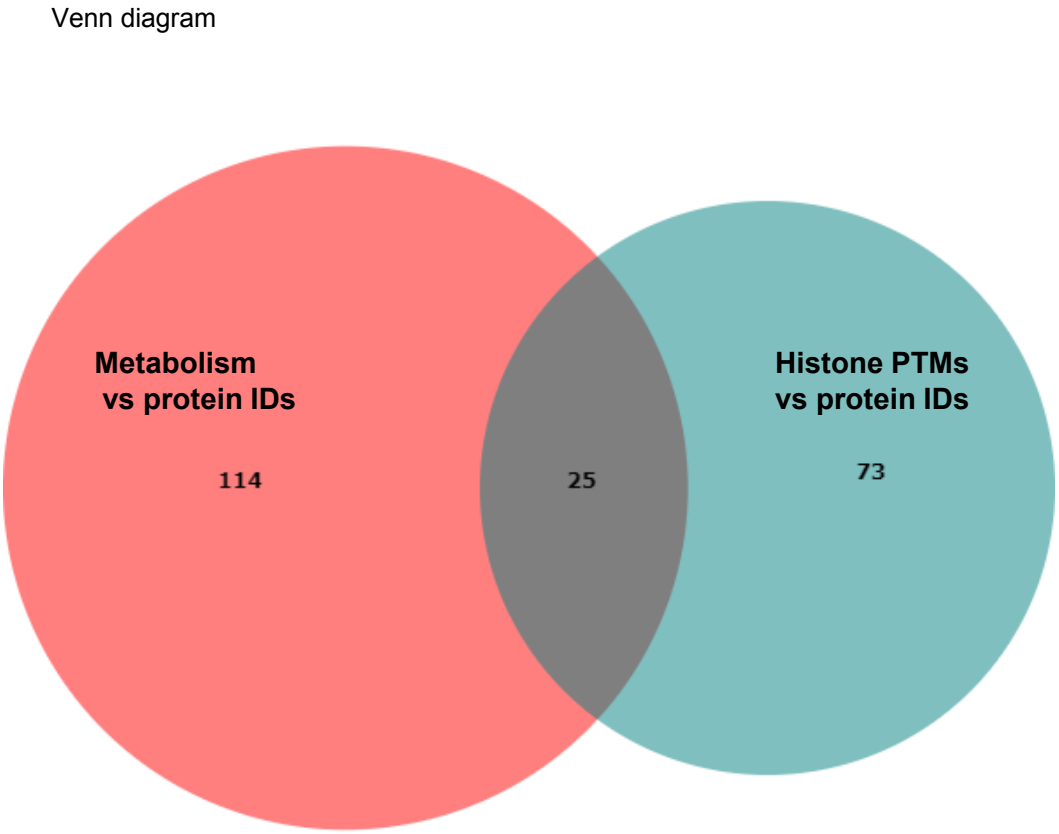

Figure 4.4. Protein correlation analysis of metabolic states and histone PTMs for 30 drug candidates

Venn diagram representing the number of protein IDs correlating with at least one metabolic state (basal OXPHOS, maximal OXPHOS, basal glycolysis, maximal glycolysis) after 72h treatments, the number of protein IDs correlating with at least one histone PTM mark and the number of protein IDs that are overlapping and correlate with both metabolic states and histone PTM marks.

appear to anticorrelate with each other (see discussion on histone PTM/metabolism correlations in Chapter 4.1.2). Interestingly, PECR which correlated with glycolysis had the opposite profile in histone PTMs with its counterpart proteins that anticorrelated with glycolysis in a one to one manner.

Interestingly proteins that anticorrelated with glycolysis correlated or anticorrelated with almost all histone PTMs in the same way, appearing almost as clusters. Also, the two proteins that correlated with glycolysis (PIKFYVE and PGDB5) appeared to have the same relationship against all histone PTM marks. (H3K27me1 was corelating with PIKFYVE and anticorrelating with PGDB5). In contrast, the proteins (anti-) correlating with oxidative phosphorylation appeared to have more versatile correlation patterns with histone PTM marks. There were some overlapping patterns between proteins AUH, CCDC186, GMEB1, VCORC1L1 mainly for the H4K20me1/2/3 peptides, emphasizing again the apparent central role H4K20 plays in metabolism according to this study (see above discussion on histone PTM/metabolism correlations in Chapter 4.1.2). Interestingly, when sorting the degree of correlation of proteins with H4K20me1, distinct clustering occurred amongst the proteins along histone PTMs, e.g. proteins correlating with glycolysis were clustered together with the same affected histone marks (e.g. low acetylation). This would suggest a potential strong function of H4K20me1 in regulating metabolism (as discussed in Chapter 4.1.2), potentially by impacting different protein networks depending on the cellular levels of its methylation state and by regulating acetylation of H3/H4.

Taken together, the points discussed in this Chapter suggested four new insights: a) identifying relevant proteins based on simply quantitative response to epigenetic drug treatments can be misleading in the identification of new metabolic regulator druggable targets; b) the analysis of correlation and overlap networks between metabolism and histone PTMs allowed to uncover several previously undescribed proteins as potential regulators of metabolism (being sensitive to epigenetic drugs directly or indirectly); c) those putative metabolic regulators were also correlating with specific histone codes; d) H4K20me1 was identified as a central previously unidentified histone PTM involved in regulating metabolism via clusters of proteins, which correlate with similar subsets of other histone PTMs in turn.

4.2 Next steps

This work presents the potential of using epigenetic inhibitors to alter metabolism and disease. It comprised the investigation of metabolic changes after utilising a large number of epigenetic treatments as they were available on the market to date, the identification of possible protein targets as metabolic regulators, and suggested a histone code for glycolysis and oxidative phosphorylation.

To expand on the results of this work, it would be interesting to look into designing specific studies focusing on identifying how the described targets are functionally relating to metabolism. For example, performing metabolic profiling characterisation using seahorse XF in knockout cell lines for proteins correlating with specific metabolic profiles, such as ARFGEF3, PIKFYVE, PECR and others would determine if these proteins are key regulators of a respective metabolic phenotype. Also, this step would determine if the main metabolic pathway used by the cell is glycolysis or oxidative phosphorylation. This could be done on a large scale using siRNA or CRISPR/Cas9 knockout libraries in combination with a high-throughput-optimized seahorse XF setup (building on the optimizations described in this work, see Chapter 2.3 and 3.2).

Apart from uncovering additional regulators of metabolism and the importance of the cell's metabolic pathways preference, many diseases are linked with alterations in energy substrates preference. For instance, cardiac disease and heart failure have been linked to either acute or progressive changes in energy substates metabolism (Evans, 2012; Fukushima et al., 2015). Cancer metabolism and cancer microenvironment metabolism are also linked with alterations in energy substrates (Thompson, 2016). Consequently, another interesting experimental series would be to explore if the above mentioned proteins alter the cell's preference for a specific main energy substrate for mitochondrial respiration (long chain fatty acids, glutamine, pyruvate). This could be done by using specific inhibitors, such as etomoxir (carnitine palmitoyltransferase-1 inhibitor), BPTES (glutaminase inhibitor) and UK5099 (mitochondrial pyruvate carrier inhibitor).

If any additional regulators are validated, it would be important to identify if these proteins physically interact with key metabolic enzymes as part of protein complexes or regulatory switches. For this, initially Co-IP experiments targeting the above mentioned proteins and analysis of co-precipitating material with mass spectrometry-based proteomics would be an option. Identified protein

complexes could then by expressed and purified in vitro to further determine interaction interfaces and structures.

To shed light into the disease relevance it would be interesting to conduct experiments on disease-specific models (cell or animal based), for instance for diabetes, obesity or other rare diseases that maybe linked with metabolic dysregulation (as discussed in Introduction Chapter 1.2). Cell lines of interest could be for example, skeletal muscle versus smooth muscle cells, brown versus white adipose tissue, given the fact that these cell lines present different metabolic profiles and would help to further investigate the metabolic and epigenetic profiles of different tissue types based on the physiological functions, and to investigate changes after pharmaceutical intervention with epigenetic inhibitors.

It would be favourable to also investigate how the epigenome changes after knocking out the above mentioned proteins and potentially compare if these results could be achieved by using an epigenetic inhibitor. It would be also important to look into not only lysine methylation but also arginine methylation and other more recently described histone PTMs, given the very scarce information about arginine methylation in context of metabolism and disease, and the complete lack thereof of other histone PTMs such as histone butyrylation, hydroxylation, lipidation and monoaminylation (Chan & Maze, 2020). Looking only at lysine methylation is only providing part of the information.

Although it has not been a focus of this study, also non-histone proteins can be modified by several enzymes that are largely considered as epigenetic writers/erasers (S. Ganai, 2016; Wesche et al., 2017). Therefore, PTMs introduced to metabolic enzymes after treatments with epigenetic inhibitors would be interesting to investigate.

The present histone PTM and cellular protein mass-spectrometry analysis provided the first step for a systematic approach of the physiological effects of epigenetically active compounds on metabolism. An important next step would be to perform RNA-seq in cells treated with epigenetic inhibitors, to characterise the transcriptional landscape and identify differentially-regulated genes. Importantly, this could uncover novel non-coding RNAs that may regulate metabolism – in addition to some that have already been described (P. Li et al., 2015; Redis et al., 2016; Sallam et al., 2016). In

addition to their rate of transcription, RNA levels are also regulated by post-transcriptional modifications, such as alternative splicing, polyA-tail length, and modification of RNA nucleotides, e.g. N6-methyladenosine and ribose-methylation (Shi et al., 2020). It has long been suggested that post-transcriptional regulation of RNAs play a role in metabolic diseases (W. Kim & Lee, 2012) but the interplay with chromatin and changes upon treatments with epigenetically-active compounds remains elusive.

Moreover, it would be very informative to uncover more molecules participating in metabolic regulation that work as signalling factors between cells and organs, such as hormones and neuronal peptides. One way to look into that would be to focus into analysing secretions of cells treated with epigenetic inhibitors that present altered metabolism. This has been very challenging to perform because identifying novel peptide coding genes of around 300bp or smaller, exist within the "genetic noise". However, focusing into that aspect is a crucial step to answer many unanswered questions for metabolic regulation and possibly identifying biomarkers and novel therapies not only for obesity and diabetes but also for rare disorders and other metabolic syndromes. At a later stage, it would be make sense to use patient-derived primary cells wherever feasible to monitor for specific metabolic changes in the context of protein networks, energy substrate preference and the histone code and to further validate hypotheses presented in this work and future studies.

4.3 Future applications

There have been 10 epigenetic drugs approved by FDA under the indication for cancer treatment (Buocikova et al., 2020; Meighan-Mantha, 2017; Qi et al., 2016). However, only very few of the epigenetic inhibitors approved are known and indicated to treat other disease conditions, such as procainamide (DNMTi, cardiac arrhythmia) and hydralazine (DNMTi, hypertension). At the moment, old drugs that were not known before for their epigenetic activity, are currently being investigated and repurposed as specific epigenetic inhibitors, including putative inhibitors of DNTMs (e.g., hydralazine, nanaomycin A), HDACs (e.g., artemisin, ginseng), and others (e.g., garcinol,

ribavirin) (Moreira-silva et al., 2020) or as drugs with dual actions (e.g., targeting both HDAC and DNMT) mainly for cancer therapy.

My study exceedingly presents novel effects of known epigenetic inhibitors on metabolism and the potential to alter metabolic states. These data leave a big window of opportunity for those drugs that had been filed under non-metabolic indications, e.g. cancer, to be tried out in treating a variety of metabolic diseases and to be repurposed under a different indication, potentially secured with novel patent application gains. Additionally, for cancer therapy itself these epigenetic inhibitors could pave the way for additional insights into cancer metabolism and interventions to halt cancerous cells via metabolic regulation.

Moreover, the output of this study regarding the histone code changes, PTM networks and inhibitor-induced metabolic profiles can be used as a tool for prediction of drug responses, metabolic state changes, and potentially other use cases. It can also be used to identify metabolism/PTM interactions in drug discovery and preclinical stages and in the design of focused chemical libraries and drug screening approaches. It might be problematic that currently there is no screening for cellular metabolic effects for drug approval (in contrast to the obligatory analysis of PK/PD assays which focus on how the drug is metabolised in the organism). Screening for metabolic effects prior to drug approval might help in avoiding side effects like cholesterol increase, heart disease, stroke and others that have been described from current treatments on the market (Gebauer et al., 2018; Himmerich et al., 2015; Wilcox, 1999). This is even more important as metabolic issues are the most frequent and strongest growing non-communicable diseases worldwide (WHO, 2018, 2019) and should therefore not be unnecessarily burdened further by side-effects of other treatments. The fact that there is no screening for metabolic effects in drug design might be a problem and limitation in drug discovery itself as it excludes the basis of the function of the cell, metabolism. This is not referring to the possibility that a molecule develops metabolic bioactivation potential (Tang & Lu, 2010) but rather that the drug holds a direct role in altering cell metabolism.

Metabolic changes are linked with the epigenome which is sensitive to environmental changes and can trigger disease and symptoms as innocent as hair loss to more severe like organ failure (Heijmans et al., 2008; Shen et al., 2019). It is a novel direction especially for Pharma companies to be

on the guard for such interactions as a quick metabolic screening in the initial stages of drug design could save resources and later on minimize patient side effects. There are currently 11 FDA approved substances to treat diabetes (FDA, 2015) but none with known epigenetic activity, and there are no epigenetic inhibitors approved for diabetes, obesity or other metabolic diseases treatments.

The epigenetic code presented in this work may also be used as biomarkers to predict metabolic diseases and others including neurodegeneration, where metabolic changes can be detected as early signs of disease (Kennedy et al., 2016).

Moreover, it may in the future be used as epigenetic reprogramming of metabolism to manipulate altered metabolic phenotypes in a variety of situations, e.g. in aging, cancer and rare diseases. There is cause for optimism that in the coming years it will be possible to improve our understanding of the regulation of the bidirectional relationship among metabolism and epigenetic switches and thus address disease development. Epigenetic interventions could advance the health status of the general population and halt disease progression or the metabolic syndrome and the transgenerational inheritance of other diseases, which is crucial to alleviate societal health burden. Novel epigenetics-based diagnostics could furthermore assist in classification of individuals suffering from chronic diseases, prescribe patient profile-based medications and treatments, and diminish possible cytotoxicity or adapt dietary requirements for the health advancement of the individual.

References

Abu-Farha, M., Lambert, J.-P., Al-Madhoun, A. S., Elisma, F., Skerjanc, I. S., & Figeys, D. (2007). *The Tale of Two Domains PROTEOMICS AND GENOMICS ANALYSIS OF SMYD2, A NEW HISTONE METHYLTRANSFERASE* □ S*. https://doi.org/10.1074/mcp.M700271-MCP200

Adachi, H., Takahashi, I., Higashimoto, K., Tsuchida, S., Noguchi, A., Tamura, H., Arai, H., Ito, T., Masue, M., Nishibori, H., Takahashi, T., & Soejima, H. (2013). Congenital hyperinsulinism in an infant with paternal uniparental disomy on chromosome 11p15: Few clinical features suggestive of Beckwith-Wiedemann syndrome. *Endocrine Journal*, 403–408. https://doi.org/10.1507/endocrj.EJ12-0242

Agnew, T., Munnur, D., Crawford, K., Palazzo, L., Mikoc, A., & Ahel, I. (2018). MacroD1 is a promiscuous ADP-ribosyl hydrolase localized to mitochondria. *Frontiers in Microbiology*, *9*(JAN). https://doi.org/10.3389/fmicb.2018.00020

Ahuja, N., Sharma, A. R., & Baylin, S. B. (2016). Epigenetic Therapeutics: A New Weapon in the War Against Cancer. *Annual Review of Medicine*, *67*(1), 73–89. https://doi.org/10.1146/annurev-med-111314-035900

Alemasova, E. E., & Lavrik, O. I. (2019). Poly(ADP-ribosyl)ation by PARP1: Reaction mechanism and regulatory proteins. In *Nucleic Acids Research* (Vol. 47, Issue 8, pp. 3811–3827). Oxford University Press. https://doi.org/10.1093/nar/gkz120

Ali, D., Hamam, R., Alfayez, M., Kassem, M., Aldahmash, A., & Alajez, N. M. (2016). Epigenetic Library Screen Identifies Abexinostat as Novel Regulator of Adipocytic and Osteoblastic Differentiation of Human Skeletal (Mesenchymal) Stem Cells. *Stem Cells Translational Medicine*, *5*(8), 1036–1047. https://doi.org/10.5966/sctm.2015-0331

Amoêdo, N. D., Rodrigues, M. F., Pezzuto, P., Galina, A., da Costa, R. M., de Almeida, F. C. L., El-Bacha, T., & David Rumjanek, F. (2011). Energy metabolism in H460 lung cancer cells: Effects of histone deacetylase inhibitors. *PLoS ONE*, *6*(7). https://doi.org/10.1371/journal.pone.0022264

Andersen, D. C., Jensen, L., Schrøder, H. D., & Jensen, C. H. (2009). "The preadipocyte factor" DLK1 marks adult mouse adipose tissue residing vascular cells that lack in vitro adipogenic differentiation potential. *FEBS Letters*, *583*(17), 2947–2953. https://doi.org/10.1016/J.FEBSLET.2009.08.002

Arpa, J., Campos, Y., Gutiérrez-Molina, M., Cruz-Martinez, A., Arenas, J., Caminero, A. B., Palomo, F., Morales, C., & Barreiro, P. (2009). Benign mitochondrial myopathy with decreased succinate cytochrome C reductase activity. *Acta Neurologica Scandinavica*, *90*(4), 281–284. https://doi.org/10.1111/j.1600-0404.1994.tb02722.x

Arsov, T., Smith, K. R., Damiano, J., Franceschetti, S., Canafoglia, L., Bromhead, C. J., Andermann, E., Vears, D. F., Cossette, P., Rajagopalan, S., McDougall, A., Sofia, V., Farrell, M., Aguglia, U., Zini, A., Meletti, S., Morbin, M., Mullen, S., Andermann, F., … Berkovic, S. F. (2011). Kufs disease, the major adult form of neuronal ceroid lipofuscinosis, caused by mutations in cln6. *American Journal of Human Genetics*, *88*(5), 566–573. https://doi.org/10.1016/j.ajhg.2011.04.004

Beck, D. B., Oda, H., Shen, S. S., & Reinberg, D. (2012a). PR-set7 and H4K20me1: At the crossroads of genome integrity, cell cycle, chromosome condensation, and transcription. *Genes and Development*, *26*(4), 325–337. https://doi.org/10.1101/gad.177444.111

Beck, D. B., Oda, H., Shen, S. S., & Reinberg, D. (2012b). PR-set7 and H4K20me1: At the crossroads of genome integrity, cell cycle, chromosome condensation, and transcription. *Genes and Development*, *26*(4), 325–337. https://doi.org/10.1101/gad.177444.111

Borck, P. C., Guo, L. W., & Plutzky, J. (2020). BET Epigenetic Reader Proteins in Cardiovascular Transcriptional Programs. *Circulation Research*, 1190–1208. https://doi.org/10.1161/CIRCRESAHA.120.315929

Boroughs, L. K., & DeBerardinis, R. J. (2015). Metabolic pathways promoting cancer cell survival and

growth. *Nature Cell Biology*, *17*(4), 351–359. https://doi.org/10.1038/ncb3124

Bowen Xua, Kyle D. Konzeb, Jian Jinb, and G. G. W. (2015). Targeting EZH2 and PRC2 dependence as novel anticancer therapy. *Exp Hematol*. https://doi.org/10.1016/j.exphem.2015.05.001.Targeting

Bricambert, J., Alves-Guerra, M. C., Esteves, P., Prip-Buus, C., Bertrand-Michel, J., Guillou, H., Chang, C. J., Vander Wal, M. N., Canonne-Hergaux, F., Mathurin, P., Raverdy, V., Pattou, F., Girard, J., Postic, C., & Dentin, R. (2018). The histone demethylase Phf2 acts as a molecular checkpoint to prevent NAFLD progression during obesity. *Nature Communications*, *9*(1). https://doi.org/10.1038/s41467-018-04361-y

Brown, M. A., Sims, R. J., Gottlieb, P. D., & Tucker, P. W. (2006). Identification and characterization of Smyd2: A split SET/MYND domain-containing histone H3 lysine 36-specific methyltransferase that interacts with the Sin3 histone deacetylase complex. *Molecular Cancer*, *5*, 26. https://doi.org/10.1186/1476-4598-5-26

Buchovecky, C. M., Turley, S. D., Brown, H. M., Kyle, S. M., McDonald, J. G., Liu, B., Pieper, A. A., Huang, W., Katz, D. M., Russell, D. W., Shendure, J., & Justice, M. J. (2013). A suppressor screen in Mecp2 mutant mice implicates cholesterol metabolism in Rett syndrome. *Nature Genetics*. https://doi.org/10.1038/ng.2714

Bulik, S., Holzhütter, H. G., & Berndt, N. (2016). The relative importance of kinetic mechanisms and variable enzyme abundances for the regulation of hepatic glucose metabolism - insights from mathematical modeling. *BMC Biology*, *14*(1), 15. https://doi.org/10.1186/s12915-016-0237-6

Buocikova, V., Rios-Mondragon, I., Pilalis, E., Chatziioannou, A., Miklikova, S., Mego, M., Pajuste, K., Rucins, M., Yamani, N. El, Longhin, E. M., Sobolev, A., Freixanet, M., Puntes, V., Plotniece, A., Dusinska, M., Cimpan, M. R., Gabelova, A., & Smolkova, B. (2020). Epigenetics in breast cancer therapy—New strategies and future nanomedicine perspectives. *Cancers*, *12*(12), 1–32. https://doi.org/10.3390/cancers12123622

Bürli, R. W., Luckhurst, C. A., Aziz, O., Matthews, K. L., Yates, D., Lyons, K. A., Beconi, M., McAllister, G., Breccia, P., Stott, A. J., Penrose, S. D., Wall, M., Lamers, M., Leonard, P., Müller, I., Richardson, C. M., Jarvis, R., Stones, L., Hughes, S., … Dominguez, C. (2013). Design, Synthesis, and Biological Evaluation of Potent and Selective Class IIa Histone Deacetylase (HDAC) Inhibitors as a Potential Therapy for Huntington's Disease. *Journal of Medicinal Chemistry*, *56*(24), 9934–9954. https://doi.org/10.1021/jm4011884

Cai, L., Sutter, B. M., Li, B., & Tu, B. P. (2011). Acetyl-CoA induces cell growth and proliferation by promoting the acetylation of histones at growth genes. *Molecular Cell*, *42*(4), 426–437. https://doi.org/10.1016/j.molcel.2011.05.004

Cai, M., Bompada, P., Atac, D., Laakso, M., Groop, L., & De Marinis, Y. (2016). Epigenetic regulation of glucose-stimulated osteopontin (OPN) expression in diabetic kidney. *Biochemical and Biophysical Research Communications*, *469*(1), 108–113. https://doi.org/10.1016/j.bbrc.2015.11.079

Campit, S. E., Meliki, A., Youngson, N. A., & Chandrasekaran, S. (2020). Nutrient Sensing by Histone Marks: Reading the Metabolic Histone Code Using Tracing, Omics, and Modeling. *BioEssays*, *42*(9), 2000083. https://doi.org/10.1002/bies.202000083

Cantor, J. R., & Sabatini, D. M. (2012). Cancer Cell Metabolism: One Hallmark, Many Faces. *Cancer Discovery*, *2*(10), 881–898. https://doi.org/10.1158/2159-8290.CD-12-0345

Cedernaes, J., Osler, M. E., Voisin, S., Broman, J.-E., Vogel, H., Dickson, S. L., Zierath, J. R., Schiöth, H. B., & Benedict, C. (2015). Acute Sleep Loss Induces Tissue-Specific Epigenetic and Transcriptional Alterations to Circadian Clock Genes in Men. *The Journal of Clinical Endocrinology & Metabolism*, *100*(9), E1255–E1261. https://doi.org/10.1210/JC.2015-2284

Chan, J. C., & Maze, I. (2020). Nothing Is Yet Set in (Hi)stone: Novel Post-Translational Modifications Regulating Chromatin Function. In *Trends in Biochemical Sciences* (Vol. 45, Issue 10, pp. 829–

844). Elsevier Ltd. https://doi.org/10.1016/j.tibs.2020.05.009

Chang, H. C., & Guarente, L. (2014). SIRT1 and other sirtuins in metabolism. In *Trends in Endocrinology and Metabolism* (Vol. 25, Issue 3, pp. 138–145). Elsevier. https://doi.org/10.1016/j.tem.2013.12.001

Charalambous, M., & Hernandez, A. (2013). Genomic imprinting of the type 3 thyroid hormone deiodinase gene: regulation and developmental implications. *Biochimica et Biophysica Acta*, *1830*(7), 3946–3955. https://doi.org/10.1016/j.bbagen.2012.03.015

Chisolm, D. A., & Weinmann, A. S. (2018). Connections Between Metabolism and Epigenetics in Programming Cellular Differentiation. *Annual Review of Immunology*, *36*(1), 221–246. https://doi.org/10.1146/annurev-immunol-042617-053127

Choi, S. Y., Kee, H. J., Jin, L., Ryu, Y., Sun, S., Kim, G. R., & Jeong, M. H. (2018). Inhibition of class IIa histone deacetylase activity by gallic acid, sulforaphane, TMP269, and panobinostat. *Biomedicine and Pharmacotherapy*, *101*, 145–154. https://doi.org/10.1016/j.biopha.2018.02.071

Chu, Y., Rosso, L. G., Huang, P., Wang, Z., Xu, Y., Yao, X., Bao, M., Yan, J., Song, H., & Wang, G. (2014). Liver Med23 ablation improves glucose and lipid metabolism through modulating FOXO1 activity. *Cell Research*, *24*(10), 1250–1265. https://doi.org/10.1038/cr.2014.120

Ciccone, D. N., Su, H., Hevi, S., Gay, F., Lei, H., Bajko, J., Xu, G., Li, E., & Chen, T. (2009). KDM1B is a histone H3K4 demethylase required to establish maternal genomic imprints. *Nature*, *461*(7262), 415–418. https://doi.org/10.1038/nature08315

Cluntun, A. A., Huang, H., Dai, L., Liu, X., Zhao, Y., & Locasale, J. W. (2015). The rate of glycolysis quantitatively mediates specific histone acetylation sites. *Cancer & Metabolism*, *3*(1), 1–12. https://doi.org/10.1186/s40170-015-0135-3

Cochran, A. G., Conery, A. R., & Sims, R. J. (2019). Bromodomains: a new target class for drug development. In *Nature Reviews Drug Discovery* (Vol. 18, Issue 8, pp. 609–628). Nature Publishing Group. https://doi.org/10.1038/s41573-019-0030-7

Corso-Díaz, X., Gentry, J., Rebernick, R., Jaeger, C., Brooks, M. J., van Asten, F., Kooragayala, K., Gieser, L., Nellissery, J., Covian, R., Cogliati, T., Mondal, A. K., Jiang, K., & Swaroop, A. (2020). Genome-wide Profiling Identifies DNA Methylation Signatures of Aging in Rod Photoreceptors Associated with Alterations in Energy Metabolism. *Cell Reports*, *31*(3). https://doi.org/10.1016/j.celrep.2020.107525

Courtnay, R., Ngo, D. C., Malik, N., Ververis, K., Tortorella, S. M., & Karagiannis, T. C. (2015). Cancer metabolism and the Warburg effect: the role of HIF-1 and PI3K. In *Molecular biology reports* (Vol. 42, Issue 4, pp. 841–851). Springer. https://doi.org/10.1007/s11033-015-3858-x

Crunkhorn, S. (2011). Metabolic disease: New role for HDACs in glucose homeostasis. *Nature Reviews Drug Discovery*, *10*(7), 492–492. https://doi.org/10.1038/nrd3483

Curtis, M., Kenny, H. A., Ashcroft, B., Mukherjee, A., Johnson, A., Zhang, Y., Helou, Y., Batlle, R., Liu, X., Gutierrez, N., Gao, X., Yamada, S. D., Lastra, R., Montag, A., Ahsan, N., Locasale, J. W., Salomon, A. R., Nebreda, A. R., & Lengyel, E. (2019). Fibroblasts Mobilize Tumor Cell Glycogen to Promote Proliferation and Metastasis. *Cell Metabolism*, *29*(1), 141-155.e9. https://doi.org/10.1016/j.cmet.2018.08.007

Dabral, S., Muecke, C., Valasarajan, C., Schmoranzer, M., Wietelmann, A., Semenza, G. L., Meister, M., Muley, T., Seeger-Nukpezah, T., Samakovlis, C., Weissmann, N., Grimminger, F., Seeger, W., Savai, R., & Pullamsetti, S. S. (2019). A RASSF1A-HIF1α loop drives Warburg effect in cancer and pulmonary hypertension. *Nature Communications*, *10*(1), 1–18. https://doi.org/10.1038/s41467-019-10044-z

Dajas, F., Juan Andres, A.-C., Florencia, A., Carolina, E., & Felicia, R.-M. (2013). Neuroprotective Actions of Flavones and Flavonols: Mechanisms and Relationship to Flavonoid Structural Features. *Central Nervous System Agents in Medicinal Chemistry*, *13*(1), 30–35.

https://doi.org/10.2174/1871524911313010005

Dang, L., White, D. W., Gross, S., Bennett, B. D., Bittinger, M. A., Driggers, E. M., Fantin, V. R., Jang, H. G., Jin, S., Keenan, M. C., Marks, K. M., Prins, R. M., Ward, P. S., Yen, K. E., Liau, L. M., Rabinowitz, J. D., Cantley, L. C., Thompson, C. B., Vander Heiden, M. G., & Su, S. M. (2009). Cancer-associated IDH1 mutations produce 2-hydroxyglutarate. *Nature*, *462*(7274), 739–744. https://doi.org/10.1038/nature08617

DeBerardinis, R. J., & Chandel, N. S. (2016). Fundamentals of cancer metabolism. *Science Advances*, *2*(5), e1600200–e1600200. https://doi.org/10.1126/sciadv.1600200

DeBerardinis, R. J., & Cheng, T. (2010). Q's next: the diverse functions of glutamine in metabolism, cell biology and cancer. *Oncogene*, *29*(3), 313–324. https://doi.org/10.1038/onc.2009.358

Del Rey, M. J., Valín, Á., Usategui, A., García-Herrero, C. M., Sánchez-Aragó, M., Cuezva, J. M., Galindo, M., Bravo, B., Cañete, J. D., Blanco, F. J., Criado, G., & Pablos, J. L. (2017). Hif-1α Knockdown Reduces Glycolytic Metabolism and Induces Cell Death of Human Synovial Fibroblasts under Normoxic Conditions. *Scientific Reports*, *7*(1). https://doi.org/10.1038/s41598-017-03921-4

Denkert, C., Budczies, J., Kind, T., Weichert, W., Tablack, P., Sehouli, J., Niesporek, S., Könsgen, D., Dietel, M., & Fiehn, O. (2006). Mass spectrometry-based metabolic profiling reveals different metabolite patterns in invasive ovarian carcinomas and ovarian borderline tumors. *Cancer Research*, *66*(22), 10795–10804. https://doi.org/10.1158/0008-5472.CAN-06-0755

Dong, Z., Yang, J., Li, L., Tan, L., Shi, P., Zhang, J., Zhong, X., Ge, L., Wu, Z., & Cui, H. (2020). FOXO3a-SIRT6 axis suppresses aerobic glycolysis in melanoma. *International Journal of Oncology*, *56*(3), 728–742. https://doi.org/10.3892/ijo.2020.4964

Donga, E., van Dijk, M., van Dijk, J. G., Biermasz, N. R., Lammers, G.-J., van Kralingen, K. W., Corssmit, E. P. M., & Romijn, J. A. (2010). A Single Night of Partial Sleep Deprivation Induces Insulin Resistance in Multiple Metabolic Pathways in Healthy Subjects. *The Journal of Clinical Endocrinology & Metabolism*, *95*(6), 2963–2968. https://doi.org/10.1210/jc.2009-2430

Duan, W. (2013). Targeting Sirtuin-1 in Huntington's Disease: Rationale and Current Status. *CNS Drugs*, *27*(5), 345–352. https://doi.org/10.1007/s40263-013-0055-0

Dueñas-Gonzalez, A., Coronel, J., Cetina, L., González-Fierro, A., Chavez-Blanco, A., & Taja-Chayeb, L. (2014). Hydralazine–valproate: a repositioned drug combination for the epigenetic therapy of cancer. *Expert Opinion on Drug Metabolism & Toxicology*, *10*(10), 1433–1444. https://doi.org/10.1517/17425255.2014.947263

Dutta, A., Abmayr, S. M., & Workman, J. L. (2016). Diverse Activities of Histone Acylations Connect Metabolism to Chromatin Function. In *Molecular Cell* (Vol. 63, Issue 4, pp. 547–552). Cell Press. https://doi.org/10.1016/j.molcel.2016.06.038

Eagle, H. (1955). The minimum vitamin requirements of the L and HeLa cells in tissue culture, the production of specific vitamin deficiencies, and their cure. *The Journal of Experimental Medicine*, *102*(5), 595–600. http://www.ncbi.nlm.nih.gov/pubmed/13271674

Etchegaray, J.-P., & Mostoslavsky, R. (2016). Interplay between Metabolism and Epigenetics: A Nuclear Adaptation to Environmental Changes. *Molecular Cell*, *62*, 695–711. https://doi.org/10.1016/j.molcel.2016.05.029

Evans, R. D. (2012). Myocardial substrate metabolism in heart disease. *Frontiers in Bioscience*, *S4*(1), 556. https://doi.org/10.2741/285

Fan, J., Krautkramer, K. A., Feldman, J. L., & Denu, J. M. (2015a). *Metabolic regulation of histone post-translational modifications*. https://doi.org/10.1021/cb500846u

Fan, J., Krautkramer, K. A., Feldman, J. L., & Denu, J. M. (2015b). Metabolic regulation of histone post-translational modifications. *ACS Chemical Biology*, *10*(1), 95–108. https://doi.org/10.1021/cb500846u

Fan, J., Krautkramer, K. A., Feldman, J. L., & Denu, J. M. (2015c). Metabolic regulation of histone post-translational modifications. In *ACS Chemical Biology* (Vol. 10, Issue 1, pp. 95–108). American Chemical Society. https://doi.org/10.1021/cb500846u

Fang, E., Wang, J., Hong, M., Zheng, L., & Tong, Q. (2019). Valproic acid suppresses Warburg effect and tumor progression in neuroblastoma. *Biochemical and Biophysical Research Communications*, *508*(1), 9–16. https://doi.org/10.1016/j.bbrc.2018.11.103

Faundes, V., Newman, W. G., Bernardini, L., Canham, N., Clayton-Smith, J., Dallapiccola, B., Davies, S. J., Demos, M. K., Goldman, A., Gill, H., Horton, R., Kerr, B., Kumar, D., Lehman, A., McKee, S., Morton, J., Parker, M. J., Rankin, J., Robertson, L., … Banka, S. (2018). Histone Lysine Methylases and Demethylases in the Landscape of Human Developmental Disorders. *American Journal of Human Genetics*, *102*(1), 175–187. https://doi.org/10.1016/j.ajhg.2017.11.013

FDA. (2015). *Diabetes Medicines*. www.fda.gov/womensdiabetes

Feinberg, A. P., Koldobskiy, M. A., & Göndör, A. (2016). Epigenetic modulators, modifiers and mediators in cancer aetiology and progression. *Nature Reviews. Genetics*, *17*(5), 284–299. https://doi.org/10.1038/nrg.2016.13

Feldhammer, M., Uetani, N., Miranda-Saavedra, D., & Tremblay, M. L. (2013). Ptp1b: A simple enzyme for a complex world. In *Critical Reviews in Biochemistry and Molecular Biology* (Vol. 48, Issue 5, pp. 430–445). Taylor & Francis. https://doi.org/10.3109/10409238.2013.819830

Feldman, J. L., Baeza, J., & Denu, J. M. (2013). Activation of the protein deacetylase SIRT6 by long-chain fatty acids and widespread deacylation by Mammalian Sirtuins. *Journal of Biological Chemistry*, *288*(43), 31350–31356. https://doi.org/10.1074/jbc.C113.511261

Feller, C., Forné, I., Imhof, A., & Becker, P. B. (2015). Global and specific responses of the histone acetylome to systematic perturbation. *Molecular Cell*, *57*(3), 559–571. https://doi.org/10.1016/j.molcel.2014.12.008

Ferrari, K. J., Scelfo, A., Jammula, S. G., Cuomo, A., Barozzi, I., Stützer, A., Fischle, W., Bonaldi, T., & Pasini, D. (2014a). Polycomb-Dependent H3K27me1 and H3K27me2 Regulate Active Transcription and Enhancer Fidelity. *Molecular Cell*, *53*(1), 49–62. https://doi.org/10.1016/j.molcel.2013.10.030

Ferrari, K. J., Scelfo, A., Jammula, S. G., Cuomo, A., Barozzi, I., Stützer, A., Fischle, W., Bonaldi, T., & Pasini, D. (2014b). Polycomb-Dependent H3K27me1 and H3K27me2 Regulate Active Transcription and Enhancer Fidelity. *Molecular Cell*, *53*(1), 49–62. https://doi.org/10.1016/j.molcel.2013.10.030

Figueroa, M. E., Lugthart, S., Li, Y., Erpelinck-Verschueren, C., Deng, X., Christos, P. J., Schifano, E., Booth, J., van Putten, W., Skrabanek, L., Campagne, F., Mazumdar, M., Greally, J. M., Valk, P. J. M., Löwenberg, B., Delwel, R., & Melnick, A. (2010). DNA Methylation Signatures Identify Biologically Distinct Subtypes in Acute Myeloid Leukemia. *Cancer Cell*, *17*(1), 13–27. https://doi.org/10.1016/j.ccr.2009.11.020

Fillmore, N., & Lopaschuk, G. D. (2013). Targeting mitochondrial oxidative metabolism as an approach to treat heart failure. *Biochimica et Biophysica Acta - Molecular Cell Research*, *1833*(4), 857–865. https://doi.org/10.1016/j.bbamcr.2012.08.014

Finkelstein, E. A., Khavjou, O. A., Thompson, H., Trogdon, J. G., Pan, L., Sherry, B., & Dietz, W. (2012). Obesity and severe obesity forecasts through 2030. *American Journal of Preventive Medicine*, *42*(6), 563–570. https://doi.org/10.1016/j.amepre.2011.10.026

Fontana, L., & Partridge, L. (2015). Promoting health and longevity through diet: from model organisms to humans. *Cell*, *161*(1), 106–118. https://doi.org/10.1016/j.cell.2015.02.020

Foy, R. L., Ihn, Y. S., Chitalia, V. C., Cohen, H. T., Saksouk, N., Cayrou, C., Vaziri, C., Côté, J., & Panchenko, M. V. (2008). Role of Jade-1 in the histone acetyltransferase (HAT) HBO1 complex. *Journal of Biological Chemistry*, *283*(43), 28817–28826.

https://doi.org/10.1074/jbc.M801407200

Fraga, M. F., Ballestar, E., Villar-Garea, A., Boix-Chornet, M., Espada, J., Schotta, G., Bonaldi, T., Haydon, C., Ropero, S., Petrie, K., Iyer, N. G., Pérez-Rosado, A., Calvo, E., Lopez, J. A., Cano, A., Calasanz, M. J., Colomer, D., Piris, M. Á., Ahn, N., … Esteller, M. (2005). Loss of acetylation at Lys16 and trimethylation at Lys20 of histone H4 is a common hallmark of human cancer. *Nature Genetics*, *37*(4), 391–400. https://doi.org/10.1038/ng1531

Fukushima, A., Milner, K., Gupta, A., & Lopaschuk, G. (2015). Myocardial Energy Substrate Metabolism in Heart Failure : from Pathways to Therapeutic Targets. *Current Pharmaceutical Design*, *21*(25), 3654–3664. https://doi.org/10.2174/1381612821666150710150445

Gabrielli, F., & Tofanelli, S. (2012). Molecular and functional evolution of human DHRS2 and DHRS4 duplicated genes. *Gene*, *511*(2), 461–469. https://doi.org/10.1016/j.gene.2012.09.013

Galbraith, M. D., Allen, M. A., Bensard, C. L., Wang, X., Schwinn, M. K., Qin, B., Long, H. W., Daniels, D. L., Hahn, W. C., Dowell, R. D., & Espinosa, J. M. (2013). XHIF1A employs CDK8-mediator to stimulate RNAPII elongation in response to hypoxia. *Cell*, *153*(6), 1327. https://doi.org/10.1016/j.cell.2013.04.048

Galdieri, L., & Vancura, A. (2012). Acetyl-CoA carboxylase regulates global histone acetylation. *The Journal of Biological Chemistry*, *287*(28), 23865–23876. https://doi.org/10.1074/jbc.M112.380519

Ganai, S. (2016). Histone deacetylase inhibitors modulating non-epigenetic players: The novel molecular targets for therapeutic intervention. *Current Drug Targets*, *17*(999), 1–1. https://doi.org/10.2174/1389450117666160527143257

Ganai, S. A., Farooq, Z., Banday, S., & Altaf, M. (2018). In silico approaches for investigating the binding propensity of apigenin and luteolin against class i HDAC isoforms. *Future Medicinal Chemistry*, *10*(16), 1925–1945. https://doi.org/10.4155/fmc-2018-0020

Gargus, J. J., Boyle, K., Bocian, M., Roe, D. S., Vianey-Saban, C., & Roe, C. R. (2003). Respiratory complex II defect in siblings associated with a symptomatic secondary block in fatty acid oxidation. *Journal of Inherited Metabolic Disease*, *26*(7), 659. https://doi.org/10.1023/B:BOLI.0000005659.52200.c1

Ge, K., Guermah, M., Yuan, C. X., Ito, M., Wallberg, A. E., Spiegelman, B. M., & Roeder, R. G. (2002). Transcription coactivator TRAP220 is required for PPARδ2-stimulated adipogenesis. *Nature*, *417*(6888), 563–567. https://doi.org/10.1038/417563a

Gebauer, J., Higham, C., Langer, T., Denzer, C., & Brabant, G. (2018). Long-Term Endocrine and Metabolic Consequences of Cancer Treatment: A Systematic Review. *Endocrine Reviews*, *40*(3), 711–767. https://doi.org/10.1210/er.2018-00092

Geng, H., Harvey, C. T., Pittsenbarger, J., Liu, Q., Beer, T. M., Xue, C., & Qian, D. Z. (2011). HDAC4 protein regulates HIF1α protein lysine acetylation and cancer cell response to hypoxia. *Journal of Biological Chemistry*, *286*(44), 38095–38102. https://doi.org/10.1074/jbc.M111.257055

Gerhäuser, C. (2012). Cancer cell metabolism, epigenetics and the potential influence of dietary components-A perspective Cancer cell metabolism. In *Cancer Metabolism) Biomedical Research* (Vol. 23, Issue 1).

German, N. J., & Haigis, M. C. (2015). Sirtuins and the Metabolic Hurdles in Cancer. In *Current Biology* (Vol. 25, Issue 13, pp. R569–R583). Cell Press. https://doi.org/10.1016/j.cub.2015.05.012

Giandomenico, V., Simonsson, M., Grönroos, E., & Ericsson, J. (2003). Coactivator-Dependent Acetylation Stabilizes Members of the SREBP Family of Transcription Factors. *Molecular and Cellular Biology*, *23*(7), 2587–2599. https://doi.org/10.1128/mcb.23.7.2587-2599.2003

Goldsworthy, M., Absalom, N. L., Schröter, D., Matthews, H. C., Bogani, D., Moir, L., Long, A., Church, C., Hugill, A., Anstee, Q. M., Goldin, R., Thursz, M., Hollfelder, F., & Cox, R. D. (2013).

Mutations in Mll2, an H3K4 Methyltransferase, Result in Insulin Resistance and Impaired Glucose Tolerance in Mice. *PLoS ONE*, *8*(6), e61870. https://doi.org/10.1371/journal.pone.0061870

Goru, S. K., Kadakol, A., Pandey, A., Malek, V., Sharma, N., & Gaikwad, A. B. (2016). Histone H2AK119 and H2BK120 monoubiquitination modulate SET7/9 and SUV39H1 in type 1 diabetes-induced renal fibrosis. *Biochemical Journal*, *473*(21), 3937–3949. https://doi.org/10.1042/BCJ20160595

Grassian, a R., Coloff, J. L., & Brugge, J. S. (2011). Extracellular Matrix Regulation of Metabolism and Implications for Tumorigenesis. *Cold Spring Harb. Symp. Quant. Biol.* https://doi.org/10.1101/sqb.2011.76.010967

Gray, S. G. (2010). Targeting Histone Deacetylases for the Treatment of Huntington's Disease. *CNS Neuroscience & Therapeutics*, *16*(6), 348–361. https://doi.org/10.1111/j.1755-5949.2010.00184.x

Greenblatt, S. M., Liu, F., & Nimer, S. D. (2016). Arginine methyltransferases in normal and malignant hematopoiesis. In *Experimental Hematology* (Vol. 44, Issue 6, pp. 435–441). Elsevier Inc. https://doi.org/10.1016/j.exphem.2016.03.009

Guan, K. L., & Xiong, Y. (2011). Regulation of intermediary metabolism by protein acetylation. *Trends in Biochemical Sciences*, *36*(2), 108–116. https://doi.org/10.1016/j.tibs.2010.09.003

Guarente, L., Mostoslavsky, R., & Kazantsev, A. (2018). Introductory review on sirtuins in biology, aging, and disease. In *Introductory Review on Sirtuins in Biology, Aging, and Disease*. Elsevier. https://doi.org/10.1016/C2016-0-04790-3

Gupta, J., Kumar, S., Li, J., Krishna Murthy Karuturi, R., & Tikoo, K. (2012). Histone H3 lysine 4 monomethylation (H3K4me1) and H3 lysine 9 monomethylation (H3K9me1): Distribution and their association in regulating gene expression under hyperglycaemic/hyperinsulinemic conditions in 3T3 cells. *Biochimie*, *94*(12), 2656–2664. https://doi.org/10.1016/j.biochi.2012.08.011

Gursoy-Yuzugullu, O., Carman, C., Serafim, R. B., Myronakis, M., Valente, V., & Price, B. D. (2017). Epigenetic therapy with inhibitors of histone methylation suppresses DNA damage signaling and increases glioma cell radiosensitivity. *Oncotarget*, *8*(15), 24518–24532. https://doi.org/10.18632/oncotarget.15543

Gut, P., & Verdin, E. (2013). The nexus of chromatin regulation and intermediary metabolism. *Nature*. https://doi.org/10.1038/nature12752

Hadden, M. J., & Advani, A. (2018). Histone deacetylase inhibitors and diabetic kidney disease. In *International Journal of Molecular Sciences* (Vol. 19, Issue 9). MDPI AG. https://doi.org/10.3390/ijms19092630

Hannum, G., Guinney, J., Zhao, L., Zhang, L., Hughes, G., Sadda, S. V., Klotzle, B., Bibikova, M., Fan, J. B., Gao, Y., Deconde, R., Chen, M., Rajapakse, I., Friend, S., Ideker, T., & Zhang, K. (2013). Genome-wide Methylation Profiles Reveal Quantitative Views of Human Aging Rates. *Molecular Cell*, *49*(2), 359–367. https://doi.org/10.1016/j.molcel.2012.10.016

Haws, S. A., Yu, D., Ye, C., Wille, C. K., Nguyen, L. C., Krautkramer, K. A., Tomasiewicz, J. L., Yang, S. E., Miller, B. R., Liu, W. H., Igarashi, K., Sridharan, R., Tu, B. P., Cryns, V. L., Lamming, D. W., & Denu, J. M. (2020). Methyl-Metabolite Depletion Elicits Adaptive Responses to Support Heterochromatin Stability and Epigenetic Persistence. *Molecular Cell*, *78*(2), 210-223.e8. https://doi.org/10.1016/j.molcel.2020.03.004

Heerboth, S., Lapinska, K., Snyder, N., Leary, M., Rollinson, S., & Sarkar, S. (2014). Use of epigenetic drugs in disease: An overview. *Genetics and Epigenetics*, *1*(6), 9–19. https://doi.org/10.4137/GeG.s12270

Heger, S., Mastronardi, C., Dissen, G. A., Lomniczi, A., Cabrera, R., Roth, C. L., Jung, H., Galimi, F.,

Sippell, W., & Ojeda, S. R. (2007). Enhanced at puberty 1 (EAP1) is a new transcriptional regulator of the female neuroendocrine reproductive axis. *Journal of Clinical Investigation*, *117*(8), 2145–2154. https://doi.org/10.1172/JCI31752

Heijmans, B. T., Tobi, E. W., Stein, A. D., Putter, H., Blauw, G. J., Susser, E. S., Slagboom, P. E., & Lumey, L. H. (2008). Persistent epigenetic differences associated with prenatal exposure to famine in humans. *Proceedings of the National Academy of Sciences of the United States of America*, *105*(44), 17046–17049. https://doi.org/10.1073/pnas.0806560105

Henriquez, B., Bustos, F. J., Aguilar, R., Becerra, A., Simon, F., Montecino, M., & van Zundert, B. (2013). Ezh1 and Ezh2 differentially regulate PSD-95 gene transcription in developing hippocampal neurons. *Molecular and Cellular Neuroscience*, *57*, 130–143. https://doi.org/10.1016/j.mcn.2013.07.012

Himmerich, H., Minkwitz, J., & Kirkby, K. (2015). Weight Gain and Metabolic Changes During Treatment with Antipsychotics and Antidepressants. *Endocrine, Metabolic & Immune Disorders-Drug Targets*, *15*(4), 252–260. https://doi.org/10.2174/1871530315666150623092031

Holoch, D., & Margueron, R. (2017). Polycomb Repressive Complex 2 Structure and Function. In V. Pirrotta (Ed.), *Polycomb Group Proteins* (pp. 191–224). Elsevier Inc. https://www.sciencedirect.com/book/9780128097373/polycomb-group-proteins

Horvath, S. (2013). DNA methylation age of human tissues and cell types. *Genome Biology*, *14*(10). https://doi.org/10.1186/gb-2013-14-10-r115

Houtkooper, R. H., Pirinen, E., & Auwerx, J. (2012). Sirtuins as regulators of metabolism and healthspan. In *Nature Reviews Molecular Cell Biology* (Vol. 13, Issue 4, pp. 225–238). Europe PMC Funders. https://doi.org/10.1038/nrm3293

Hoyo, C., Fortner, K., Murtha, A. P., Schildkraut, J. M., Soubry, A., Demark-Wahnefried, W., Jirtle, R. L., Kurtzberg, J., Forman, M. R., Overcash, F., Huang, Z., & Murphy, S. K. (2012). Association of cord blood methylation fractions at imprinted insulin-like growth factor 2 (IGF2), plasma IGF2, and birth weight. *Cancer Causes & Control : CCC*, *23*(4), 635–645. https://doi.org/10.1007/s10552-012-9932-y

Huang, L., Liu, J., Zhang, X. O., Sibley, K., Najjar, S. M., Lee, M. M., & Wu, Q. (2018). Inhibition of protein arginine methyltransferase 5 enhances hepatic mitochondrial biogenesis. *Journal of Biological Chemistry*, *293*(28), 10884–10894. https://doi.org/10.1074/jbc.RA118.002377

Hyun, K., Jeon, J., Park, K., & Kim, J. (2017). Writing, erasing and reading histone lysine methylations. *Experimental and Molecular Medicine*, *49*(4). https://doi.org/10.1038/emm.2017.11

IDF, D. A. 9th E. (2019). *IDF Atlas*. https://www.diabetesatlas.org/en/resources/

Iida, S., Chen, W., Nakadai, T., Ohkuma, Y., & Roeder, R. G. (2015). PRDM16 enhances nuclear receptordependent transcription of the brown fat-specific Ucp1 gene through interactions with mediator subunit MED1. *Genes and Development*, *29*(3), 308–321. https://doi.org/10.1101/gad.252809.114

Ikonomov, O. C., Sbrissa, D., Delvecchio, K., A. Rillema, J., & Shisheva, A. (2016). Unexpected severe consequences of Pikfyve deletion by aP2- or Aq-promoter-driven Cre expression for glucose homeostasis and mammary gland development. *Physiological Reports*, *4*(11). https://doi.org/10.14814/phy2.12812

Ikonomov, O. C., Sbrissa, D., Dondapati, R., & Shisheva, A. (2007). ArPIKfyve-PIKfyve interaction and role in insulin-regulated GLUT4 translocation and glucose transport in 3T3-L1 adipocytes. *Experimental Cell Research*, *313*(11), 2404–2416. https://doi.org/10.1016/j.yexcr.2007.03.024

Jakovcevski, M., & Akbarian, S. (2012). Epigenetic mechanisms in neurological disease. *Nature Medicine*, *18*(8), 1194–1204. https://doi.org/10.1038/nm.2828

Jankevicius, G., Hassler, M., Golia, B., Rybin, V., Zacharias, M., Timinszky, G., & Ladurner, A. G. (2013). A family of macrodomain proteins reverses cellular mono-ADP-ribosylation. *Nature*

Structural and Molecular Biology, *20*(4), 508–514. https://doi.org/10.1038/nsmb.2523

Janssen, F., Bardoutsos, A., & Vidra, N. (2020). Obesity Prevalence in the Long-Term Future in 18 European Countries and in the USA. *Obesity Facts*, *13*(5), 514–527. https://doi.org/10.1159/000511023

Jia, Y., Qi, C., Kashireddi, P., Surapureddi, S., Zhu, Y. J., Rao, M. S., Le Roith, D., Chambon, P., Gonzalez, F. J., & Reddy, J. K. (2004). Transcription coactivator PBP, the peroxisome proliferator-activated receptor (PPAR)-binding protein, is required for PPARα-regulated gene expression in liver. *Journal of Biological Chemistry*, *279*(23), 24427–24434. https://doi.org/10.1074/jbc.M402391200

Jia, Y., Viswakarma, N., Fu, T., Yu, S., Rao, M. S., Borensztajn, J., & Reddy, J. K. (2009). Conditional ablation of mediator subunit MED1 (MED1/PPARBP) gene in mouse liver attenuates glucocorticoid receptor agonist dexamethasone-induced hepatic steatosis. *Gene Expression*, *14*(5), 291–306. https://doi.org/10.3727/105221609788681213

Jiang, L., Zhou, W., Lu, B., & Yan, Q. (2020). ITCH regulates oxidative stress induced by high glucose through thioredoxin interacting protein in cultured human lens epithelial cells. *Molecular Medicine Reports*, *22*(5), 4307–4319. https://doi.org/10.3892/mmr.2020.11499

Jih, G., Iglesias, N., Currie, M. A., Bhanu, N. V., Paulo, J. A., Gygi, S. P., Garcia, B. A., & Moazed, D. (2017). Unique roles for histone H3K9me states in RNAi and heritable silencing of transcription. *Nature*, *547*(7664), 463–467. https://doi.org/10.1038/nature23267

Jiujie Cui., et al. (2019). A novel KDM5A/MPC-1 signaling pathway promotes pancreatic cancer progression via redirecting mitochondrial pyruvate metabolism. *Oncogene*. https://doi.org/https://doi.org/10.1038/s41388-019-1051-8

Jose, C., Bellance, N., & Rossignol, R. (2011). Choosing between glycolysis and oxidative phosphorylation: A tumor's dilemma? *Biochimica et Biophysica Acta - Bioenergetics*, *1807*(6), 552–561. https://doi.org/10.1016/j.bbabio.2010.10.012

Jumpertz von Schwartzenberg, R., & Turnbaugh, P. J. (2015). Siri, What Should I Eat? *Cell*, *163*(5), 1051–1052. https://doi.org/10.1016/j.cell.2015.11.012

Justice, M. J., Buchovecky, C. M., Kyle, S. M., & Djukic, A. (2013). A role for metabolism in Rett syndrome pathogenesis: New clinical findings and potential treatment targets. *Rare Diseases (Austin, Tex.)*, *1*, e27265. https://doi.org/10.4161/rdis.27265

Kaelin, W. G., McKnight, S. L., & McKnight, S. L. (2013). Influence of metabolism on epigenetics and disease. *Cell*, *153*(1), 56–69. https://doi.org/10.1016/j.cell.2013.03.004

Kang, B., & Sun, X.-H. (2014). Regulation of cancer stem cells by RING finger ubiquitin ligases. *Stem Cell Investigation*, *1*, 5–5. https://doi.org/10.3978/j.issn.2306-9759.2014.01.01

Kang, J., Kim, J., Kim, K., Park, J. W., Cho, H., Hahm, J. Y., Chae, Y., Kim, D., Kook, H., Rhee, S., Ha, N., & Seo, S. (2018). KDM2B is a histone H3K79 demethylase and induces transcriptional repression *via* sirtuin-1-mediated chromatin silencing. *The FASEB Journal*, *32*(10), 5737–5750. https://doi.org/10.1096/fj.201800242R

Kaniskan, H. Ü., Martini, M. L., & Jin, J. (2018). Inhibitors of Protein Methyltransferases and Demethylases. *Chemical Reviews*, *118*(3), 989–1068. https://doi.org/10.1021/acs.chemrev.6b00801

Kawada, I., Hasina, R., Lennon, F. E., Bindokas, V. P., Usatyuk, P., Tan, Y. H. C., Krishnaswamy, S., Arif, Q., Carey, G., Hseu, R. D., Robinson, M., Tretiakova, M., Brand, T. M., Iida, M., Ferguson, M. K., Wheeler, D. L., Husain, A. N., Natarajan, V., Vokes, E. E., … Salgia, R. (2013). Paxillin mutations affect focal adhesions and lead to altered mitochondrial dynamics: Relevance to lung cancer. *Cancer Biology and Therapy*, *14*(7), 679–691. https://doi.org/10.4161/cbt.25091

Kelly, T., Yang, W., Chen, C.-S., Reynolds, K., & He, J. (2008). Global burden of obesity in 2005 and projections to 2030. *International Journal of Obesity*, *32*(9), 1431–1437.

https://doi.org/10.1038/ijo.2008.102

Kennedy, B. E., Hundert, A. S., Goguen, D., Weaver, I. C. G., & Karten, B. (2016). Presymptomatic Alterations in Amino Acid Metabolism and DNA Methylation in the Cerebellum of a Murine Model of Niemann-Pick Type C Disease. *The American Journal of Pathology*, *186*(6), 1582–1597. https://doi.org/10.1016/j.ajpath.2016.02.012

Khanna, I. (2012). Drug discovery in pharmaceutical industry: Productivity challenges and trends. In *Drug Discovery Today* (Vol. 17, Issues 19–20, pp. 1088–1102). https://doi.org/10.1016/j.drudis.2012.05.007

Khera, A. V., Emdin, C. A., Drake, I., Natarajan, P., Bick, A. G., Cook, N. R., Chasman, D. I., Baber, U., Mehran, R., Rader, D. J., Fuster, V., Boerwinkle, E., Melander, O., Orho-Melander, M., Ridker, P. M., & Kathiresan, S. (2016). Genetic Risk, Adherence to a Healthy Lifestyle, and Coronary Disease. *New England Journal of Medicine*, *375*(24), 2349–2358. https://doi.org/10.1056/NEJMoa1605086

Kim, A., & Yun, J.-M. (2017). Combination Treatments with Luteolin and Fisetin Enhance Anti-Inflammatory Effects in High Glucose-Treated THP-1 Cells Through Histone Acetyltransferase/Histone Deacetylase Regulation. *Journal of Medicinal Food*, *20*(8), 782–789. https://doi.org/10.1089/jmf.2017.3968

Kim, D.-H., Kim, J., Kwon, J.-S., Sandhu, J., Tontonoz, P., Lee, S.-K., Lee, S., & Lee, J. W. (2016). Critical Roles of the Histone Methyltransferase MLL4/KMT2D in Murine Hepatic Steatosis Directed by ABL1 and PPARγ2. *Cell Reports*, *17*(6), 1671–1682. https://doi.org/10.1016/j.celrep.2016.10.023

Kim, D.-H., Rhee, J. C., Yeo, S., Shen, R., Lee, S.-K., Lee, J. W., & Lee, S. (2015). Crucial roles of mixed-lineage leukemia 3 and 4 as epigenetic switches of the hepatic circadian clock controlling bile acid homeostasis in mice. *Hepatology (Baltimore, Md.)*, *61*(3), 1012–1023. https://doi.org/10.1002/hep.27578

Kim, J., Kim, J. Y., Song, K. S., Lee, Y. H., Seo, J. S., Jelinek, J., Goldschmidt-Clermont, P. J., & Issa, J.-P. J. (2007). Epigenetic changes in estrogen receptor β gene in atherosclerotic cardiovascular tissues and in-vitro vascular senescence. *Biochimica et Biophysica Acta (BBA) - Molecular Basis of Disease*, *1772*(1), 72–80. https://doi.org/10.1016/j.bbadis.2006.10.004

Kim, S., Jeong, J., Park, J. A. E., Lee, J., Seo, J. I. H. A. E., Jung, B., Bae, M., & Kim, K. (2007). or_17_3_647_PDF. *Oncology Reports*, *17*, 647–651.

Kim, S. Y., Zhang, X., Schiattarella, G. G., Altamirano, F., Ramos, T. A. R., French, K. M., Jiang, N., Szweda, P. A., Evers, B. M., May, H. I., Luo, X., Li, H., Szweda, L. I., Maracaja-Coutinho, V., Lavandero, S., Gillette, T. G., & Hill, J. A. (2020). Epigenetic Reader BRD4 Governs Nucleus-encoded Mitochondrial Transcriptome to Regulate Cardiac Function. *Circulation*, *4*, 2356–2370. https://doi.org/10.1161/circulationaha.120.047239

Kim, W., & Lee, E. K. (2012). Post-transcriptional regulation in metabolic diseases. In *RNA Biology* (Vol. 9, Issue 6, pp. 772–780). Taylor and Francis Inc. https://doi.org/10.4161/rna.20091

Kirtana, R., Manna, S., & Patra, S. K. (2020). Molecular mechanisms of KDM5A in cellular functions: Facets during development and disease. In *Experimental Cell Research* (Vol. 396, Issue 2). Elsevier Inc. https://doi.org/10.1016/j.yexcr.2020.112314

Kok, D. E. G., Dhonukshe-Rutten, R. A. M., Lute, C., Heil, S. G., Uitterlinden, A. G., van der Velde, N., van Meurs, J. B. J., van Schoor, N. M., Hooiveld, G. J. E. J., de Groot, L. C. P. G. M., Kampman, E., & Steegenga, W. T. (2015). The effects of long-term daily folic acid and vitamin B12 supplementation on genome-wide DNA methylation in elderly subjects. *Clinical Epigenetics*, *7*(1), 121. https://doi.org/10.1186/s13148-015-0154-5

Kollmann, K., Uusi-Rauva, K., Scifo, E., Tyynelä, J., Jalanko, A., & Braulke, T. (2013). Cell biology and function of neuronal ceroid lipofuscinosis-related proteins. In *Biochimica et Biophysica Acta - Molecular Basis of Disease* (Vol. 1832, Issue 11, pp. 1866–1881).

https://doi.org/10.1016/j.bbadis.2013.01.019

Kopelman, P., Jebb, S. A., & Butland, B. (2007). Executive summary: Foresight "tackling obesities: Future choices" project. *Obesity Reviews*, *8*(SUPPL. 1). https://doi.org/10.1111/j.1467-789X.2007.00344.x

Koren, D., & Palladino, A. (2016). Hypoglycemia. In *Genetic Diagnosis of Endocrine Disorders* (pp. 31–75). Elsevier. https://doi.org/10.1016/B978-0-12-800892-8.00003-8

Kriaucionis, S., Paterson, A., Curtis, J., Guy, J., MacLeod, N., & Bird, A. (2006). Gene Expression Analysis Exposes Mitochondrial Abnormalities in a Mouse Model of Rett Syndrome. *Molecular and Cellular Biology*. https://doi.org/10.1128/MCB.01665-05

Kwak, S. H., & Park, K. S. (2016). Recent progress in genetic and epigenetic research on type 2 diabetes. *Experimental & Molecular Medicine*, *48*(3), e220. https://doi.org/10.1038/emm.2016.7

Kyle, S. M., Saha, P. K., Brown, H. M., Chan, L. C., & Justice, M. J. (2016). MeCP2 co-ordinates liver lipid metabolism with the NCoR1/HDAC3 corepressor complex. *Human Molecular Genetics*, *25*(14), 3029–3041. https://doi.org/10.1093/hmg/ddw156

Lau, P., Fitzsimmons, R. L., Raichur, S., Wang, S.-C. M., Lechtken, A., & Muscat, G. E. O. (2008). The Orphan Nuclear Receptor, RORα, Regulates Gene Expression That Controls Lipid Metabolism. *Journal of Biological Chemistry*, *283*(26), 18411–18421. https://doi.org/10.1074/jbc.M710526200

Laugesen, A., Højfeldt, J. W., & Helin, K. (2019). Molecular Mechanisms Directing PRC2 Recruitment and H3K27 Methylation. *Molecular Cell*, *74*(1), 8–18. https://doi.org/10.1016/j.molcel.2019.03.011

Laukka, T., Mariani, C. J., Ihantola, T., Cao, J. Z., Hokkanen, J., Kaelin, W. G., Godley, L. A., & Koivunen, P. (2016). Fumarate and Succinate Regulate Expression of Hypoxia-inducible Genes via TET Enzymes. *Journal of Biological Chemistry*, *291*(8), 4256–4265. https://doi.org/10.1074/jbc.M115.688762

Lavarone, E., Barbieri, C. M., & Pasini, D. (2019). Dissecting the role of H3K27 acetylation and methylation in PRC2 mediated control of cellular identity. *Nature Communications*, *10*(1), 1–16. https://doi.org/10.1038/s41467-019-09624-w

Lee, H. S., & Park, T. (2020). The influences of DNA methylation and epigenetic clocks, on metabolic disease, in middle-aged Koreans. *Clinical Epigenetics*, *12*(1), 1–10. https://doi.org/10.1186/s13148-020-00936-z

Lee, J.-E., Wang, C., Xu, S., Cho, Y.-W., Wang, L., Feng, X., Baldridge, A., Sartorelli, V., Zhuang, L., Peng, W., & Ge, K. (2013). H3K4 mono- and di-methyltransferase MLL4 is required for enhancer activation during cell differentiation. *ELife*, *2*, e01503. https://doi.org/10.7554/eLife.01503

Li, H., Wei, S., Cheng, K., Gounko, N. V., Ericksen, R. E., Xu, A., Hong, W., & Han, W. (2014). BIG3 inhibits insulin granule biogenesis and insulin secretion. *EMBO Reports*, *15*(6), 714–722. https://doi.org/10.1002/embr.201338181

Li, P., Ruan, X., Yang, L., Kiesewetter, K., Zhao, Y., Luo, H., Chen, Y., Gucek, M., Zhu, J., & Cao, H. (2015). A liver-enriched long non-coding RNA, lncLSTR, regulates systemic lipid metabolism in mice. *Cell Metabolism*, *21*(3), 455–467. https://doi.org/10.1016/j.cmet.2015.02.004

Li, Q., Cao, L., Tian, Y., Zhang, P., Ding, C., Lu, W., Jia, C., Shao, C., Liu, W., Wang, D., Ye, H., & Hao, H. (2018). Butyrate suppresses the proliferation of colorectal cancer cells via targeting pyruvate kinase M2 and metabolic reprogramming. *Molecular and Cellular Proteomics*, *17*(8), 1531–1545. https://doi.org/10.1074/mcp.RA118.000752

Li, T., & Deng, P. (2017). Nuclear Magnetic Resonance technique in tumor metabolism. *Genes & Diseases*, *4*(1), 28–36. https://doi.org/10.1016/J.GENDIS.2016.12.001

Li, X., Li, C., & Sun, G. (2016). Histone Acetylation and Its Modifiers in the Pathogenesis of Diabetic Nephropathy. In *Journal of Diabetes Research* (Vol. 2016). Hindawi Limited. https://doi.org/10.1155/2016/4065382

Liu, F., Xu, Y., Lu, X., Hamard, P. J., Karl, D. L., Man, N., Mookhtiar, A. K., Martinez, C., Lossos, I. S., Sun, J., & Nimer, S. D. (2020). PRMT5-mediated histone arginine methylation antagonizes transcriptional repression by polycomb complex PRC2. *Nucleic Acids Research*, *48*(6), 2956–2968. https://doi.org/10.1093/nar/gkaa065

Liu, N., & Zhu, B. (2017). Regulation of PRC2 Activity. In V. Pirrotta (Ed.), *Polycomb Group Proteins* (pp. 225–258). Elsevier Inc. https://www.sciencedirect.com/book/9780128097373/polycomb-group-proteins#book-info

Liu, X. G., Xu, H., Chen, M., Tan, X. Y., Chen, X. F., Yang, Y. G., Lin, M. Z., Liu, G. H., Liang, X. L., Qian, Y. Bin, Yuan, G. J., Chen, M. Q., Li, W. T., Miao, H. L., Li, M. Y., Liao, X. W., Dai, W., & Chen, N. P. (2020). Identify potential clinical significance of long noncoding RNA forkhead box P4 antisense RNA 1 in patients with early stage pancreatic ductal adenocarcinoma. *Cancer Medicine*, *9*(6), 2062–2076. https://doi.org/10.1002/cam4.2818

Liu, Y., Lai, Y. C., Hill, E. V., Tyteca, D., Carpentier, S., Ingvaldsen, A., Vertommen, D., Lantier, L., Foretz, M., Dequiedt, F., Courtoy, P. J., Erneux, C., Viollet, B., Shepherd, P. R., Tavare, J. M., Jensen, J., & Rider, M. H. (2013). Phosphatidylinositol 3-phosphate 5-kinase (PIKfyve) is an AMPK target participating in contraction-stimulated glucose uptake in skeletal muscle. *Biochemical Journal*, *455*(2), 195–206. https://doi.org/10.1042/BJ20130644

Livingstone, C., & Borai, A. (2014). Insulin-like growth factor-II: its role in metabolic and endocrine disease. *Clinical Endocrinology*, *80*(6), 773–781. https://doi.org/10.1111/cen.12446

Lloyd, J. T., & Glass, K. C. (2018). Biological function and histone recognition of family IV bromodomain-containing proteins. In *Journal of Cellular Physiology* (Vol. 233, Issue 3, pp. 1877–1886). Wiley-Liss Inc. https://doi.org/10.1002/jcp.26010

Lobera, M., Madauss, K. P., Pohlhaus, D. T., Wright, Q. G., Trocha, M., Schmidt, D. R., Baloglu, E., Trump, R. P., Head, M. S., Hofmann, G. A., Murray-Thompson, M., Schwartz, B., Chakravorty, S., Wu, Z., Mander, P. K., Kruidenier, L., Reid, R. A., Burkhart, W., Turunen, B. J., … Nolan, M. A. (2013). Selective class IIa histone deacetylase inhibition via a nonchelating zinc-binding group. *Nature Chemical Biology*, *9*(5), 319–325. https://doi.org/10.1038/nchembio.1223

Loftus, S. K., Baxter, L. L., Cronin, J. C., Fufa, T. D., Pavan, W. J., Barnabas, B. B., Bouffard, G. G., Brooks, S. Y., Coleman, H., Dekhtyar, L., Guan, X., Han, J., Ho, S. L., Legaspi, R., Maduro, Q. L., Masiello, C. A., McDowell, J. C., Montemayor, C., Mullikin, J. C., … Young, A. C. (2017). Hypoxia-induced HIF1α targets in melanocytes reveal a molecular profile associated with poor melanoma prognosis. *Pigment Cell and Melanoma Research*, *30*(3), 339–352. https://doi.org/10.1111/pcmr.12579

Losman, J.-A., Kaelin, W. G., & Jr. (2013). What a difference a hydroxyl makes: mutant IDH, (R)-2-hydroxyglutarate, and cancer. *Genes & Development*, *27*(8), 836–852. https://doi.org/10.1101/gad.217406.113

Lu, C., & Thompson, C. B. (2012). Metabolic regulation of epigenetics. *Cell Metabolism*, *16*(1), 9–17. https://doi.org/10.1016/j.cmet.2012.06.001

Lu, D., Ventura-Holman, T., Li, J., McMurray, R. W., Subauste, J. S., & Maher, J. F. (2005). Abnormal Glucose Homeostasis and Pancreatic Islet Function in Mice with Inactivation of the Fem1b Gene. *Molecular and Cellular Biology*, *25*(15), 6570–6577. https://doi.org/10.1128/mcb.25.15.6570-6577.2005

Lu, T. T. H., Heyne, S., Dror, E., Casas, E., Leonhardt, L., Boenke, T., Yang, C. H., Sagar, Arrigoni, L., Dalgaard, K., Teperino, R., Enders, L., Selvaraj, M., Ruf, M., Raja, S. J., Xie, H., Boenisch, U., Orkin, S. H., Lynn, F. C., … Pospisilik, J. A. (2018). The Polycomb-Dependent Epigenome Controls β Cell Dysfunction, Dedifferentiation, and Diabetes. *Cell Metabolism*, *27*(6), 1294-

1308.e7. https://doi.org/10.1016/j.cmet.2018.04.013

Lv, X., Han, Z., Chen, H., Yang, B., Yang, X., Xia, Y., Pan, C., Fu, L., Zhang, S., Han, H., Wu, M., Zhou, Z., Zhang, L., Li, L., Wei, G., & Zhao, Y. (2016). A positive role for polycomb in transcriptional regulation via H4K20me1. *Cell Research*, *26*(5), 529–542. https://doi.org/10.1038/cr.2016.33

Madhukar, N. S., Warmoes, M. O., & Locasale, J. W. (2015). Organization of enzyme concentration across the metabolic network in cancer cells. *PLoS ONE*, *10*(1). https://doi.org/10.1371/journal.pone.0117131

Maes, T., Mascaró, C., Rotllant, D., Cavalcanti, F., Carceller, E., Ortega, A., Molinero, C., & Buesa, C. (2016). ORY-2001: AN EPIGENETIC DRUG FOR THE TREATMENT OF COGNITION DEFECTS IN ALZHEIMER'S DISEASE AND OTHER NEURODEGENERATIVE DISORDERS. *Alzheimer's & Dementia*, *12*(7), P1192. https://doi.org/10.1016/j.jalz.2016.07.149

Maitituoheti, M., Keung, E. Z., Tang, M., Yan, L., Alam, H., Han, G., Singh, A. K., Raman, A. T., Terranova, C., Sarkar, S., Orouji, E., Amin, S. B., Sharma, S., Williams, M., Samant, N. S., Dhamdhere, M., Zheng, N., Shah, T., Shah, A., … Rai, K. (2020). Enhancer Reprogramming Confers Dependence on Glycolysis and IGF Signaling in KMT2D Mutant Melanoma. *Cell Reports*, *33*(3), 108293. https://doi.org/10.1016/j.celrep.2020.108293

Marino, A., Menghini, R., Fabrizi, M., Casagrande, V., Mavilio, M., Stoehr, R., Candi, E., Mauriello, A., Moreno-Navarrete, J. M., Gómez-Serrano, M., Peral, B., Melino, G., Lauro, R., Fernandez Real, J. M., & Federici, M. (2014). ITCH Deficiency Protects From Diet-Induced Obesity. *Diabetes*, *63*, 550–561. https://doi.org/10.2337/db13-0802

Martínez-Redondo, P., & Vaquero, A. (2013). The Diversity of Histone Versus Nonhistone Sirtuin Substrates. In *Genes and Cancer* (Vol. 4, Issues 3–4, pp. 148–163). Impact Journals, LLC. https://doi.org/10.1177/1947601913483767

Masuyama, H., & Hiramatsu, Y. (2012). Effects of a high-fat diet exposure in utero on the metabolic syndrome-like phenomenon in mouse offspring through epigenetic changes in adipocytokine gene expression. *Endocrinology*, *153*(6), 2823–2830. https://doi.org/10.1210/en.2011-2161

Mau, T., & Yung, R. (2014). Potential of epigenetic therapies in non-cancerous conditions. *Frontiers in Genetics*, *5*, 438. https://doi.org/10.3389/fgene.2014.00438

Mehedint, M. G., Niculescu, M. D., Craciunescu, C. N., & Zeisel, S. H. (2010). Choline deficiency alters global histone methylation and epigenetic marking at the Rel site of the calbindin 1 gene. *The FASEB Journal*, *24*(1), 184–195. https://doi.org/10.1096/fj.09-140145

Mehrmohamadi, M., Mentch, L. K., Clark, A. G., & Locasale, J. W. (2016). Integrative modelling of tumour DNA methylation quantifies the contribution of metabolism. *Nature Communications*, *7*, 13666. https://doi.org/10.1038/ncomms13666

Meighan-Mantha, R. (2017). *Epigenetic Drugs in Oncology: Current Clinical Landscape and Emerging Trends*.

Metallo, C. M., & Vander Heiden, M. G. (2013). Understanding Metabolic Regulation and Its Influence on Cell Physiology. In *Molecular Cell* (Vol. 49, Issue 3, pp. 388–398). NIH Public Access. https://doi.org/10.1016/j.molcel.2013.01.018

Mokbel, N., Hoffman, N. J., Girgis, C. M., Small, L., Turner, N., Daly, R. J., Cooney, G. J., & Holt, L. J. (2014). Grb10 Deletion Enhances Muscle Cell Proliferation, Differentiation and GLUT4 Plasma Membrane Translocation. *Journal of Cellular Physiology*, *229*(11), 1753–1764. https://doi.org/10.1002/jcp.24628

Mora-García, G., Ruiz-Díaz, M. S., Espitia-Almeida, F., & Gómez-Camargo, D. (2017). Variations in ADIPOR1 but not ADIPOR2 are associated with hypertriglyceridemia and diabetes in an admixed Latin American population. *Review of Diabetic Studies*, *14*(2–3), 311–328. https://doi.org/10.1900/RDS.2017.14.311

Moreira-silva, F., Camilo, V., Gaspar, V., Mano, J. F., Henrique, R., & Jerónimo, C. (2020). Repurposing old drugs into new epigenetic inhibitors: Promising candidates for cancer treatment? In *Pharmaceutics* (Vol. 12, Issue 5). MDPI AG. https://doi.org/10.3390/pharmaceutics12050410

Morey, L., Aloia, L., Cozzuto, L., Benitah, S. A., & Di Croce, L. (2013). RYBP and Cbx7 Define Specific Biological Functions of Polycomb Complexes in Mouse Embryonic Stem Cells. *Cell Reports*, *3*(1), 60–69. https://doi.org/10.1016/j.celrep.2012.11.026

Morris, C. J., Purvis, T. E., Mistretta, J., & Scheer, F. A. J. L. (2016). Effects of the Internal Circadian System and Circadian Misalignment on Glucose Tolerance in Chronic Shift Workers. *The Journal of Clinical Endocrinology and Metabolism*, *101*(3), 1066–1074. https://doi.org/10.1210/jc.2015-3924

Muller, B., Lewis, N., Adeniyi, T., Leese, H. J., Brison, D. R., & Sturmey, R. G. (2019). Application of extracellular flux analysis for determining mitochondrial function in mammalian oocytes and early embryos. *Scientific Reports*, *9*(1), 1–14. https://doi.org/10.1038/s41598-019-53066-9

Näär, A. M., Beaurang, P. A., Zhou, S., Abraham, S., Solomon, W., & Tjian, R. (1999). Composite co-activator ARC mediates chromatin-directed transcriptional activation. *Nature*, *398*(6730), 828–832. https://doi.org/10.1038/19789

Nauta, T. D., van den Broek, M., Gibbs, S., van der Pouw-Kraan, T. C. T. M., Oudejans, C. B., van Hinsbergh, V. W. M., & Koolwijk, P. (2017). Identification of HIF-2α-regulated genes that play a role in human microvascular endothelial sprouting during prolonged hypoxia in vitro. *Angiogenesis*, *20*(1), 39–54. https://doi.org/10.1007/s10456-016-9527-4

Neul, J. L., Skinner, S. A., Annese, F., Lane, J., Heydemann, P., Jones, M., Kaufmann, W. E., Glaze, D. G., & Percy, A. K. (2020). Metabolic Signatures Differentiate Rett Syndrome From Unaffected Siblings. *Frontiers in Integrative Neuroscience*, *14*(February), 1–10. https://doi.org/10.3389/fnint.2020.00007

Nguyen, T. T. T., Zhang, Y., Shang, E., Shu, C., Torrini, C., Zhao, J., Bianchetti, E., Mela, A., Humala, N., Mahajan, A., Harmanci, A. O., Lei, Z., Maienschein-Cline, M., Quinzii, C. M., Westhoff, M. A., Karpel-Massler, G., Bruce, J. N., Canoll, P., & Siegelin, M. D. (2020). HDAC inhibitors elicit metabolic reprogramming by targeting super-enhancers in glioblastoma models. *Journal of Clinical Investigation*, *130*(7), 3699–3716. https://doi.org/10.1172/JCI129049

Nicholas, D. A., Proctor, E. A., Agrawal, M., Belkina, A. C., Van Nostrand, S. C., Panneerseelan-Bharath, L., Jones, A. R., Raval, F., Ip, B. C., Zhu, M., Cacicedo, J. M., Habib, C., Sainz-Rueda, N., Persky, L., Sullivan, P. G., Corkey, B. E., Apovian, C. M., Kern, P. A., Lauffenburger, D. A., & Nikolajczyk, B. S. (2019). Fatty Acid Metabolites Combine with Reduced β Oxidation to Activate Th17 Inflammation in Human Type 2 Diabetes. *Cell Metabolism*, *30*(3), 447-461.e5. https://doi.org/10.1016/j.cmet.2019.07.004

Nicholas, L. M., Rattanatray, L., MacLaughlin, S. M., Ozanne, S. E., Kleemann, D. O., Walker, S. K., Morrison, J. L., Zhang, S., Muhlhausler, B. S., Martin-Gronert, M. S., & McMillen, I. C. (2013). Differential effects of maternal obesity and weight loss in the periconceptional period on the epigenetic regulation of hepatic insulin-signaling pathways in the offspring. *The FASEB Journal*, *27*(9), 3786–3796. https://doi.org/10.1096/fj.13-227918

Nicklin, P., Bergman, P., Zhang, B., Triantafellow, E., Wang, H., Nyfeler, B., Yang, H., Hild, M., Kung, C., Wilson, C., Myer, V. E., MacKeigan, J. P., Porter, J. A., Wang, Y. K., Cantley, L. C., Finan, P. M., & Murphy, L. O. (2009). Bidirectional Transport of Amino Acids Regulates mTOR and Autophagy. *Cell*, *136*(3), 521–534. https://doi.org/10.1016/j.cell.2008.11.044

Nicolaou, K. C. (2014). Advancing the Drug Discovery and Development Process. *Angewandte Chemie*, *126*(35), 9280–9292. https://doi.org/10.1002/ange.201404761

NIH. (2016). *What Is Metabolic Syndrome?* What Is Metabolic Syndrome? https://www.nhlbi.nih.gov/health/health-topics/topics/ms

Nikolaou, K. C., Moulos, P., Harokopos, V., Chalepakis, G., & Talianidis, I. (2017). Kmt5a Controls

Hepatic Metabolic Pathways by Facilitating RNA Pol II Release from Promoter-Proximal Regions. *Cell Reports*, *20*(4), 909–922. https://doi.org/10.1016/j.celrep.2017.07.003

Ninova, M., Tóth, K. F., & Aravin, A. A. (2019). The control of gene expression and cell identity by H3K9 trimethylation. *Development (Cambridge)*, *146*(19). https://doi.org/10.1242/dev.181180

Nogueiras, R., Habegger, K. M., Chaudhary, N., Finan, B., Banks, A. S., Dietrich, M. O., Horvath, T. L., Sinclair, D. A., Pfluger, P. T., & Tschöp, M. H. (2012). Sirtuin 1 and sirtuin 3: Physiological modulators of metabolism. *Physiological Reviews*, *92*(3), 1479–1514. https://doi.org/10.1152/physrev.00022.2011

Nouws, J., Te brinke, H., Nijtmans, L. G., & Houten, S. M. (2014). ACAD9, a complex i assembly factor with a moonlighting function in fatty acid oxidation deficiencies. *Human Molecular Genetics*, *23*(5), 1311–1319. https://doi.org/10.1093/hmg/ddt521

Nunn, A. D. G., Scopigno, T., Pediconi, N., Levrero, M., Hagman, H., Kiskis, J., Enejder, A., Allfrey, V. G., Faulkner, R., Mirsky, A. E., Kuo, M. H., Allis, C. D., Riester, D., Hildmann, C., Schwienhorst, A., Oiso, H., Sun, Z., Cantley, J. L., Guguen-Guillouzo, C., … Unser, M. (2016). The histone deacetylase inhibiting drug Entinostat induces lipid accumulation in differentiated HepaRG cells. *Scientific Reports*, *6*, 28025. https://doi.org/10.1038/srep28025

OECD. (2017). *Policy insights*. www.oecd.org/health/obesity-update.htm

Okamoto, K., Tanaka, Y., & Tsuneoka, M. (2017). SF-KDM2A binds to ribosomal RNA gene promoter, reduces H4K20me3 level, and elevates ribosomal RNA transcription in breast cancer cells. *International Journal of Oncology*, *50*(4), 1372–1382. https://doi.org/10.3892/ijo.2017.3908

Olie, C. S., Riaz, M., Konietzny, R., Charles, P. D., Pinto-Fernandez, A., Kiełbasa, S. M., Aartsma-Rus, A., Goeman, J. J., Kessler, B. M., & Raz, V. (2019). Deacetylation Inhibition Reverses PABPN1-Dependent Muscle Wasting. *IScience*, *12*, 318–332. https://doi.org/10.1016/j.isci.2019.01.024

Omori, E., Inagaki, M., Mishina, Y., Matsumoto, K., & Ninomiya-Tsuji, J. (2012). Epithelial transforming growth factor β-activated kinase 1 (TAK1) is activated through two independent mechanisms and regulates reactive oxygen species. *Proceedings of the National Academy of Sciences of the United States of America*, *109*(9), 3365–3370. https://doi.org/10.1073/pnas.1116188109

Pang, B., Zheng, X. R., Tian, J. xia, Gao, T. hong, Gu, G. yan, Zhang, R., Fu, Y. B., Pang, Q., Li, X. G., & Liu, Q. (2016). EZH2 promotes metabolic reprogramming in glioblastomas through epigenetic repression of EAF2-HIF1α signaling. *Oncotarget*, *7*(29), 45134–45143. https://doi.org/10.18632/oncotarget.9761

Peleg, S., Feller, C., Forne, I., Schiller, E., Sévin, D. C., Schauer, T., Regnard, C., Straub, T., Prestel, M., Klima, C., Schmitt Nogueira, M., Becker, L., Klopstock, T., Sauer, U., Becker, P. B., Imhof, A., & Ladurner, A. G. (2016). Life span extension by targeting a link between metabolism and histone acetylation in *Drosophila*. *EMBO Reports*, *17*(3), 455–469. https://doi.org/10.15252/embr.201541132

Perfilyev, A., Dahlman, I., Gillberg, L., Rosqvist, F., Iggman, D., Volkov, P., Nilsson, E., Risérus, U., & Ling, C. (2017). Impact of polyunsaturated and saturated fat overfeeding on the DNA-methylation pattern in human adipose tissue: a randomized controlled trial. *The American Journal of Clinical Nutrition*, *105*(4), 991–1000. https://doi.org/10.3945/ajcn.116.143164

Phillips, C. M. (2016). Metabolically Healthy Obesity: Personalised and Public Health Implications. *Trends in Endocrinology & Metabolism*, *27*(4), 189–191. https://doi.org/10.1016/j.tem.2016.02.001

Pietrocola, F., Galluzzi, L., Bravo-San Pedro, J. M., Madeo, F., & Kroemer, G. (2015). Acetyl coenzyme A: a central metabolite and second messenger. *Cell Metabolism*, *21*(6), 805–821. https://doi.org/10.1016/j.cmet.2015.05.014

Prickett, A. R., Ishida, M., Böhm, S., Frost, J. M., Puszyk, W., Abu-Amero, S., Stanier, P., Schulz, R., Moore, G. E., & Oakey, R. J. (2015). Genome-wide methylation analysis in Silver-Russell syndrome patients. *Human Genetics*, *134*(3), 317–332. https://doi.org/10.1007/s00439-014-1526-1

Qi, Y., Wang, D., Wang, D., Jin, T., Yang, L., Wu, H., Li, Y., Zhao, J., Du, F., Song, M., & Wang, R. (2016). HEDD: the human epigenetic drug database. *Database : The Journal of Biological Databases and Curation*, *2016*. https://doi.org/10.1093/database/baw159

Qian, D. Z., Kachhap, S. K., Collis, S. J., Verheul, H. M. W., Carducci, M. A., Atadja, P., & Pili, R. (2006). Class II histone deacetylases are associated with VHL-independent regulation of hypoxia-inducible factor 1α. *Cancer Research*, *66*(17), 8814–8821. https://doi.org/10.1158/0008-5472.CAN-05-4598

Rando, O. J., & Simmons, R. A. (2015). I'm eating for two: Parental dietary effects on offspring metabolism. *Cell*, *161*(1), 93–105. https://doi.org/10.1016/j.cell.2015.02.021

Rao, R. C., & Dou, Y. (2015). Hijacked in cancer: the KMT2 (MLL) family of methyltransferases. *Nature Reviews. Cancer*, *15*(6), 334–346. https://doi.org/10.1038/nrc3929

Raynal, N. J.-M., Da Costa, E. M., Lee, J. T., Gharibyan, V., Ahmed, S., Zhang, H., Sato, T., Malouf, G. G., & Issa, J.-P. J. (2017). Repositioning FDA-Approved Drugs in Combination with Epigenetic Drugs to Reprogram Colon Cancer Epigenome. *Molecular Cancer Therapeutics*, *16*(2), 397–407. https://doi.org/10.1158/1535-7163.MCT-16-0588

Rea, S., Eisenhaber, F., O'Carroll, D., Strahl, B. D., Sun, Z.-W., Schmid, M., Opravil, S., Mechtler, K., Ponting, C. P., Allis, C. D., & Jenuwein, T. (2000). Regulation of chromatin structure by site-specific histone H3 methyltransferases. *Nature*, *406*(6796), 593–599. https://doi.org/10.1038/35020506

Redis, R. S., Vela, L. E., Lu, W., Ferreira de Oliveira, J., Ivan, C., Rodriguez-Aguayo, C., Adamoski, D., Pasculli, B., Taguchi, A., Chen, Y., Fernandez, A. F., Valledor, L., Van Roosbroeck, K., Chang, S., Shah, M., Kinnebrew, G., Han, L., Atlasi, Y., Cheung, L. H., … Calin, G. A. (2016). Allele-Specific Reprogramming of Cancer Metabolism by the Long Non-coding RNA CCAT2. *Molecular Cell*, *61*(4), 520–534. https://doi.org/10.1016/j.molcel.2016.01.015

Reid, M. A., Dai, Z., & Locasale, J. W. (2017). The impact of cellular metabolism on chromatin dynamics and epigenetics. In *Nature Cell Biology* (Vol. 19, Issue 11, pp. 1298–1306). Nature Publishing Group. https://doi.org/10.1038/ncb3629

Reid, M. A., Lowman, X. H., Pan, M., Tran, T. Q., Warmoes, M. O., Ishak Gabra, M. B., Yang, Y., Locasale, J. W., & Kong, M. (2016). IKKβ promotes metabolic adaptation to glutamine deprivation via phosphorylation and inhibition of PFKFB3. *Genes and Development*, *30*(16), 1837–1851. https://doi.org/10.1101/gad.287235.116

Riising, E. M., & Helin, K. (2012). A New Role for the Polycomb Group Protein Ezh1 in Promoting Transcription. *Molecular Cell*, *45*(2), 145–146. https://doi.org/10.1016/j.molcel.2012.01.003

Roe, J.-S., Hwang, C.-I., Somerville, T. D. D., Milazzo, J. P., Lee, E. J., Da Silva, B., Maiorino, L., Tiriac, H., Young, C. M., Miyabayashi, K., Filippini, D., Creighton, B., Burkhart, R. A., Buscaglia, J. M., Kim, E. J., Grem, J. L., Lazenby, A. J., Grunkemeyer, J. A., Hollingsworth, M. A., … Vakoc, C. R. (2017). Enhancer Reprogramming Promotes Pancreatic Cancer Metastasis. *Cell*, *170*(5), 875-888.e20. https://doi.org/10.1016/j.cell.2017.07.007

Russell, S., Wojtkowiak, J., Neilson, A., & Gillies, R. J. (2017). Metabolic Profiling of healthy and cancerous tissues in 2D and 3D. *Scientific Reports*, *7*(1), 15285. https://doi.org/10.1038/s41598-017-15325-5

Sallam, T., Jones, M. C., Gilliland, T., Zhang, L., Wu, X., Eskin, A., Sandhu, J., Casero, D., Vallim, T. Q. D. A., Hong, C., Katz, M., Lee, R., Whitelegge, J., & Tontonoz, P. (2016). Feedback modulation of cholesterol metabolism by the lipid-responsive non-coding RNA LeXis. *Nature*, *534*(7605), 124–128. https://doi.org/10.1038/nature17674

Salzberg, A. C., Harris-Becker, A., Popova, E. Y., Keasey, N., Loughran, T. P., Claxton, D. F., & Grigoryev, S. A. (2017). Genome-wide mapping of histone H3K9me2 in acute myeloid leukemia reveals large chromosomal domains associated with massive gene silencing and sites of genome instability. In *PLoS ONE* (Vol. 12, Issue 3). https://doi.org/10.1371/journal.pone.0173723

Sang, N., & Chen, S. (2011). Histone deacetylase inhibitors: The epigenetic therapeutics that repress hypoxia-inducible factors. *Journal of Biomedicine and Biotechnology*, *2011*. https://doi.org/10.1155/2011/197946

Scharping, N., & Delgoffe, G. (2016). Tumor Microenvironment Metabolism: A New Checkpoint for Anti-Tumor Immunity. *Vaccines*, *4*(4), 46. https://doi.org/10.3390/vaccines4040046

Schneider, A. C., Heukamp, L. C., Rogenhofer, S., Fechner, G., Bastian, P. J., Von Ruecker, A., Müller, S. C., & Ellinger, J. (2011). Global histone H4K20 trimethylation predicts cancer-specific survival in patients with muscle-invasive bladder cancer. *BJU International*, *108*(8 B), 290–296. https://doi.org/10.1111/j.1464-410X.2011.10203.x

Schoepflin, Z. R. (2016). Class I and IIa HDACs mediate HIF-1α stability through PHD2- dependent mechanism while HDAC6, a class IIb member, promotes HIF-1α transcriptional activity in nucleus pulposus cells of the intervertebral disc. *J Bone Miner Res*. https://doi.org/10.1002/jbmr.2787.Class

Schönherr, N., Meyer, E., Eggermann, K., Ranke, M. B., Wollmann, H. A., & Eggermann, T. (2006). (Epi)mutations in 11p15 significantly contribute to Silver–Russell syndrome: but are they generally involved in growth retardation? *European Journal of Medical Genetics*, *49*(5), 414–418. https://doi.org/10.1016/J.EJMG.2006.03.001

Scott, R. H., & Moore, G. E. (2012). Epigenetic Mechanisms of Human Imprinting Disorders. In *Epigenetics in Human Disease* (pp. 253–271). Elsevier. https://doi.org/10.1016/B978-0-12-388415-2.00013-5

Seki, Y., Williams, L., Vuguin, P. M., & Charron, M. J. (2012). Minireview: Epigenetic programming of diabetes and obesity: animal models. *Endocrinology*, *153*(3), 1031–1038. https://doi.org/10.1210/en.2011-1805

Sekine, H., Okazaki, K., Ota, N., Shima, H., Katoh, Y., Suzuki, N., Igarashi, K., & Ito, M. (2016). *into Antioxidant Gene Expression*. *36*(3), 407–420. https://doi.org/10.1128/MCB.00785-15.Address

Semenza, G. L. (2007). HIF-1 mediates the Warburg effect in clear cell renal carcinoma. In *Journal of Bioenergetics and Biomembranes* (Vol. 39, Issue 3, pp. 231–234). Springer. https://doi.org/10.1007/s10863-007-9081-2

Shen, L., Li, C., Wang, Z., Zhang, R., Shen, Y., Miles, T., Wei, J., & Zou, Z. (2019). Early-life exposure to severe famine is associated with higher methylation level in the IGF2 gene and higher total cholesterol in late adulthood: The Genomic Research of the Chinese Famine (GRECF) study. *Clinical Epigenetics*, *11*(1), 88. https://doi.org/10.1186/s13148-019-0676-3

Shi, H., Chai, P., Jia, R., & Fan, X. (2020). Novel insight into the regulatory roles of diverse RNA modifications: Re-defining the bridge between transcription and translation. In *Molecular Cancer* (Vol. 19, Issue 1, pp. 1–17). BioMed Central Ltd. https://doi.org/10.1186/s12943-020-01194-6

Sho Morioka1, 3, , Kazuhito Sai1, 2, Emily Omori1, Yuka Ikeda1, Kunihiro Matsumoto2, A., & Ninomiya-Tsuji1, J. (2016). TAK1 regulates hepatic lipid homeostasis through SREBP. *Oncogene*. https://doi.org/10.1038/onc.2015.453

Shogren-Knaak, M., Ishii, H., Sun, J. M., Pazin, M. J., Davie, J. R., & Peterson, C. L. (2006). Histone H4-K16 acetylation controls chromatin structure and protein interactions. *Science*, *311*(5762), 844–847. https://doi.org/10.1126/science.1124000

Soubry, A., Schildkraut, J. M., Murtha, A., Wang, F., Huang, Z., Bernal, A., Kurtzberg, J., Jirtle, R. L., Murphy, S. K., & Hoyo, C. (2013). Paternal obesity is associated with IGF2hypomethylation in newborns: results from a Newborn Epigenetics Study (NEST) cohort. *BMC Medicine*, *11*(1),

29. https://doi.org/10.1186/1741-7015-11-29

Sparago, A., Cerrato, F., Vernucci, M., Ferrero, G. B., Silengo, M. C., & Riccio, A. (2004). Microdeletions in the human H19 DMR result in loss of IGF2 imprinting and Beckwith-Wiedemann syndrome. *Nature Genetics*, *36*(9), 958–960. https://doi.org/10.1038/ng1410

Stein, E. M., Garcia-Manero, G., Rizzieri, D. A., Tibes, R., Berdeja, J. G., Savona, M. R., Jongen-Lavrenic, M., Altman, J. K., Thomson, B., Blakemore, S. J., Daigle, S. R., Waters, N. J., Suttle, A. B., Clawson, A., Pollock, R., Krivtsov, A., Armstrong, S. A., DiMartino, J., Hedrick, E., … Tallman, M. S. (2018). The DOT1L inhibitor pinometostat reduces H3K79 methylation and has modest clinical activity in adult acute leukemia. *Blood*, *131*(24), 2662–2669. https://doi.org/10.1182/blood-2017-12-818948

Stöhr, R., Mavilio, M., Marino, A., Casagrande, V., Kappel, B., Möllmann, J., Menghini, R., Melino, G., & Federici, M. (2015). ITCH modulates SIRT6 and SREBP2 to influence lipid metabolism and atherosclerosis in ApoE null mice. *Scientific Reports*, *5*, 1–8. https://doi.org/10.1038/srep09023

Stojic, L., Jasencakova, Z., Prezioso, C., Stützer, A., Bodega, B., Pasini, D., Klingberg, R., Mozzetta, C., Margueron, R., Puri, P., Schwarzer, D., Helin, K., Fischle, W., & Orlando, V. (2011). Chromatin regulated interchange between polycomb repressive complex 2 (PRC2)-Ezh2 and PRC2-Ezh1 complexes controls myogenin activation in skeletal muscle cells. *Epigenetics and Chromatin*, *4*(1), 16. https://doi.org/10.1186/1756-8935-4-16

Su, L., Liang, D., Kuang, S.-Y., Dong, Q., Han, X., & Wang, Z. (2020). Neuroprotective mechanism of TMP269, a selective class IIA histone deacetylase inhibitor, after cerebral ischemia/reperfusion injury. *Neural Regeneration Research*, *15*(2), 277. https://doi.org/10.4103/1673-5374.265562

Suganuma, T., & Workman, J. L. (2018). Chromatin and Metabolism. In *Annual Review of Biochemistry* (Vol. 87, pp. 27–49). Annual Reviews Inc. https://doi.org/10.1146/annurev-biochem-062917-012634

Sumegi, B., & Srere, P. A. (1984). Complex I binds several mitochondrial NAD-coupled dehydrogenases. *Journal of Biological Chemistry*, *259*(24), 15040–15045.

Swain, P., Kam, Y., Caradonna, K., Rogers, G. W., & Dranka, B. P. (n.d.). *Rapid, Real-time Detection of T Cell Activation Using an Agilent Seahorse XFp Analyzer Application Note*. Retrieved May 23, 2017, from https://www.hemacare.com/wp-content/uploads/2015/12/T-cell-App-Note.pdf

Tallis, M., Morra, R., Barkauskaite, E., & Ahel, I. (2014). Poly(ADP-ribosyl)ation in regulation of chromatin structure and the DNA damage response. In *Chromosoma* (Vol. 123, Issues 1–2, pp. 79–90). Springer Science and Business Media Deutschland GmbH. https://doi.org/10.1007/s00412-013-0442-9

Tang, W., & Lu, A. Y. H. (2010). Metabolic bioactivation and drug-related adverse effects: Current status and future directions from a pharmaceutical research perspective. In *Drug Metabolism Reviews* (Vol. 42, Issue 2, pp. 225–249). Drug Metab Rev. https://doi.org/10.3109/03602530903401658

Taylor, W. A., Mejia, E. M., Mitchell, R. W., Choy, P. C., Sparagna, G. C., & Hatch, G. M. (2012). Human Trifunctional Protein Alpha Links Cardiolipin Remodeling to Beta-Oxidation. *PLoS ONE*, *7*(11), 1–12. https://doi.org/10.1371/journal.pone.0048628

Thomas, D. M., Weedermann, M., Fuemmeler, B. F., Martin, C. K., Dhurandhar, N. V., Bredlau, C., Heymsfield, S. B., Ravussin, E., & Bouchard, C. (2014). Dynamic model predicting overweight, obesity, and extreme obesity prevalence trends. *Obesity*, *22*(2), 590–597. https://doi.org/10.1002/oby.20520

Thompson, N. N. P. and C. B. (2016). Emerging metabolic hallmarks of cancer. *Cell Metabolism*. https://doi.org/10.1016/j.cmet.2015.12.006.

Tiganis, T. (2013). PTP1B and TCPTP - nonredundant phosphatases in insulin signaling and glucose homeostasis. *FEBS Journal*, *280*(2), 445–458. https://doi.org/10.1111/j.1742-4658.2012.08563.x

Tobi, E. W., Goeman, J. J., Monajemi, R., Gu, H., Putter, H., Zhang, Y., Slieker, R. C., Stok, A. P., Thijssen, P. E., Müller, F., van Zwet, E. W., Bock, C., Meissner, A., Lumey, L. H., Eline Slagboom, P., & Heijmans, B. T. (2015). Corrigendum: DNA methylation signatures link prenatal famine exposure to growth and metabolism. *Nature Communications*, *6*, 7740. https://doi.org/10.1038/ncomms8740

Toth, J. I., Datta, S., Athanikar, J. N., Freedman, L. P., & Osborne, T. F. (2004). Selective Coactivator Interactions in Gene Activation by SREBP-1a and -1c. *Molecular and Cellular Biology*, *24*(18), 8288–8300. https://doi.org/10.1128/mcb.24.18.8288-8300.2004

Tran Mau-Them, F., Guibaud, L., Duplomb, L., Keren, B., Lindstrom, K., Marey, I., Mochel, F., van den Boogaard, M. J., Oegema, R., Nava, C., Masurel, A., Jouan, T., Jansen, F. E., Au, M., Chen, A. H., Cho, M., Duffourd, Y., Lozier, E., Konovalov, F., … Vitobello, A. (2019). De novo truncating variants in the intronless IRF2BPL are responsible for developmental epileptic encephalopathy. *Genetics in Medicine*, *21*(4), 1008–1014. https://doi.org/10.1038/s41436-018-0143-0

Trollet, C., Anvar, S. Y., Venema, A., Hargreaves, I. P., Foster, K., Vignaud, A., Ferry, A., Negroni, E., Hourde, C., Baraibar, M. A., 't Hoen, P. A. C., Davies, J. E., Rubinsztein, D. C., Heales, S. J., Mouly, V., van der Maarel, S. M., Butler-Browne, G., Raz, V., & Dickson, G. (2010). Molecular and phenotypic characterization of a mouse model of oculopharyngeal muscular dystrophy reveals severe muscular atrophy restricted to fast glycolytic fibres. *Human Molecular Genetics*, *19*(11), 2191–2207. https://doi.org/10.1093/hmg/ddq098

Tsuda, H., & Komatsu, S. (2010). Gene Section Mini Review Atlas of Genetics and Cytogenetics in Oncology and Haematology SMYD2 (SET and MYND domain containing 2) Identity DNA/RNA. *Atlas Genet Cytogenet Oncol Haematol*, *14*(10). https://doi.org/10.4267/2042/46056

Tuorkey, M. J. (2016). Molecular targets of luteolin in cancer. *European Journal of Cancer Prevention*, *25*(1), 65–76. https://doi.org/10.1097/CEJ.0000000000000128

Tyanova, S., Temu, T., Carlson, A., Sinitcyn, P., Mann, M., & Cox, J. (2015). Visualization of LC-MS/MS proteomics data in MaxQuant. *Proteomics*, *15*(8), 1453–1456. https://doi.org/10.1002/pmic.201400449

Tyni, T., Palotie, A., Viinikka, L., Valanne, L., Salo, M. K., Von Dobeln, U., Jackson, S., Wanders, R., Venizelos, N., & Pihko, H. (1997). Long-chain 3-hydroxyacyl-coenzyme A dehydrogenase deficiency with the G1528C mutation: Clinical presentation of thirteen patients. *Journal of Pediatrics*, *130*(1), 67–76. https://doi.org/10.1016/S0022-3476(97)70312-3

U.Selker, E. T. W. and E. (2017). H3K27 methylation: a promiscuous repressive chromatin mark. *Curr Opin Genet Dev*. https://doi.org/10.1016/j.gde.2016.11.001.

Valverde, Á. M., & González-Rodríguez, Á. (2011). IRS2 and PTP1B: Two opposite modulators of hepatic insulin signalling. *Archives of Physiology and Biochemistry*, *117*(3), 105–115. https://doi.org/10.3109/13813455.2011.557386

Van Damme, M., Crompot, E., Meuleman, N., Maerevoet, M., Mineur, P., Bron, D., Lagneaux, L., & Stamatopoulos, B. (2016). Characterization of TET and IDH gene expression in chronic lymphocytic leukemia: comparison with normal B cells and prognostic significance. *Clinical Epigenetics*, *8*, 132. https://doi.org/10.1186/s13148-016-0298-y

van Dijk, S. J., Molloy, P. L., Varinli, H., Morrison, J. L., Muhlhausler, B. S., Buckley, M., Clark, S. J., McMillen, I. C., Noakes, M., Samaras, K., & Tellam, R. L. (2015). Epigenetics and human obesity. *International Journal of Obesity*. https://doi.org/10.1038/ijo.2014.34

Van Laarhoven, P. M., Neitzel, L. R., Quintana, A. M., Geiger, E. A., Zackai, E. H., Clouthier, D. E., Artinger, K. B., Ming, J. E., & Shaikh, T. H. (2015). Kabuki syndrome genes KMT2D and KDM6A: functional analyses demonstrate critical roles in craniofacial, heart and brain

development. *Human Molecular Genetics*, *24*(15), 4443–4453. https://doi.org/10.1093/hmg/ddv180

Vander Heiden, M. G., & DeBerardinis, R. J. (2017). Understanding the Intersections between Metabolism and Cancer Biology. *Cell*, *168*(4), 657–669. https://doi.org/10.1016/j.cell.2016.12.039

Verdin, E., Dequiedt, F., & Kasler, H. G. (2003). Class II histone deacetylases: Versatile regulators. In *Trends in Genetics* (Vol. 19, Issue 5, pp. 286–293). Elsevier Ltd. https://doi.org/10.1016/S0168-9525(03)00073-8

Wakeling, E. L., Brioude, F., Lokulo-Sodipe, O., O'Connell, S. M., Salem, J., Bliek, J., Canton, A. P. M., Chrzanowska, K. H., Davies, J. H., Dias, R. P., Dubern, B., Elbracht, M., Giabicani, E., Grimberg, A., Grønskov, K., Hokken-Koelega, A. C. S., Jorge, A. A., Kagami, M., Linglart, A., … Netchine, I. (2017). Diagnosis and management of Silver–Russell syndrome: first international consensus statement. *Nature Reviews Endocrinology*, *13*(2), 105–124. https://doi.org/10.1038/nrendo.2016.138

Wang, G., Balamotis, M. A., Stevens, J. L., Yamaguchi, Y., Handa, H., & Berk, A. J. (2005). Mediator requirement for both recruitment and postrecruitment steps in transcription initiation. *Molecular Cell*, *17*(5), 683–694. https://doi.org/10.1016/j.molcel.2005.02.010

Wang, H., Zhang, H., Deng, P., Liu, C., Li, D., Jie, H., Zhang, H., Zhou, Z., & Zhao, Y.-L. (2016). Tissue metabolic profiling of human gastric cancer assessed by (1)H NMR. *BMC Cancer*, *16*, 371. https://doi.org/10.1186/s12885-016-2356-4

Wang, W., Huang, L., Huang, Y., Yin, J. wen, Berk, A. J., Friedman, J. M., & Wang, G. (2009). Mediator MED23 Links Insulin Signaling to the Adipogenesis Transcription Cascade. *Developmental Cell*, *16*(5), 764–771. https://doi.org/10.1016/j.devcel.2009.04.006

Wang, Y., Beydoun, M. A., Liang, L., Caballero, B., & Kumanyika, S. K. (2008). Will all Americans become overweight or obese? Estimating the progression and cost of the US obesity epidemic. *Obesity*, *16*(10), 2323–2330. https://doi.org/10.1038/oby.2008.351

Wang, Zhen, Long, Q. Y., Chen, L., Fan, J. D., Wang, Z. N., Li, L. Y., Wu, M., & Chen, X. (2017a). Inhibition of H3K4 demethylation induces autophagy in cancer cell lines. *Biochimica et Biophysica Acta - Molecular Cell Research*, *1864*(12), 2428–2437. https://doi.org/10.1016/j.bbamcr.2017.08.005

Wang, Zhen, Long, Q. Y., Chen, L., Fan, J. D., Wang, Z. N., Li, L. Y., Wu, M., & Chen, X. (2017b). Inhibition of H3K4 demethylation induces autophagy in cancer cell lines. *Biochimica et Biophysica Acta - Molecular Cell Research*, *1864*(12), 2428–2437. https://doi.org/10.1016/j.bbamcr.2017.08.005

Wang, Zhibin, Zang, C., Rosenfeld, J. A., Schones, D. E., Barski, A., Cuddapah, S., Cui, K., Roh, T. Y., Peng, W., Zhang, M. Q., & Zhao, K. (2008). Combinatorial patterns of histone acetylations and methylations in the human genome. *Nature Genetics*, *40*(7), 897–903. https://doi.org/10.1038/ng.154

Wapenaar, H., & Dekker, F. J. (2016). Histone acetyltransferases: challenges in targeting bi-substrate enzymes. *Clinical Epigenetics*, *8*(1), 59. https://doi.org/10.1186/s13148-016-0225-2

Warburg, O., Wind, F., & Negelein, E. (1927). THE METABOLISM OF TUMORS IN THE BODY. *The Journal of General Physiology*, *8*(6), 519–530. http://www.ncbi.nlm.nih.gov/pubmed/19872213

Wardell, S. E., Ilkayeva, O. R., Wieman, H. L., Frigo, D. E., Rathmell, J. C., Newgard, C. B., & McDonnell, D. P. (2009). Glucose metabolism as a target of histone deacetylase inhibitors. *Molecular Endocrinology*, *23*(3), 388–401. https://doi.org/10.1210/me.2008-0179

Wasko, M. J., Pellegrene, K. A., Madura, J. D., & Surratt, C. K. (2015). A role for fragment-based drug design in developing novel lead compounds for central nervous system targets. In *Frontiers*

in Neurology (Vol. 6, Issue SEP, p. 197). Frontiers Media S.A. https://doi.org/10.3389/fneur.2015.00197

Weipeng Mu, Joshua Starmer, Yoichiro Shibata, Della Yee, and T. M. (2017). EZH1 in Germ Cells Safeguards the Function of PRC2 during Spermatogenesis. *Developmental Biology*. https://doi.org/10.1016/j.ydbio.2017.02.017.EZH1

Wesche, J., Kühn, S., Kessler, B. M., Salton, M., & Wolf, A. (2017). Protein arginine methylation: a prominent modification and its demethylation. In *Cellular and Molecular Life Sciences* (Vol. 74, Issue 18, pp. 3305–3315). Birkhauser Verlag AG. https://doi.org/10.1007/s00018-017-2515-z

WHO. (2014). Prevention and Control of Noncommunicable diseases in the European Region: a progress report. *World Health Organization Regional Officer for Europe*, 62.

WHO. (2018). *No Title*. Fact Sheets. https://www.who.int/data/gho/data/themes/noncommunicable-diseases

WHO. (2019). *The top 10 causes of death*. Fact Sheets. https://www.who.int/news-room/fact-sheets/detail/the-top-10-causes-of-death

Wilcox, C. S. (1999). Metabolic and adverse effects of diuretics. *Semin Nephrol*. https://pubmed.ncbi.nlm.nih.gov/10598543/

Williams, R., Karuranga, S., Malanda, B., Saeedi, P., Basit, A., Besançon, S., Bommer, C., Esteghamati, A., Ogurtsova, K., Zhang, P., & Colagiuri, S. (2020). Global and regional estimates and projections of diabetes-related health expenditure: Results from the International Diabetes Federation Diabetes Atlas, 9th edition. *Diabetes Research and Clinical Practice*, *162*. https://doi.org/10.1016/j.diabres.2020.108072

Wilson, D. F. (2017). Oxidative phosphorylation: regulation and role in cellular and tissue metabolism. *Journal of Physiology*, *595*(23), 7023–7038. https://doi.org/10.1113/JP273839

Wilson, S., Fan, L., Sahgal, N., Qi, J., & Filipp, F. V. (2017). The histone demethylase KDM3A regulates the transcriptional program of the androgen receptor in prostate cancer cells. *Oncotarget*, *8*(18), 30328–30343. https://doi.org/10.18632/oncotarget.15681

Wilson, S., Qi, J., & Filipp, F. V. (2016). Refinement of the androgen response element based on ChIP-Seq in androgen-insensitive and androgen-responsive prostate cancer cell lines. *Scientific Reports*, *6*, 32611. https://doi.org/10.1038/srep32611

Wolfinbarger, L. (2017). Enzyme Regulation in Metabolic Pathways. In *Enzyme Regulation in Metabolic Pathways*. John Wiley & Sons, Inc. https://doi.org/10.1002/9781119155423

Wood, K., Tellier, M., & Murphy, S. (2018). DOT1L and H3K79 methylation in transcription and genomic stability. In *Biomolecules* (Vol. 8, Issue 1). MDPI AG. https://doi.org/10.3390/biom8010011

Wu, S. P., Kao, C. Y., Wang, L., Creighton, C. J., Yang, J., Donti, T. R., Harmancey, R., Vasquez, H. G., Graham, B. H., Bellen, H. J., Taegtmeyer, H., Chang, C. P., Tsai, M. J., & Tsai, S. Y. (2015). Increased COUP-TFII expression in adult hearts induces mitochondrial dysfunction resulting in heart failure. *Nature Communications*, *6*. https://doi.org/10.1038/ncomms9245

Xia, L., Sun, J., Xie, S., Chi, C., Zhu, Y., Pan, J., Dong, B., Huang, Y., Xia, W., Sha, J., & Xue, W. (2020). PRKAR2B-HIF-1α loop promotes aerobic glycolysis and tumour growth in prostate cancer. *Cell Proliferation*. https://doi.org/10.1111/cpr.12918

Xia, O., Lemieux, M. E., Li, W., Carroll, J. S., Brown, M., Shirley Liu, X., & Kung, A. L. (2009a). Integrative analysis of HIF binding and transactivation reveals its role in maintaining histone methylation homeostasis. *Proceedings of the National Academy of Sciences of the United States of America*, *106*(11), 4260–4265. https://doi.org/10.1073/pnas.0810067106

Xia, O., Lemieux, M. E., Li, W., Carroll, J. S., Brown, M., Shirley Liu, X., & Kung, A. L. (2009b). Integrative analysis of HIF binding and transactivation reveals its role in maintaining histone

methylation homeostasis. *Proceedings of the National Academy of Sciences of the United States of America*, *106*(11), 4260–4265. https://doi.org/10.1073/pnas.0810067106

Xiao, L., Zhao, Z., He, F., & Du, Z. (2019). Multivariable regulation of gene expression plasticity in metazoans. *BioRxiv*. https://doi.org/10.1101/692863

Xiao, M., Yang, H., Xu, W., Ma, S., Lin, H., Zhu, H., Liu, L., Liu, Y., Yang, C., Xu, Y., Zhao, S., Ye, D., Xiong, Y., & Guan, K.-L. (2012). Inhibition of α-KG-dependent histone and DNA demethylases by fumarate and succinate that are accumulated in mutations of FH and SDH tumor suppressors. *Genes & Development*, *26*(12), 1326–1338. https://doi.org/10.1101/gad.191056.112

Xiong, Y., & Guan, K. L. (2012). Mechanistic insights into the regulation of metabolic enzymes by acetylation. *Journal of Cell Biology*, *198*(2), 155–164. https://doi.org/10.1083/jcb.201202056

Xu, J., & Kidder, B. L. (2018). H4K20me3 co-localizes with activating histone modifications at transcriptionally dynamic regions in embryonic stem cells. *BMC Genomics*, *19*(1), 1–15. https://doi.org/10.1186/s12864-018-4886-4

Yadav, R. K., Chauhan, A. S., Zhuang, L., & Gan, B. (2018). FoxO transcription factors in cancer metabolism. In *Seminars in Cancer Biology* (Vol. 50, pp. 65–76). Academic Press. https://doi.org/10.1016/j.semcancer.2018.01.004

Yang, F., Vought, B. W., Satterlee, J. S., Walker, A. K., Jim Sun, Z. Y., Watts, J. L., DeBeaumont, R., Mako Saito, R., Hyberts, S. G., Yang, S., Macol, C., Iyer, L., Tjian, R., Van Den Heuvel, S., Hart, A. C., Wagner, G., & Näär, A. M. (2006). An ARC/Mediator subunit required for SREBP control of cholesterol and lipid homeostasis. *Nature*, *442*(7103), 700–704. https://doi.org/10.1038/nature04942

Yang, J., Jin, X., Yan, Y., Shao, Y., Pan, Y., Roberts, L. R., Zhang, J., Huang, H., & Jiang, J. (2017). Inhibiting histone deacetylases suppresses glucose metabolism and hepatocellular carcinoma growth by restoring FBP1 expression. *Scientific Reports*, *7*(1), 1–13. https://doi.org/10.1038/srep43864

Yao, C.-H., Liu, G.-Y., Wang, R., Moon, S. H., Gross, R. W., & Patti, G. J. (2018). Identifying off-target effects of etomoxir reveals that carnitine palmitoyltransferase I is essential for cancer cell proliferation independent of β-oxidation. *PLOS Biology*, *16*(3), e2003782. https://doi.org/10.1371/journal.pbio.2003782

Yao, W., King, D. A., Beckwith, S. L., Gowans, G. J., Yen, K., Zhou, C., & Morrison, A. J. (2016). The INO80 Complex Requires the Arp5-Ies6 Subcomplex for Chromatin Remodeling and Metabolic Regulation. *Molecular and Cellular Biology*, *36*(6), 979–991. https://doi.org/10.1128/mcb.00801-15

Yu, J., & Auwerx, J. (2009). The role of sirtuins in the control of metabolic homeostasis. In *Annals of the New York Academy of Sciences* (Vol. 1173, Issue SUPPL. 1, p. E10). Blackwell Publishing Inc. https://doi.org/10.1111/j.1749-6632.2009.04952.x

Yu, L., Lu, M., Jia, D., Ma, J., Ben-Jacob, E., Levine, H., Kaipparettu, B. A., & Onuchic, J. N. (2017). Modeling the genetic regulation of cancer metabolism: Interplay between glycolysis and oxidative phosphorylation. *Cancer Research*, *77*(7), 1564–1574. https://doi.org/10.1158/0008-5472.CAN-16-2074

Yuan, W., Xu, M., Huang, C., Liu, N., Chen, S., & Zhu, B. (2011). H3K36 methylation antagonizes PRC2-mediated H3K27 methylation. *Journal of Biological Chemistry*, *286*(10), 7983–7989. https://doi.org/10.1074/jbc.M110.194027

Yuneva, M. O., Fan, T. W. M., Allen, T. D., Higashi, R. M., Ferraris, D. V, Tsukamoto, T., Matés, J. M., Alonso, F. J., Wang, C., Seo, Y., Chen, X., & Bishop, J. M. (2012). The metabolic profile of tumors depends on both the responsible genetic lesion and tissue type. *Cell Metabolism*, *15*(2), 157–170. https://doi.org/10.1016/j.cmet.2011.12.015

Zaidi, S., Choi, M., Wakimoto, H., Ma, L., Jiang, J., Overton, J. D., Romano-Adesman, A., Bjornson,

R. D., Breitbart, R. E., Brown, K. K., Carriero, N. J., Cheung, Y. H., Deanfield, J., DePalma, S., Fakhro, K. A., Glessner, J., Hakonarson, H., Italia, M. J., Kaltman, J. R., … Lifton, R. P. (2013). De novo mutations in histone-modifying genes in congenital heart disease. *Nature*, *498*(7453), 220–223. https://doi.org/10.1038/nature12141

Zeevi, D., Korem, T., Zmora, N., Halpern, Z., Elinav, E., & Correspondence, E. S. (2015). Personalized Nutrition by Prediction of Glycemic Responses. *Cell*, *163*, 1079–1094. https://doi.org/10.1016/j.cell.2015.11.001

Zhang, C., Gao, S., Molascon, A. J., Liu, Y., & Andrews, P. C. (2014). Quantitative proteomics reveals histone modifications in crosstalk with h3 lysine 27 methylation. *Molecular and Cellular Proteomics*, *13*(3), 749–759. https://doi.org/10.1074/mcp.M113.029025

Zhang, S., Rattanatray, L., McMillen, I. C., Suter, C. M., & Morrison, J. L. (2011). Periconceptional nutrition and the early programming of a life of obesity or adversity. *Progress in Biophysics and Molecular Biology*, *106*(1), 307–314. https://doi.org/10.1016/j.pbiomolbio.2010.12.004

Zhang, T., Gong, Y., Meng, H., Li, C., & Xue, L. (2020). Symphony of epigenetic and metabolic regulation - Interaction between the histone methyltransferase EZH2 and metabolism of tumor. In *Clinical Epigenetics* (Vol. 12, Issue 1, pp. 1–15). BioMed Central Ltd. https://doi.org/10.1186/s13148-020-00862-0

Zhao, J., Li, H., Zhou, R., Ma, G., Dekker, J. D., Tucker, H. O., Yao, Z., & Guo, X. (2015). Foxp1 regulates the proliferation of hair follicle stem cells in response to oxidative stress during hair cycling. *PLoS ONE*, *10*(7). https://doi.org/10.1371/journal.pone.0131674

Zhong, Q., & Kowluru, R. A. (2010). Role of histone acetylation in the development of diabetic retinopathy and the metabolic memory phenomenon. *Journal of Cellular Biochemistry*, *110*(6), 1306–1313. https://doi.org/10.1002/jcb.22644

Zhu, P., Liu, Y., Zhang, F., Bai, X., Chen, Z., Shangguan, F., Zhang, B., Zhang, L., Chen, Q., Xie, D., Lan, L., Xue, X., Liang, X. J., Lu, B., Wei, T., & Qin, Y. (2018). Human elongation factor 4 regulates cancer bioenergetics by acting as a mitochondrial translation switch. *Cancer Research*, *78*(11), 2813–2824. https://doi.org/10.1158/0008-5472.CAN-17-2059

Appendix

A

Seahorse 72h basal

Type of compound :R / ECAR response		cluster 1 Up Up	cluster 2 Up NC	cluster 3 Up Down	cluster 4 NC Up	cluster 5 Down Up	cluster 6 Down NC	cluster 7 NC Down	cluster 8 Down Down	cluster 9 NC NC
Fragment cluster	1	0	0	0	1	0	2	2	0	5
	2	0	2	0	1	0	0	1	2	11
	3	0	0	0	0	0	0	0	0	1
	4	0	0	0	0	0	0	0	0	0
	5	0	3	1	3	0	3	4	0	27
	6	1	1	0	1	0	0	2	3	6
	7	0	0	0	0	0	0	0	0	0
	8	0	1	0	0	0	0	0	0	1
	9	1	0	0	0	0	1	0	1	2
	10	0	0	0	0	0	0	0	0	1
MOE cluster	1	2	7	1	6	0	2	7	5	43
	8	0	0	0	0	0	1	0	0	0
	16	0	0	0	0	0	0	0	0	1
	17	0	0	0	0	0	0	1	1	2
	18	0	0	0	0	0	0	0	0	2
	26	0	0	0	0	0	0	0	0	1
	44	0	0	0	0	0	1	0	0	0
	48	0	0	0	0	0	0	1	0	1
	53	0	0	0	0	0	0	0	0	1
	54	0	0	0	0	0	0	0	0	1
	57	0	0	0	0	0	0	0	0	1
	58	0	0	0	0	0	1	0	0	0
	62	0	0	0	0	0	1	0	0	0
	76	0	0	0	0	0	0	0	0	0
	88	0	0	0	0	0	0	0	0	0
	92	0	0	0	0	0	0	0	0	0
	98	0	0	0	0	0	0	0	0	0
	101	0	0	0	0	0	0	0	0	1
Macro classes	A	0	2	0	2	0	2	3	2	17
	B	1	4	1	4	0	0	5	3	30
	C	0	0	0	0	0	3	1	0	5
	D	1	1	0	0	0	1	0	1	2

Figure A.1. Pharmacophore fragment based analysis did not show underlying drug structure similarities to explain metabolic readouts of 100 inhibitors

A. The screened compounds cluster in 4 large groups defined by statistical proximity within a fragment cluster or MOE gpiDAPH3.

B. 72h basal respiration rates were used to cluster the inhibitors in the macro classes corresponding to the fragment cluster method.

C. 72h maximal respiration rates were used to cluster the inhibitors in the macro classes corresponding to the fragment cluster method.

A

Seahorse 72h max

Type of compound		cluster 1	cluster 2	cluster 3	cluster 4	cluster 5	cluster 6	cluster 7	cluster 8	cluster 9
OCR / ECAR response		Up Up	Up NC	Up Down	NC Up	Down Up	Down NC	NC Down	Down Down	NC NC
Fragment cluster	1	1	2	0	0	0	3	3	0	1
	2	3	1	0	0	0	1	0	3	9
	3	0	0	0	0	0	0	0	0	1
	4	0	0	0	0	0	0	0	0	0
	5	2	5	1	1	0	4	2	2	24
	6	1	1	1	0	1	0	1	4	5
	7	0	0	0	0	0	0	0	0	0
	8	1	0	0	0	0	0	0	0	1
	9	1	0	0	0	0	1	0	2	1
	10	0	0	0	0	0	1	0	0	0
MOE cluster	1	9	9	2	1	1	5	6	8	32
	8	0	0	0	0	0	1	0	0	0
	16	0	0	0	0	0	0	0	0	1
	17	0	0	0	0	0	0	0	1	3
	18	0	0	0	0	0	0	0	0	2
	26	0	0	0	0	0	0	0	0	1
	44	0	0	0	0	0	1	0	0	0
	48	0	0	0	0	0	0	0	2	0
	53	0	0	0	0	0	0	0	0	1
	54	0	0	0	0	0	0	0	0	1
	57	0	0	0	0	0	0	0	0	1
	58	0	0	0	0	0	1	0	0	0
	62	0	0	0	0	0	1	0	0	0
	76	0	0	0	0	0	0	0	0	0
	88	0	0	0	0	0	0	0	0	0
	92	0	0	0	0	0	0	0	0	0
	98	0	0	0	0	0	0	0	0	0
	101	0	0	0	0	0	1	0	0	0
Kelly class	A	4	3	0	0	0	4	3	3	11
	B	3	6	2	1	1	1	3	5	26
	C	0	0	0	0	0	4	0	2	3
	D	2	0	0	0	0	1	0	1	2

Figure A.2. Pharmacophore fragment based analysis did not show underlying drug structure similarities to explain metabolic readouts of 100 inhibitors

A. The screened compounds cluster in 4 large groups defined by statistical proximity within a fragment cluster or MOE gpiDAPH3.

B. 72h basal respiration rates were used to cluster the inhibitors in the macro classes corresponding to the fragment cluster method.

C. 72h maximal respiration rates were used to cluster the inhibitors in the macro classes corresponding to the fragment cluster method.

A

Seahorse 1h basal

Type of compound		cluster 1	cluster 2	cluster 3	cluster 4	cluster 5	cluster 6	cluster 7	cluster 8	cluster 9
OCR / ECAR response		Up Up	Up NC	Up Down	NC Up	Down Up	Down NC	NC Down	Down Down	NC NC
Fragment cluster	1	0	0	0	0	0	0	0	1	8
	2	0	1	0	0	0	0	0	0	15
	3	0	0	0	0	0	0	0	0	1
	4	0	0	0	0	0	0	0	0	1
	5	0	1	0	0	0	1	1	0	37
	6	0	0	0	0	0	0	2	0	11
	7	0	0	0	0	0	0	0	0	1
	8	0	0	0	0	0	0	0	0	2
	9	0	0	0	0	0	0	0	0	6
	10	0	0	0	0	0	0	0	0	1
MOE cluster	1	0	2	0	0	0	1	3	1	63
	8	0	0	0	0	0	0	0	0	1
	16	0	0	0	0	0	0	0	0	1
	17	0	0	0	0	0	0	0	0	4
	18	0	0	0	0	0	0	0	0	2
	26	0	0	0	0	0	0	0	0	1
	44	0	0	0	0	0	0	0	0	1
	48	0	0	0	0	0	0	0	0	2
	53	0	0	0	0	0	0	0	0	1
	54	0	0	0	0	0	0	0	0	1
	57	0	0	0	0	0	0	0	0	1
	58	0	0	0	0	0	0	0	0	1
	62	0	0	0	0	0	0	0	0	1
	76	0	0	0	0	0	0	0	0	0
	88	0	0	0	0	0	0	0	0	0
	92	0	0	0	0	0	0	0	0	1
	98	0	0	0	0	0	0	0	0	1
	101	0	0	0	0	0	0	0	0	1
Kelly class	A	0	1	0	0	0	0	0	1	24
	B	0	1	0	0	0	1	3	0	42
	C	0	0	0	0	0	0	0	0	11
	D	0	0	0	0	0	0	0	0	6

Figure A.3. Pharmacophore fragment based analysis did not show underlying drug structure similarities to explain metabolic readouts of 100 inhibitors

A. The screened compounds cluster in 4 large groups defined by statistical proximity within a fragment cluster or MOE gpiDAPH3.

B. 72h basal respiration rates were used to cluster the inhibitors in the macro classes corresponding to the fragment cluster method.

C. 72h maximal respiration rates were used to cluster the inhibitors in the macro classes corresponding to the fragment cluster method.

A

Seahorse 1h max										
Type of compound		**cluster 1**	**cluster 2**	**cluster 3**	**cluster 4**	**cluster 5**	**cluster 6**	**cluster 7**	**cluster 8**	**cluster 9**
OCR / ECAR response		Up Up	Up NC	Up Down	NC Up	Down Up	Down NC	NC Down	Down Down	NC NC
Fragment cluster	1	0	0	0	0	0	1	0	1	7
	2	1	1	0	0	0	2	0	1	11
	3	0	0	0	0	0	0	0	0	1
	4	0	0	0	0	0	0	0	0	1
	5	2	2	0	0	0	2	2	0	32
	6	0	3	0	0	0	1	0	1	8
	7	0	0	0	0	0	0	0	0	1
	8	0	0	0	0	0	0	0	0	2
	9	0	1	0	0	0	0	0	1	4
	10	0	0	0	0	0	0	0	0	1
MOE cluster	1	2	6	0	0	0	6	2	4	50
	8	0	0	0	0	0	0	0	0	1
	16	0	0	0	0	0	0	0	0	1
	17	0	0	0	0	0	0	0	0	4
	18	0	1	0	0	0	0	0	0	1
	26	0	0	0	0	0	0	0	0	1
	44	0	0	0	0	0	0	0	0	1
	48	0	0	0	0	0	0	0	0	2
	53	0	0	0	0	0	0	0	0	1
	54	0	0	0	0	0	0	0	0	1
	57	1	0	0	0	0	0	0	0	0
	58	0	0	0	0	0	0	0	0	1
	62	0	0	0	0	0	0	0	0	1
	76	0	0	0	0	0	0	0	0	0
	88	0	0	0	0	0	0	0	0	0
	92	0	0	0	0	0	0	0	0	1
	98	0	0	0	0	0	0	0	0	1
	101	0	0	0	0	0	0	0	0	1
Kelly class	A	1	1	0	0	0	3	0	2	19
	B	1	5	0	0	0	3	2	1	35
	C	1	0	0	0	0	0	0	0	10
	D	0	1	0	0	0	0	0	1	4

Figure A.4. Pharmacophore fragment based analysis did not show underlying drug structure similarities to explain metabolic readouts of 100 inhibitors

A. The screened compounds cluster in 4 large groups defined by statistical proximity within a fragment cluster or MOE gpiDAPH3.

B. 72h basal respiration rates were used to cluster the inhibitors in the macro classes corresponding to the fragment cluster method.

C. 72h maximal respiration rates were used to cluster the inhibitors in the macro classes corresponding to the fragment cluster method.

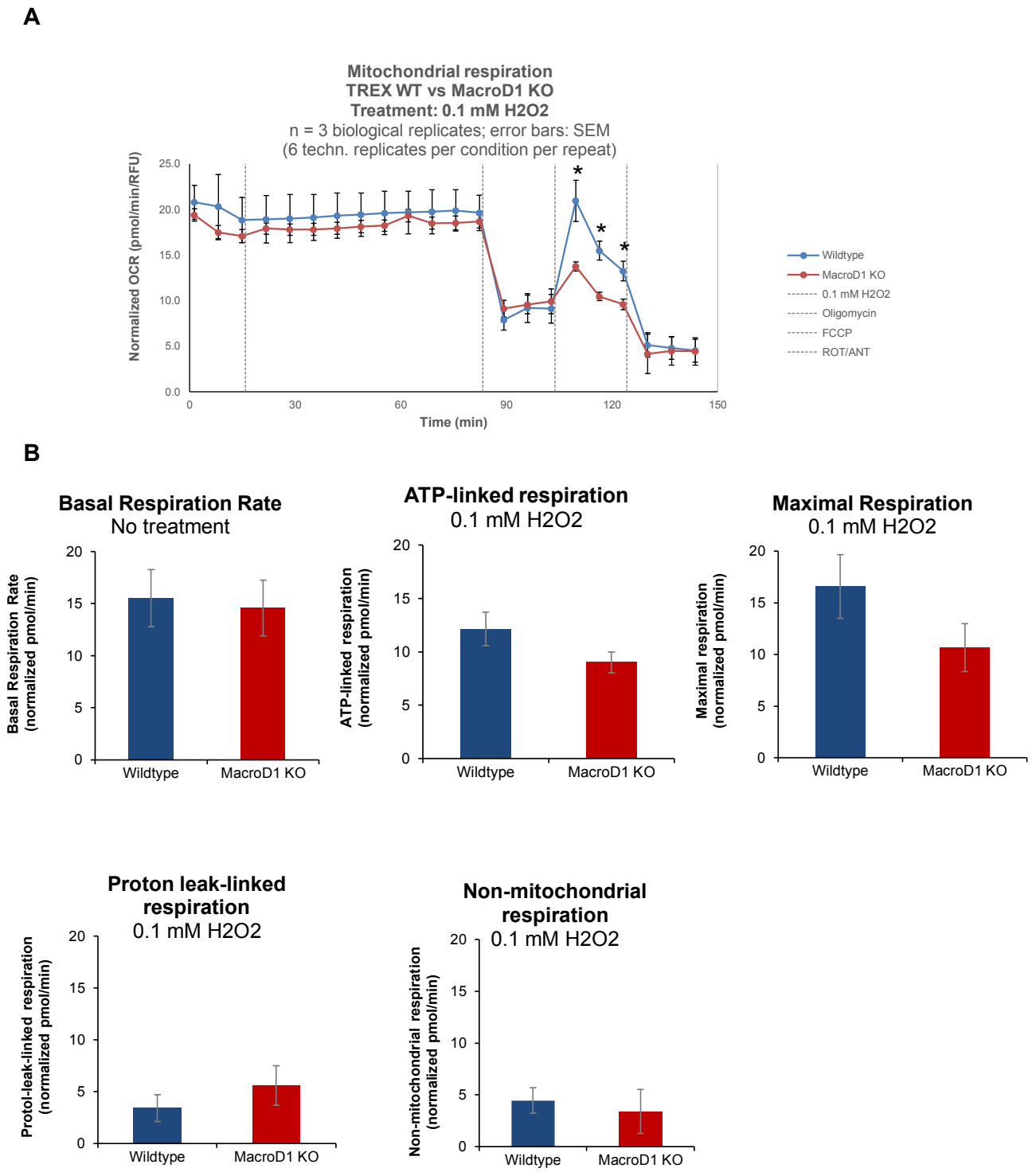

Figure A.5. MacroD1 regulated metabolism in TREX cells by promoting oxidative respiration, even under DNA stress induced by 0.1 mM H_2O_2

A. Seahorse XF analysis of mitochondrial respiration of TREX WT vs MacroD1 KO before and after addition of 0.1 mM H_2O_2 (at t=15min). N=3 biological replicates; error bars: SEM, 6 technical replicates per condition per biological repeat. X-axis represents time (min) and y-axis represents normalized OCR ([pmol/min]/RFU)

B. Normalized respiration rate parameters measured with seahorse XF based on time course experiments depicted in A.

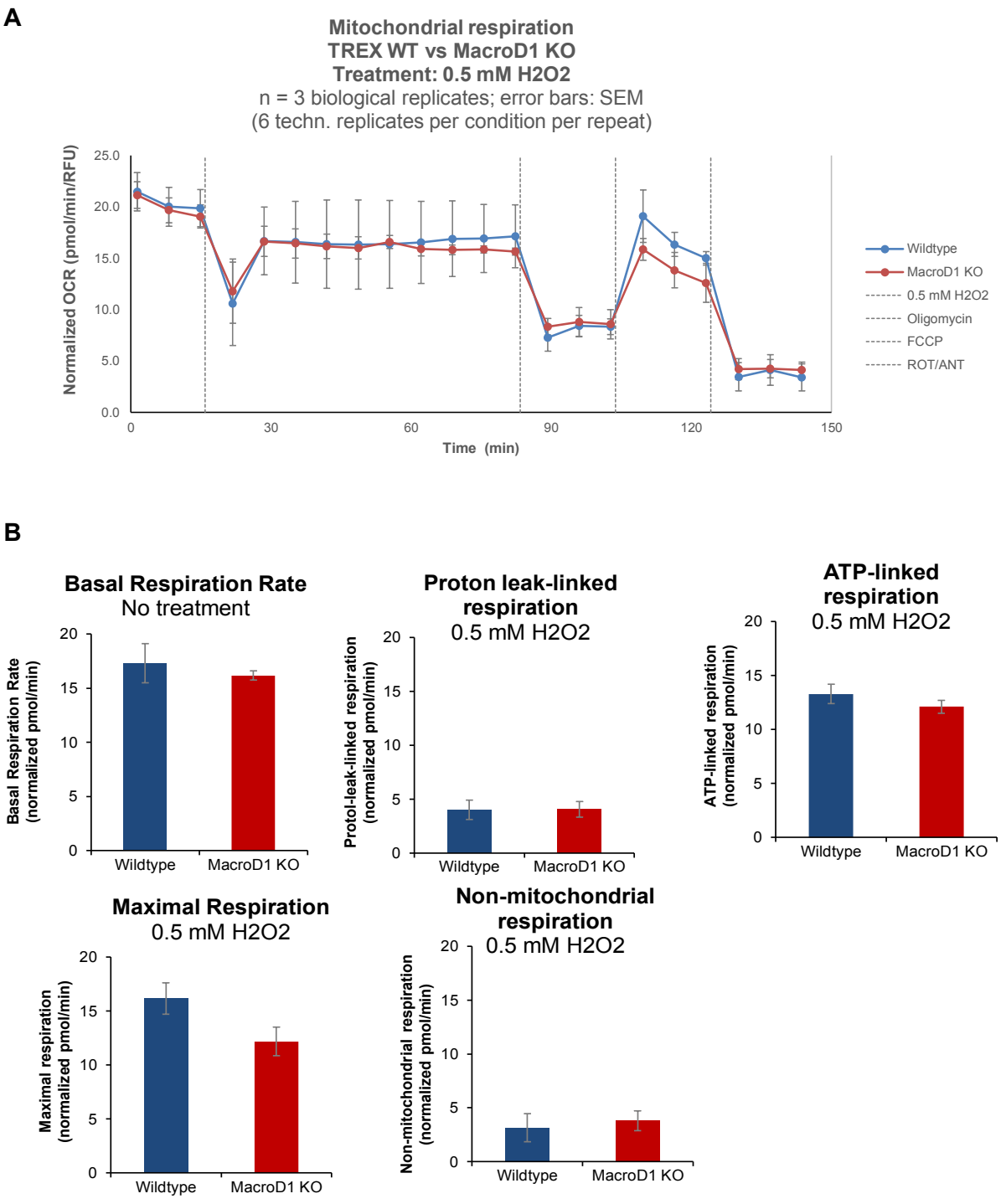

Figure A.6. MacroD1 regulated metabolism in TREX cells by promoting oxidative respiration, even under DNA stress induced by 0.5 mM H_2O_2

A. Seahorse XF analysis of mitochondrial respiration of TREX WT vs MacroD1 KO before and after addition of 0.5 mM H_2O_2 (at t=15min). N=3 biological replicates; error bars: SEM, 6 technical replicates per condition per biological repeat. X-axis represents time (min) and y-axis represents normalized OCR ([pmol/min]/RFU)

B. Normalized respiration rate parameters measured with seahorse XF based on time course experiments depicted in A.

A

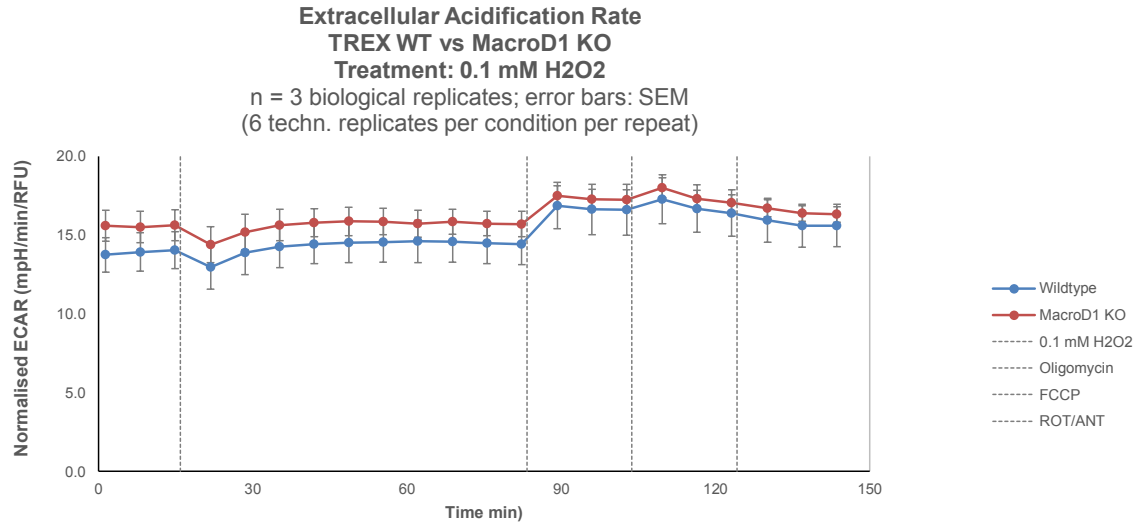

B

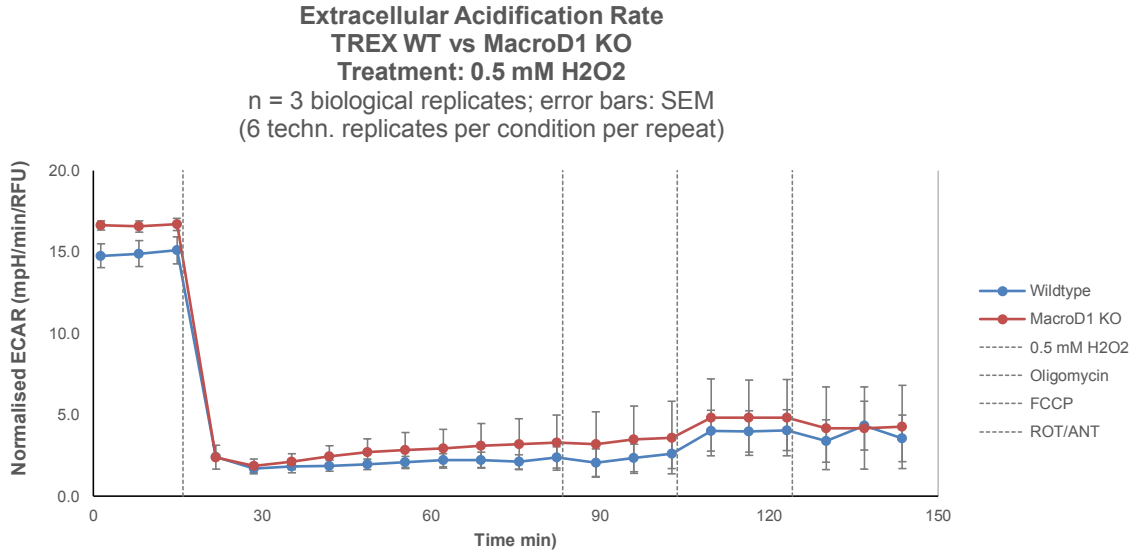

Figure A.7. MacroD1 regulated metabolism in TREX cells by inhibiting glycolysis, even under DNA stress induced by 0.1 or 0.5 mM H_2O_2

A. Seahorse XF analysis of glycolysis of TREX WT vs MacroD1 KO before and after addition of 0.1 mM H_2O_2 (at t=15min). N=3 biological replicates; error bars: SEM, 6 technical replicates per condition per biological repeat. X-axis represents time (min) and y-axis represents normalized ECAR ([mpH/min]/RFU)

B. Seahorse XF analysis of glycolysis of TREX WT vs MacroD1 KO before and after addition of 0.5 mM H_2O_2 (at t=15min). N=3 biological replicates; error bars: SEM, 6 technical replicates per condition per biological repeat. X-axis represents time (min) and y-axis represents normalized ECAR ([mpH/min]/RFU)

A

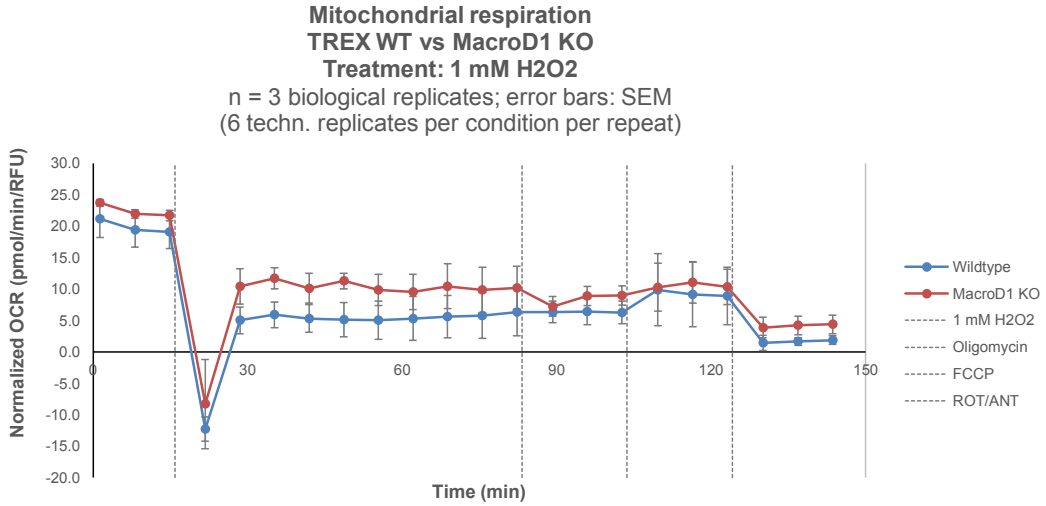

B

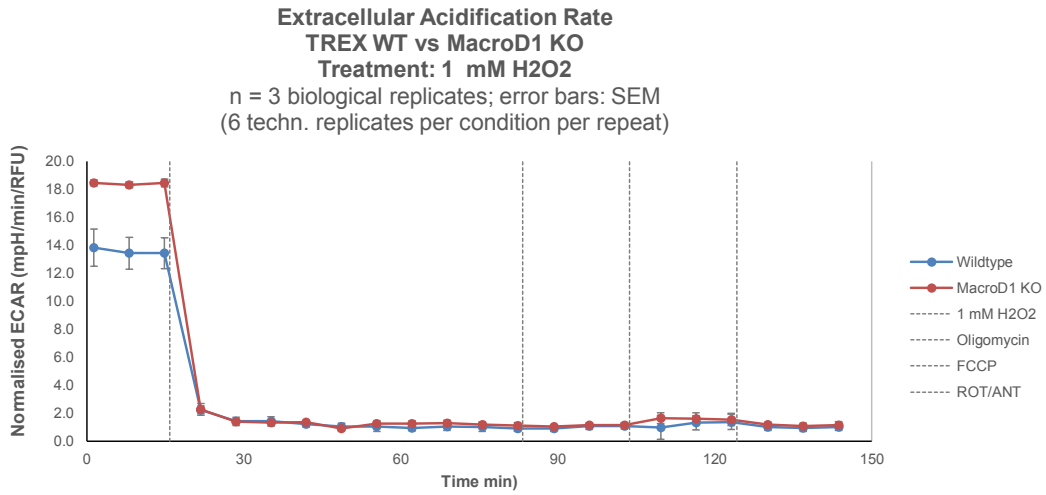

Figure A.8. Treatment of TREX cells with 1 mM H_2O_2 abrogated normal cellular metabolism

A. Seahorse XF analysis of mitochondrial respiration of TREX WT vs MacroD1 KO before and after addition of 1 mM H_2O_2 (at t=15min). N=3 biological replicates; error bars: SEM, 6 technical replicates per condition per biological repeat. X-axis represents time (min) and y-axis represents normalized OCR ([pmol/min]/RFU)

B. Seahorse XF analysis of glycolysis of TREX WT vs MacroD1 KO before and after addition of 1 mM H_2O_2 (at t=15min). N=3 biological replicates; error bars: SEM, 6 technical replicates per condition per biological repeat. X-axis represents time (min) and y-axis represents normalized ECAR ([mpH/min]/RFU)

A

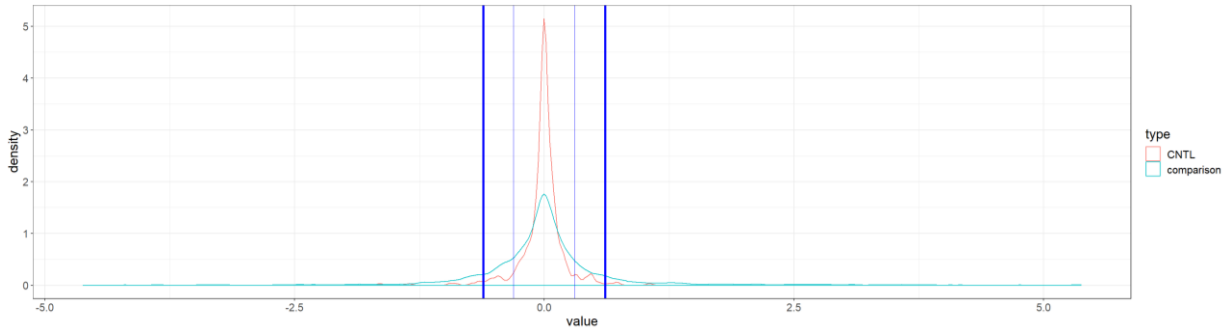

B

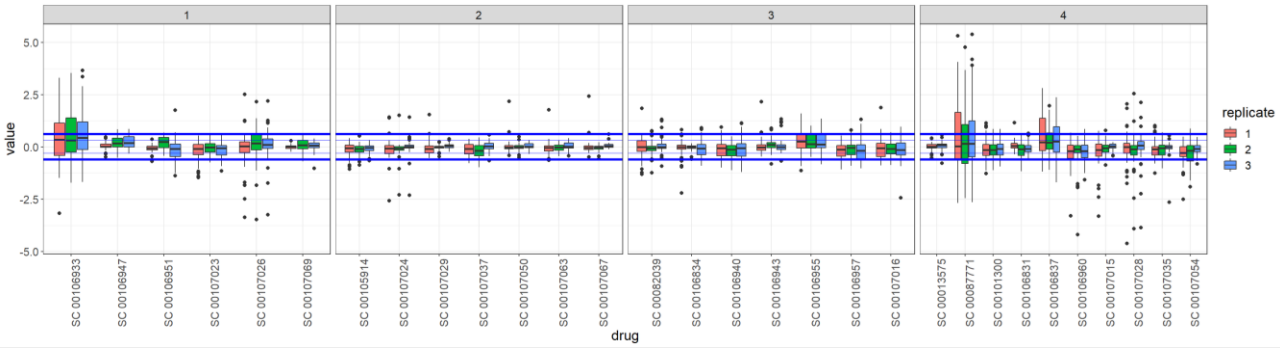

Figure A.9. Basic histone PTM mass spec statistics

A. Density plot comparing the histone PTMs ctrl replicates and the histone PTMs induced by treatments versus ctrl. Log2 ratios of ctrl vs treatment.

B. Log2 ratios of histone PTM levels depicted as box plots of ctrl vs treatment for all 30 treatments, with the three biological replicates shown as separate box plots.

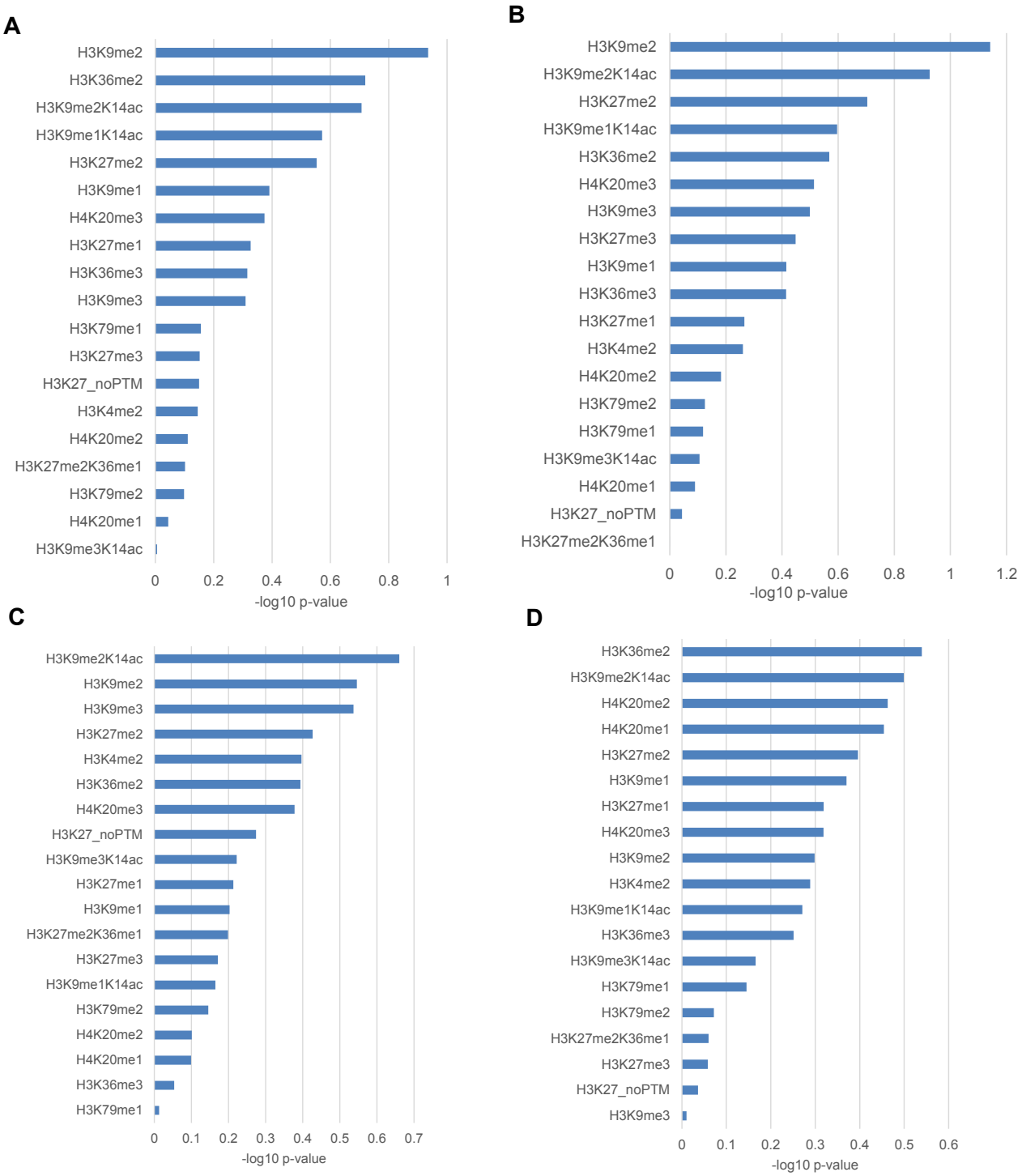

Figure A.10. Correlation of methylation marks on H3 and H4 and metabolic states

Multivariate linear modelling was performed between all histone PTMs levels and metabolic states induced by treatments with 30 different drug candidates. Values depict -log 10 p value where $p>1.3$ indicates a significant correlation (corresponding to $p<0.05$) between the respective PTM and metabolic state.

A. Correlation between histone lysine methylation and basal glycolysis

B. Correlation between histone lysine methylation and maximum glycolysis

C. Correlation between histone lysine methylation and maximum oxidative phosphorylation

D. Correlation between histone lysine methylation and base oxidative phosphorylation

Pearson correlation matrix: metabolism vs most-affected proteins

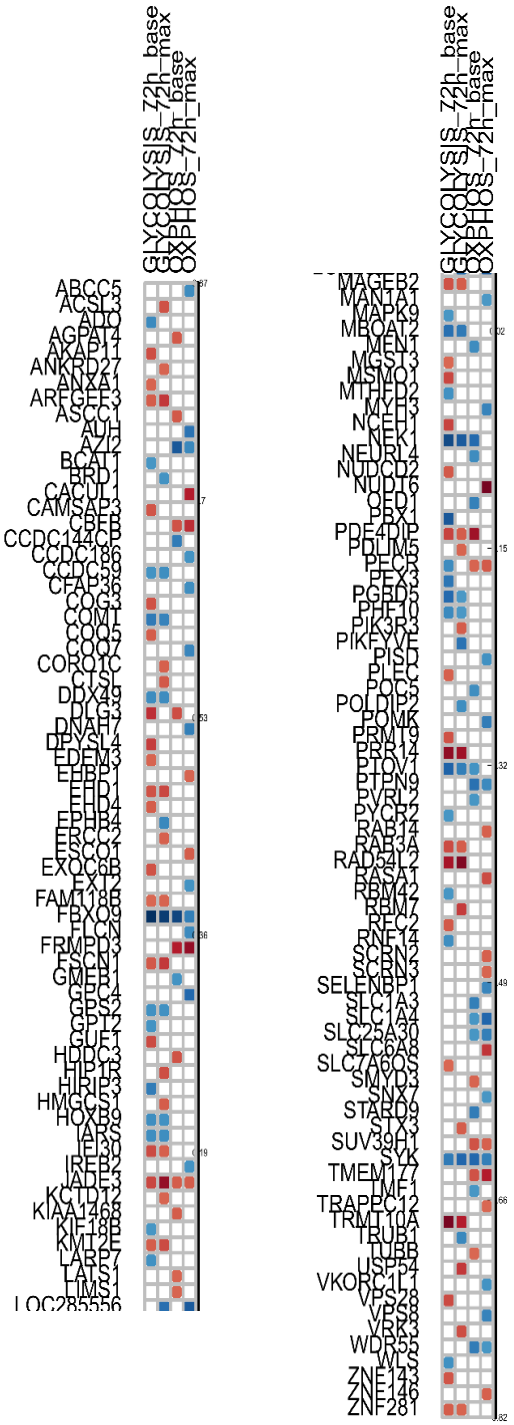

Figure A.11. Pearson correlation analysis of acetylation and methylation modifications on histones H3 and H4, as well as proteins, induced by treatments with 30 different small molecules

Correlation matrix based on Pearson's correlation coefficient. The size and colour of the bubble indicates a higher degree of correlation between respective PTM marks, as shown on the right-hand side legend, ranging from strong anticorrelation (red, -1) to strong correlation (blue, +1). The threshold for correlations selected in this graph was +/- 0.50.